



Asphalt Research Consortium

Quarterly Technical Progress Report April 1-June 30, 2010

July 2010

Prepared for
Federal Highway Administration
Contract No. DTFH61-07-H-00009

By
Western Research Institute
Texas A&M University
University of Wisconsin-Madison
University of Nevada-Reno
Advanced Asphalt Technologies

www.westernresearch.org
www.ARC.unr.edu

TABLE OF CONTENTS

INTRODUCTION	1
GENERAL CONSORTIUM ACTIVITIES	3
PROGRAM AREA: MOISTURE DAMAGE.....	5
Category M1: Adhesion.....	5
Category M2: Cohesion.....	17
Category M3: Aggregate Surface	19
Category M4: Modeling.....	20
Category M5: Moisture Damage Prediction System	21
PROGRAM AREA: FATIGUE.....	25
Category F1: Material and Mixture Properties	25
Category F2: Test Method Development.....	53
Category F3: Modeling.....	77
PROGRAM AREA: ENGINEERED MATERIALS.....	99
Category E1: Modeling.....	99
Category E2: Design Guidance.....	124
PROGRAM AREA: VEHICLE-PAVEMENT INTERACTION.....	165
Category VP1: Workshop.....	165
Category VP2: Design Guidance.....	165
Category VP3: Modeling.....	170
PROGRAM AREA: VALIDATION	177
Category V1: Field Validation.....	177
Category V2: Accelerated Pavement Testing.....	178
Category V3: R&D Validation	179
PROGRAM AREA: TECHNOLOGY DEVELOPMENT.....	189
PROGRAM AREA: TECHNOLOGY TRANSFER.....	207
Category TT1: Outreach and Databases	207

INTRODUCTION

This document is the Quarterly Report for the period of April 1 to June 30, 2010 for the Federal Highway Administration (FHWA) Contract DTFH61-07-H-00009, the Asphalt Research Consortium (ARC). The Consortium is coordinated by Western Research Institute with partners Texas A&M University, the University of Wisconsin-Madison, the University of Nevada Reno, and Advanced Asphalt Technologies.

The Quarterly Report is grouped into seven areas, Moisture Damage, Fatigue, Engineered Paving Materials, Vehicle-Pavement Interaction, Validation, Technology Development, and Technology Transfer. The format of the report is based upon the Research Work Plan that is grouped by Work Element and Subtask.

This Quarterly Report summarizes the work accomplishments, data, and analysis for the various Work Elements and Subtasks. This report is being presented in a brief summary form. Please note that in many cases the report is briefer than in the past at the request of FHWA AOTR Mr. Eric Weaver. The Quarter of April 1 to June 30, 2010 is first quarter of the Year 4 contract year. Reviewers may want to reference the Year 4 Work Plan and perhaps the earlier Work Plans. There is also background information regarding the research plan contained in the Revised Year 2 Work Plan. The more detailed information about the research such as approaches to test method development, data collection, and analyses will be reported in research publications as part of the deliverables. All of the Work Plans, as well as many other documents, including quarterly reports, are posted on the ARC website, www.ARC.unr.edu.

SUPPORT OF FHWA AND DOT STRATEGIC GOALS

The Asphalt Research Consortium research is responsive to the needs of asphalt engineers and technologists, state DOT's, and supports the FHWA Strategic Goals and the Asphalt Pavement Road Map. More specifically, the research reported here supports the Strategic Goals of safety, mobility, and environmental stewardship. By addressing the causes of pavement failure and thus determining methods to improve asphalt pavement durability and longevity, this research will provide the motoring public with increased safety and mobility. The research directed at improved use of recycled asphalt pavement (RAP), warm mix asphalt, and cold mix asphalt supports the Strategic Goal of environmental stewardship.

GENERAL CONSORTIUM ACTIVITIES

PROGRESS THIS QUARTER

ARC members attended and made presentations at the European Asphalt Technology Association (EATA) meeting in Parma, Italy in June.

ARC members, Dr. Hussain Bahia, Dr. Elie Hajj, and Dr. Eric Kalberer, attended the RAP Expert Task Group meeting in Auburn, Alabama on May 19 & 20, 2010 that was hosted by Auburn University and the National Center for Asphalt Technology. An update on the RAP research being conducted by the ARC was presented.

Dr. Ramon Bonaquist of Advanced Asphalt Technologies continued to work with Mr. Frank Fee of NuStar Energy to coordinate sampling of materials for the flow number study requested and approved by the Mixture and Construction ETG.

Dr. Donald Christensen of Advanced Asphalt Technologies visited NCAT and presented a seminar on the simplified continuum damage fatigue testing and analysis that is being developed in Work Element TD2. NCAT is considering using continuum damage fatigue testing in some of their projects.

WORK PLANNED FOR NEXT QUARTER

Several ARC members will attend and make presentations at the 47th Petersen Asphalt Research Conference and the 2010 Pavement Performance Prediction Symposium in Laramie, Wyoming in July.

The ARC Asphalt Microstructural Modeling team members Mr. Troy Pauli, Dr. Michael Greenfield, Dr. Linbing Wang, and Dr. Jeffrey Bullard met during the week of the Petersen Conference to discuss project progress, coordination, and work plans.

Several ARC members are planning to attend and make presentations at the Binder, Mix & Construction, and Fundamental Properties & Advanced Models ETG meetings planned for Madison, Wisconsin during the week of September 13 – 17, 2010.

Dr. Ramon Bonaquist will continue to work with Mr. Frank Fee to coordinate sampling of materials for the Mixtures and Construction ETG's flow number study and will assist with coordination of the testing at the National Institute of Standards and Technology (NIST) and the University of Nevada, Reno.

PROGRAM AREA: MOISTURE DAMAGE

CATEGORY M1: ADHESION

Work Element M1a: Affinity of Asphalt to Aggregate (UWM)

Work Done This Quarter

In this quarter, the research team focused its efforts on evaluating the reproducibility (operator variability) of the Bitumen Bond Strength (BBS) test. An experimental matrix, which included different binders and aggregate types, was used to estimate the effect of different device operators on the pull-off strength obtained from the BBS test. The materials used are listed in table M1a.1.

Table M1a.1. Materials used to evaluate the reproducibility of the BBS test.

Solution	Tap Water
Mineral Surfaces	Granite and Diabase
Asphalt Binder	FH 64-22
Modified Asphalt Binder	FH 64-22 + 0.7% ELV + 0.17% PPA

ELV = Elvaloy. PPA = polyphosphoric acid.

Samples were conditioned in tap water for 0, 6 and 24 hours. The effect of conditioning time on the pull-off strength of the asphalt-aggregate systems tested by different operators can be observed in figure M1a.1. The conditioning of specimens in water has a significant effect on the pull-off strength and on the failure mechanism, regardless of the selected asphalt binder or aggregate type. As can be seen in figure M1a.1, the values of pull-off strength for each aggregate-binder system were similar for both operators.

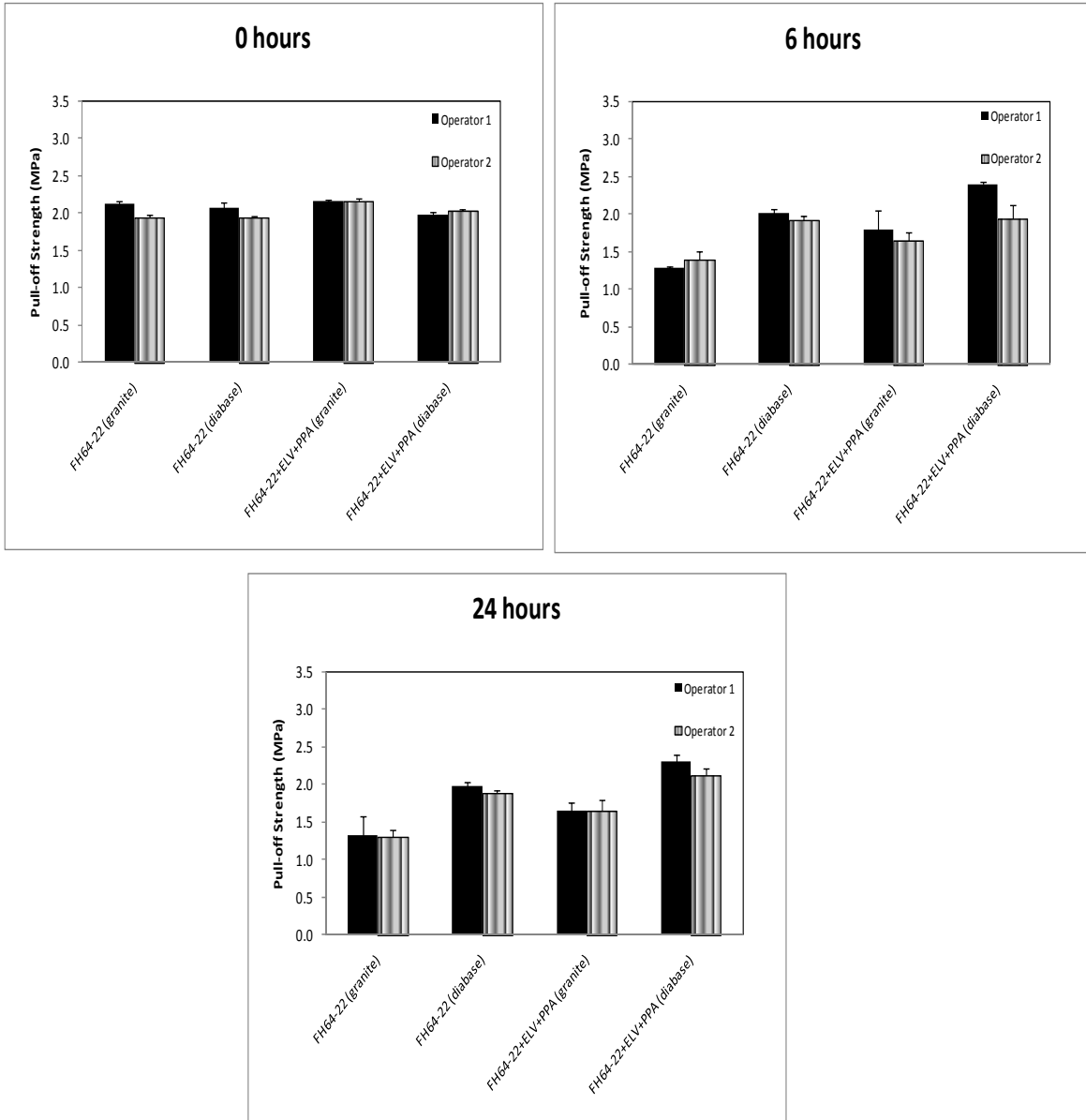


Figure M1a.1. Charts. Influence of operators in the BBS pull-off tensile strength at 0 hours, 6 hours and 24 hours.

Statistical analyses were performed to evaluate the reproducibility of the BBS test. Specifically, tests of hypotheses were used to determine if there is any statistically significant difference between the means of the pull-off tensile strength obtained with two operators. Table M1a.2 shows the results of the statistical analysis of the operator variability of the BBS test data for all asphalt-aggregate systems. Note that the average pull-off strength was calculated from three replicates for each operator and that $\alpha = 0.05$ is used.

Table M1a.2. Statistical analysis of the operator variability of BBS test.

Materials	Operator 1		Operator 2		Sp ²	t _{statistic}	t _α	-t _α	Result
	u ₁	σ	u ₂	σ					
FH64-22, Granite (0 h)	2.110	0.040	1.937	0.040	0.00	-5.297	2.776	-2.776	Reject Ho
FH64-22, Diabase (0 h)	2.058	0.080	1.932	0.030	0.00	-2.554			Accept Ho
FH64-22+ELV+PPA, Granite (0 h)	2.150	0.030	2.164	0.030	0.00	0.572			Accept Ho
FH64-22+ELV+PPA, Diabase (0 h)	1.966	0.040	2.024	0.020	0.00	2.246			Accept Ho
FH64-22, Granite (6 h)	1.284	0.010	1.388	0.120	0.01	1.496			Accept Ho
FH64-22, Diabase (6 h)	2.017	0.050	1.925	0.050	0.00	-2.254			Accept Ho
FH64-22+ELV+PPA, Granite (6 h)	1.787	0.260	1.650	0.100	0.04	-0.852			Accept Ho
FH64-22+ELV+PPA, Diabase (6 h)	2.387	0.040	1.930	0.190	0.02	-4.077			Reject Ho
FH64-22, Granite (24 h)	1.321	0.260	1.305	0.090	0.04	-0.101			Accept Ho
FH64-22, Diabase (24 h)	1.981	0.050	1.880	0.040	0.00	-2.732			Accept Ho
FH64-22+ELV+PPA, Granite (24 h)	1.644	0.120	1.656	0.130	0.02	0.117			Accept Ho
FH64-22+ELV+PPA, Diabase (24 h)	2.298	0.100	2.127	0.090	0.01	-2.201			Accept Ho

Note that, generally, the BBS test is not sensitive to the operator performing the test. In only two conditions was the average of the pull-off tensile strength statistically different between operators: FH62-22, Granite, at 0 hours and FH62-22+ELV+PPA, Diabase, at 6 hours of conditioning time. Figure M1a.2 shows one of the two cases where the null hypothesis was rejected for $\alpha = 0.05$.

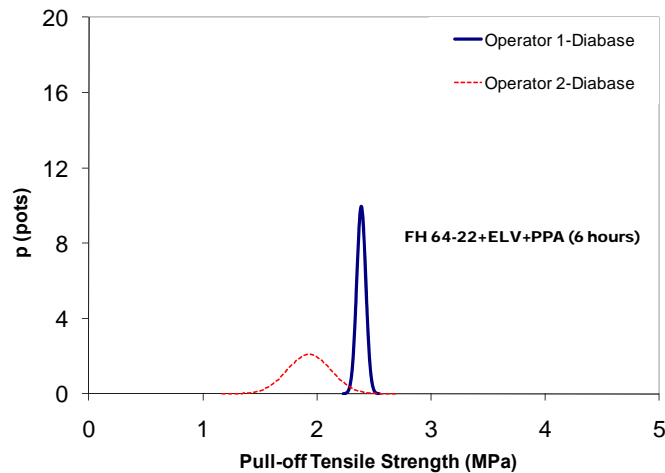


Figure M1a.2. Graph. Distributions of the BBS test results from two operators: null hypothesis was rejected for $\alpha = 0.05$.

On the other hand, figure M1a.3 presents an example of the very similar probability distributions obtained for the BBS test results by different operators.

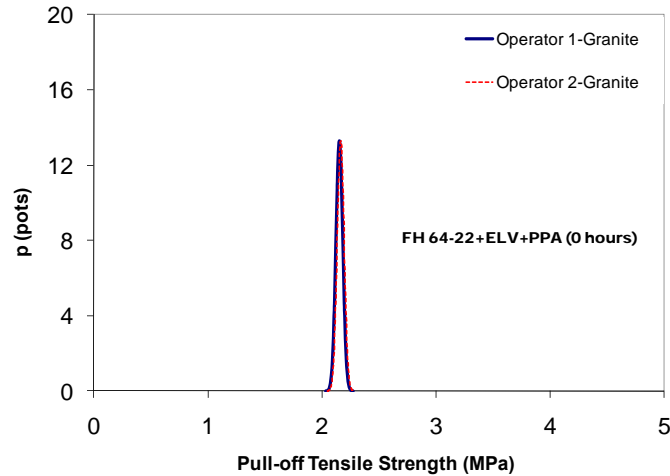


Figure M1a.3. Graph. Distributions of the BBS test results from two operators: null hypothesis was accepted for $\alpha = 0.05$.

Significant Results

The research team obtained promising results regarding reproducibility (operator variability) of the BBS test for the characterization of asphalt-aggregate interface. It was observed that the test is repeatable and applicable to quantify the bonding between asphalt and aggregate under moist conditions. Furthermore, the research team modified the BBS test to minimize the effect of eccentric loading on the pull-off tensile strength. The four blocks used as supports for the piston were replaced by a metallic ring, which significantly reduces any rotation of the BBS loading system during testing.

Significant Problems, Issues and Potential Impact on Progress

None.

Work Planned Next Quarter

Efforts for next quarter will focus on understanding the mechanisms of adhesion between asphalt and aggregate based on fundamental physical and chemical theories. The team will use surface energy (physical-chemical) and zeta potential (electrostatic) to quantify asphalt-aggregate adhesion. Also, the team will continue testing the experimental matrix in the Year 4 work plan. The validation/verification of the BBS test procedure will start next quarter by performing limited modified Dynamic Shear Rheometer (DSR) strain sweep tests and Tensile Strength Ratio (TSR) tests for asphalt mixtures.

Work Element M1b: Work of Adhesion Based on Surface Energy

Subtask M1b-1: Surface Free Energy and Micro-Calorimeter Based Measurements for Work of Adhesion (TAMU)

Work Done This Quarter

The main goal of this subtask is to provide material property inputs required in other work elements as required. Any data obtained from this subtask will be included in the material properties database. In the last quarter surface free energy of some aggregates and asphalt binders that are being used to develop test methods were measured.

Significant Results

None

Significant Problems, Issues and Potential Impact on Progress

None

Work Planned Next Quarter

Work on this subtask will be conducted in conjunction with and as required by other work elements.

Subtask M1b-2: Work of Adhesion at Nano-Scale using AFM (WRI)

Work Done This Quarter

During this past quarter a number of experiments were conducted with the objective of providing a better understanding of the adhesive properties of neat asphalt films at low temperature. A series of experiments was conducted in which thin-film samples of the various SHRP core asphalts were prepared as a “sandwich” between two glass microscope slides. Selected samples were also prepared using a low surface energy plastic film and a cleaved mica surface in place of one of the microscope slides. Sandwich samples were prepared by placing a small spot of asphalt on a clean borosilicate glass microscope slide, covering the asphalt spot with a second slide (or other solid substrate) and then placing the resulting “sandwich” in an oven at ~120° C for one half hour with a small weight on top. After removal from the oven, samples were allowed to cool to room temperature, frozen by the application of a few drops of liquid nitrogen, and then popped apart. The asphalt and glass surfaces thus exposed were imaged using non-contact (wavemode) AFM.

Significant Results

For all of the experiments, regardless of what asphalt or combination of solid substrates was used, a residual film of asphalt was always observed on solid surfaces that appeared to be bare.

That is, in no case did we observe a purely adhesive failure (fracture) in these experiments. Even at very low (liquid nitrogen) temperatures with one low-energy surface (plastic film as used to line BBR molds) asphalt was observed on both substrates. Bee-type structures were not observed on any surface except at the very perimeter of the sample spot (for some asphalt types) where an air/asphalt interface was present during sample preparation. An apparent wetting front that may indicate selective wetting of the surface by a specific phase within the bulk asphalt was frequently observed.

While not conclusive, the results of experiments conducted this quarter with eight SHRP core asphalts and several solid substrates strongly indicate that fracture always occurs in a nearly planar interfacial zone some distance into the asphalt and parallel to the asphalt/solid interface. This, in turn, would indicate that prior to aging and environmental exposure, a purely adhesive failure of the asphalt/aggregate bond is unlikely. Instead, we observed fracture in an interfacial zone of some apparently specific thickness. Thus, fracture, in the absence of aging and moisture, would appear to be neither strictly adhesive, nor cohesive, being limited to a narrow interfacial zone some small distance from the solid surface.

Also, fracture surfaces exhibited areas with patterns of parallel bands that we believe to be evidence of shear banding behavior upon fracture. With more carefully controlled experiments, shear banding can be analyzed to reveal a great deal about the specific behavior of materials during fracture.

Significant Problems, Issues and Potential impact on Progress

None.

Work Planned Next Quarter

Next quarter we will begin to investigate the effects of moisture and aging using the experimental techniques developed this quarter to determine the fracture mode and the location of the fracture with respect to the aggregate surface. We also plan to conduct similar experiments using representative samples of various common aggregate stones with different degrees of surface polish. We will try to arrange for the preparation of these aggregate samples during this next quarter.

Subtask M1b-3: Identify Mechanisms of Competition Between Water and Organic Molecules for Aggregate Surface (TAMU)

Work Done This Quarter

This sub task is investigating the mechanisms responsible for adhesion and debonding of model organic compounds (representing functional groups in asphalt binder) to minerals and representative aggregates. We are measuring the heat of reactions of the chemical mechanisms using a dual-mode flow adsorption calorimeter. Differences in molar heats of reaction of different organics bonding to the same absorbent are indicative of differences in the bonding strength of each absorbate with the absorbent of interest.

Work during this quarter focused on continued development of the instrument. We are in the process of re-tooling the calorimetry instrument in order to best accommodate the minerals and aggregate chosen for the experiment, and to increase the overall robustness and accuracy of the instrument.

Significant Results

There are no significant results for this quarter as we focused on aggregate characterizations.

Significant Problems, Issues and Potential Impact on Progress

There are no significant issues.

Work Planned Next Quarter

We intend to continue are currently conducting studies to validate the ability of the instrument to differentiate between bonding characteristics of materials produced under different conditions, and modify the instrument as needed based on these results. We plan to continue ongoing flow through experiments to measure the molar heat of reaction of the adhesion of model organic compounds that represent asphalt to minerals and aggregates, as well as the molar heats of reactions of water adsorption to organic-coated minerals and aggregates.

Adhesion will be modeled in the flow-through calorimeter by organic sorption from nonaqueous phase solvents to aggregates and pure phase minerals with have already been characterized. Model compounds will be chosen to represent potential functional groups found in asphalt. Potential model compounds include benzoic acid, phenol, valerophenone, benzyl benzoate, quinoline, phenyl sulfoxide, phenyl sulfone, naphthalene, and dibenzanthracene. Solutions containing the model compounds individually and then together will be run through the instrument and the sample chamber containing the aggregates samples. The molar heat of reaction of the adsorption reaction will be measured using the temperature difference between the solution entering and exiting the sample chamber. Experimental variables include the chemistry of the model organics, single versus mixtures of model organics, ionic salt content of the nonaqueous phase solvent, and the surface chemistry of the mineral or aggregate.

Competition of water and the model organics for the mineral or aggregate surfaces will be characterized using flow-through experiments where increasing concentrations of water in a non-aqueous solution are introduced to aggregates coated with the model organic compounds. Coating will be achieved by dissolving small quantities of the model compound(s) in a volatile organic solvent (hexane). The aggregate will be added to the solution, and following mixing the solvent will be allowed to evaporate. Following coating, the aggregates will be placed in instrument, and increasing amounts of water will be added to the non-aqueous carrier solvent. The instrument will measure any heat generated resulting from water's displacement of the model organic compounds at the aggregate surface. Following each experiment the concentration of the model organic compounds in the carrier solution will be determined using a GC/MS.

Work Element M1c: Quantifying Moisture Damage Using DMA (TAMU)

Work Done This Quarter

This work element has been completed. The main two objectives of this work element were as follows:

- Establish a new standard test procedure for preparing FAM samples in order to replicate the composition and structure of fine portion of asphalt mixtures.
- Develop user-friendly software that is capable of executing the analysis of the DMA data and present the results in simple formats. Such software can be used to analyze both stress- and strain-controlled DMA tests.

The proposed test method and software development were discussed in details in the previous report. In this quarter, the software development was completed and it was used to analyze the DMA test data with the aim of validation the analysis procedure and fixing any bugs with the software. This software was developed using C++ programming language. In this software the user is required to load the DMA test raw data and specify some test information through a friendly user interface as presented in figure M1c.1. The DMA test was conducted on four mixtures (table M1c.1) prepared with different aggregates and binders. The aim of this test was to evaluate the proposed standard test procedure for preparing FAM mixtures and DMA specimens. The DMA test was conducted on FAM specimens produced based on the new proposed method and the old method that was proposed by Castelo Branco (2008). After the test was completed, the software was used to analyze the data. Table M1c.2 shows the labels of the different FAM test specimens. Figure M1c.2 shows the crack growth index, $\Delta R(N)$, plotted against number of load cycles for the limestone, gravel, and granite FAM test specimens in dry and wet conditions. It was decided to evaluate the effect of the lime and anti-strip on the performance on the Texas mixture and the results are presented in figure M1c.3.

The FAM mixtures that were prepared using the new proposed method were always testable. However, some tests had to be conducted at a higher temperature (30°C) because of the limited torque capacity (0.2 N.m) of the DMA machine. A new DMA that has a torque capacity of 5.2 N.m was recently acquired. Consequently, there will be no need to raise the temperature to overcome the limited torque. The developed software was used to analyze the DMA test data and present the results in simple formats as presented in figures M1c.2 and M1c.3.

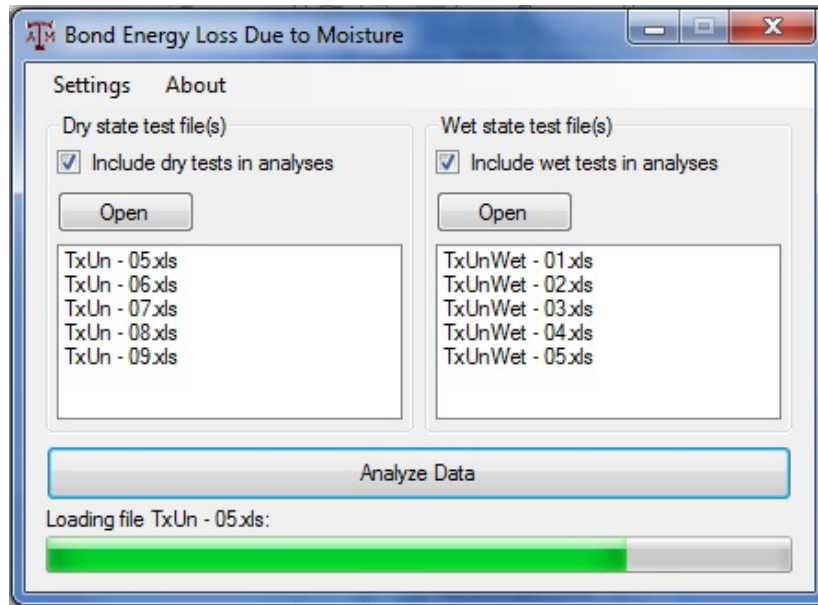
Table M1c.1. Mixtures composition details.

Mixture type	Binder	Material origin
Limestone	PG 70-22C	Sabinal/Knippla, TX
Granite	PG 70-28	Childress, TX
Gravel	PG 64-22S	Fordyce, TX
Texas	PG 76-22	Freer, TX

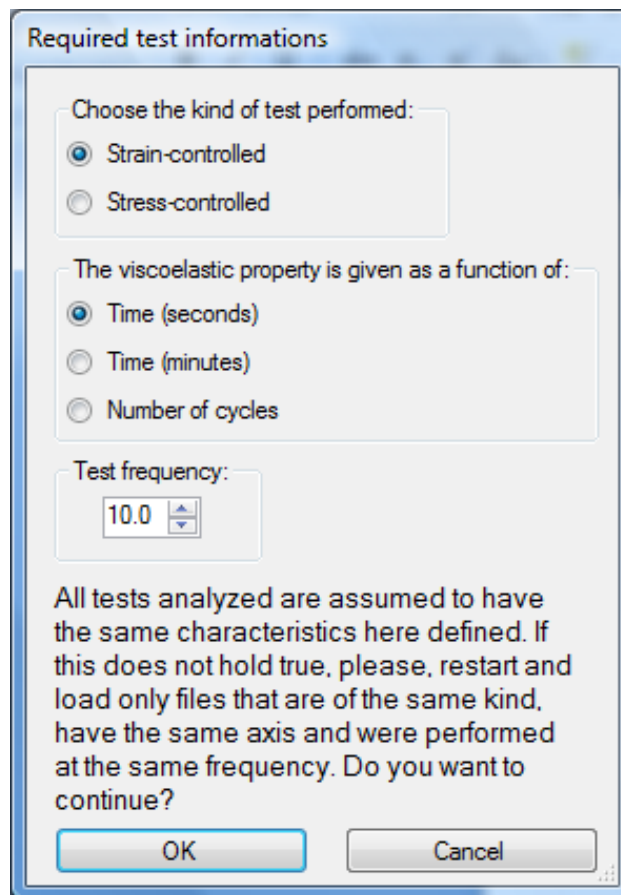
Table M1c.2. FAM test specimens ID.

Specimen type	Test condition			
	Dry		Wet	
	Old method	New Method	Old method	New Method
Limestone	LsOD	LsND	*	LsNW
Granite	GtOD	GtND	*	GtNW
Gravel	GvOD	GvND	GvOW	GvNW
Texas	*	TxND	*	TxNW

* The old method did not produce testable FAM specimens.

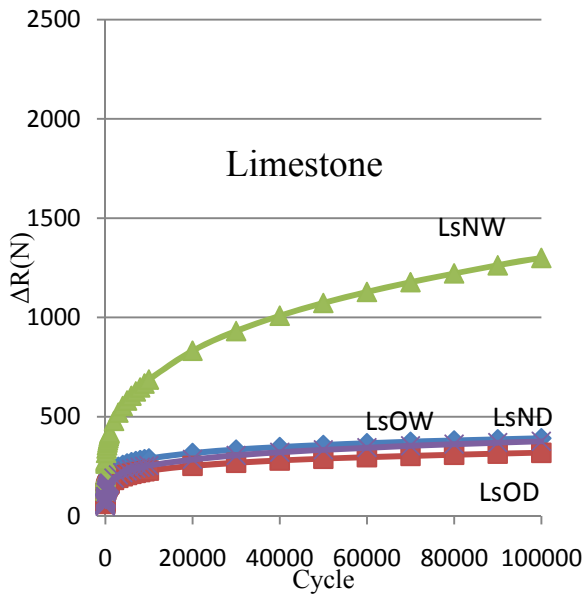


(a)

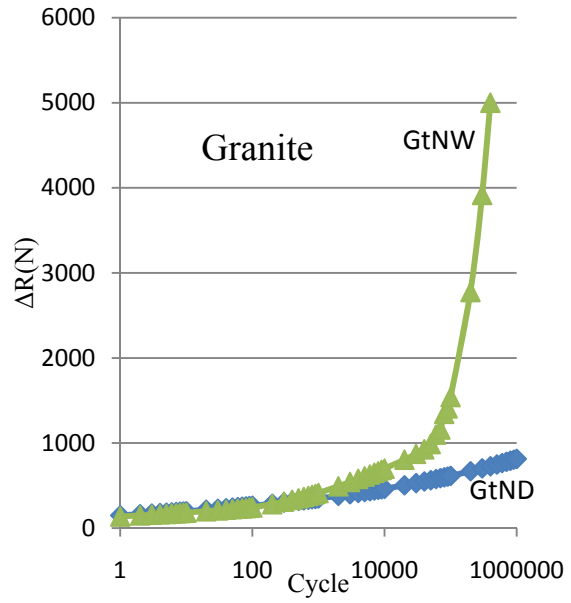


(b)

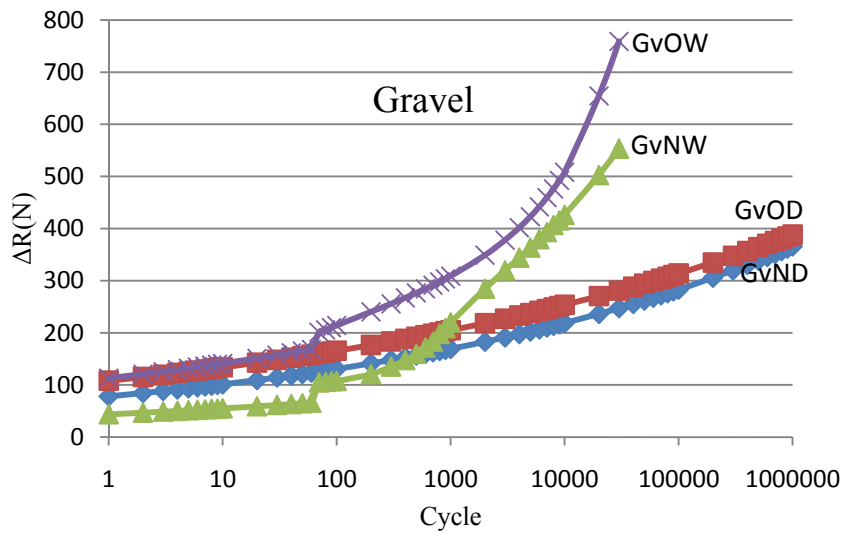
Figure M1c.1. User input interface.



(a)



(b)



(c)

Figure M1c.2. Crack growth index, $\Delta R(N)$, vs. number of load cycles (a) in dry conditions, (b) in wet conditions.

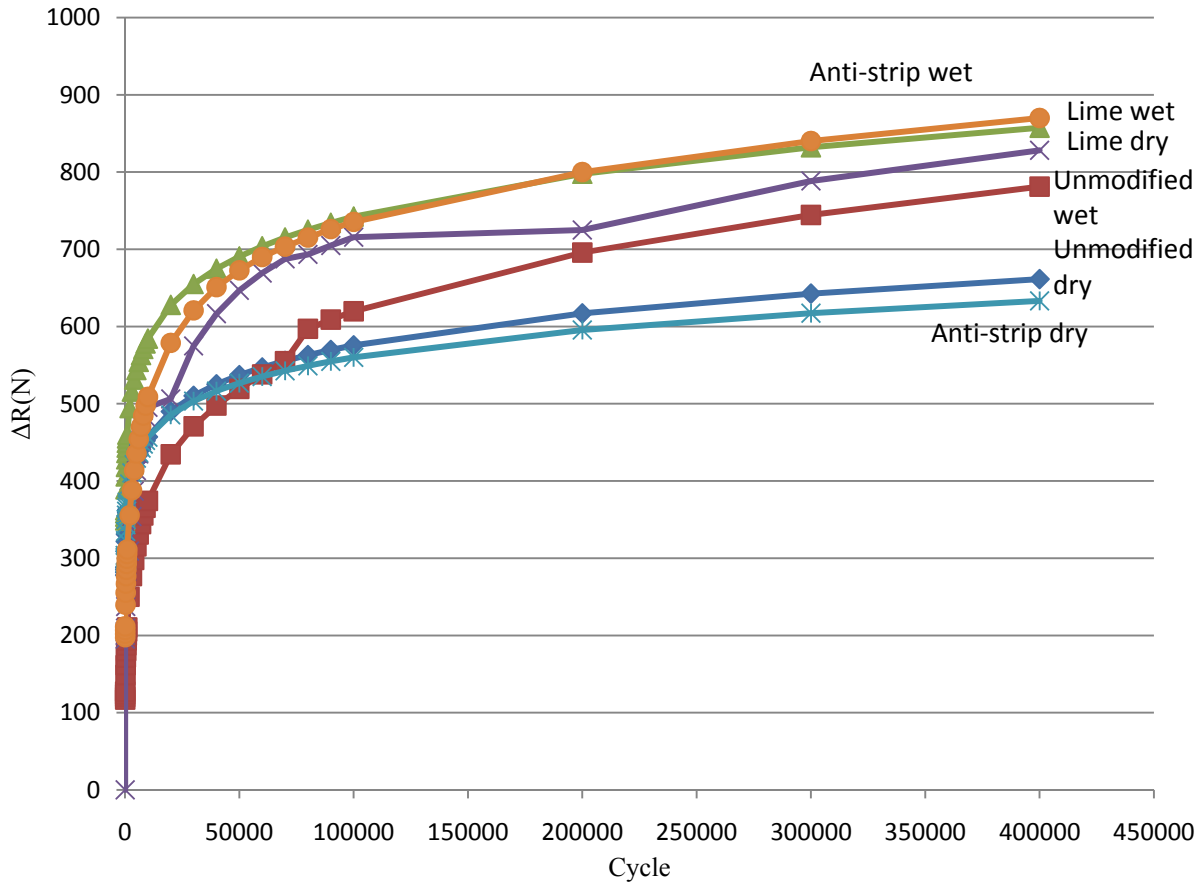


Figure M1c.3. Crack growth index, $\Delta R(N)$, vs. number of load cycles for Texas mixture.

Significant Results

The validation of the developed software was completed. Both the new proposed method for preparing DMA test specimens and the developed software to analyze the data were used and validated successfully.

Significant Problems, Issues and Potential Impact on Progress

None

Work Planned Next Quarter

This task is completed.

Reference

Castelo Branco, V.T.F., 2008. *A unified method for the analysis of nonlinear viscoelasticity and fatigue cracking of asphalt mixes using the dynamic mechanical analyzer*. Dissertation (PhD). Texas A&M University.

CATEGORY M2: COHESION

Work Element M2a: Work of Cohesion Based on Surface Energy

Subtask M2a-1: Methods to Determine Surface Free Energy of Saturated Asphalt Binders (TAMU)

Work Done This Quarter

No activity was planned for this quarter.

Work Planned Next Quarter

Work on this task is anticipated to start in year 4 of the project.

Subtask M2a-2: Work of Cohesion Measured at Nano-Scale using AFM (WRI)

Work Done This Quarter

During this quarter force versus distance curves collected at various approach/retract rates were analyzed to provide calibrated results in terms of force and distance for our experimental system. These data were combined with the results of experiments in which the probe was modulated sinusoidally while in contact with the sample. This work resulted in significant progress in our effort toward the development of a method for using the AFM to measure rheological properties at nano-scale, and, subsequently, to apply this tool in our effort to measure work of cohesion as a function of location within an asphalt film. A number of experiments were conducted using a 45- μm diameter polystyrene AFM probe tip and a commercial viscosity standard. For these experiments, both amplitude and phase angle data was collected with respect to the applied forces and the resulting response.

Significant Results

Phase angles were measured as very near to 0 degrees for bare glass (essentially purely elastic) and 90 degrees for a commercial viscosity standard (essentially purely Newtonian) at a nominal frequency of 10 radians per second. The measured phase angles are appropriate for the types of samples for which they were collected. Obtaining the correct phase angle information for these sample types is our first significant success in the attempt to develop useful nano-rheology tools. With the ability to measure the rheological phase angle demonstrated, at least in preliminary work, we looked toward the next part of this effort, that is, the determination of complex modulus (G^*) for a visco-elastic material. This part of the effort is complicated due to the need to establish the exact (Z-axis) location of the sample surface. Attractive forces between the probe tip and the sample and substrate surfaces become quite large as the distance between the probe and the surface becomes very small. Attractive forces cause the tip to snap-in to contact from some finite distance above the surface. This “snap-in” motion causes the tip to bury itself an unknown distance into the soft surface. Various models can be used to estimate how far the tip

will penetrate into the surface, but the validity of these models at nano-scale needs to be demonstrated more thoroughly.

An equation has been developed (WRI 2010) that relates complex modulus to parameters that are, in theory at least, measureable with an AFM and/or other instruments. These include probe tip radius, amplitude of incident and response forces, and cantilever spring constant as well as the distance between the substrate surface and the surface of the film and the measured phase angle. Using a test material with a known complex modulus and the nominal cantilever spring constant (as supplied by the manufacturer) we were able to rearrange our equation to solve for the distance between the substrate surface and the surface of the film (film thickness) which in turn would allow us to assign a precise location for the sample surface. This calculation gave a result approximately one order of magnitude larger than our estimated nominal thickness and somewhat greater than the maximum that could have been accommodated within our system. Our thought was that if this calculation gave a result that was several orders of magnitude different than the nominal value (calculated essentially as volume divided by area) it would indicate that the force picture was dominated by some uncontrolled variable and that a new approach or different equations would be needed to solve this problem. Considering the possibility of experimental error and the use of nominal values for the tip radius and cantilever spring constant, our result, off only by approximately one order of magnitude, has to be viewed as inconclusive.

Measurement of the full suite of rheological properties at nano-scale would be quite useful in the effort to illuminate nano-scale changes associated with cohesive failure of an asphalt binder. However, the ability to measure the rheological phase angle at nano/micro-scale also provides some very useful information with respect to cohesive properties at specific locations within the bulk. The rheological phase angle provides a measure of the ratio between solid and liquid characteristics (i.e. cohesive energy density) relative to a specific location within the sample. Based upon experiments conducted in an associated subtask (see Subtask M1b-2 this quarter), we believe that fracture tends to occur in an essentially planar zone within the interfacial region. Rheological phase angle measurements on the two sides of a fracture zone could help to determine if material on one side of the fracture is more solid-like in character. This type of information could lead to a much better understanding of fracture in an interracial zone some distance from the solid surface.

Significant Problems, Issues and Potential Impact on Progress

None.

Work Planned Next Quarter

We plan to further investigate the concept of AFM nano-rheology and to apply this technique, as well as other available AFM methodologies to the study of surfaces resulting after cohesive fracture. We also plan experiments to determine if we can measure a rheological phase angle using a sharp probe tip that is also suitable for surface imaging.

Cited Reference

Western Research Institute, 2010, Quarterly Technical Progress Report, FHWA Contract DTFH61-07-00005, Fundamental Properties of Asphalts and Modified Asphalts, III, March 2010, p 76.

Work Element M2b: Impact of Moisture Diffusion in Asphalt Mixtures

Subtask M2b-1: Measurements of Diffusion in Asphalt Binders and Mixtures (TAMU)

Subtask M2b-2: Kinetics of Debonding at the Binder-Aggregate Interface (TAMU)

Work Done This Quarter

No activity this quarter.

Significant Problems, Issues and Potential Impact on Progress

None.

Work Planned Next Quarter

Work will proceed as time allows.

Work Element M2c: Measuring Thin Film Cohesion and Adhesion Using the PATTI Test and the DSR (UWM)

Most work is completed. The remaining activity is reported under Work Element M1a.

CATEGORY M3: AGGREGATE SURFACE

Work Element M3a: Aggregate Surface Characterization (TAMU)

Work Done This Quarter

No significant work was done on this task during this quarter.

Significant Results

The results from earlier studies have been reported, and no additional results were generated during this quarter.

Work Planned Next Quarter

Work planned in the next quarter centers around continued development of a predictive model of surface energy.

CATEGORY M4: MODELING

Work Element M4a: Micromechanics Model (TAMU)

The reader is referred to Work Element F3b.

Work Element M4b: Analytical Fatigue Model for Mixture Design

This work is addressed under Work Elements F1b-1, F3c-1, and E1a.

Work Element M4c: Unified Continuum Model

Work Done This Quarter

In this quarter, the moisture damage model has been verified against a large set of experimental data from the literature. Moreover, the model has been modified to accurately capture the degradation in the mechanical properties due to moisture diffusion. Moreover, the developed moisture damage model along with the viscoelastic, viscoplastic, and mechanical damage models has been used to predict the damage evolution in micromechanical representative volume elements of the asphalt mixture microstructure. The model is found to be capable of predicting damage evolution at the micro and macro scales. Therefore, one can use the developed models for guiding the design of asphalt mixture as well as predict performance of asphalt pavements.

Significant Results

None

Significant Problems, Issues and Potential Impact on Progress

None

Work Planned Next Quarter

The focus of the coming quarter is on formulating the moisture-induced damage model based on the laws of thermodynamics in order to include the effects of porosity (air void) and the development of pore water pressures due to traffic movement. Moreover, a systematic procedure is under development for identifying the material parameters associated with the constitutive models based on well-designed experiments at TAMU. The experiments include moisture

conditioned pull-off tests on mastic-aggregate systems using the materials from the ARC 2x2 matrix validation plan. Furthermore, the experimental verification of the moisture damage component of the unified continuum damage model and the constitutive model itself will be initiated by conducting the mixture-level tests after subjecting the specimens to different levels of moisture conditioning.

CATEGORY M5: MOISTURE DAMAGE PREDICTION SYSTEM

This area is planned to start later in the project.

Moisture Damage Year 4		Year 4 (4/10-3/11)												Team
		4	5	6	7	8	9	10	11	12	1	2	3	
Adhesion														
M1a	Affinity of Asphalt to Aggregate - Mechanical Tests													
M1a-1	Select Materials													UWM
M1a-2	Conduct modified DSR tests													
M1a-3	Evaluate the moisture damage of asphalt mixtures	P					JP					P		
M1a-4	Correlate moisture damage between DSR and mix tests													
M1a-5	Propose a Novel Testing Protocol											JP	F	
M1a-6	Standard Testing Procedure and Recommendation for Specifications							P						
M1b	Work of Adhesion													
M1b-1	Adhesion using Micro calorimeter and SFE													TAMU
M1b-2	Evaluating adhesion at nano scale using AFM													WRI
M1b-3	Mechanisms of water-organic molecule competition													TAMU
M1c	Quantifying Moisture Damage Using DMA													
M1c-1	Evaluate load and deflection measurements using the modified PATTI test						JP				D		F	TAMU
Cohesion														
M2a	Work of Cohesion Based on Surface Energy													
M2a-1	Methods to determine SFE of saturated binders													TAMU
M2a-2	Evaluating cohesion at nano scale using AFM													WRI
M2b	Impact of Moisture Diffusion in Asphalt													
M2b-1	Diffusion of moisture through asphalt/mastic films				D			F						TAMU
M2b-2	Kinetics of debonding at binder-aggregate interface													
M2c	Thin Film Rheology and Cohesion													
M2c-1	Evaluate load and deflection measurements using the modified PATTI test													UWM
M2c-2	Evaluate effectiveness of the modified PATTI test for Detecting Modification													
M2c-3	Conduct Testing													
M2c-4	Analysis & Interpretation													
M2c-5	Standard Testing Procedure and Recommendation for Specifications							see Subtask M1a-6						
Aggregate Surface														
M3a	Impact of Surface Structure of Aggregate													
M3a-1	Aggregate surface characterization				JP					P				TAMU
Modeling														
M4a	Micromechanics model development									JP				TAMU
M4b	Analytical fatigue model for use during mixture design													TAMU
M4c	Unified continuum model									JP		DP	M&A	TAMU
M5	Moisture Damage Prediction System													ALL

LEGEND

Deliverable codes

- D: Draft Report
- F: Final Report
- M&A: Model and algorithm
- SW: Software
- JP: Journal paper
- P: Presentation
- DP: Decision Point
- [x]

- Work planned
- Work completed
- Parallel topic

Deliverable Description

- Report delivered to FHWA for 3 week review period.
- Final report delivered in compliance with FHWA publication standards
- Mathematical model and sample code
- Executable software, code and user manual
- Paper submitted to conference or journal
- Presentation for symposium, conference or other
- Time to make a decision on two parallel paths as to which is most promising to follow through
- Indicates completion of deliverable x

Moisture Damage Year 2 - 5		Year 2 (4/08-3/09)				Year 3 (4/09-3/10)				Year 4 (04/10-03/11)				Year 5 (04/11-03/12)				Team
		Q1	Q2	Q3	Q4	Q1	Q2	Q3	Q4	Q1	Q2	Q3	Q4	Q1	Q2	Q3	Q4	
Adhesion																		
M1a	Affinity of Asphalt to Aggregate - Mechanical Tests																	
M1a-1	Select Materials		DP														UWM	
M1a-2	Conduct modified DSR tests		P		P													
M1a-3	Evaluate the moisture damage of asphalt mixtures				DP		P			P	JP		P					
M1a-4	Correlate moisture damage between DSR and mix tests						P			P								
M1a-5	Propose a Novel Testing Protocol				P				P, D						JP, F			
M1a-6	Standard Testing Procedure and Recommendation for Specifications										P							
M1b	Work of Adhesion																	
M1b-1	Adhesion using Micro calorimeter and SFE						JP										TAMU	
M1b-2	Evaluating adhesion at nano scale using AFM							JP								JP, F	WRI	
M1b-3	Mechanisms of water-organic molecule competition				JP												TAMU	
M1c	Quantifying Moisture Damage Using DMA										JP	D	F				TAMU	
Cohesion																		
M2a	Work of Cohesion Based on Surface Energy																	
M2a-1	Methods to determine SFE of saturated binders													JP			TAMU	
M2a-2	Evaluating cohesion at nano scale using AFM							JP								JP, F	WRI	
M2b	Impact of Moisture Diffusion in Asphalt																	
M2b-1	Diffusion of moisture through asphalt/mastic films						JP	D	F	D	F						TAMU	
M2b-2	Kinetics of debonding at binder-aggregate interface																	
M2c	Thin Film Rheology and Cohesion																	
M2c-1	Evaluate load and deflection measurements using the modified PATTI test	DP	JP	D	F												UWM	
M2c-2	Evaluate effectiveness of the modified PATTI test for Detecting Modification			D	DP, F													
M2c-3	Conduct Testing						JP											
M2c-4	Analysis & Interpretation				P				D									
M2c-5	Standard Testing Procedure and Recommendation for Specifications					D											see Subtask M1a-6	
Aggregate Surface																		
M3a	Impact of Surface Structure of Aggregate																	
M3a-1	Aggregate surface characterization									JP		P					TAMU	
Models																		
M4a	Micromechanics model development				JP				JP		JP			D	DP	F, SW	TAMU	
M4b	Analytical fatigue model for use during mixture design															M&A, D	F	
M4c	Unified continuum model								JP		JP	DP	M&A	D	DP	F, SW	TAMU	
M5	Moisture Damage Prediction System																ALL	

LEGEND

Deliverable codes

- D: Draft Report
- F: Final Report
- M&A: Model and algorithm
- SW: Software
- JP: Journal paper
- P: Presentation
- DP: Decision Point

[x]

- Work planned
- Work completed
- Parallel topic

Deliverable Description

- Report delivered to FHWA for 3 week review period.
- Final report delivered in compliance with FHWA publication standards
- Mathematical model and sample code
- Executable software, code and user manual
- Paper submitted to conference or journal
- Presentation for symposium, conference or other
- Time to make a decision on two parallel paths as to which is most promising to follow through
- Indicates completion of deliverable x

PROGRAM AREA: FATIGUE

CATEGORY F1: MATERIAL AND MIXTURE PROPERTIES

Work Element F1a: Cohesive and Adhesive Properties

Work Done This Quarter

The experiments shown in table F1a.1 were completed in the past quarter. The results were analyzed to determine the relationships between fracture energy and changes in film thickness, loading rate, temperature, and moisture conditioning time. A final report documenting these relationships will be submitted as an appendix in the following quarter.

Table F1a.1. Testing matrix for asphalt-aggregate pull-off tests.

Testing Matrix																		
Replicate	Asphalt	Film Sweep - 45 Tests 0.01 mm/sec @ 23°C					Master Curve - 81 Tests									Moisture Conditioning - 27 Tests 0.01 mm/sec @ 23°C & 30µm		
		Film Thicknesses (µm)					Loading Rate - Temperature Combinations - 30µm									Conditioning Time		
		5	10	30	50	100	0.01 mm/sec			0.02 mm/sec			0.05 mm/sec			12 hrs	24 hrs	48 hrs
		10°C	23°C	36°C	10°C	23°C	36°C	10°C	23°C	36°C	10°C	23°C	36°C					
1	AAB																	
2																		
3																		
1	AAD																	
2																		
3																		
1	ABD																	
2																		
3																		

Significant Results

The relationships between fracture energy and changes in film thickness, loading rate, temperature, and moisture conditioning time were developed.

Significant Problem, Issues and Potential Impact on Progress

None

Work Planned Next Quarter

In addition to the monotonic loading until failure, we have also collected preliminary data on the viscoelastic creep and E^* of thin films subjected to direct tension-compression loading. Additional work to model the effect of multi-axial stress state (that is due to thin films in these test geometries) on the rheological properties of the asphalt binder will be continued as described in Subtask F1b.

Work Element F1b: Viscoelastic Properties (Year 1 start)

Subtask F1b-1: Viscoelastic Properties under Cyclic Loading

Work Done This Quarter

In the last quarter we obtained results to demonstrate that at intermediate to high stress or strain levels, the free volume of the binder increases. When subjected to shear stresses, restrictions on the increase in free volume resulted in the generation of stresses normal to the shear plane. It was also demonstrated that the nonlinear response of asphalt binders observed using measurements with the DSR is due to interaction between normal stresses and applied shear stresses. In this quarter we focused on incorporating this response into a constitutive equation.

The data from the DSR indicated that the G^* of the binder reduced with time upon cyclic loading at a given stress amplitude or reduced with the increment of the stress amplitude. A cursory examination of this data would suggest that the binder is undergoing some sort of a fatigue failure or exhibiting nonlinear viscoelastic response. However, upon examining the normal force it appears that the drop in G^* is correlated with an increase in the normal compressive stress. Therefore, this apparent fatigue or apparent nonlinearity can be explained at least in part due to the interaction between normal and shear stresses in the specimen. We have also conducted limited tests that indicate the presence of interaction nonlinearity in fine aggregate mortars.

The octahedral shear stress was computed and used to compute the shear modulus instead of the direct applied shear stress that does not account for the normal force. We are currently using Schapery's nonlinear viscoelastic model (with the four terms a_0 , g_0 , g_1 , and g_2) to represent the interaction nonlinearity observed using the DSR.

Significant Results

None

Significant Problems, Issues and Potential Impact on Progress

None

Work Planned Next Quarter

In the next quarter we plan to finalize the procedure to calibrate the model that accounts for interaction nonlinearity. The expectation is that the findings from this subtask will result in a more robust constitutive model for the time and stress state dependent response for asphalt materials that can significantly improve the accuracy of micromechanical models.

Subtask F1b-2: Separation of Nonlinear Viscoelastic Deformation from Fracture Energy under Repeated and Monotonic Loading (TAMU)

Work Done This Quarter

In this quarter, the proposed pilot test was finished using the test protocols that were developed in past quarters and were detailed in previous Quarterly Reports and in the technical report entitled “Aging Experiment Design Including Revised CMSE* Testing Protocols and Analysis to Characterize Mixture Fatigue Resistance” (Luo et al. 2009). The materials used to fabricate the asphalt mixture specimens and the test procedures were documented in the last Quarterly Report. The results of the pilot test are presented as follows.

First, the complex modulus of the undamaged asphalt mixtures was obtained as the reference state for the damaged material. The phase angle (ϕ_{LVE}) and the magnitude (E_{LVE}) of the complex modulus of the undamaged linear viscoelastic material are given in figures F1b-2.1 and F1b-2.2, respectively. The mixture with the binder AAM has a lower ϕ_{LVE} and higher E_{LVE} than that with the binder AAD, indicating that the mixture with AAM exhibits more elastic behavior and the mixture with AAD exhibits more viscous behavior. The increase of the air void content causes the increase of ϕ_{LVE} and the decrease of E_{LVE} . Aging results in significant decrease of ϕ_{LVE} and significant increase of E_{LVE} , which demonstrates the significant effect of aging on the complex modulus. As a result, three different aging periods are planned in the expanded experiment to better address the aging effect on asphalt mixtures.

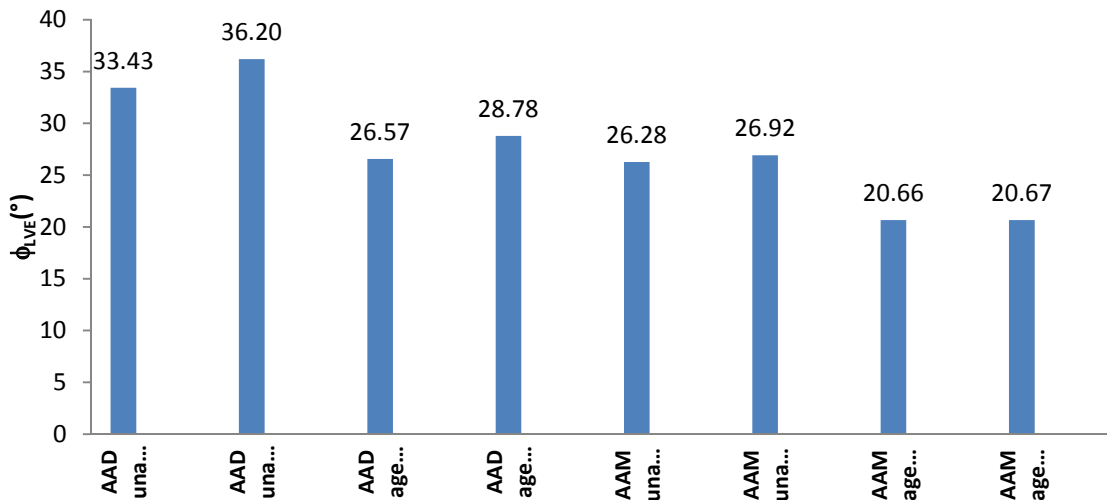


Figure F1b-2.1. The phase angle of complex modulus of undamaged asphalt mixtures.

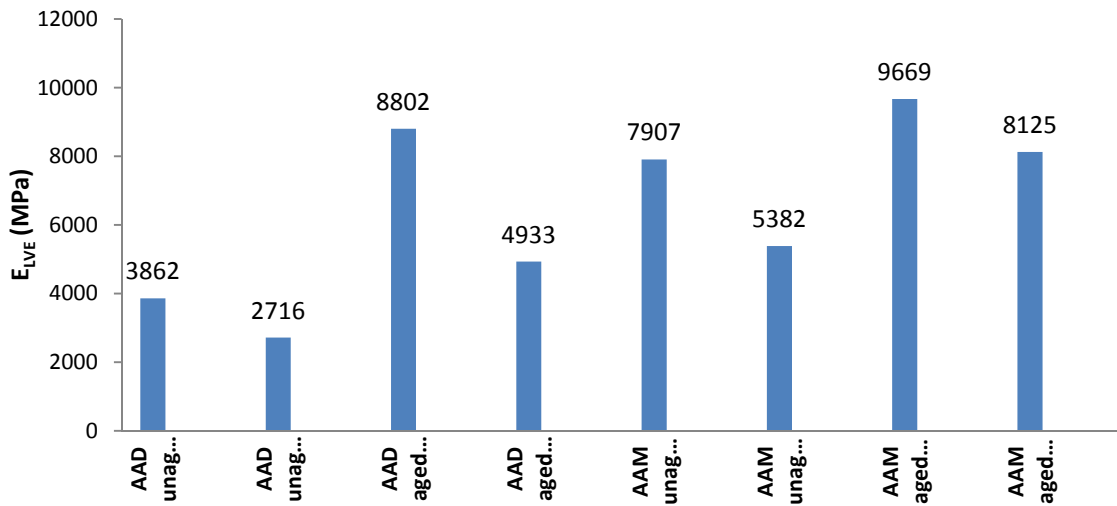


Figure F1b-2.2. The magnitude of complex modulus of undamaged asphalt mixtures.

The rate of fracture damage accumulation (b) of each asphalt mixture is shown in figure F1b-2.3, in which b is the slope of the plot of the dissipated pseudo strain energy (DPSE) for fracture, W_{R1} , versus the number of loading cycles. It was used as an indicator of the fracture resistance of asphalt mixtures in the calibrated mechanistic with surface energy (CMSE) approach (Walubita et al. 2005). A larger value of b indicates the faster of accumulation of fracture in the material. Figure F1b-2.3 suggests that both binder type and aging have a significant influence on the fatigue resistance. With respect to the fracture resistance indicated by the parameter b , the binder AAD is better than AAM. In addition, aging accelerates the speed of fracture damage accumulation because the material becomes more brittle when it is aged.

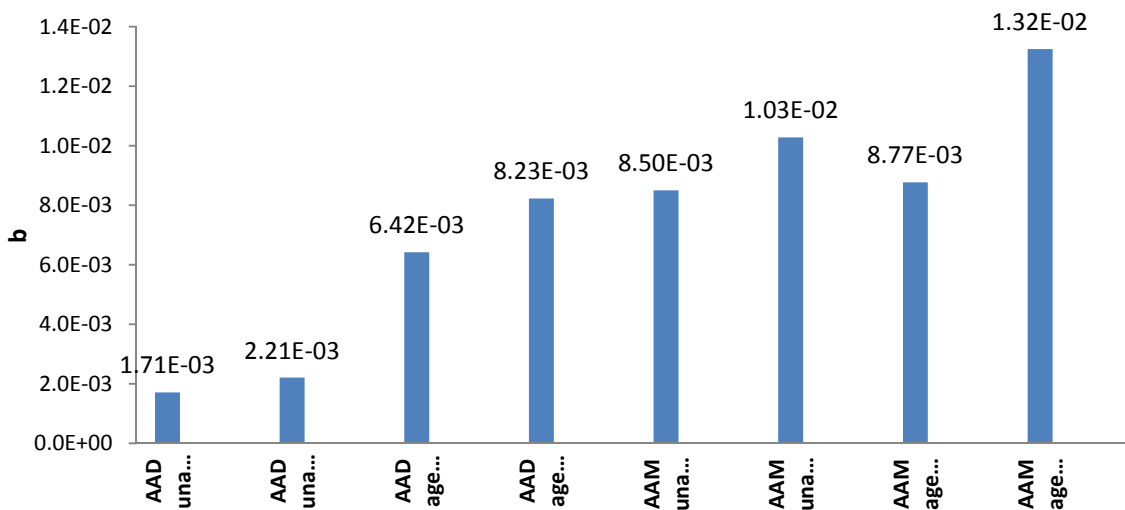


Figure F1b-2.3. The rate of fracture damage accumulation.

The damage density of each asphalt mixture at the end of the repeated direct tension (RDT) test is presented in figure F1b-2.4, which demonstrates the extent of fracture damage for 1000 loading cycles. The mixture with binder AAM has a higher damage density than that with AAD, and the aged mixture has a higher damage density than the corresponding undamaged mixture. These findings confirm what is observed for the parameter b in figure F1b-2.3.

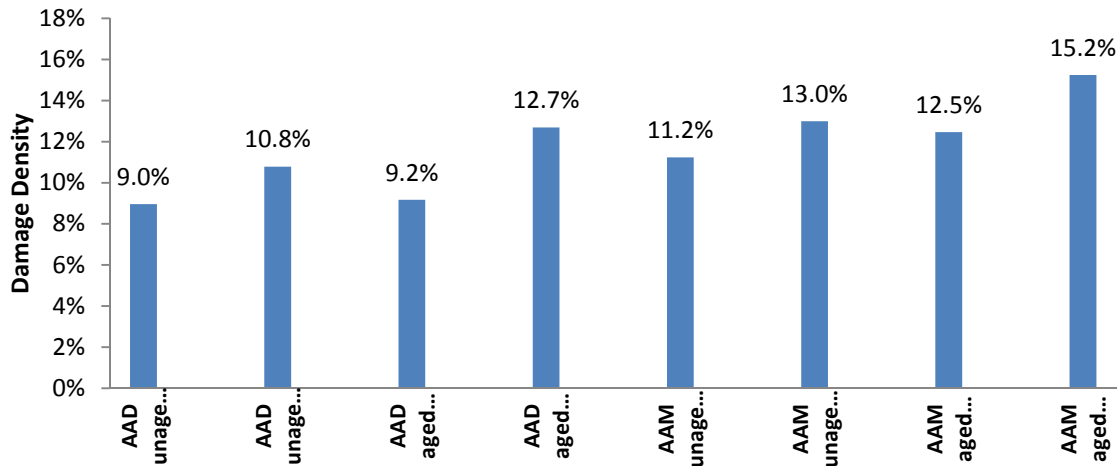


Figure F1b-2.4. The damage density at the end of the RDT test.

The initial mean air void radius (c_0) and the number of air voids (M_0) are presented in figures F1b-2.5 and F1b-2.6, respectively. Both c_0 and M_0 are determined from two methods respectively: 1) the energy balance approach that was developed in previous quarters, and 2) the X-ray Computed Tomography (X-ray CT). When comparing the values of c_0 and M_0 from the two methods, figure F1b-2.5 shows that the value of c_0 calculated from the energy balance approach is much smaller than that measured by the X-ray CT, and figure F1b-2.6 presents higher values of M_0 determined by the energy balance approach than that is measured by the X-ray CT. The reasons that cause this difference in c_0 and M_0 between the energy balance approach and the X-ray CT include limitation of the X-ray CT resolution and the threshold gray intensity chosen in the analysis of the X-ray CT data. In the X-ray CT analysis, two parameters are needed: image resolution and threshold gray intensity (Masad et al. 2002; Arambula et al. 2007). The image resolution is usually about 0.2 mm/pixel, indicating that the air voids which are smaller than 0.2 mm cannot be detected by the X-ray CT system. In the analysis of the X-ray CT images, the threshold gray intensity must be chosen to differentiate the air voids from the asphalt binder and the aggregates. The arbitrary selection of the threshold gray intensity causes errors in identifying the percentage of air voids and its average size. Therefore, compared to the X-ray CT, the energy balance approach provides a more accurate estimate of c_0 and M_0 .

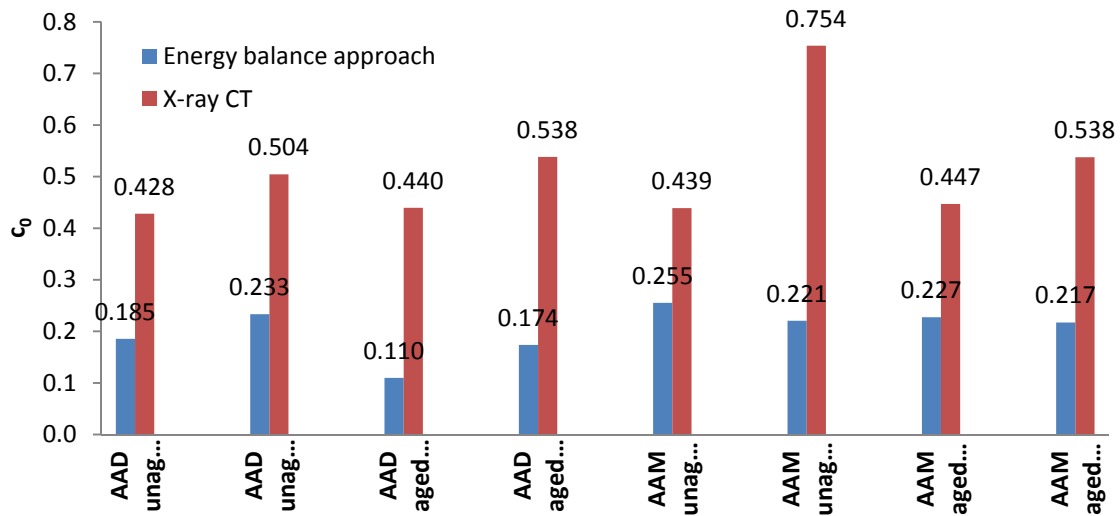


Figure F1b-2.5. The initial mean air void radius.

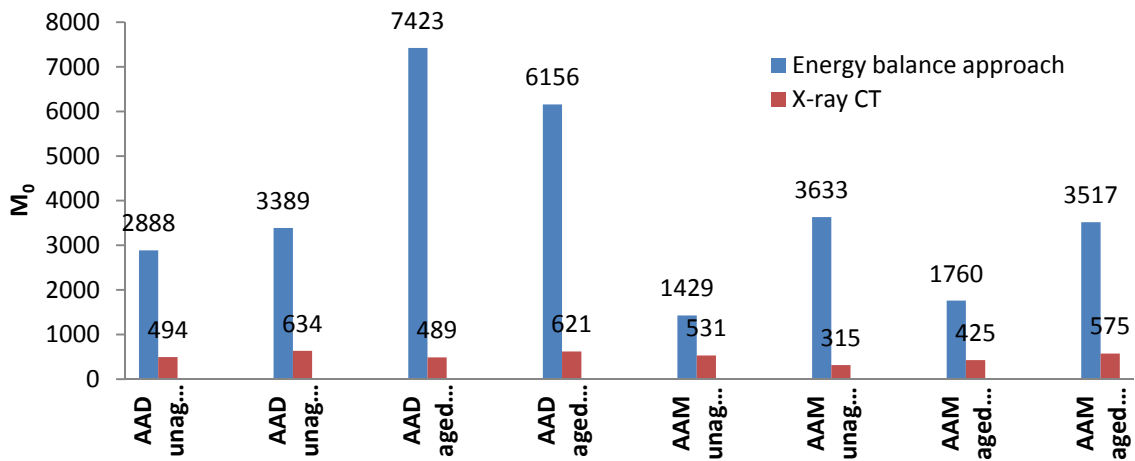


Figure F1b-2.6. The number of initial air voids.

Significant Results

The pilot test was finished this quarter to examine the application of the test protocols developed in previous quarterly reports. The results show that the test protocols are capable of obtaining reliable undamaged material properties of asphalt mixtures as the reference state for fatigue analysis. The rate of the fracture damage accumulation obtained from the accumulation of the DPSE indicates the fatigue resistance of the material. The damage density, including both the crack radius and the number of cracks, provides an integrated description of the extent of fracture damage. Compared to the X-ray CT, the energy balance approach provides more accurate estimate of the initial average air void radius and the number of initial air voids.

The pilot test examined the effects of the type of binder, air void content, and aging on the fatigue properties of asphalt mixtures. The test results show that AAD is better than AAM with respect to fracture resistance. Aging changes the material properties and accelerates the process of fracture. Compared to the air void content, aging demonstrates a more significant influence on the fatigue resistance.

Significant Problems, Issues and Potential Impact on Progress

The results of the pilot test showed relatively high variability between replicate specimens, which was caused by the variability of specimens. The coefficient of variation of the complex modulus was in the range of 1% to 20%. The quality of the specimen is critical to obtain accurate and reliable data. This issue will be addressed in the fabrication of specimens for the expanded experiment.

Work Planned Next Quarter

The current characterization of asphalt mixtures in a damaged state is based on the RDT test without rest periods between loading cycles. Therefore, the healing of the asphalt mixture is not investigated in the RDT test. In the next quarter, the current RDT test protocol will be modified to incorporate rest periods in the repeated loading cycles. As a result, the healing of the asphalt mixture will be taken into account using the energy balance approach.

References

Arambula, E., E. Masad, and A. Epps Martin, 2007, Influence of Air Void Distribution the Moisture Susceptibility of Asphalt Mixes. *Journal of Materials in Civil Engineering*, 19 (8), 655-664.

Luo, X., A. Epps Martin, R. Luo, R. L. Lytton, and C. J. Glover, 2009, *Aging Experiment Design Including Revised CMSE* Testing Protocols and Analysis to Characterize Mixture Fatigue Resistance*. Report No. FHWA-DTFH61-07H-0009, Texas Transportation Institute, College Station, Texas.

Masad, E., V. K. Jandhyala, N. Dasgupta, N. Somadevan, and N. Shashidhar, 2002, Characterization of Air Void Distribution in Asphalt Mixes Using X-ray Computed Tomography. *Journal of Materials in Civil Engineering*, 14 (2), 122-129.

Walubita, L. F., A. Epps Martin, S. H. Jung, C. J. Glover, A. Chowdhury, A. E. Park, and R. L. Lytton, 2005, "Comparison of Fatigue Analysis Approach for Two Hot Mix Asphalt Concrete (HMAC) Mixtures." Technical Research Report 0-4468-2. Texas Transportation Institute, College Station, Texas.

Work Element F1c: Aging

Subtask F1c-1: Critical Review of Binder Oxidative Aging and Its Impact on Mixtures (TAMU)

Work Done This Quarter

The correlation between D/T and the asphalt's low shear rate limiting viscosity (η_0^*), developed in TxDOT study 0-6009 and described in the previous report, were evaluated with an additional five binders in this quarter.

Significant Results

Figure F1c.1 shows a complete plot with data obtained from all eight binders in this study. The entire plot shows a good correlation between (D/T) and (η_0^*) . The correlation is:

$$\frac{D_{O_2}}{T} = 3.01 \times 10^{-11} (\eta_0^*)^{-0.54} \quad (\text{F1c-1.1})$$

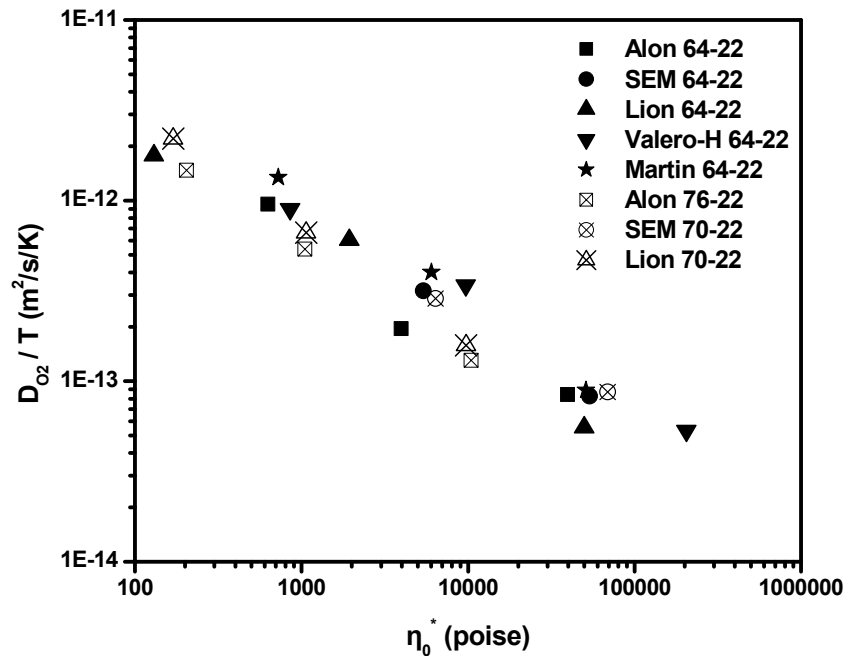


Figure F1c-1. Correlation of D/T with low shear rate limiting viscosity (η_0^*).

To summarize research findings: estimates of oxygen diffusivity in binders were successfully made based on laboratory oxidation measurements in binder films of known reaction kinetics and of sufficient thickness for diffusion to be a significant factor. Analysis of the data to obtain

diffusivities was performed using a flat film oxygen diffusion model in which diffusivity is a function of viscosity, which in turn varies with the level of oxidation.

For neat asphalts, oxygen diffusivities (D) ranged from 10^{-10} to 10^{-11} m²/s, varying with temperature (T) and asphalt low shear rate limiting viscosity (η_o^*); $\log(D/T)$ varied linearly with $\log(\eta_o^*)$ for both base asphalts and polymer modified binders. For asphalt mastics, oxygen diffusivity was observed to decrease as filler volume fraction increased. Quantitatively, this effect follows estimates based on common transport theories of the effect of a dilute suspension of spherical inclusions on diffusivity.

Significant Problems, Issues and Potential Impact on Progress

There are no problems or issues.

Work Planned Next Quarter

Review of the literature and work on other research projects is ongoing.

Subtask F1c-2: Develop Experimental Design (TAMU)

Work Done This Quarter

No work this quarter.

Significant Results

None

Significant Problems, Issues and Potential Impact on Progress

Conducting the planned experiments using ARC core binders is awaiting the arrival of ARC binders. Measurements on mixtures fabricated using other binders are underway.

Work Planned Next Quarter

Measurements of mixture rheology and fatigue continue. Also, rheological measurements of binders extracted and recovered from these mixtures will be made as part of the effort to link binder oxidation to changes in mixture properties.

Subtask F1c-3: Develop a Transport Model of Binder Oxidation in Pavements (TAMU)

Work Done This Quarter

Measurements of Recovered Binder Properties

As planned in previous report, field cores from pavement sites in different climate zones will be collected to provide 1) data on binder oxidation as a function of time and depth in pavements for the purpose of evaluating and improving the pavement transport oxidation model, and 2) data on changes to mixture rheology and fatigue resistance that occur in response to binder oxidation. In this quarter, post-construction field cores from the Arizona test section have been tested.

The Arizona site is on US 93 about 50 miles north of Wickenburg at about milepost 153. The project consisted of new four-lane construction of two 2½-inch lifts of unmodified PG 76-16, one project asphalt and the three comparative asphalts, followed by a ¾-inch lift of a rubber-modified asphalt friction course. Cores were taken from those two 2½-inch lifts with replicates for all four different asphalts (AZ 1-1 to AZ 1-4) by WRI shortly after pavement construction.

Those cores were measured with CoreLok and X-ray CT for total air voids and interconnected air voids determinations, then sliced to 0.5 inch thicknesses to measure the air void properties of each slice. After that, the binder in each slice was extracted, recovered, and analyzed for oxidation (FTIR) and rheological properties (DSR) to provide data on binder oxidative aging and hardening as a function of depth in pavement. These data provide a baseline starting point for these Arizona sections.

Figure F1c-3.1 shows the carbonyl content for the recovered binders as a function of depth in field cores AZ 1-1. Letter T in y axis refers to the top lift, and B refers to the bottom lift. Clearly, there is no significant difference in carbonyl content at the different pavement depths; because these cores were taken post-construction; there was not enough time for binders to oxidize in service and to develop an oxidation gradient with depth.

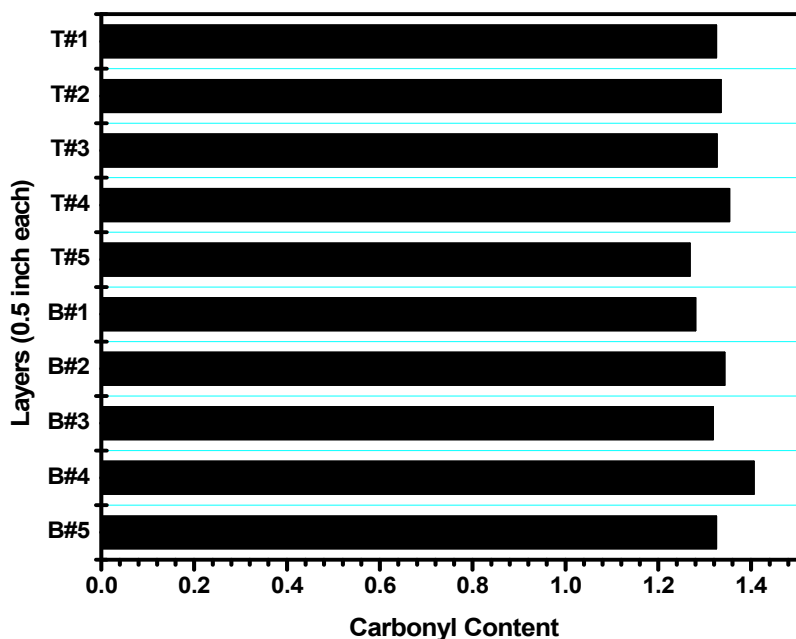


Figure F1c-3.1. Carbonyl content of recovered binder of AZ1-1 at different depths.

Measurements of Binder Density as a Function of Oxidation

Background. Asphalt density is the result of both the asphalt's chemical composition and its colloidal state. Oxidative aging changes both of these factors, thereby producing density changes. Furthermore, the density of asphalt materials decreases with temperature. In pavements, the temperature will vary from day to night, roughly following a sinusoidal fluctuation. As a result, the densities of both asphalt and aggregate will change, but to different degrees. Such changes will introduce contraction and expansion forces on the asphalt-aggregate mixture, which is fundamentally important for thermal stress analysis.

In summary, asphalt density, as an important physical property that varies with the degree of oxidation (as indicated by FTIR carbonyl measurements) and temperature, will be a valuable companion to existing rheological data.

Objectives. The objective of this work is to measure the densities of several asphalt materials as a function of the extent of oxidative aging. Ultimately, the experiments will be expanded to measure density versus temperature.

Experimental Methodology. Binders were aged in POVs at five different temperatures and atmospheric pressure and sampled at different aging times for analysis. Carbonyl area (CA) was measured using FTIR to obtain the area under the spectrum from 1650 to 1820 cm^{-1} . To measure density, binders at different aging levels were prepared in small drops (of approximately 5 mm diameter) and floated in a density gradient column (DGC). Three replicates were measured. The density gradient of the fluid in the DGC is built by filling the column with two completely

miscible liquids of distinct densities that define the range of fluid density in the column. Mixing and filling is performed so as to achieve a stable linear density gradient by varying the composition of the mixture from bottom to top. Calibration beads were used to indicate the mixture density at 10 points in the column. For asphalt materials, deionized water was used as the low-density fluid, and saline water was used as the high-density fluid.

Preliminary Data. Table F1c-3.1 shows preliminary data for three binders aged at one elevated temperature over several days. Densities were measured at room temperature.

Table F1c-3.1. Preliminary binder density values at various levels of oxidation.

Binder	Aging T (F)	Aging Days	Carbonyl Area	Density (g/cc)
ALON PG64-22	208	0	0.587	1.034
		6	1.236	1.041
		13	1.734	1.045
SEM PG64-22	208	0	0.548	1.037
		6	1.232	1.042
		15	1.631	1.049
MARTIN PG64-22	192	0	0.585	1.026
		6	0.907	1.039
		16	1.423	1.045

Figure F1c-3.2 shows density as a function of carbonyl area. All data show a trend of increasing density with increases in oxidative aging, although the linear correlation for Martin PG 64-22 is not as well defined as for the other two binder types. Again, these are only preliminary data but nevertheless indicate the level of density change that result from oxidation.

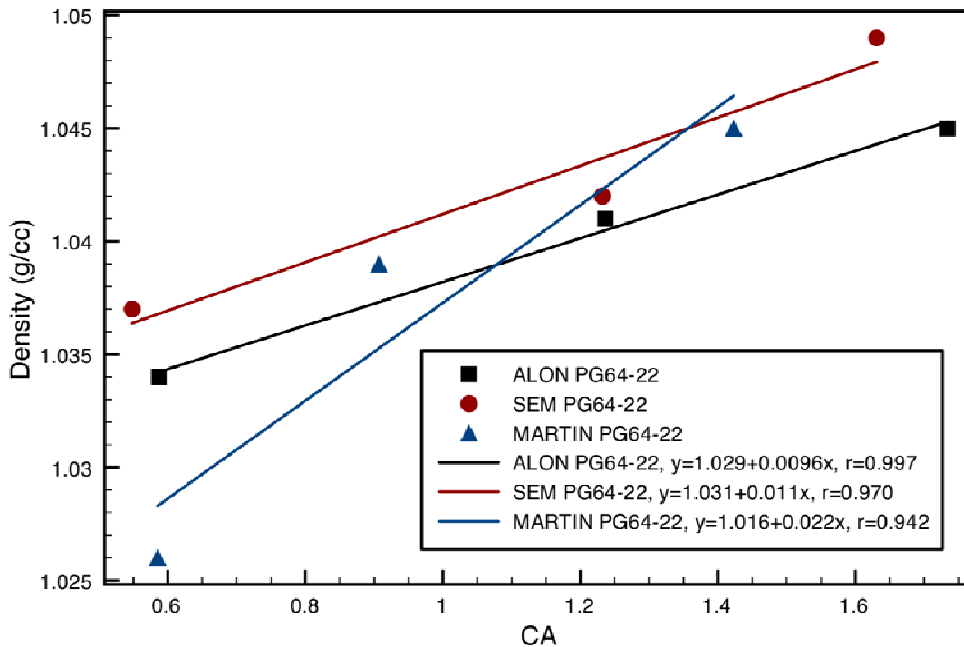


Figure F1c-3.2. Density increases with binder oxidation for three asphalts.

Significant Results

The paper submitted to the Journal of Materials in Civil Engineering to document the improved pavement temperature model is under final review.

Significant Problems, Issues and Potential Impact on Progress

The effort to obtain cores from pavement sites in different climate zones continues. Discussion with researchers at WRI have been held to evaluate which of their test sites might be best used for providing information on binder and mixture changes in pavements as a function of service time. Cores from such sites will provide 1) data on binder oxidation as a function of time and depth in pavements and 2) data on changes to mixture rheology and fatigue resistance that occur in response to binder oxidation.

Work Planned Next Quarter

Field cores from other sites and Arizona site as available from WRI will be tested to provide data on binder oxidation as a function of time and depth in pavements in different climate zones.

Density Measurements on asphalt binders continue, with a focus on improving measurement precision and accuracy.

Subtask F1c-4: The Effects of Binder Aging on Mixture Viscoelastic, Fracture, and Permanent Deformation Properties (TAMU)

Work Done This Quarter

The reader is referred to Work Elements F1b-2 and F2c.

Work Planned Next Quarter

The reader is referred to Work Elements F1b-2 and F2c.

Subtask F1c-5: Polymer Modified Asphalt Materials (TAMU)

Work Done This Quarter

In this quarter, FTIR spectra for a number of commercial asphalts from different manufacturers were obtained and their SBS polymer contents (total polymer content and content of each SBS components) were determined using established calibration curves of FTIR absorption of PS at 699 cm^{-1} , trans-PB at 966 cm^{-1} , and vinyl at 911 cm^{-1} and with known PS/PB ratio.

Significant Results

The total SBS content of these commercial binders has been specified in the product data sheet, while the content of each polymer component is unknown. Table F1c-5.1 summarizes the weight percentage of each polymer component measured with FTIR for base asphalts (PG 64-22) and their corresponding polymer modified binders (PG 70-22 and PG 76-22). The calculated total SBS content, in general, is about one percentage point higher than what is specified (2-3% for PG 70-22 binders and 3 to 5% for PG 76-22) for most of the studied PMAs. Tentatively, we suspect this overestimation of total polymer content is caused by the accuracy of PB calibration curve, which was not perfectly established due to the sample preparation technique (PB is very difficult to mix with asphalt) and the spectrum analysis method (selecting a proper baseline for peak height measurement is problematic). Because there is no value available for the weight content of each polymer component, it is difficult to evaluate the calculated values.

Table F1c-5.1. Polymer content measured with FTIR spectra.

Asphalt	Grade	PB-trans (wt%, m ^a)	PB-vinyl (wt%, m)	PS (wt%, m)	PB-cis (wt%, c ^b)
Alon	64-22	0.000	0.000	0.000	0.000
	70-22	2.200	0.469	2.646	2.278
	76-22	2.247	0.578	3.334	2.640
SEM	64-22	0.000	0.000	0.000	0.000
	70-22	0.361	0.859	0.302	0.653
	76-22	0.739	1.391	1.388	1.507
Valero-H	64-22	0.000	0.000	0.000	0.000
	70-22	1.084	0.125	1.548	1.182
	76-22	1.917	0.250	2.369	1.944
Valero-C	64-22	0.000	0.000	0.000	0.000
	70-22	1.100	0.297	1.583	1.277
	76-22	1.807	0.438	2.336	1.963
Lion	64-22	0.000	0.000	0.000	0.000
	70-22	1.367	0.516	1.008	1.239
	76-22	2.341	1.000	1.440	2.049

^am, measured content based on FTIR peak height

^bc, calculated content based on PS/PB ratio and measured content of other components

Significant Problems, Issues and Potential Impact on Progress

None

Work Planned Next Quarter

In next quarter, PB calibration curves will be revisited with better mixing methods and proper selection of PB peak baseline.

Work Element F1d: Healing

Subtask F1d-1: Critical review of the literature

Subtask F1d-2: Material selection

Subtask F1d-3: Experiment design

Subtask F1d-4: Test methods to measure properties related to healing

Work Done This Quarter

Influence of temperature and aging on the intrinsic healing properties of asphalt binders

In the previous quarter, a test procedure to determine intrinsic healing of asphalt binders using the DSR was refined to improve repeatability and reduce artifacts that may appear as healing, especially at lower temperatures. This test procedure was used in this quarter to measure the intrinsic healing rates of asphalt binders at different temperatures and aging conditions. The modified form of the Avrami equation, shown below, was used to model the intrinsic healing of asphalt binders:

$$R_h(t) = R_0 + p(1 - e^{-qt^r})$$

The above equation represents the sum effect of: i) instantaneous strength gain due to interfacial cohesion at the crack interface, represented by the parameter R_0 which is also equal to $1-p$, and ii) time dependent strength gain due to inter diffusion of molecules between the crack surfaces, represented by $1 - e^{-qt^r}$. Figures F1d.1 and F1d.2 illustrate the typical change in intrinsic healing with temperature and aging. There is a small increase in the initial healing with an increase in temperature and a small decrease due to long-term aging. The time dependent component of self-healing is represented by the parameter q . As expected this parameter increases with an increase in temperature and decreases due to aging. Figures F1d.3 and F1d.4 illustrate the increase in this parameter for three different asphalt binders with an increase in temperature and a significant decrease in this parameter due to long-term aging.

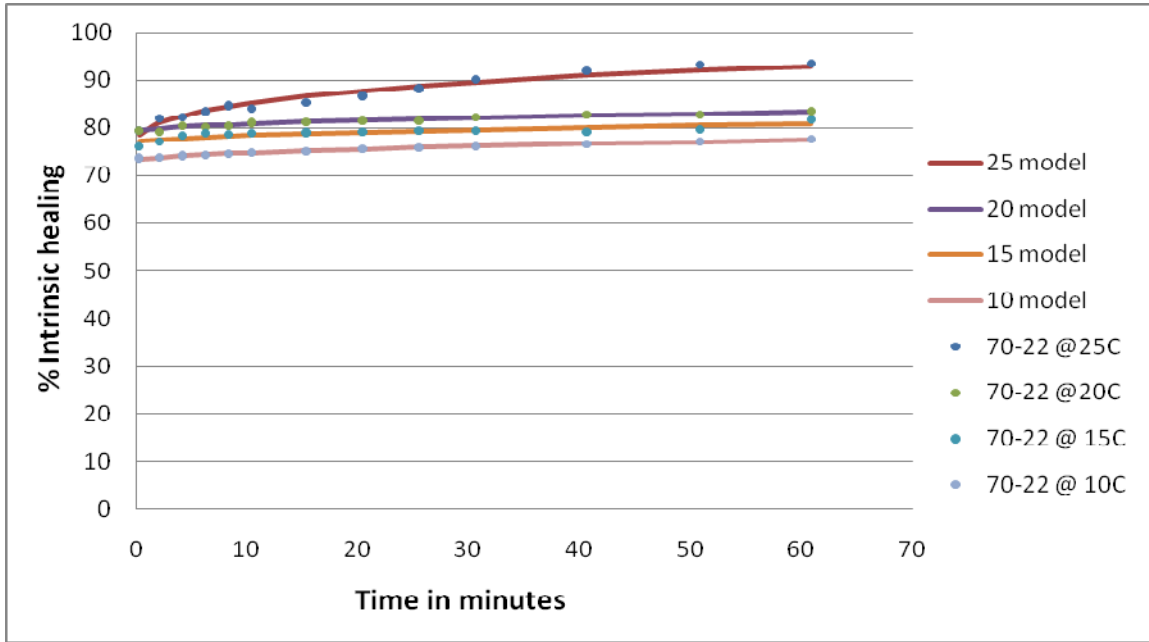


Figure F1d.1. Intrinsic healing of PG 70-22 after short term aging for 10 through 25C.

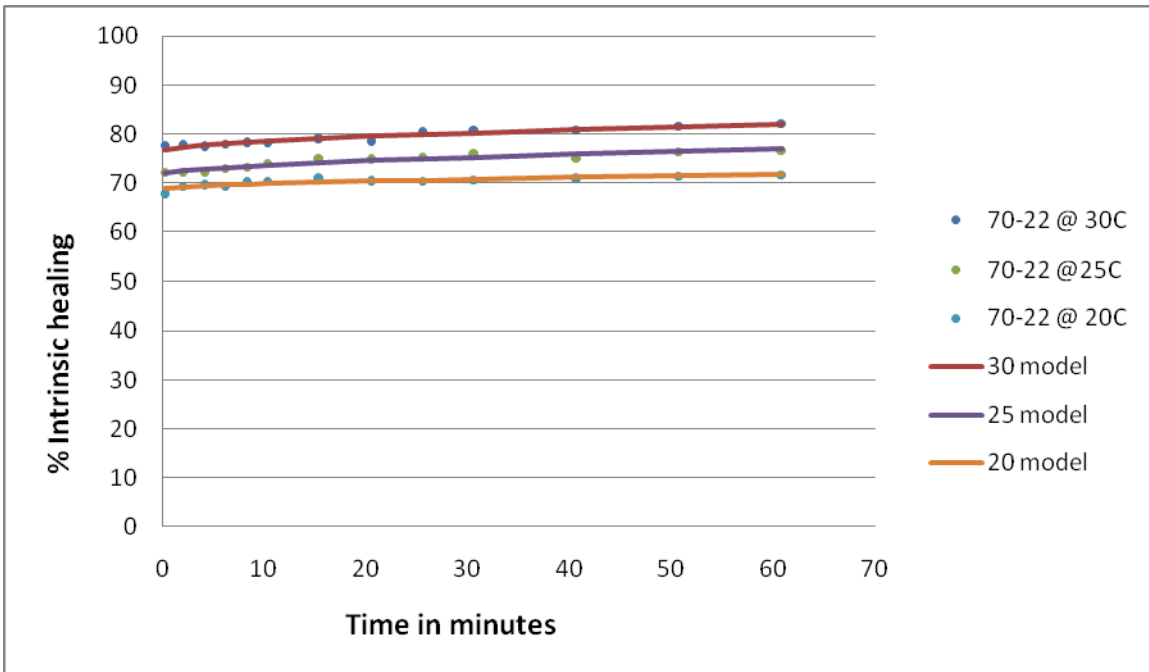


Figure F1d.2. Intrinsic healing of PG 70-22 after long term aging for 20 through 30C. (NOTE: range of temperature is different compared to above figure)

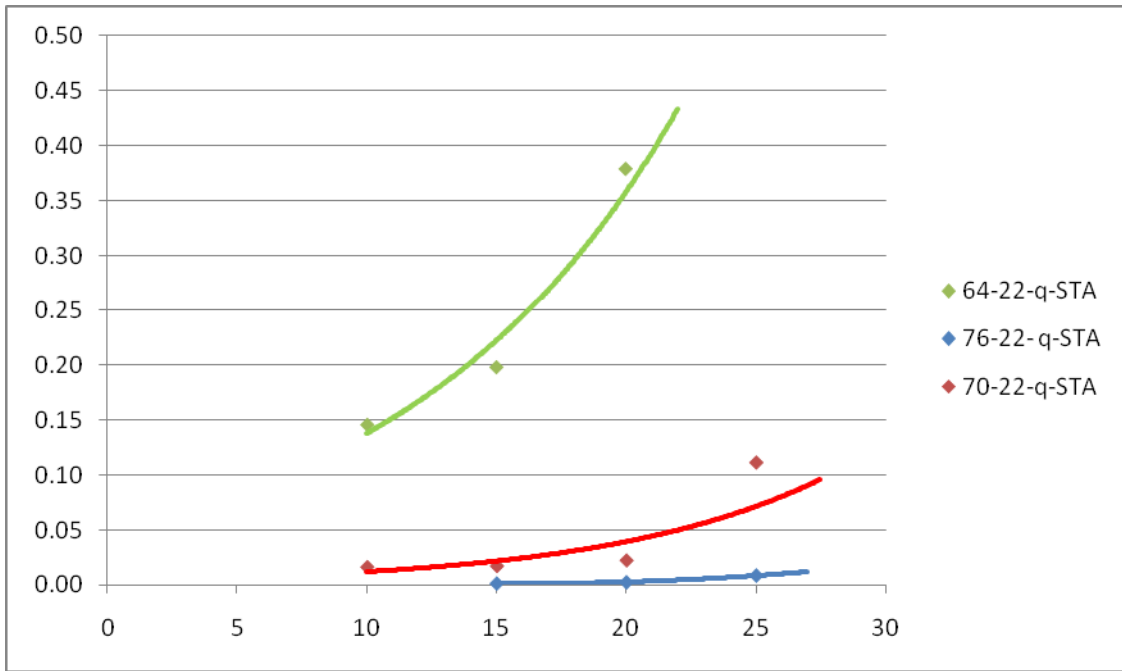


Figure F1d.3. q for three short term aged binders as a function of temperature.

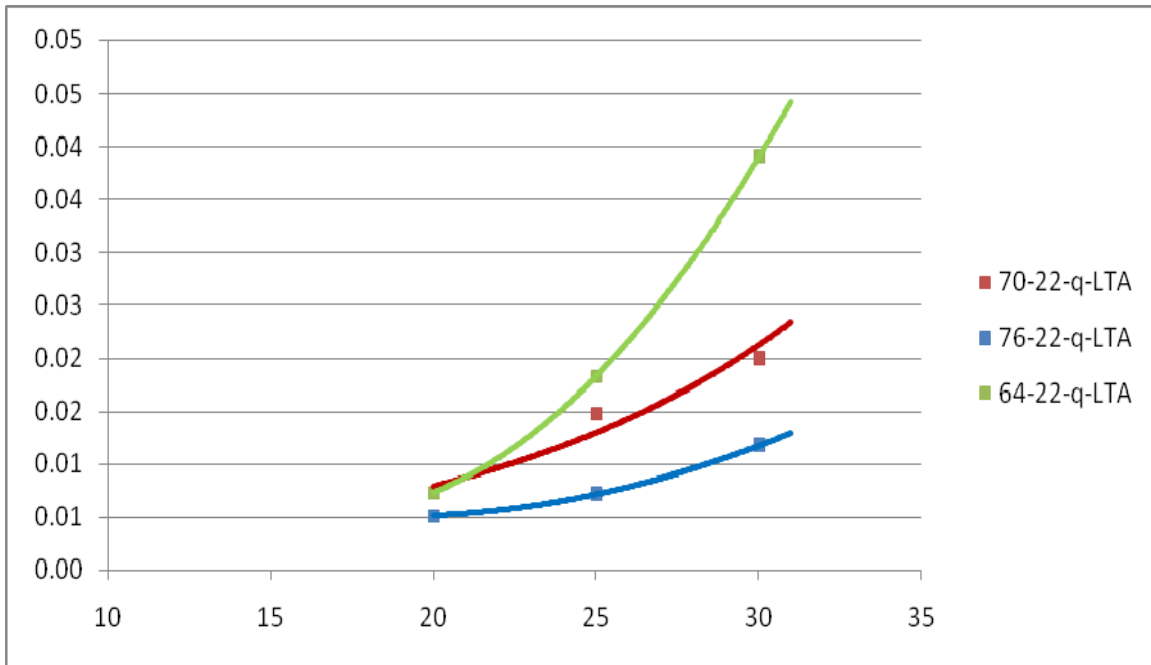


Figure F1d.4. q for three long term aged binders as a function of temperature.

Overall healing (rate of wetting x rate of intrinsic healing) in fine aggregate matrix

While the test procedure described above measures the rate of intrinsic healing of asphalt binder, the overall rate of healing is defined by the convolution of the rate of crack wetting and the rate of intrinsic healing. In this quarter we conducted preliminary experiments to measure the overall rate of healing in fine aggregate matrix (FAM) specimens. The overall objective of this test is to measure the overall rate of wetting for different material combinations and validate the relationship to the fundamental material properties described in the models presented in the previous quarterly reports. The following is a brief discussion of some of the results from preliminary testing of the FAM specimens.

Preliminary tests were performed on FAM specimens to measure the rate of overall healing in a specimen using DMA. The linear viscoelastic properties of the test specimen were measured prior to initiating a cyclic load fatigue test. The specimen was subjected to fatigue cracking by applying sinusoidal loading with a high constant stress amplitude at a frequency of 5 Hz. The test was stopped when the dynamic shear modulus, G^* , of the specimen dropped to 50% of the linear viscoelastic shear modulus. During this rest period, the linear viscoelastic modulus of the material was measured at specified time intervals by applying sinusoidal loading with a low constant stress amplitude at a frequency of 5 Hz in order not to disturb the sample during the rest period. By recording the change in G^* over time, the entire trajectory of the gain in stiffness was recorded. Following the rest period, the specimen was once again subjected to sinusoidal loading until it once again reached 50% of the initial shear modulus. Figures F1d.5 through F1d.6 summarize the results.

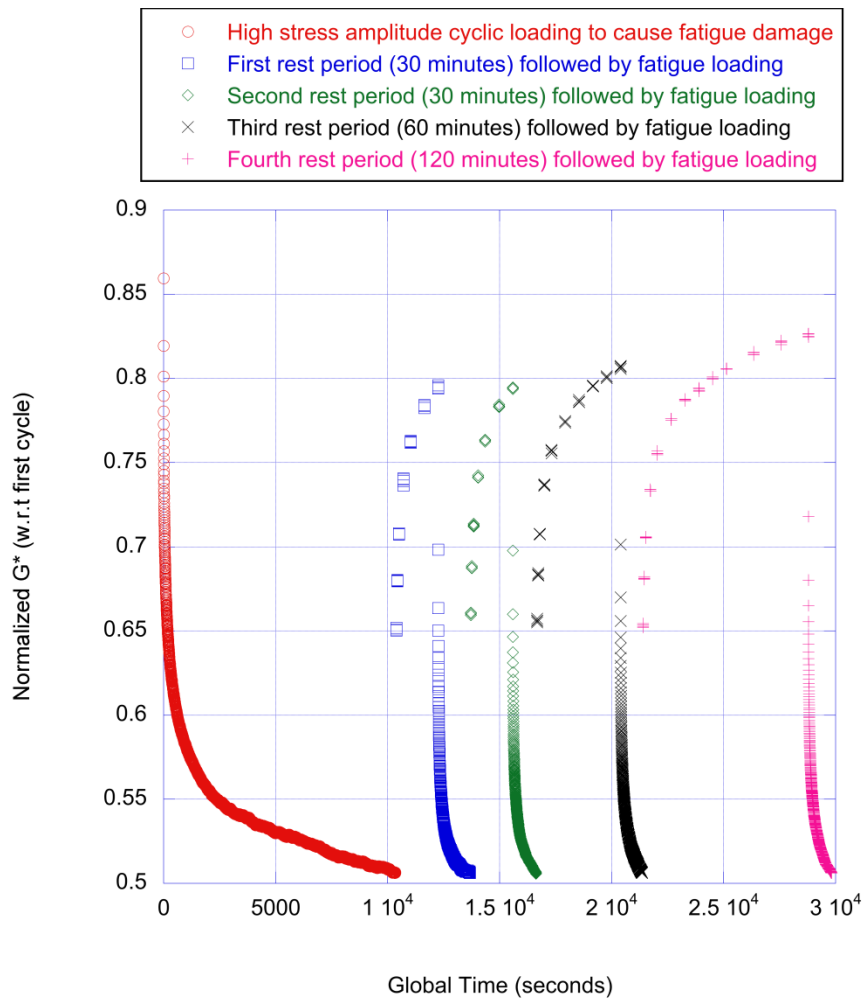


Figure F1d.5. Stiffness of FAM specimen on being subjected to a sequence of cyclic loading to cause fatigue damage and rest period.

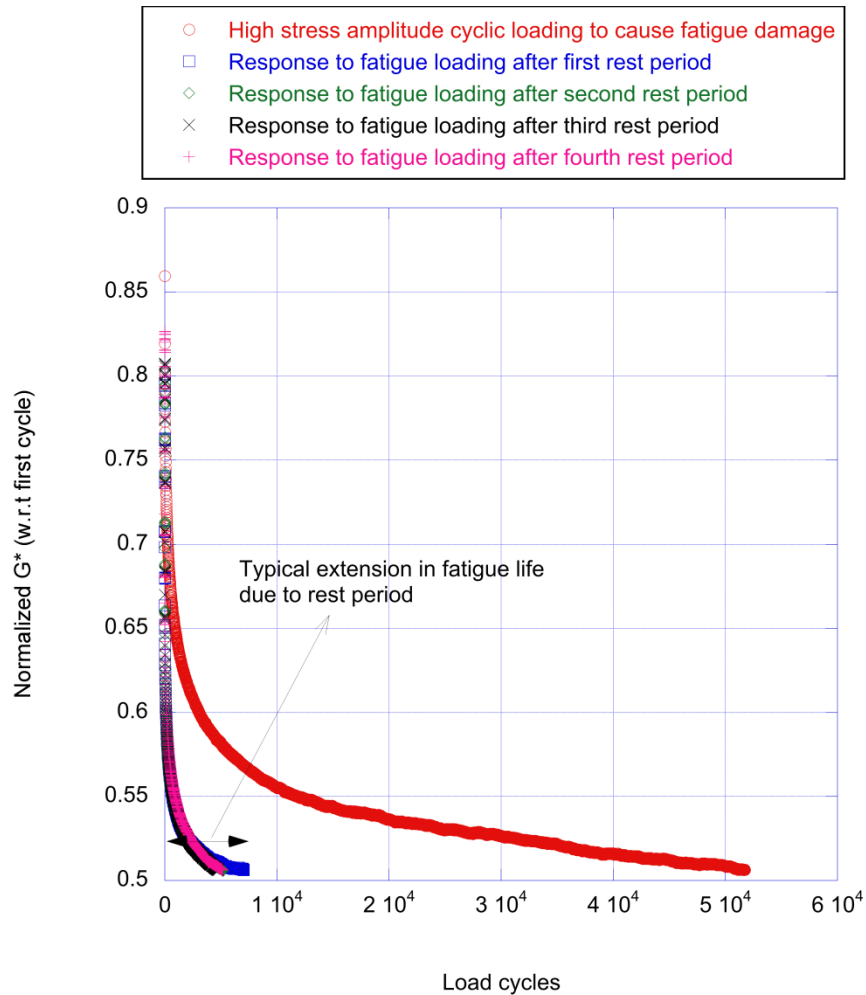


Figure F1d.6. Response to cyclic loading to induce fatigue for the original specimen and after rest periods.

Although this data is preliminary, a few observations can be made from figures F1d.2 and F1d.3:

- The extended rest period after subjecting the specimen to significant fatigue damage does in fact help extend the fatigue cracking life of the FAM (figure F1d.2). Also, the fatigue damage after each rest period was very consistent, although there was a slight increase in rate of damage after each subsequent rest period.
- The rate of stiffness gain during the four rest periods was very consistent with a very slight decrease in the rate of stiffness gain with every subsequent rest period (figure F1d.3).
- Each rest period (of 30 minutes to 2 hours) was introduced after the specimen reached 50% of its linear viscoelastic G^* . At the end of the rest periods, the stiffness of the FAM specimen increased from 50% to approximately 80%. However, when subjected to fatigue loading after the rest period the subsequent rate of reduction of G^* with increasing number of load cycles was not the same as the original specimen. For

example, it took approximately 50 million cycles for the complex modulus of the original specimen to drop from 80% to 50% of its original value. Whereas, after the first rest period it took only about 8 million cycles for the complex modulus of the specimen to drop from 80% to 50%. However, following the first rest period, the rate of fatigue failure was consistent and only decreased slightly after each subsequent rest period for the same window of 80% to 50%. Similar trends were observed with the phase angle. Based on this preliminary data, it appears that G^* and phase angle alone may not reflect the integrity or level of damage within the specimen. A possible explanation for this is that the typical 80% recovery in stiffness at the end of the rest period was measured using low stress amplitude and therefore due to material nonlinearity the material may not have the same internal state when 80% stiffness is recorded using high stress amplitude. Simply stated 80% G^* on the first (red curve) measured using high stress amplitude may not reflect the same material state as 80% G^* at the end of rest periods measured using low stress amplitude due to material non linearity. The partial recovery of the fatigue life during the rest period can be largely attributed to the fact that the rest period was introduced much later during the test, i.e. after 50% reduction in modulus. The two aforementioned aspects will be examined further by accounting for nonlinearity and introducing longer rest periods early on during the test.

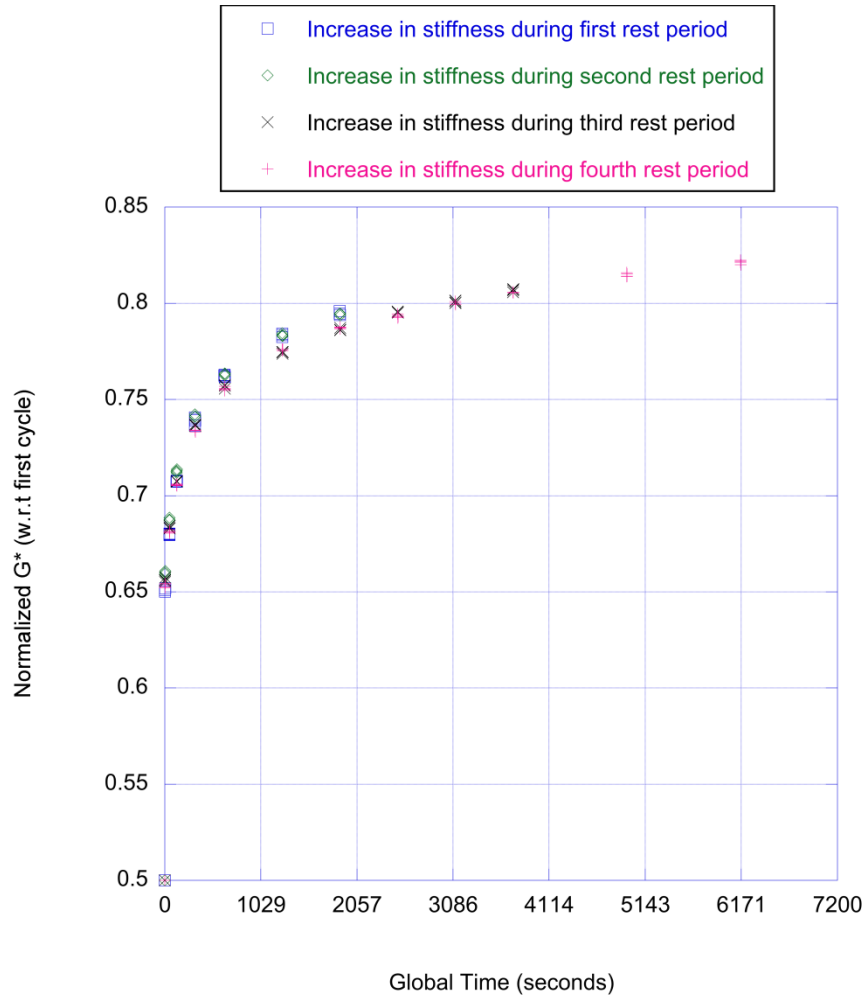


Figure F1d.7. Rate of stiffness gain during rest periods (each rest period was started when the specimen reached 50% of its linear viscoelastic complex modulus).

Significant Problems, Issues and Potential Impact on Progress

None

Work Planned Next Quarter

We plan to start using the core materials to measure intrinsic healing as well as prepare FAM specimens to measure overall healing. We also plan to finalize and start the test plan on the characterization of wetting using the DMA with mortar samples.

Subtask F1d-6: Evaluate Relationship Between Healing and Endurance Limit of Asphalt Binders (UWM)

Work Done This Quarter

The Dynamic Shear Rheometer (DSR) used for healing tests was unavailable for much of the past quarter due to maintenance. Thus, the majority of research team's effort during the past quarter was focused on modeling cyclic loading with and without rest to determine the significance of stress relaxation on the benefit observed from the addition of rest periods in time sweep testing. The modeling of cyclic loading with and without rest periods using a generalized Maxwell model (i.e., Prony series) has been conducted to simulate the linear viscoelastic response of asphalt binders under time sweep testing with and without rest periods. The coefficients of the Prony series used in the time sweep simulations were obtained by fitting frequency sweep data. Both the change in complex modulus and the change in dissipated energy with the inclusion of rest periods in the model-predicted responses were investigated using three loading patterns. Results of the three loading patterns gave similar responses. For brevity, only the results of sinusoidal loading modeling will be discussed, as this is the type of loading actually used in DSR testing.

The complex modulus predicted by the generalized Maxwell model was found to decrease over the first few cycles of loading and then reach a constant, steady-state value when no rests were included. Upon inclusion of rest periods, the modulus was found to increase following the rest period. If loading continued for a long period of time, the modulus would decrease to the steady-state value as in the no-rest case. The effect of different rest period duration on the magnitude of the modulus is presented in figure F1d-6.1. Note that the results are for a typical asphalt binder loaded at a frequency of 10 Hz.

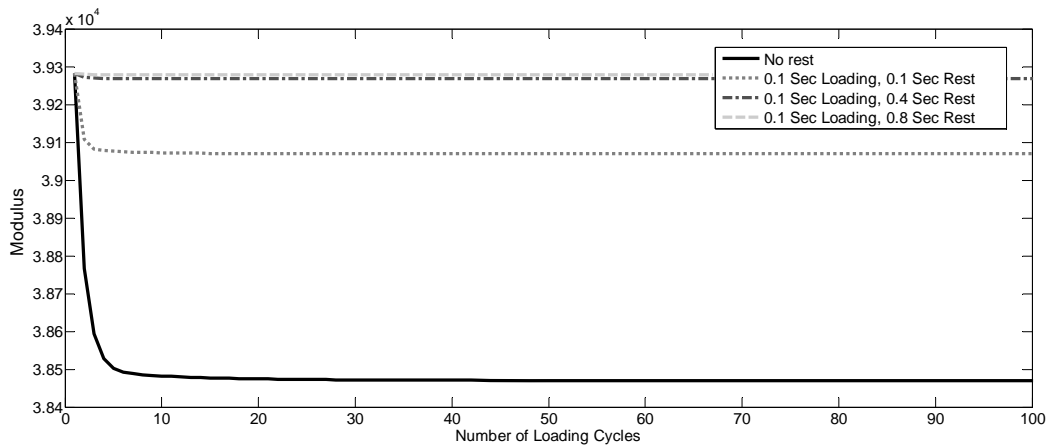


Figure F1d-6.1. Graph. Effect of rest periods on complex modulus.

It appears that the effect of the rest period on complex modulus diminishes with increasing rest period duration. That is, inclusion of a long rest period has little benefit over a short rest period.

Based on the modeling of four binders, it was found that the modulus was typically increased by 1% to 3% with inclusion of rest periods under sinusoidal loading.

The effect of rest periods on dissipated energy was also investigated this quarter. The dissipated energy was calculated as the area of the hysteresis for each loading cycle using numerical integration. Much like the complex modulus, an increase in dissipated energy was observed over the first several cycles of loading and then a constant, steady-state value was reached for the no-rest case. For the rest case, an analogous phenomenon was observed. Following each rest period, the dissipated energy was observed to increase over the first few loading cycles and then reach a steady-state value. This steady-state value was higher than the no-rest case, indicating a benefit from rest periods that is purely due to linear viscoelastic response. Increasing rest period duration proved to be insignificant in the steady-state dissipated energy, which is in agreement with the effect of rest on complex modulus.

Predictions of dissipated energy as a function of the number of loading cycles for a typical asphalt binder are shown in figure F1d-6.2. For this simulation, a frequency of 10 Hz was used; for the rest case, a 1-second loading period followed by a 5-second rest period was utilized. The rest period led to an increase in steady-state dissipated energy of approximately 1%. For the same binder, rest periods of 1 second and 10 seconds were also simulated and the same 1% increase in steady-state dissipated energy from the no-rest case was observed.

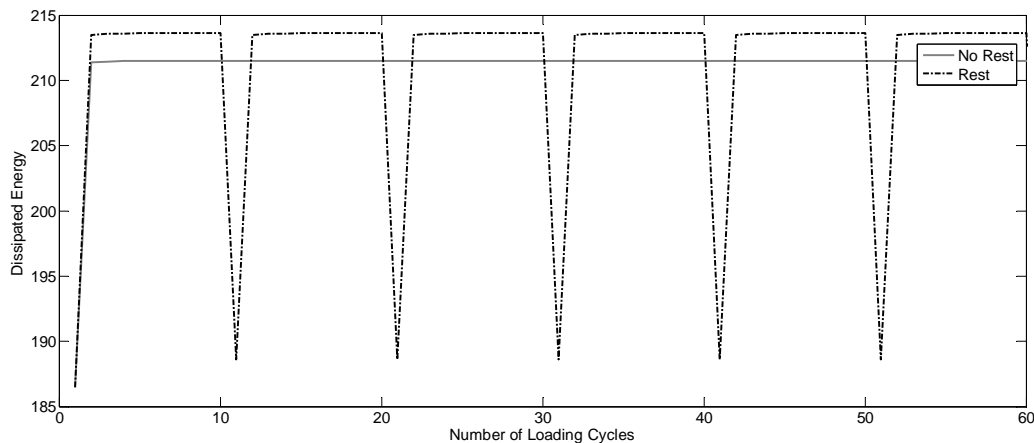


Figure F1d-6.2. Graph. Effect of rest on dissipated energy.

Based on modeling results, it appears there is an increase in complex modulus and dissipated energy due solely to viscoelastic response. The research team intends to continue the investigation of the viscoelastic response that occurs during rest periods to allow for separation of stress relaxation healing in actual time sweep results. The research team will also assess if this viscoelastic phenomenon is important for healing characterization of asphalt binders.

Limited time sweep with rest period testing was performed due to machine availability. Based on the results of testing conducted in the previous quarter, the research team considered using frequencies below 10 Hz to eliminate machine problems with reaching target strains. However,

when time sweeps with rest periods were performed using 5 Hz there were still problems reaching the target strain after each rest period. It was interesting to observe that the target strain was reached quickly during the first loading period, but in each successive loading period it took almost the entire 2.2-second loading period to reach the target strain amplitude. Thus, it appears that the rheometer requires significant time to ramp up to the desired strain amplitude. Test results of the measured strain during the first loading period and all other loading periods applied in between rest periods is shown in figure F1d-6.3. The target strain in this test was 4%.

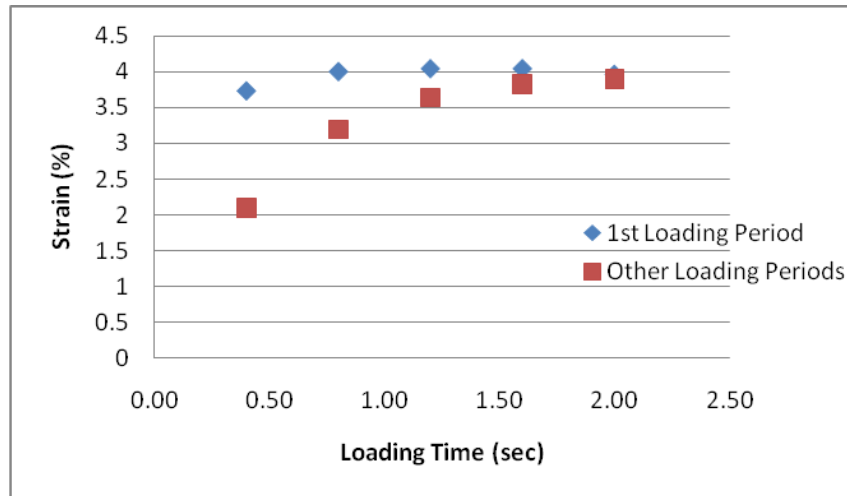


Figure F1d-6.3. Graph. Strain versus loading time.

The research team decided to adopt a loading sequence that includes a step which allows for ramping of strain amplitude to be compliant with machine capabilities. For the no-rest case, this procedure employs a 3-second period of oscillatory loading that linearly increases from zero to 4% strain followed by 100 cycles of loading at 4% strain. The strain amplitude is then set to zero; when this is reached the ramp and 100 cycles at constant strain is repeated. It takes a short period of time for the strain to be set to zero. However, this has been found to be consistent among tests so it is not considered to be an issue. For the rest case, an additional period of time at zero strain is included. A frequency of 10 Hz was used for these tests. A depiction of the idealized loading sequence with and without rest periods is depicted in figure F1d-6.4.

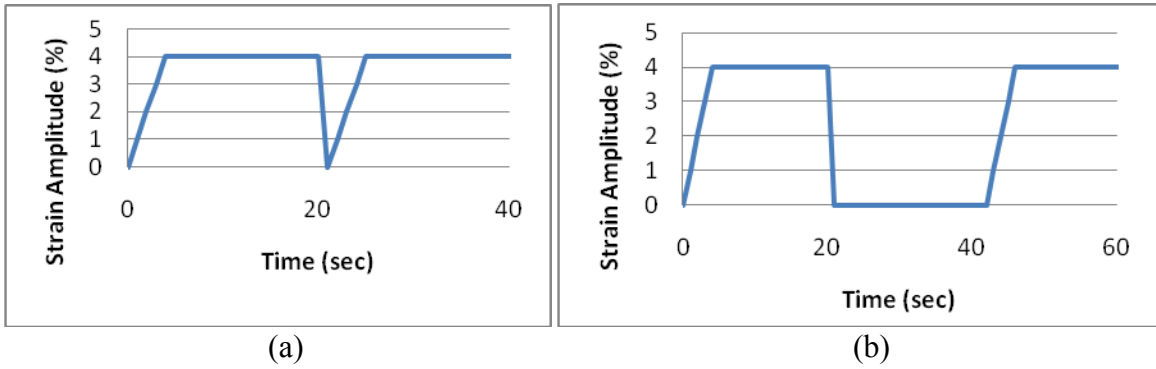
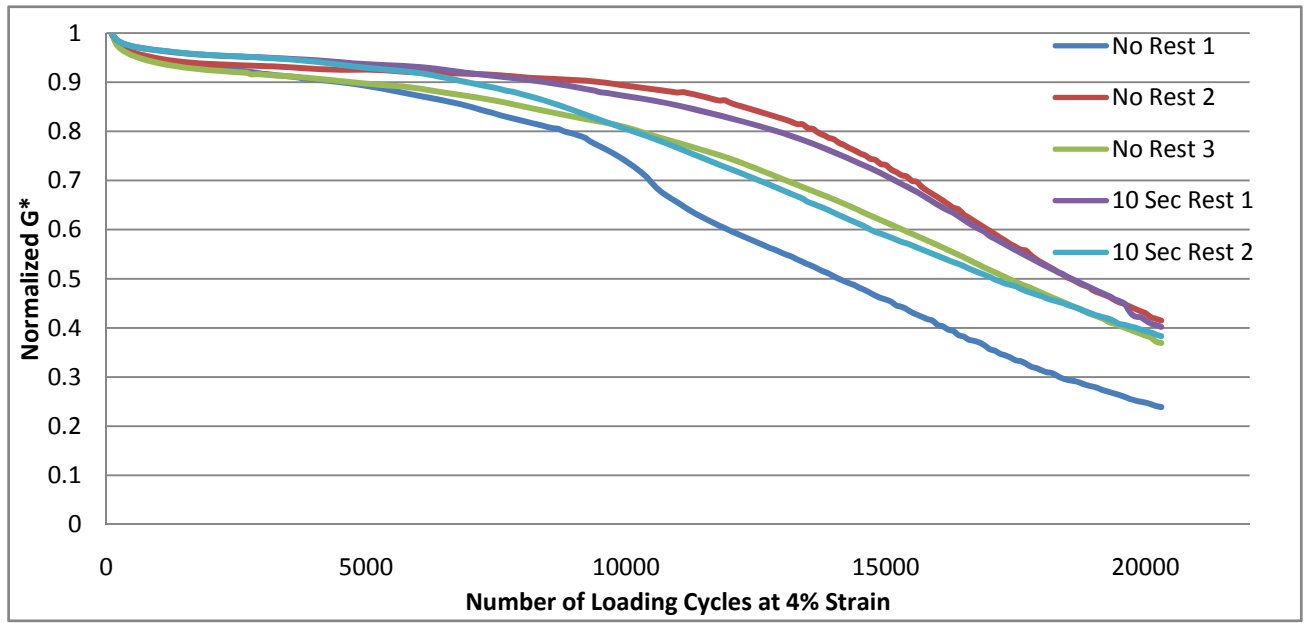


Figure F1d-6.4. Graphs. Proposed loading sequences for: (a) no-rest case; and (b) rest case.

Tests were run on a neat rolling thin film oven (RTFO)-aged PG 64-22 binder using no rest and 10 seconds rest. Figure F1d-6.5 shows the normalized complex modulus versus number of loading cycles at 4% strain. That is, the number of cycles recorded is the number of cycles of loading excluding the ramping step. As the figure indicates, the test was not able to clearly distinguish between the rest and no-rest cases. Furthermore, test results proved to be unrepeatable.



F1d-6.5. Graph. Normalized G^* versus number of loading cycles.

The research team intends to investigate modifications of the procedure described above. The goal will be to define a test procedure that is repeatable and allows for clear distinction between tests run with and without rest to allow for quantification of healing.

Significant Results

The research team has made progress on modeling the viscoelastic response of asphalt binders that occurs during time sweeps with rest periods. It has been shown that if viscoelastic effects are not carefully considered, misleading healing effects could be assumed.

Significant Problems, Issues and Potential Impact on Progress

The DSR was unavailable due to maintenance for much of the past quarter, which reduced the amount of testing that could be done.

Work Planned Next Quarter

Efforts will be focused on defining a reliable test procedure to evaluate healing that is compliant with the laboratory DSR.

Subtask F1d-7: Coordinate with Atomic Force Microscopic (AFM) Analysis (WRI)

Work Done This Quarter

Nothing to report.

Significant Problems, Issues and Potential Impact on Progress

None

Work Planned Next Quarter

Continuation: Analysis of existing data will continue in the next quarter. In these analyses, morphological features observed in asphalt and asphalt chromatographic fraction thin films prepared from validation site asphalts will be compared to performance data of the field site pavements. Image analysis of AFM scans will be developed to define a roughness “lumpiness” index.

Subtask F1d-8: Coordinate Form of Healing Parameter with Micromechanics and Continuum Damage Models (TAMU)

Work Done This Quarter

The focus of this quarter is on relating the developed micro-damage healing model to micromechanical aspects of healing. The continuum-based healing model’s parameters have been related to fundamental material properties such as the surface energy, bond strength, and the size of the healing process zone. The micro-damage healing model is coupled to the viscoelastic, viscoplastic, and continuum damage mechanics constitutive models in the unified continuum damage mechanics model PANDA. Moreover, the formulated model is validated initially against uniaxial compression and tension fatigue data from the Nottingham database on

asphalt mixtures. Thermodynamic aspects of the developed healing model will be explored based on the laws of thermodynamics.

Significant Results

None

Significant Problems, Issues and Potential Impact on Progress

None

Work Planned Next Quarter

Formulating the thermodynamic aspects of the developed healing model will be based on the laws of thermodynamics will continue in this quarter. Moreover, the micro-damage healing model will be validated against ALF experimental data and other existing data on another asphalt mixture in the Nottingham database. Special emphasis will be placed on relating the associated material parameters to fundamental properties (e.g. surface energy, bond strength, length of the healing process zone) based on micro-mechanical arguments.

CATEGORY F2: TEST METHOD DEVELOPMENT

Work Element F2a: Binder Tests and Effect of Composition (UWM)

Work Done This Quarter

Work this quarter focused on evaluating the elastic recovery-Dynamic Shear Rheometer (DSR) test developed in previous quarters. The research team evaluated the feasibility of running the test for shorter periods of time (less than 60 minutes). The elastic recovery results for the binders selected for testing in this task were compared to fatigue time sweep testing results, as well as the percent recovery (%R) from the Multiple Stress Creep and Recovery (MSCR) test.

Significant effort was dedicated to the analysis of Binder Yield Energy Test (BYET) collected data, the effect of modification type and level on BYET results, and the relationship between BYET results and the elastic recovery in DSR.

Significant Results

One of the advantages of running the elasticity in the DSR is the continuous monitoring of the data collected during the loading and unloading phases. The DSR elastic recovery procedure collects data every 0.065 seconds. To investigate effects of shortening the test, elastic recovery values were calculated at different unloading time intervals: 15, 30, 45 and 60 minutes. The plots of the elastic recovery in the ductility bath versus elastic recovery in the DSR at the different time intervals are shown in figure F2a.1. The R^2 values and the corresponding linear

equations are shown in table F2a.1. The results show a very good correlation ($R^2=0.97$) even after 15 minutes of unloading time, which suggest that the testing time can be reduced to 15 minutes. However, until additional tests are run to validate this time, 30 minutes unloading (relaxation) time is recommended.

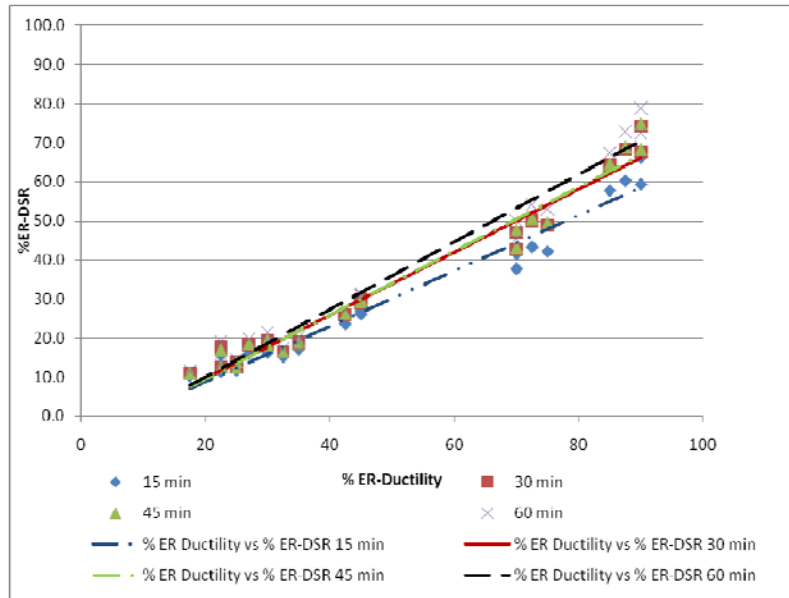


Figure F2a.1. Graph. Correlation between elastic recoveries in the ductility bath and elastic recoveries in the DSR measured at different time intervals. (ER = elastic recovery.)

Table F2a.1. Relation between elastic recovery in the ductility bath and DSR.

Time (minutes)	Equation	R^2
15	$Y=0.7077X-5.2502$	0.97
30	$Y= 0.8074X-6.4782$	0.97
45	$Y= 0.8181X-6.7169$	0.97
60	$Y=0.8631X-7.0721$	0.97

Y =ER-DSR. X = ER-ductility.

Another important subject addressed this quarter is the relationship between fatigue of binders as measured by the time sweep test and elastic recovery. The correlation between elastic recovery results and time sweep results at 10 kPa and 30 kPa is shown in figure F2a.2. The plots present the elastic recovery measured in the DSR versus the number of cycles to failure measured in the time sweep. The number of cycles to failure was determined using the dissipated energy concept and correspond to the point where the dissipated energy ratio was the maximum. The results presented in figure F2a.2 show that there is some correlation between elastic recovery results and time sweep results at both energy levels ($R^2=0.508$ and $R^2=0.536$). A closer inspection of the plots reveals that there are some outliers. In figure F2a.2(a), at 10 kPa it can be noticed that the

Flint Hills binder modified with 4% linear styrene-butadiene-styrene (LSBS) data point is an outlier. Eliminating this point improved the correlation ($R^2=0.623$).

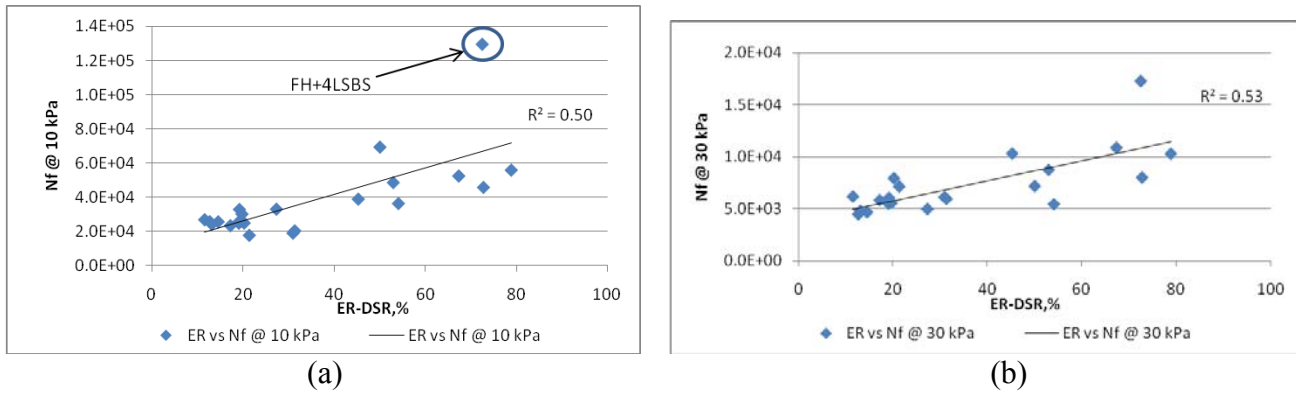


Figure F2a.2 Graphs. Correlation between elastic recovery and time sweep for: (a) ER versus Nf at 10 kPa; and (b) ER versus Nf at 30 kPa. (Nf = fatigue life.)

Figure F2a.3 shows the correlation between the elastic recovery measured in the DSR at 25 °C and %R from MSCR test measured at 0.1 kPa and 3.2 kPa at the PG temperature of the base binder. As shown, a very poor correlation ($R^2=0.04$) exists between ER-DSR and %R-MSCR at 0.1 kPa. This poor correlation can be attributed to the very high elastic recovery exhibited by the plastomers at the 0.1 stress level. A good correlation ($R^2=0.71$) between elastic recovery in the DSR and %R from the MSCR tests was observed when the results at 3.2 kPa were used.

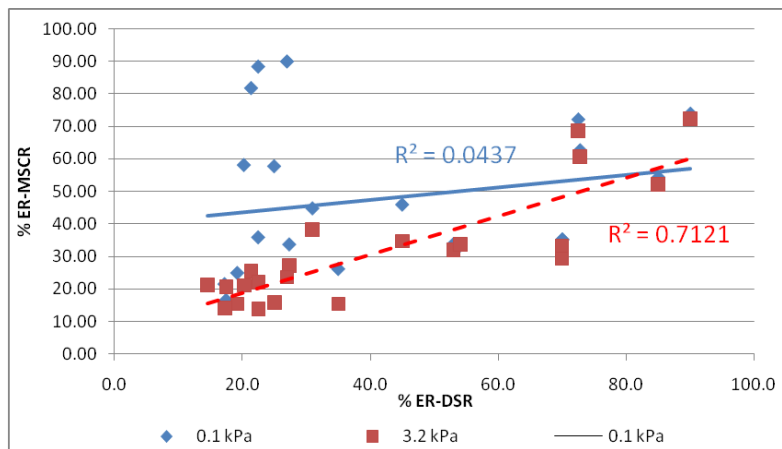


Figure F2a.3 Graph. Correlation between elastic recoveries in the DSR and elastic recoveries from MSCR tested at base binder PG temperature.

Four bitumen yield energy parameters were calculated from the response measured:

- BYET energy at the maximum stress point (BYEpeak).
- BYET energy at 20 strain (BYE20).
- BYET energy/G* (BYEpeak/G*).
- BYET energy at 20 strain/G* (BYE20/G*).

The four energies are described in the ARC Q2 2010 report for work element E2a. Figure F2a.4 summarizes the Flint Hills (FH)-based binder results, which shows that modification plays an important role in the fatigue performance. Styrene-butadiene-styrene (SBS) polymer-modified binder shows better performance than the Elvaloy (ELV)-modified binders. The plastomers have a negative effect on performance compared with the unmodified binder, while the acids show a contradictory response: 1% polyphosphoric acid (PPA) has a negative effect while the 1.5% PPA has a positive effect.

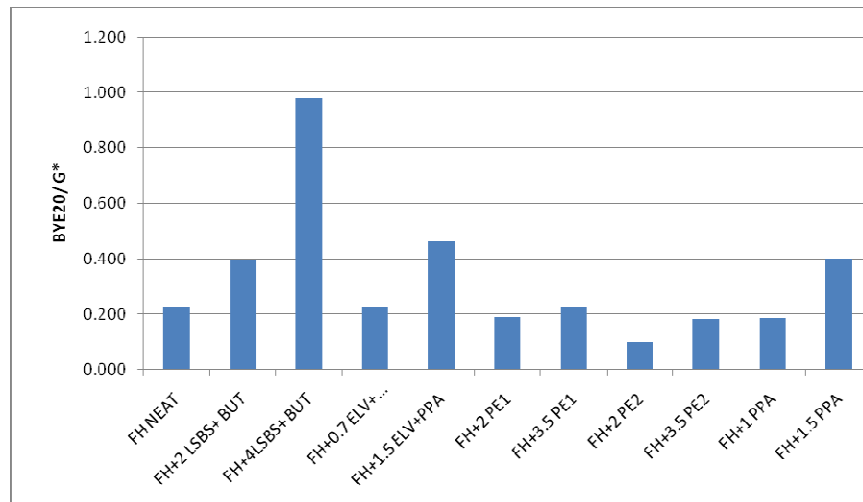
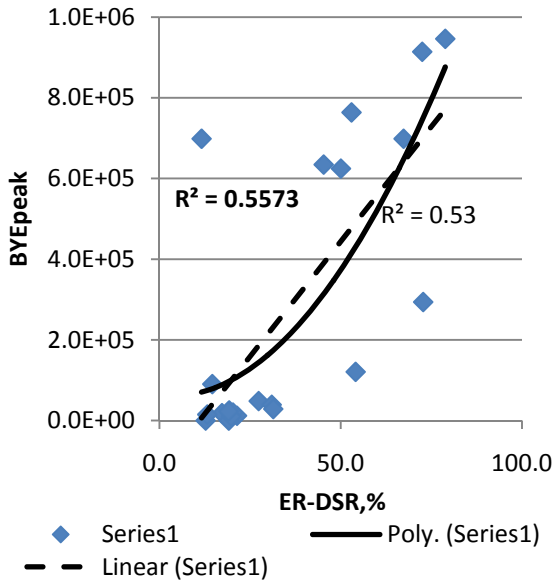
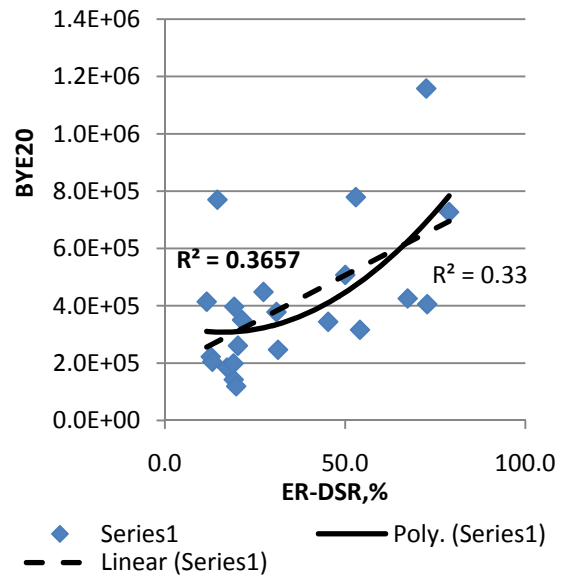


Figure F2a.4. Chart. Effect of the polymer type on BYE20/G*.

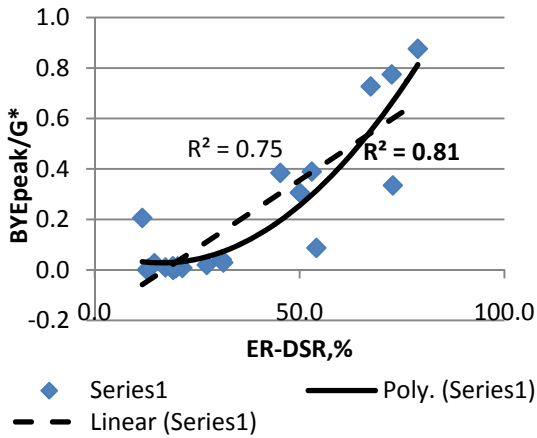
The results of the elastic recovery in the DSR were compared with the four different BYET energies described above, as shown in figure F2a.5. A second-order polynomial and a linear equation were used to correlate the results. The linear equation is represented by the dashed line, while the solid line represents the polynomial equation. The R^2 for the polynomial function is presented in bold. The plots show that the polynomial equation fit the results much better than the linear equation. It also shows that normalizing the energy by the stiffness (G^*) produces a better correlation for both BYEpeak (R^2 from 0.55 to 0.81) and BYE20 (R^2 from 0.36 to 0.71).



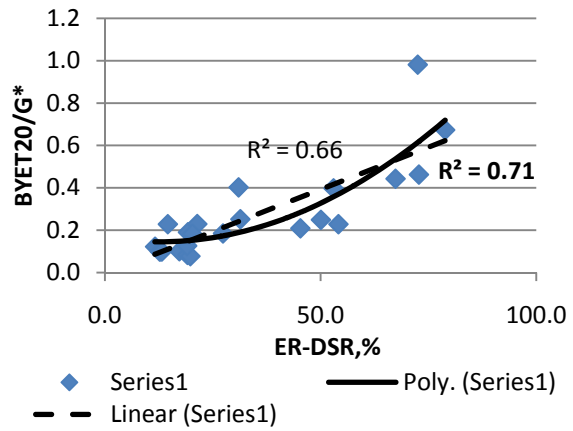
(a)



(b)



(c)



(d)

Figure F2a.5. Graphs. Comparison between elastic recoveries in the DSR and BYET results for: (a) BYET energy at the maximum stress point; (b) BYET energy at 20 strain; (c) BYET energy/G*; and (d) BYET energy at 20 strain/G*.

Significant Problems, Issues and Potential Impact on Progress

None.

Work Planned Next Quarter

The research team plans to prepare material for the second phase of the approved testing matrix, which includes testing mastics. Material preparation includes modifying the binders and mixing with the fillers. A subset of the testing matrix will be selected as a starting point for testing the mastics.

Work Element F2b: Mastic Testing Protocol (TAMU)

Work Done This Quarter

The reader is referred to work element M1c where the procedure for preparing FAM specimens and software development is presented.

Work planned next Quarter

Work will be conducted and presented in work element M1c.

Work Element F2c: Mixture Testing Protocol (TAMU)

Work Done This Quarter

Further investigation was made in this quarter on the anisotropic and viscoplastic properties of asphalt mixtures. The comprehensive viscoplastic damage model that was developed in past quarters was further improved in this quarter by establishing two more relationships between the viscoplastic parameters and the measurable material properties. Specifically, the following four achievements were made:

- A more general and more consistent formula was proposed for the modified effective stress to address the inherent and stress-induced anisotropy in asphalt mixtures;
- The inherent anisotropic relationship between the microstructural vector magnitude and the anisotropic modulus ratio was theoretically established and experimentally validated; a technical paper was finished that presents this relationship in detail (Zhang et al. 2010);
- A relationship was proposed to relate the yield stress ratio to the friction angle of asphalt mixtures; the limitations of the modified Drucker-Prager model were addressed and general yield surface and plastic potential models were proposed; and
- A method was developed to calculate the slope of the yield surface of asphalt mixtures based on the microstructural vector magnitude and the yield stress ratio.

Details of the achievements made in this quarter are presented as follows:

1) A General Modified Effective Stress Model

According to the nature of anisotropy, granular materials, such as soils, aggregate base and asphalt mixtures, consist of two types of anisotropy: i) inherent anisotropy and ii) stress-induced anisotropy. The inherent anisotropy of the asphalt mixture is attributed to the preferential orientation of aggregates. Since the aggregates tend to “lie flat” during the compaction of asphalt mixtures, the major axis of the aggregate has a preferential direction in the horizontal plane. The stress-induced anisotropy is the result of the crack growth under the load applications. The increase of the crack surface area leads to the loss of the intact material area, which causes the modulus degradation. The crack growth speed differs in different directions, which results in different modulus degradation in different directions and produces the stress-induced anisotropy in the asphalt mixture. To address those two types of anisotropy in asphalt mixtures, the continuum viscoplastic damage model was employed and the modified effective stress was generalized as:

$$\bar{\sigma}_{ij}^e = M_{imnj} F_{mabn} \sigma_{ab} \quad (\text{F2c.1})$$

where $\bar{\sigma}_{ij}^e$ = modified effect stress tensor; M_{imnj} = stress-induced anisotropic fourth order tensor; F_{mabn} = inherent anisotropic fourth order tensor; σ_{ab} = nominal stress tensor that is defined in the damaged configuration. The stress-induced anisotropic fourth order tensor, M_{imnj} , and the inherent anisotropic fourth order tensor, F_{mabn} , are formulated as follows:

$$M_{imnj} = \frac{1}{2} \left[\delta_{im} (\delta_{nj} - \xi_{nj})^{-1} + (\delta_{im} - \xi_{im})^{-1} \delta_{nj} \right] \quad (\text{F2c.2})$$

$$F_{mabn} = \frac{1}{6} (\delta_{ma} F'_{bn} + F'_{ma} \delta_{bn}) \quad (\text{F2c.3})$$

where, δ_{ij} = Kronecker delta tensor; $\xi_{ij}(N)$ = anisotropic damage density tensor representing the damage due to stress at the N-th load cycle; F'_{ij} = fabric tensor representing the microstructural properties, which is formulated as:

$$F'_{ij} = \begin{bmatrix} F'_1 & 0 & 0 \\ 0 & F'_2 & 0 \\ 0 & 0 & F'_3 \end{bmatrix} = \frac{1}{3 + \Delta'} \begin{bmatrix} 1 - \Delta' & 0 & 0 \\ 0 & 1 + \Delta' & 0 \\ 0 & 0 & 1 + \Delta' \end{bmatrix} \quad (\text{F2c.4})$$

in which Δ' is the new vector magnitude and can be determined using the following equation:

$$\Delta' = \frac{1}{A_0} \sqrt{\left(\sum_{k=1}^M \rho^{(k)} \lambda^{(k)} \sin 2\theta_k \right)^2 + \left(\sum_{k=1}^M \rho^{(k)} \lambda^{(k)} \cos 2\theta_k \right)^2} \quad (\text{F2c.5})$$

where $A_0 = \sum_{k=1}^M (\rho^{(k)} \lambda^{(k)})$; $\rho^{(k)}$ = area of the k-th aggregate; $\lambda^{(k)}$ = aspect ratio of the k-th aggregate and θ_k = inclination angle of the k-th aggregate relative to horizontal direction. Equation F2c.5 indicates that the new vector magnitude takes into account not only the aggregate orientation but also the aggregate size and the aggregate shape.

2) Relationship of Vector Magnitude (Δ') with Modulus Ratio E_{11}/E_{22}

A mechanistic relationship was developed in last quarter to relate the vector magnitude defined in equation F2c.5 to the anisotropic modulus ratio, which is shown as follows:

$$\Delta' = \frac{3 \left(\frac{E_{11}}{E_{22}} - 1 \right)}{4(q-1) - \left(\frac{E_{11}}{E_{22}} - 1 \right)} \quad (\text{F2c.6})$$

where E_{11} = vertical modulus in the compaction direction; E_{22} = horizontal modulus in the direction perpendicular to the compaction direction; q = maximum value of the anisotropic modulus ratio, E_{11}/E_{22} .

In this quarter, a series of laboratory experiments were conducted on 16 asphalt mixture specimens that varied in binder type, air void content and aging period to verify the relationship in equation F2c.6. First, an efficient and economical testing protocol was developed to measure the vector magnitude, in which the lateral surfaces of the cylinder specimens were scanned (see figure F2c.1) and the outline of the aggregates was plotted (see figure F2c.2). The scanned lateral surface of the asphalt mixture specimen was used to measure the aggregate characteristics including inclination angle, cutting surface area and aspect ratio, which were later employed to calculate the vector magnitude.

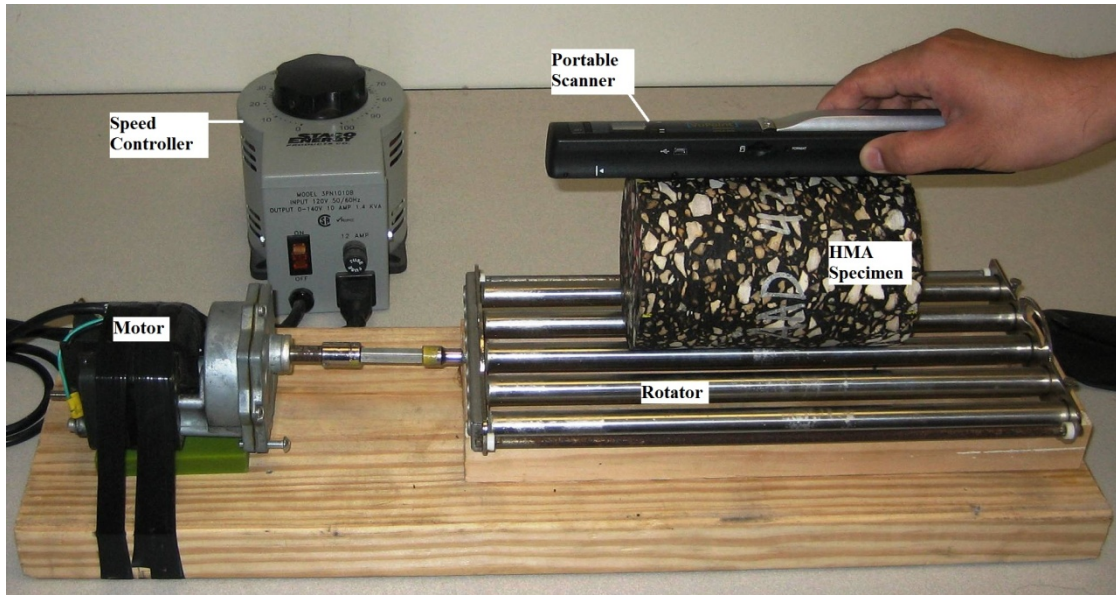


Figure F2c.1. Configuration of lateral surface scanning of asphalt mixture sample.

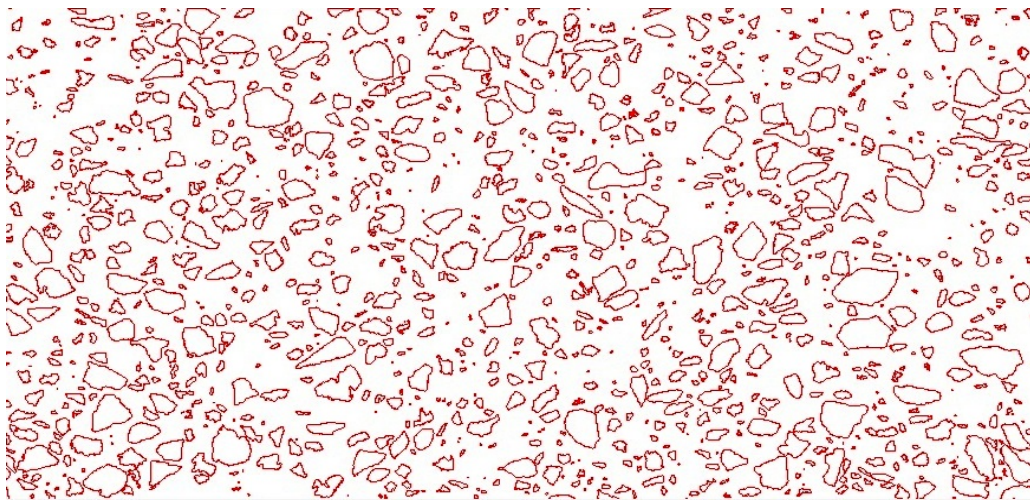


Figure F2c.2. Aggregate outline on the lateral surface of a cylinder asphalt mixture sample.

Second, three nondestructive tests (Zhang et al. 2009) including the compressive creep test, tensile creep test and indirect tensile creep test were performed on the 16 specimens at three temperatures and the master curves of the vertical and horizontal complex modulus were constructed using a mechanistic model (Luo and Lytton 2010). Plot of the vector magnitude against the modulus ratio shown in figure F2c.3 revealed that the ratio of the vertical modulus to the horizontal modulus normally ranged from 1.2 to 2.0 corresponding to a range of the vector magnitude from 0.2 to 0.5. Regression of the 16 data showed that the maximum modulus ratio (q) tended to be 2.553 ($R^2 = 0.9312$), which demonstrated that the relationship between the new

vector magnitude and the anisotropic modulus ratio was consistent with the derived theoretical relationship. Binder type, air void content or aging condition did not show significant effect on this relationship, which accordingly connected the microstructural characteristics to the physical properties of the asphalt mixture directly.

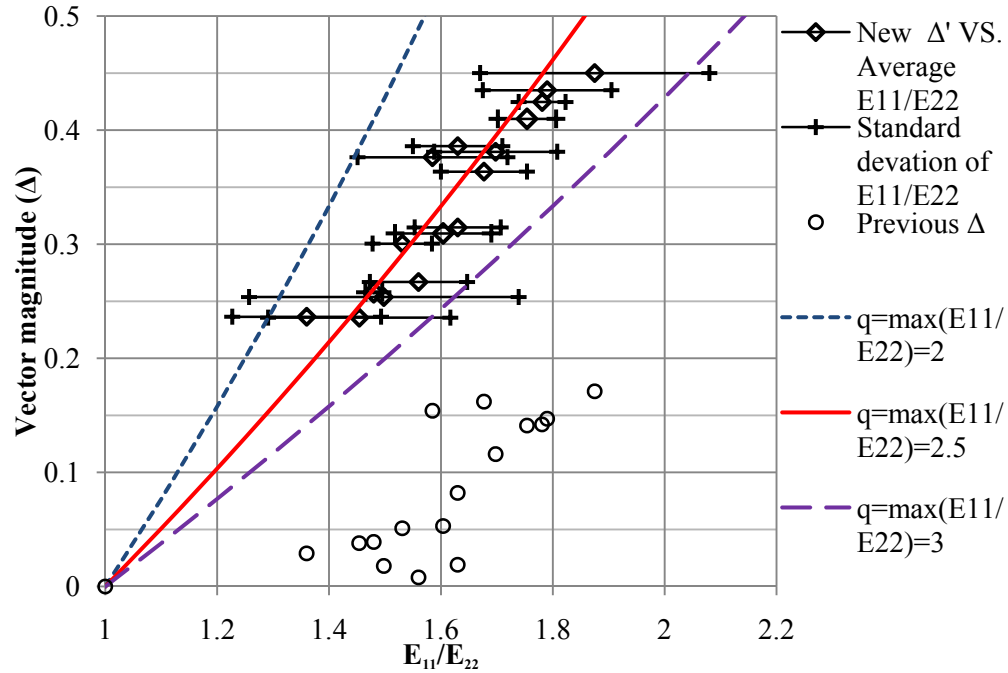


Figure F2c.3. Relationship of vector magnitude with anisotropic modulus ratio.

3) Relationship of Yield Stress Ratio (d) with Friction Angle (ϕ)

For a material, such as metal, with identical compressive and extensive properties, the traditional Drucker-Prager yield function can be used and the shape of the yield surface is a circle on the octahedral plane as shown in figure F2c.4. If a material, such as asphalt mixtures, has significantly different compressive and extensive properties, the modified Drucker-Prager yield function is more appropriate and the shape of its yield surface is shown as the dashed curve in figure F2c.4.

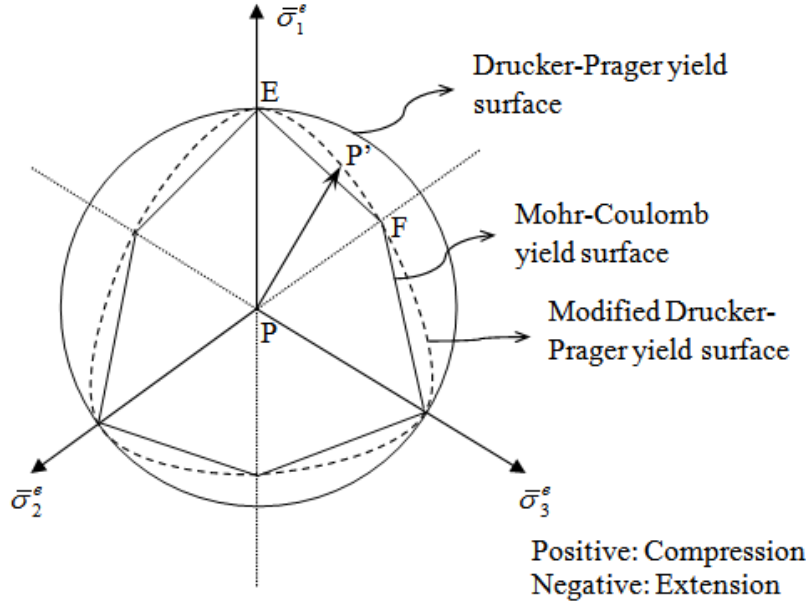


Figure F2c.4. Yield surfaces of Drucker-Prager and Mohr-Coulomb models.

A parameter d was defined as the ratio of a certain stress state on the modified Drucker-Prager yield surface (point P' in figure F2c.4) to the stress state in pure compression (point E in figure F2c.4). The use of the parameter d differentiated the compressive properties from the extensive properties of the asphalt mixture in the viscoplastic model. By superposing the Mohr-Coulomb yield surface with the extended Drucker-Prager yield surface at the pure stress states (vertices of hexagon), the d is derived as:

$$d = \frac{PP'}{PE} = \frac{3 - \sin \varphi}{3 + \bar{n} \sin \varphi} \sqrt{\frac{\bar{n}^2 + 3}{4}} \quad (\text{F2c.7})$$

where φ = friction angle of asphalt mixture; \bar{n} = Lode parameter and, if $\bar{\sigma}_1^e$, $\bar{\sigma}_2^e$, and $\bar{\sigma}_3^e$ ($\bar{\sigma}_1^e \geq \bar{\sigma}_2^e \geq \bar{\sigma}_3^e$) are effective principal stresses, then

$$\bar{n} = \frac{2\bar{\sigma}_2^e - \bar{\sigma}_1^e - \bar{\sigma}_3^e}{\bar{\sigma}_1^e - \bar{\sigma}_3^e} \quad (\text{F2c.8})$$

Figure F2c.5 shows the values of d varying with friction angles based on equation F2c.7. To ensure a convex yield surface so that the Drucker's hardening postulate is satisfied, the values of d are restricted from 0.778 to 1.0 in the triaxial stress state (where $d_1 = (3 - \sin \varphi)/(3 + \sin \varphi)$ when $\bar{n} = 1$), which corresponds to a range of friction angle from 0 to 22 degrees; however, many real materials such as asphalt mixtures has a friction angle larger than 22 degrees. One solution in this circumstance is to choose $d = 0.778$ and then to use the remaining equations to define the yield condition. However, if the friction angle is significantly larger than 22 degrees,

such as an asphalt mixture at a relative high temperature, the vertices of the Mohr-Coulomb yield surface will not be located on the modified Drucker-Prager yield surface and the modified Drucker-Prager yield surface will become non-convex.

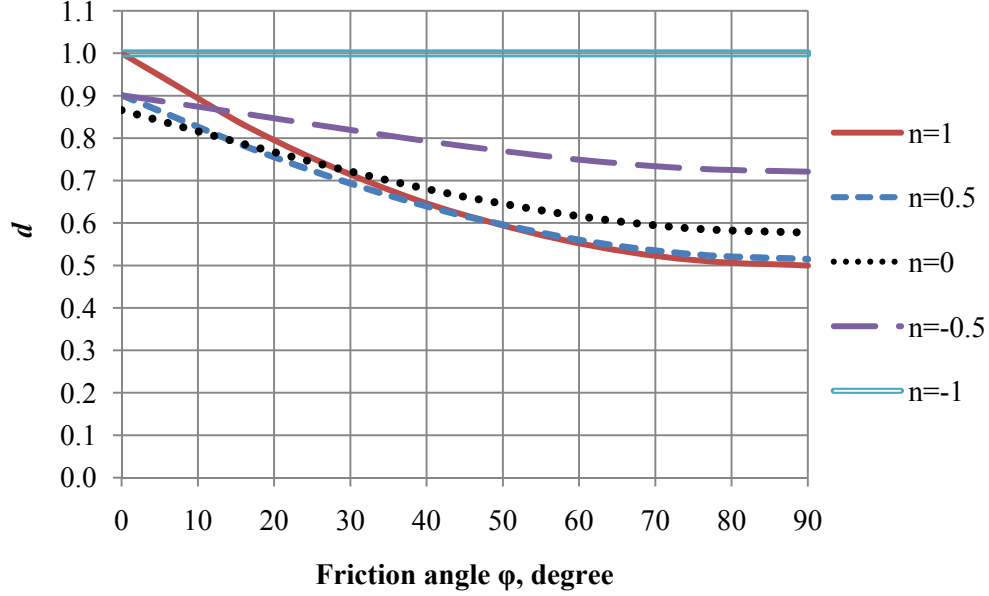


Figure F2c.5. Yield stress ratio of extension to compression (d) at different friction angles.

In order to address materials with a friction angle larger than 22 degrees, the modified Drucker-Prager yield surface function was further improved by introducing an elliptical yield surface so that the yield function satisfies the convexity condition in the full range of d (from 0.5 to 1) that corresponds to a range of friction angles from 0 to 90 degrees. The original modified Drucker-Prager yield surface function that was developed in last quarter has the following form:

$$f = \bar{\tau}^e - \alpha \bar{I}_1^e - \left(\kappa_1 \left[\varepsilon_{ij}^{vp} (N) \right]^{\kappa_2} + \kappa_0 \right) \quad (\text{F2c.9})$$

where:

$$\bar{\tau}^e = \frac{\sqrt{\bar{J}_2^e}}{2} \left[1 + \frac{1}{d} + \left(1 - \frac{1}{d} \right) \frac{\bar{J}_3^e}{(\bar{J}_2^e)^{3/2}} \right] \quad (\text{F2c.10})$$

In the improved modified Drucker-Prager yield surface function, an elliptical yield surface was used to replace equation F2c.10 as follows:

$$\bar{\tau}^e = \frac{\sqrt{\bar{J}_2^e}}{\eta(\theta)} \quad (\text{F2c.11})$$

where θ = Lode angle, and

$$\eta(\theta) = \frac{2(1-d^2)\cos\theta + (2d-1)\sqrt{4(1-d^2)\cos^2\theta + d(5d-4)}}{4(1-d^2)\cos^2\theta + (2d-1)^2} \quad (\text{F2c.12})$$

$$\cos\theta = \frac{1}{3} \arccos\left(\frac{3\sqrt{3}}{2} \frac{\bar{J}_3^e}{(\bar{J}_2^e)^{3/2}}\right) \quad (\text{F2c.13})$$

Equations F2c.11 and F2c.12 give a convex yield surface in the octahedral plane over the entire range of friction angle from 0 to 90 degree as shown in figure F2c.6.

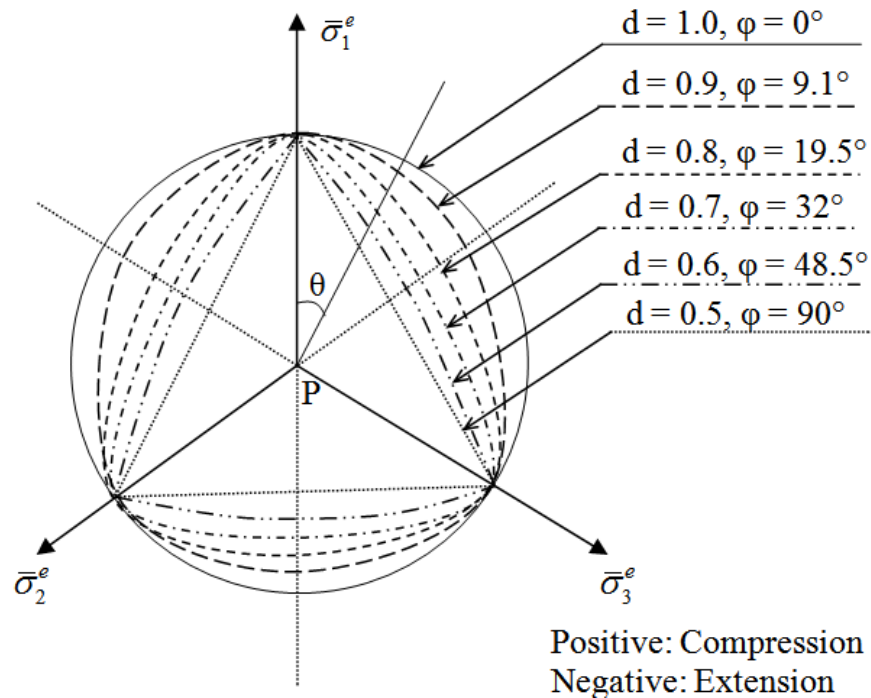


Figure F2c.6. Schematic non-convex yield surface for various values of d .

4) Relationship of Slope of Plastic Potential Function (β) with Δ' and d

The non-associated flow rule applies to the asphalt mixture, which means that the direction of the viscoplastic strain increment is perpendicular not to the yield surface but to the plastic potential surface. Therefore, assuming that the plastic potential surface has a form as:

$$g = \bar{\tau}^e - \beta \bar{I}_1^e - \kappa_3 \quad (\text{F2c.14})$$

where β = the slope of the viscoplastic potential surface, the normality condition between the plastic potential function and the viscoplastic strain function yields:

$$\beta = \frac{43a - 22b}{12(a-b)} - \frac{9}{4d} - \frac{3}{2d(a-b)} \left[a^2 \left(\frac{47d-27}{18} \right)^2 - ab \left(\frac{491}{81}d^2 - \frac{61}{6}d + \frac{9}{2} \right) + b^2 \left(\frac{14d-27}{18} \right)^2 \right]^{0.5} \quad (\text{F2c.15})$$

where $a = (3 + \Delta')/(1 - \Delta')$ and $b = (3 + \Delta')/(1 - \Delta')$. Equation F2c.15 indicates that a non-associated flow rule applies to asphalt mixtures during the viscoplastic deformation. This non-associated flow rule may result from the inherent anisotropy (Δ') and different properties in extension and compression (d). Figure F2c.7 illustrates the relationships between β , d , Δ' , and α in the triaxial compressive condition. The slope of the plastic potential function (β) decreases with an increasing vector magnitude (Δ') and an increasing yield stress ratio (d). The slope of the yield surface function (α) also decreases as d increases, and α is always greater than β , which is consistent with previous findings.

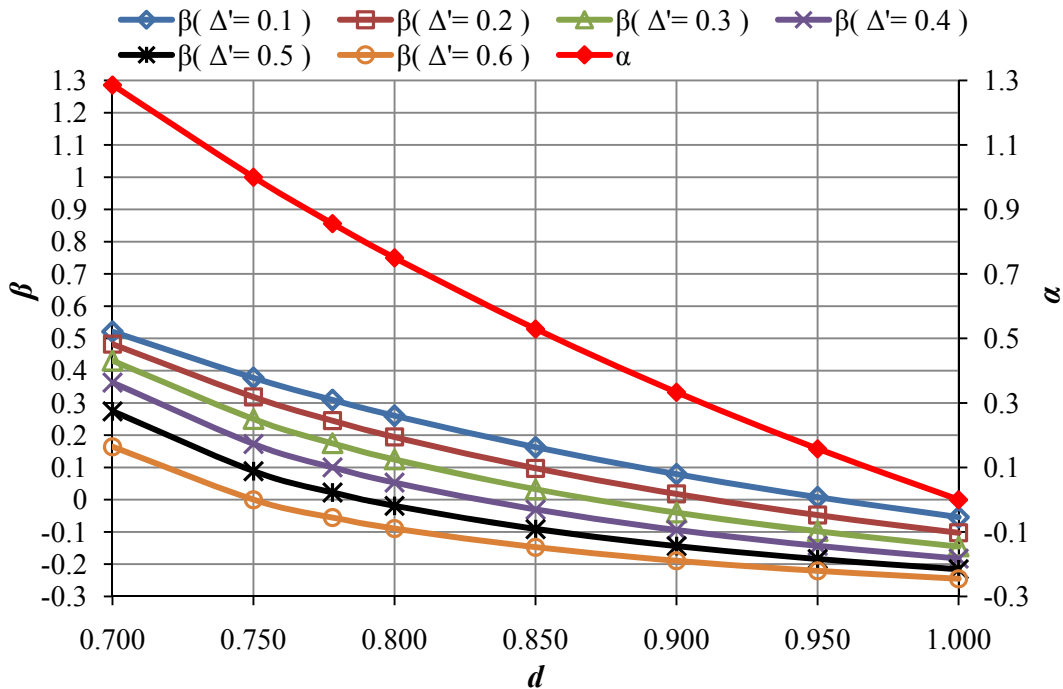


Figure F2c.7 Relationships between β , d , Δ' , and α .

Significant Results

In this quarter, further investigation was conducted on the characterization of the anisotropic and viscoplastic-damage properties of asphalt mixtures in compression. First, the modified effective stress tensor used in viscoplastic model was improved by using a fabric tensor and a damage density tensor to consistently address the inherent and stress-induced anisotropy of asphalt mixtures. Second, laboratory experiments were conducted in this quarter to verify the relationship between the microstructural anisotropic parameter (updated vector magnitude) and the modulus ratio of the vertical modulus to the horizontal modulus. A new test protocol was developed to measure the aggregate characteristics that were then used to calculate the vector magnitude. The test data proved to be consistent with the developed theoretical relationship between aggregate characteristics and vector magnitude.

Furthermore, a relationship was developed to relate the yield stress ratio to the friction angle of the asphalt mixture, based on which the modified Drucker-Prager yield surface was found to be applicable only for materials with a friction angle less than 22° . Therefore, an elliptical yield surface was proposed to address the full range of the friction angle of asphalt mixtures from 0° to 90° . As a result, the non-associated flow rule applied to asphalt mixtures since the plastic potential function differed from the yield surface. The slope of the plastic potential function was estimated using the yield stress ratio and the vector magnitude and was found to be always less than the slope of the yield surface.

Finally, based on the work accomplished in this quarter and last quarter, reasonable relationships were formulated between the measurable material properties (such as modulus, friction angle and cohesion) and the viscoplastic model parameters including vector magnitude (Δ), slope of yield function (α), slope of plastic potential function (β), yield strength (κ_0), yield stress ratio (d).

Significant Problems, Issues and Potential Impact on Progress

The comprehensive viscoplastic models for asphalt mixtures have not been completed because: i) the separated dissipated pseudo-strain energy for permanent deformation (W_{R2}) is not well defined for an asphalt mixture in compression which must be considered to be anisotropic, and ii) the anisotropic damage density tensor is not explicitly specified to account for the direction-dependent degradation of asphalt mixture properties due to the increasing radius of cracks/voids under a compressive load. In addition, testing protocols and data analysis methods for viscoplastic-damage properties of asphalt mixtures under the repeated compressive loading need to be developed to evaluate and calibrate the proposed viscoplastic-damage models.

Work Planned Next Quarter

- Improvement of the anisotropic viscoplastic damage model for asphalt mixtures under repeated compressive load;
- Definition and calculation of the separated dissipated pseudo-strain energy for permanent deformation in an asphalt mixture under repeated compressive loading;

- Definition and calculation of the anisotropic damage density due to the increasing radius of cracks/voids in an asphalt mixture under the repeated compressive loading; and
- Testing protocols and data analysis methods for the anisotropic and viscoplastic properties of asphalt mixtures under repeated compressive loading.

References

Luo, R., and R. L. Lytton, 2010, Characterization of the Tensile Viscoelastic Properties of an Undamaged Asphalt Mixture. *Journal of Transportation Engineering*, 136 (3), 173-180.

Zhang, Y., R. Luo, and R. L. Lytton, 2009, Anisotropic Viscoelastic Properties of Undamaged Asphalt Mixtures under Compressive Loading. *Journal of Transportation Engineering, American Society of Civil Engineers (ASCE)*, Submitted for review.

Zhang, Y., R. Luo, and R. L. Lytton, 2010, Microstructure-Based Inherent Anisotropy of Asphalt Mixtures. *Draft available*.

Work Element F2d: Structural Characterization of Micromechanical Properties in Bitumen using Atomic Force Microscopy (TAMU)

Background:

In the previous quarterly report, a sample preparation method and protocol for this experiment was developed and implemented. The preliminary findings indicated that dissimilar phase detection microscopy (PDM) phases exhibited different material behavior and mechanical properties. These findings vindicated the need to further pursue the extent of these differences and eliminate any possible errors and/or artifacts that may have contributed to the results.

Work Done This Quarter

To build on findings from the previous quarter, some of the AFM technical issues were studied, including the influence of artifacts and the effects of varying cantilever alignments and probes. The aforementioned procedures have been fine-tuned during this quarter prior to the implementation of a comprehensive study of the micromechanical properties in bitumen, which includes the change in microstructure and micromechanical behavior due to oxidative aging. The following tasks were carried out during the quarter:

Task 1: Sample Preparation

In this step, multiple thin-film specimens of different binder types were prepared for testing using a spin coating method, which involves completed dissolution of a known weight of binder in toluene. A number of these samples were aged in the rolling thin-film oven (RTFO) pressure aging vessel (PAV) to evaluate the effects of long-term oxidative aging on the binder's microstructure.

Task 2: Cantilever Tip Calibration and Trial Testing

The probe and tip geometry, cantilever spring constant, and cantilever resonant frequencies can vary significantly from cantilever to cantilever, which can cause problems for gathering analogous data during AFM experiments. These variations, in addition to irrepressible changes in the manual cantilever alignment were studied to determine the sensitivity of these parameters in the event that a single probe could not be used throughout this experiment. Maintaining a useable probe that has been calibrated presents challenges during testing, because probes can be damaged or contaminated while performing force experiments on stiff materials and while engaging with sticky materials such as asphalt. To determine the consequence of changing cantilevers and/or alignments, the deflection sensitivity of multiple cantilevers was measured. This was performed by allowing the probe to interact with a hard surface, such as a clean glass slide or silicon, while a constant force was applied. The slope of the corresponding force vs. distance curve yielded the deflection sensitivity of the cantilever.

After evaluating the cantilever sensitivity, trial testing was necessary to fine-tune the experimental procedure, identify potential artifacts, and ensure that accurate and comparable results could be obtained throughout the experiment. The entire experiment would require roughly 120-240 force measurements for six binders (three aged and three unaged), depending on the number of phases identified using PDM. The primary objective of the trial run was to observe any type of systematic change in data during the progression of data collection. This trial experiment was performed using two separate methods to effectively identify a systematic shift in data:

1. Identify different phases in an asphalt specimen and perform a force measurement in each of the different phases, then repeat a force measurement in the **same** location of each phase. Note any systematic shift.
2. Identify different phases in an asphalt specimen and perform a force measurement in each of the different phases, then repeat a force measurement in a **different** location of each phase. Note any systematic shift.

The trial test consisted of precisely three force measurements taken in each apparent PDM-identified phase change. An illustration of the PDM bitumen phases and locations of each measurement for the two trial experiments are shown in figure F2d.1.

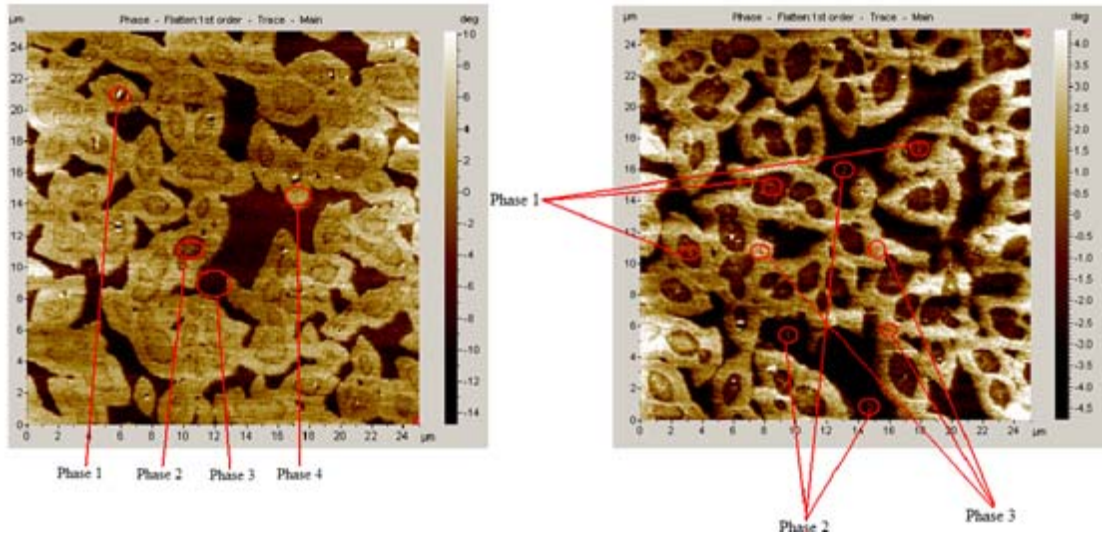


Figure F2d.1. Location of force measurements for two trial experiment methods.

Task 3: Experimental Testing and Data Collection

Once trial testing and calibrations were completed, individual specimens were studied and tested with the AFM. The preparation and testing was performed according to the flowchart shown in figure F2d.2.

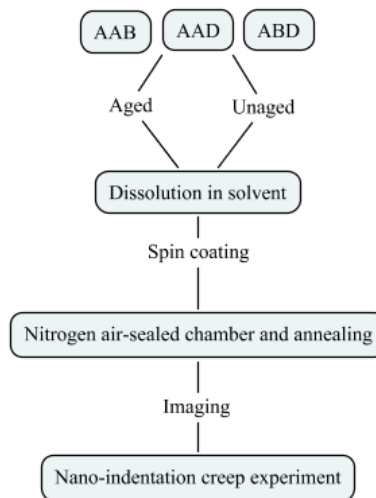


Figure F2d.2. Experimental flowchart.

Significant Results

It was determined that the deflection sensitivity of each cantilever, and thus the force measurements, varies significantly due to changing or re-alignment, as shown in figure F2d.3. The AFM software, PicoView, allows the user to enter the force constant and the deflection sensitivity (slope of force vs. distance calibration curve) of the cantilever tip prior to taking measurements, but due to the high variability and sensitivity of each cantilever, it is reasonable to assume that the likelihood of attaining invalid results increases by removing or changing cantilever tips during a single experiment.

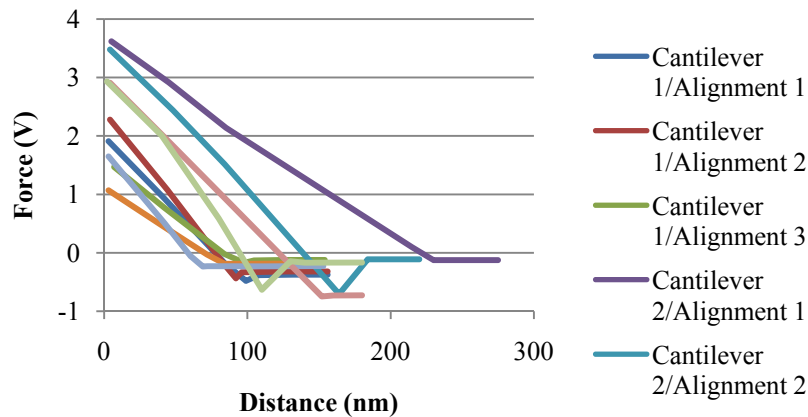


Figure F2d.3. Deflection sensitivity changes with varying cantilevers and alignments.

Due to the cantilever sensitivity findings previously described and the lack of a sound method for accurately measuring the force constant of each cantilever tip, the ability to repeat accurate and consistent measurements with the same cantilever tip became a key focus for the experiment. It was revealed through trial testing that accurate and repeatable measurements **can** be obtained by the using a single cantilever during the experiment. The primary concern with using a single tip for multiple force measurements in asphalt was the highly adhesive nature of the material. It was believed that material could conceivably accumulate on the cantilever tip and result in a systematic change in force measurements as the experiment progressed, but the trial experiment alleviated those concerns. As shown in figure F2d.4, force measurements taken in the same exact location consistently results in a systematic shift upwards in data, which indicates a higher stiffness with each measurement. As shown in figure F2d.5, the next trial of measurements taken at different locations within each phase yielded consistent measurements with no apparent systematic shift in data. These findings suggest that the systematic increase observed during the first trial was the result of disturbing or compacting the test location with each progressive measurement.

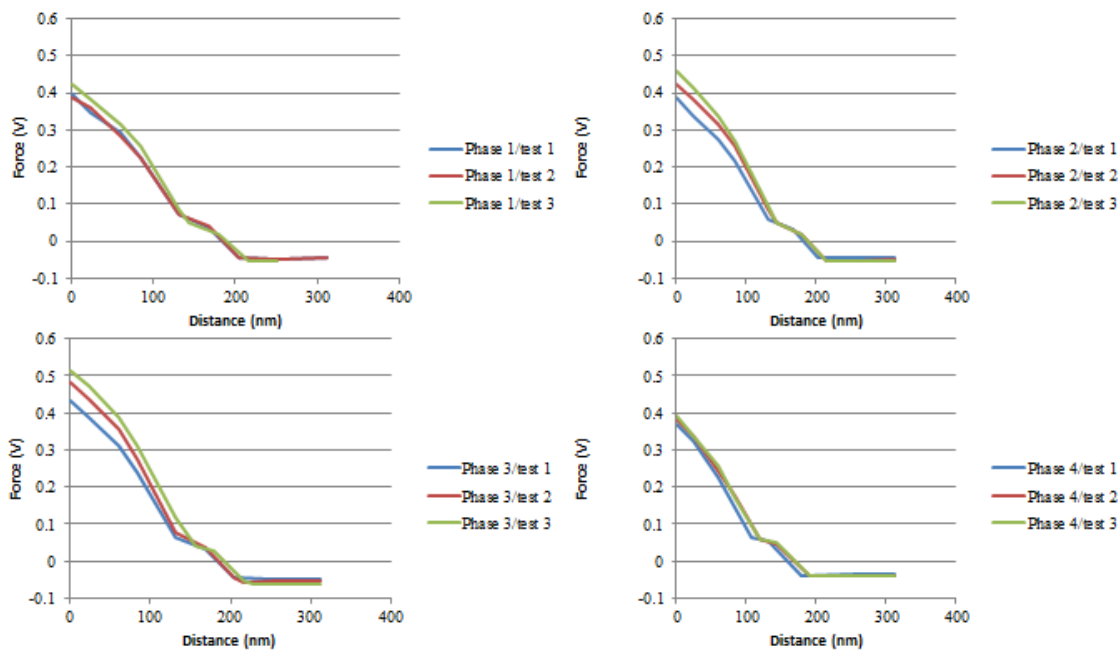


Figure F2d.4. Repeating force measurements in the same location of four identified phases.

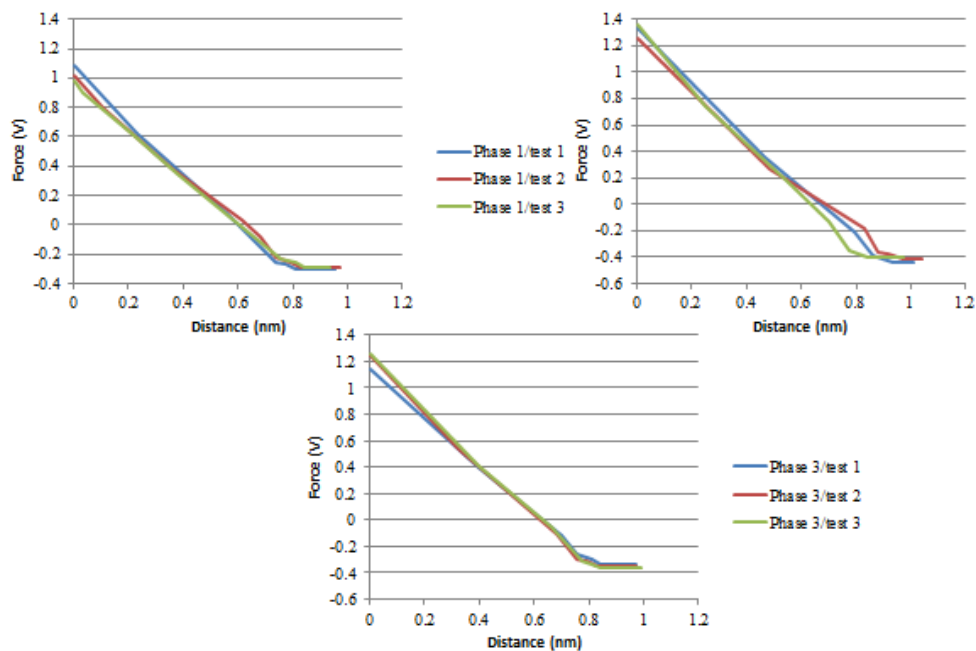


Figure F2d.5. Repeating force measurements in different locations of three identified phases.

It was determined that by avoiding data collection in repetitive locations, a single cantilever could confidently be used to collect accurate and consistent force measurements throughout the experiment.

Significant Problems, Issues and Potential Impact on Progress

The accurate measurement of cantilever force constants continues to be a problem for AFM researchers. A method for consistently and accurately measuring this value is still needed. The problem will not impact the progression of this experiment, but an AFM study of larger scale would likely require more than one cantilever to gather the necessary measurements.

Work Planned Next Quarter

A significant amount of data has been collected during the experiment, but the results and data analysis are still incomplete. This step will be performed during the next quarter according to task 4.

Task 4: Data Analysis and Characterization

In this step, all data measurements will be organized and compiled for evaluation and characterization. The analysis will include evaluation of topography images, PDM phase images, and force measurements for various samples. Finally, an assessment will be performed to characterize the microstructural properties and behavior of the binders.

Work Element F2e: Verification of the Relationship between DSR Binder Fatigue Tests and Mixture Fatigue Performance (UWM)

Work Done This Quarter

In the past quarter significant effort has been placed on revising the viscoelastic continuum damage (VECD) data analysis template for the Linear Amplitude Sweep (LAS) to make it more user-friendly.

For the analysis of the LAS results, a damage rate is defined in accordance with that proposed by Schapery (1984):

$$\frac{dD}{dt} = \left(\frac{dW}{dD} \right)^\alpha \quad (\text{F2e.1})$$

where D = damage intensity

α = material constant related to the rate at which damage progresses

The ultimate goal in analyzing LAS results is to predict the number of loading cycles a binder can withstand prior to a predefined failure criterion. Thus, equation F2e.1 must be solved to obtain damage as a function of time (or alternatively as number of loading cycles). In the study

of binder fatigue, the reduction of dissipated energy as function of the number of loading cycles has been selected to define damage growth where dissipated energy is defined as:

$$W = \pi \cdot I_D \cdot \gamma_0^2 \cdot |G^*| \cdot \sin \delta \quad (\text{F2e.2})$$

where I_D = normalized initial undamaged dynamic shear modulus

γ_0 = applied shear strain amplitude

$|G^*|$ = dynamic shear modulus

δ = phase angle

It can be observed that the loss modulus is the only portion of equation F2e.2 that is determined by the binder response. Thus, in order to utilize equation F2e.1, one must determine a numeric relation between $|G^*| \cdot \sin \delta$ and damage (D). Previously, equation F2e.3 was fit to experimental data using Excel Solver to perform a least squares optimization. However, this proved to be problematic as the quality of the fit was dependent on an initial guess for parameters C_1 and C_2 . (C_0 is simply taken to be the average $|G^*| \cdot \sin \delta$ at 0.1% strain amplitude.)

$$|G^*| \cdot \sin \delta = C_0 - C_1 D^{C_2} \quad (\text{F2e.3})$$

Thus, to reduce the chance of error due to guessing, equation F2e.3 was linearized using a logarithmic transform as shown in equation F2e.4. This allowed for use of Excel's slope and intercept functions to determine model parameters C_1 and C_2 rather than Excel Solver.

$$\log(C_0 - |G^*| \sin \delta) = \log C_1 + C_2 \log D \quad (\text{F2e.4})$$

Initially, C_1 and C_2 were determined using all test data. However, it was found that the logarithmic transform of data was not perfectly linear at low damage levels. Therefore, C_1 and C_2 were determined based on data corresponding to damage levels (D) greater than 100. Typically, this occurs when strain amplitudes are at 4% to 5%.

LAS test results were analyzed for eight binders (two replicates per binder) using both Excel Solver and the linearization method previously described. The research team compared the model parameter A_{35} (included in the fatigue law derived from LAS results) obtained from both analysis methods. Note that the parameter B is not related to the representation of $|G^*| \sin \delta$ as a function of damage. Therefore, parameter B is the same irrespective of the computation method. Table F2e.1 shows the results for A_{35} for the two methods. It can be seen that there is very little difference between the two methods.

Table F2e.1. Comparison of model parameter A_{35} determined through use of Excel Solver and logarithmic transformation.

Sample ID	A_{35} (Solver)	A_{35} (Linearization)	COV A
04-B901 1	2.26E+06	2.21E+06	1.65%
04-B901 2	1.90E+06	1.86E+06	1.44%
09-0902 1	5.13E+06	5.08E+06	0.70%
09-0902 2	4.83E+06	4.72E+06	1.65%
34-0961 1	4.32E+06	3.98E+06	5.71%
34-0961 2	3.78E+06	3.69E+06	1.68%
37-0962 1	1.17E+08	1.23E+08	3.44%
37-0962 2	9.37E+07	9.71E+07	2.52%
09-0961 1	1.27E+07	1.20E+07	4.32%
09-0961 2	1.22E+07	1.16E+07	3.69%
34-0901 1	5.13E+06	5.02E+06	1.52%
34-0901 2	5.68E+06	5.54E+06	1.79%
89-A902 1	5.22E+06	5.33E+06	1.47%
89-A902 2	5.71E+06	5.82E+06	1.27%
35-0902 1	7.81E+06	7.27E+06	5.11%
35-0902 2	7.74E+06	7.05E+06	6.59%

COV = coefficient of variation.

An attempt was also made to use a fifth-degree polynomial to represent $|G^*| \cdot \sin \delta$ as a function of damage, as high-order polynomials can represent data better than equation F2e.3 and can also be implemented without the use of Excel Solver. However, the use of a fifth-degree polynomial requires numerical integration of equation F2e.1 to obtain the relationship between load amplitude and number of cycles to failure, as a closed-form solution does not exist. The research team found that numerical integration could not be conducted due to the presence of singularities in the integral. Thus, a fifth-degree polynomial representation cannot be used to represent $|G^*| \cdot \sin \delta$ as a function of damage.

In addition to simplifying the estimation method for the coefficients used to represent $|G^*| \cdot \sin \delta$ as a function of damage, an effort was placed on developing an easy method to determine the parameter α . The parameter α is based on undamaged rheological properties and is typically determined from the slope of a log-log plot of relaxation modulus versus time. This time-intensive process was accomplished by fitting a model to frequency sweep data and then converting to the time domain using approximate interconversion methods. The conversion between frequency sweep and relaxation modulus relies primarily on the relationship between storage modulus and frequency. Thus, the applicability of using storage modulus and frequency to determine alpha directly from frequency sweep results was examined. It was determined that the slope of a log-log plot of storage modulus versus frequency can also be used to obtain α with:

$$\alpha = 1 + \frac{1}{m} \quad (\text{F2e.5})$$

where m = slope of a log-log plot of storage modulus versus frequency

A comparison between α as determined using relaxation modulus (original) and storage modulus versus frequency (revised) for four binders is shown in table F2e.2. As is evident by these results, the two methods produce very similar values of α .

Table F2e.2. Comparison of α derived using original and revised methods.

Binder	Original α	Revised α
64-SBS	2.416	2.430
64-ELV	2.388	2.401
58-ELV	2.389	2.403
64-Neat	2.451	2.460

SBS = styrene-butadiene-styrene. ELV = Elvaloy.

Significant Results

Simplification of the VECD analysis of the LAS test results was accomplished. The research team eliminated the use of interconversion methods to determine the model parameter α , and eliminated the need for the use of Excel Solver in binder fatigue analysis.

Significant Problems, Issues and Potential Impact on Progress

None.

Work Planned Next Quarter

The effect of asphalt binder age on LAS test results is currently under investigation. Six asphalt binders used in LTPP sections have been selected for this study. The LAS will be run on un-aged, rolling thin film oven (RTFO)-aged, pressure aging vessel (PAV)-aged, and double PAV-aged materials. The six binders represent a wide range of performance grades and include both modified and unmodified binders. The research team plans on publishing a paper on the findings of this study.

Cited References

Schapery, R. A. Correspondence Principles and a Generalized J Integral for Large Deformation and Fracture Analysis of Viscoelastic Media. *International Journal of Fracture*, Vol. 25, No. 3, 1984, pp. 195–223.

CATEGORY F3: MODELING

Work Element F3a: Asphalt Microstructural Model

Work Done This Quarter

Members of the modeling team met at TUDelft (June 8-18, 2010) in cooperation with the Delft Healing Consortium to continue development of a fracture-healing phase field model which is implemented through a finite element platform, CAPA3D. Members of the team also met after the Petersen Asphalt Conference to discuss work to be implemented by the researchers at NIST and Virginia Tech University.

During the second quarter of 2010, the Virginia Tech efforts focused on the characterization of 3D nano structure of asphalt binder and mastics using a NanoCT. Efforts were also devoted to the phase field theory and MD simulations of asphalt binder behavior.

Significant Problems, Issues and Potential Impact on Progress

The NIST subcontract has not been signed yet due to the slow process in the Department of Commerce. Nevertheless, the NIST researcher has started to get involved in the project.

Work Planned Next Quarter

Experimental measures of physico-chemical properties of asphalt, including molecular mass distributions of asphalts and asphalt fractions, phase transition temperatures of wax melting, crystallization energies, and flow activation energies, will be used as input in the FEM-Phase field model implemented at Delft to simulate structuring of wax in the healing process as a function of the nature of the asphalt. This approach assumes that asphalts differ based on molecular mass distribution and wax concentration. Additional parameters, including stiffness of waxy species (micro-domains) and increased stiffness of binder will be studied by low temperature 4-mm plate DSR to serve as input to this model to study stress-riser phenomena of heterogeneous binder properties.

In this upcoming quarter, the Virginia Tech focus will be on the development of a Matlab code to implement the phase field theory to include visualization capability.

Work Element F3b: Micromechanics Model (TAMU)

Subtask F3b-1: Model Development

Work Done This Quarter

Cohesive Zone Model

During this quarter we have mainly progressed towards three activities:

- We analyzed semi-circular bend (SCB) fracture test results to more accurately identify fracture characteristics of fine aggregate matrix (FAM) materials. To accomplish this task, simulation results were compared to the experimental results for a wide range of loading rates.
- Another primary task we focused on during this quarter was the further elaboration of the mixing-compaction-production protocol of the FAM phase with more test data and simulation results to reach more conclusive findings. This effort is to provide more accurate mechanical properties (viscoelastic properties and cohesive zone properties) of the FAM phase in the asphalt mixture to accomplish more accurate finite element-based micromechanics modeling.

The research outcomes were summarized in two journal papers that are submitted to the 2011 TRB annual meeting. Work progress and significance of each activity can be summarized as follows.

- Analysis of SCB Fracture Test Results

In the previous quarters, the testing protocol developed to obtain cohesive zone fracture parameters was presented. As shown in the previous reports, several loading displacement rates were applied to the top center line of SCB specimens. Test results were plotted relating reaction forces to the vertical displacements at the line of load application, to the crack-mouth opening displacements (CMOD) and to the crack-tip opening displacements (CTOD), respectively. Numerical simulations using the finite element method (FEM) incorporated with a bilinear cohesive zone model were performed to identify rate-dependent cohesive zone fracture parameters by matching the numerical simulations with the experimental test results. The good match between experimental and numerical results has been presented in the previous reports.

During this quarter, we focused on the analysis of test results. Opening displacements at the mouth and at the tip of the initial notch were monitored with high speed cameras of a digital image correlation (DIC) system. The DIC is an easy-to-use, non-contact technique that can capture time-varying variations in the deformation of specimen with high-resolution video cameras. It compares full-field deformation including the crack tip behavior at a certain loading time with the initial configuration by image analyses. The DIC test results at the local fracture process zone can be incorporated with the numerical cohesive zone fracture modeling so that the locally identified fracture properties of FAM mixtures subjected to different loading rates can be determined. Figure F3b-1.1 shows the SCB testing set-up incorporated with the high speed cameras of the DIC system. Figure F3b-1.1(a) shows an overview of the testing set-up including the DIC cameras, light source, a calibration panel of the DIC system, and the SCB testing specimen installed in a universal mechanical testing machine. Figure F3b-1.1(b) is a closer view of the SCB specimen. Note that, in order to capture more accurate deformation characteristics, the front face of the specimen were painted in white and were then stamped with black dot patterns. This improves the contrast of the images processed by the DIC system. Furthermore, in an attempt to trace opening displacements at the mouth and at the tip of notch in a more accurate manner, two pairs of extra dot gauges were glued as shown in the figure.

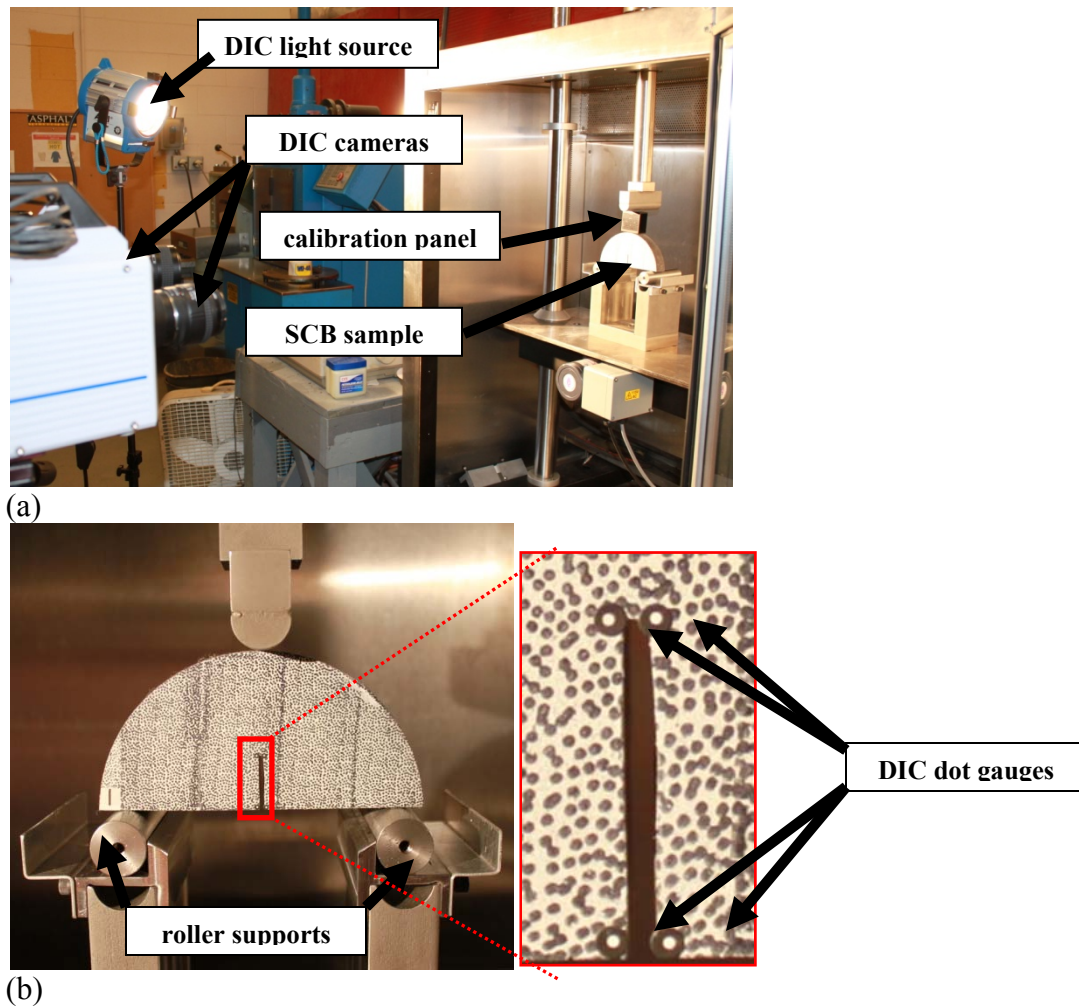


Figure F3b-1.1. Experimental testing set-up: (a) an overview of the whole testing set-up; (b) a closer view of a SCB specimen ready to be tested.

The viscoelastic nature of the FAM mixture creates a further complication on the identification of cohesive zone fracture properties. Global energy dissipation monitored by simply calculating the area below the experimental force-displacement (or loading time) curves is related to the energy dissipated due to the viscoelastic behavior of the matrix material as well as the fracture process initiated at the notch tip. Thus, fracture parameters along the fracture process zone should be identified locally, not by the global force-displacement results. Based on this fact, numerical simulations of the SCB tests were conducted to determine the cohesive zone fracture parameters required to initiate and propagate cracks through the specimens.

Figure F3b-1.2 presents a finite element mesh constructed and its corresponding boundary conditions to model the SCB fracture testing of the FAM specimens. As shown, the mesh contains cohesive zone elements along the center line of the virtual SCB specimen. Viscoelastic properties obtained from the linear viscoelastic dynamic frequency sweep tests of the FAM mixture were used for the solid elements, and the bilinear cohesive zone model was used to simulate fracture in the middle of the SCB specimen as the opening displacements increased.

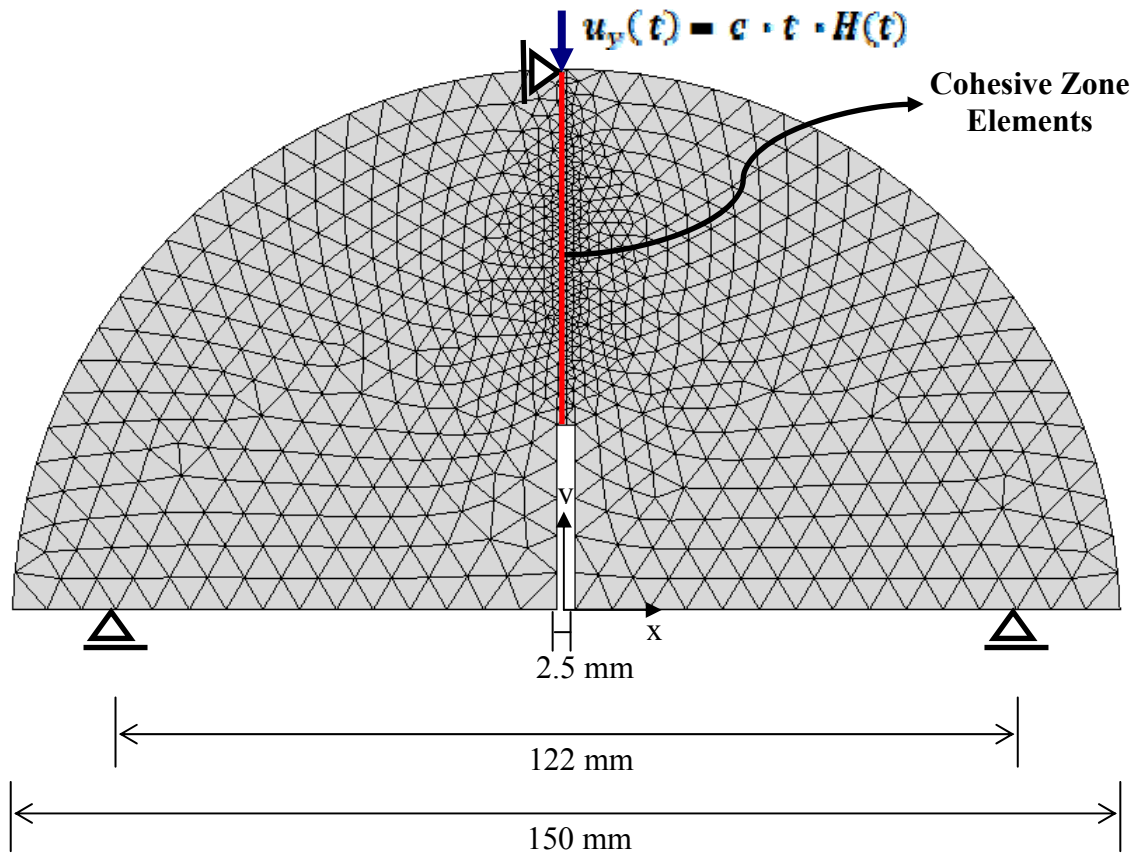
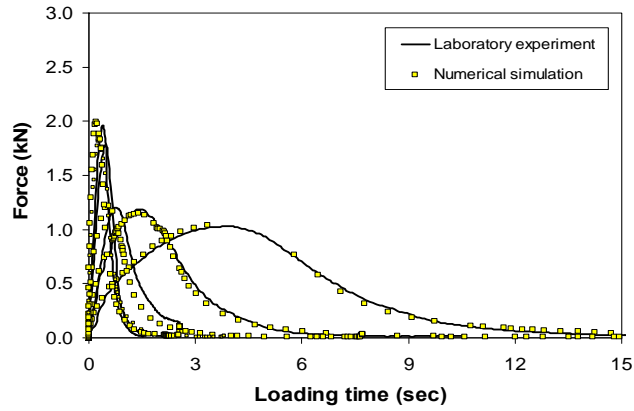
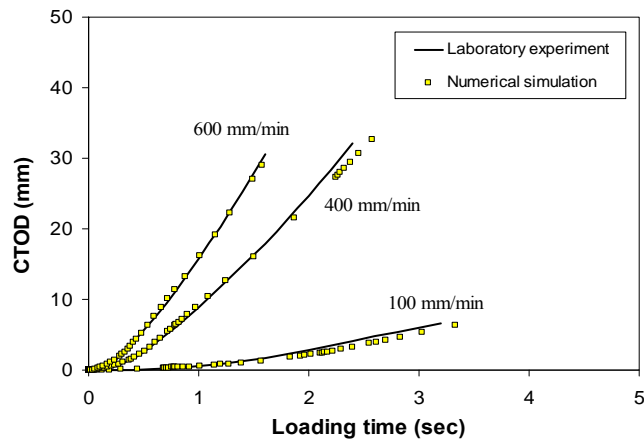


Figure F3b-1.2. A finite element mesh and its boundary conditions to model the SCB fracture testing.

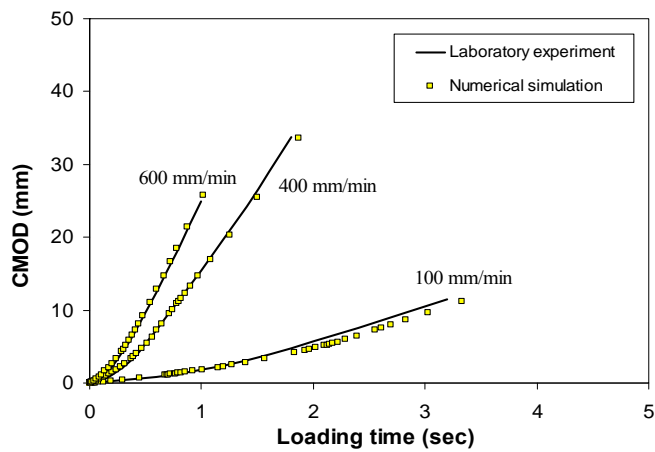
Cohesive zone parameters were found until a good match between experimental results and numerical simulations was observed. Figure F3b-1.3 (a) presents a strong agreement between the test results and numerical simulations of the reaction force – loading time plots. Validity of the cohesive zone properties determined herein are further verified from figures F3b-1.3(b) and (c) where test results and numerical simulations for the crack (notch) mouth opening displacements (CMOD) and the crack (notch) tip opening displacements are plotted respectively as the loading time increased. Figures F3b-1.3 (a) to (c) clearly demonstrates that the model parameters were accurately defined with no major discrepancies between experimental and numerical results.



(a)



(b)



(c)

Figure F3b-1.3. Comparisons between experimental and numerical simulation results: (a) reaction force at the line of load application; (b) CTOD; and (c) CMOD.

- Development of a protocol for mixing, compaction, and production of FAM phase to provide mechanical properties for the micromechanical modeling

During the previous quarters, we have developed an experimental-numerical framework for predicting dynamic modulus of asphalt concrete mixtures based on a computational micromechanics approach. One of primary purposes of the effort is to construct a reasonable experimental protocol for mixing, compaction, and production of FAM phase which is one of two distinct phases (i.e., the FAM and coarse aggregate phase) typically observed in digital images of asphalt concrete microstructure. The more accurate characterization of individual phase properties in the mixture will guarantee the more accurate predictions of overall mixture performance. To that, the finite element method has been incorporated with laboratory tests to characterize the properties of individual mixture constituents and with the two-dimensional digital image technique to represent detailed mixture microstructure characteristics. Mechanical properties of each phase are experimentally determined by conducting well-designed constitutive tests: oscillatory torsional tests of cylindrical FAM specimens and quasi-static nanoindentation tests of aggregates particles. Material properties of each mixture component are used in the finite element simulation, and simulation results are compared to experimental dynamic moduli of asphalt concrete mixtures so that the predicting power of the approach and the reasonableness of the FAM mixing-compaction-production protocol can be assessed.

In the previous quarter, fair agreement between simulated moduli and measured moduli was observed. The dynamic modulus master curves predicted by finite element simulations were within the range of experimental variations of the asphalt concrete samples, when the simulations were conducted with FAM phase that contains some air voids. This has been expected, since the FAM, by definition, is a mixture of asphalt binder, fine aggregates, and some entrained air voids.

The results in the previous quarter seem reasonable and are expected; however there were some uncertain and/or incomplete factors in the previous process such as the use of an average value for the elastic modulus of aggregates which are from various different mineralogical origins and the use of only one digital image for the micromechanical simulation. Therefore, during this quarter, we fabricated asphalt concrete mixtures and FAM mixtures using only one type of aggregate (i.e., limestone). The microstructure characterization through the digital image processing and its use for the finite element simulation is the same approach presented in the previous quarter, but a total of three images instead of the one were simulated to reach a better generality.

Dynamic modulus tests were performed on three replicate cylindrical asphalt concrete specimens. Three linear variable differential transformers (LVDTs) were mounted onto the surface of the specimen at 120° radial intervals with a 100-mm gauge length. As suggested in the AASHTO TP-62, five temperatures (-10, 4.4, 21.1, 37.8, and 54.4° C) and six loading frequencies (25, 10, 5, 1.0, 0.5, and 0.1 Hz) were used, and the frequency-temperature superposition concept was applied to develop a master curve representing the dynamic modulus of each specimen. Testing results in a form of frequency-domain master curve at the reference temperature of 23° C are presented in figure F3b-1.4. As shown, all three replicates were highly repeatable.

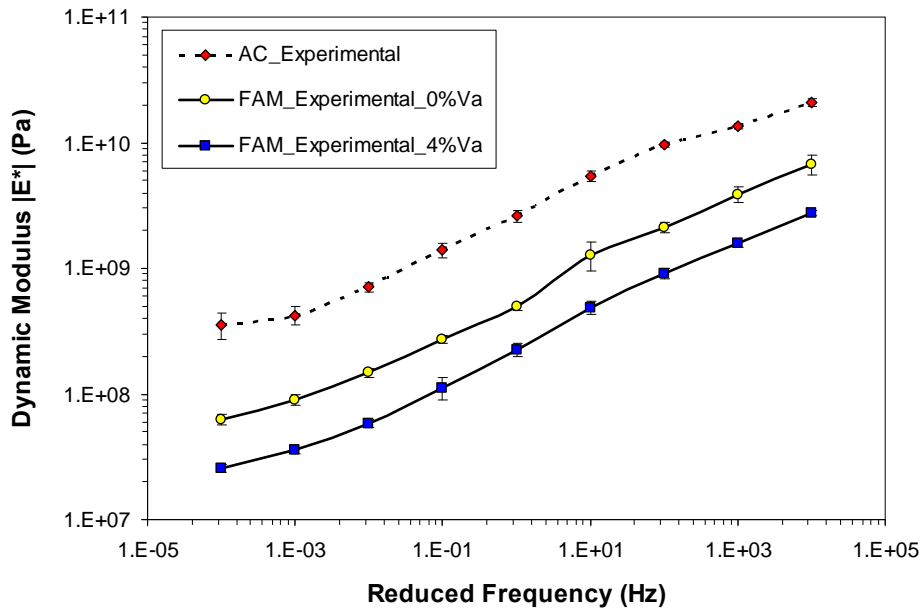


Figure F3b-1.4. Dynamic modulus master curves of asphalt concrete mixture and FAM mixtures.

The FAM mixtures were then fabricated and tested to characterize the linear viscoelastic properties. Using a Superpave gyratory compactor (SGC), two different amounts of FAM mixtures were compacted to represent two different levels of density (i.e., air voids of 0% and 4%). As previously noted, the compaction density of the FAM is not trivial to determine, since the volume occupied by the FAM phase in the asphalt mixture is unclear. An exact density of FAM phase in the mixture can be estimated only if the value of air void content in the FAM phase is known. However, the determination of air void content in the FAM is not easy to identify experimentally. Therefore, two possible extreme air voids, 0% and 4%, were attempted to fabricate FAM specimens.

For each level of density, a cylindrical FAM sample of 80 mm tall and 150 mm diameter were compacted. Then, the bulk matrix sample was sliced into three parts; the middle part of 45 mm thick and the top and bottom slices. Keeping the three parts intact in a 150 mm diameter cylindrical case open at both ends, the 45 mm long and 12.25 mm diameter cylindrical bar specimens were cored out of the compacted sample. The top and bottom slices of the matrix, and the cylindrical case were used to produce the high-quality FAM specimens without any problems at their two ends during the coring process. A total of four replicates were extracted from the FAM sample to characterize their linear viscoelastic properties by performing dynamic frequency sweep tests within a range of frequencies (0.01 Hz to 25 Hz) and at three different temperatures (5, 20, and 40° C), which provides a master curve of each FAM mixture. Figure F3b-1.4 also presents the dynamic shear modulus curves of the two FAM mixtures at the reference temperature of 23° C. A general trend seen in the figure is that the asphalt matrix mixture with higher density (0% air voids) exhibited higher stiffness over the entire loading frequencies. The testing results from the four replicates were highly repeatable with small

variances which are signified by error bars placed at different loading frequencies on each master curve.

To determine the elastic modulus of coarse aggregate phase in the mixture, 37 nanoindentation measurements were made by indenting a Berkovich diamond tip to the surface of limestone aggregates. Young's modulus of the limestone aggregate resulted in a mean value of 68.4 GPa with its standard deviation of 8.6 GPa.

The same asphalt concrete specimens which were used for the dynamic modulus tests were used to conduct the finite element micromechanical modeling. The 150 mm tall and 100 mm diameter cylindrical asphalt concrete specimens were sawn into two halves along the diametric plane in order to expose two 150 mm by 100 mm two-dimensional rectangular surfaces. The clean and dry rectangular surfaces were digitally scanned, and then cropped to a length of 135 mm and a width of 90 mm to make edges clearer as shown in figure F3b-1.5 (a). The two dimensional original gray images were converted into black and white images to identify two separate phases: coarse aggregates in white and FAM phase in black (Figure F3b-1.5 (b)). The original black and white images of mixture microstructure were then further treated to distinguish the two phases clearly. Figure F3b-1.5 (c) presents a final black and white image after completing all image treatment processes. The treated digital image of mixture microstructure was then discretized to produce three-node linear triangular elements. Figure F3b-1.5 (d) shows the finite element mesh generated from the original image shown in figure F3b-1.5 (a).

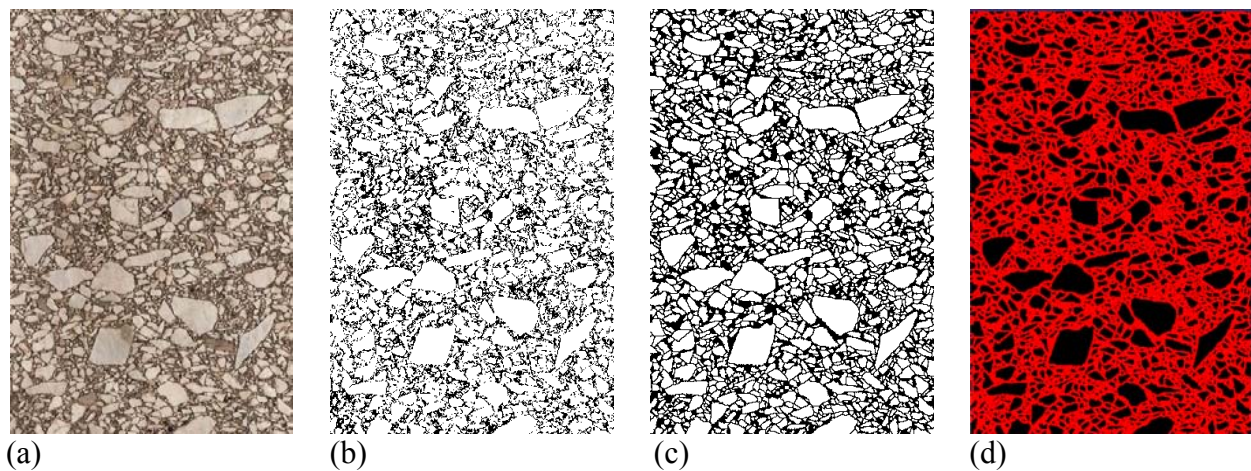


Figure F3b-1.5. Digital image process of mixture microstructure and its finite element mesh.

With the treated digital images and the mechanical properties of each component, dynamic modulus predictions can be made through the computational micromechanics modeling. Isotropic symmetry was considered for both the FAM phase and the coarse aggregate particles, which were modeled to be linear viscoelastic and linear elastic materials, respectively. For the finite element simulation, commercial software, *ABAQUS* was used. With the mesh developed as exemplified in figure F3b-1.5 (d), boundary conditions were applied to constrain the vertical displacements of the nodes at the bottom. Compressive haversine tractions were evenly applied

to the top nodes. To construct a dynamic modulus master curve, a wide spectrum of loading frequencies was simulated (10^{-4} to 10^4 Hz).

Figure F3b-1.6 shows dynamic modulus comparisons between the model predictions (obtained from the three microstructure images) and the experimental data (obtained from the three replicates). The predicted dynamic moduli were cross-plotted to the experimental dynamic moduli at each corresponding loading frequencies. In general, predicted dynamic moduli at the two different levels of air voids were in fair agreement with the experimental dynamic moduli. Experimental modulus values are placed between the two predictions, which is an expected observation, with slightly better match to the 0% air void FAM. In spite of several assumptions made and some inevitable technical limitations, based on the reasonable agreement between the experimental dynamic moduli and the simulated moduli, it can be inferred that the current development of the FAM fabrication protocol and the computational micromechanics modeling approach, although it is not perfect yet, seems attractive to characterize mechanical properties of asphalt concrete mixtures.

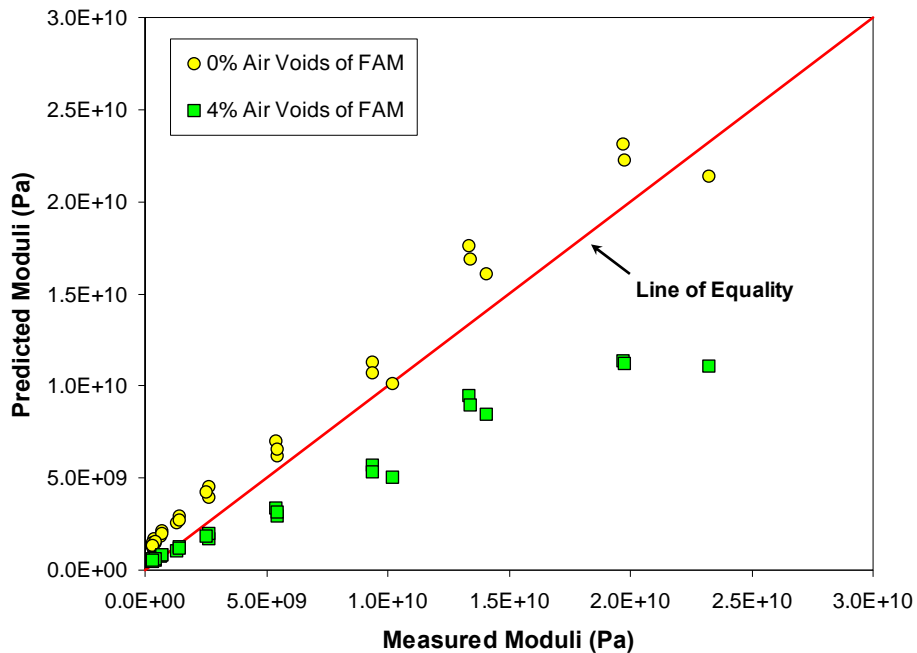


Figure F3b-1.6. Cross-plots between experimental dynamic moduli and model predictions.

Lattice Micromechanical Model

The main effort of the previous quarter focused on the quantitative verification of the recently implemented VECD-based approach using experimental results. It is observed that the simulations do not yield satisfactory results. Among many possible reasons for this outcome, the most likely is the change in time dependency with scale-up. Further investigations are underway to understand the physics of the process that lead to this observed behavior. The effort in the

current quarter has focused on enhancing the lattice model so that it has the capability to model air voids.

Experiments show that air voids can have a significant effect on the behavior of asphalt concrete. For example, air voids can cause a considerable drop in the initial stiffness of the specimen. This type of effect can change the behavior of the material from the outset. Air voids can also force changes to the direction of the crack path while the material is subjected to damage. Therefore, including air voids in the lattice model is deemed necessary.

There are different ways to consider the effects of air voids in the model. For example, the effect of air voids can be included within the mechanical properties of the material as a reduction factor. However, such an approach may neglect the effect of air voids on the microstructure and also the load path. In addition, air voids can have a significant effect on the initiation and propagation of cracks. Including air voids as a phase in material can address most of the aforementioned issues. Therefore, the research team has decided to add air voids to the model as a separate phase. The air voids will be modeled as cavities in each of the specimens.

Experimental research conducted at Texas A&M University indicates that air void size follows a lognormal distribution. Such a distribution is used to generate air “particles” (voids) using the same procedure as that used in generating aggregate particles. It should be mentioned that the inclusion of air voids using this procedure is not straightforward; techniques such as interlacing and scale splitting are important to obtain reasonable microstructures that contain air voids. For the NCSU research, the mesh generator has been modified accordingly so that it can handle the existence of cavities inside the specimen.

Figure F3b-1.7 shows a virtually fabricated specimen and the mesh that is generated using the initial image. The air voids in the image may seem big compared to the size of the aggregates. However, it should be noted that in some scales the size of the air voids can indeed be comparable to the size of the aggregate particles. In other words, it is not unusual to find relatively large air voids in some of the multiple scales that are being analyzed.

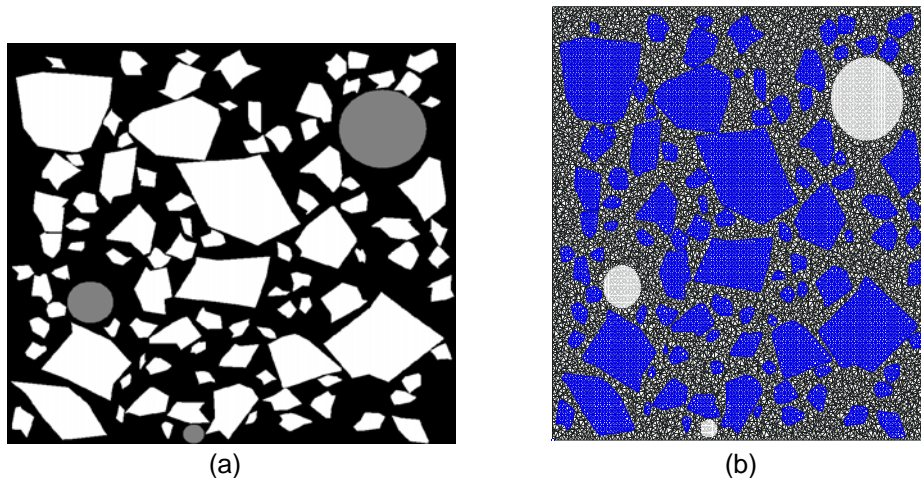


Figure F3b-1.7. (a) Virtually fabricated image; (b) mesh associated with the image.

Using the virtually fabricated microstructure, the effect of air voids on the behavior of the asphalt concrete can be investigated. Because voids are being added to the specimen, it is necessary to review the basic rules that apply for specimens that do not contain air voids. For example, the number of replicates that must be analyzed in each scale in order to obtain a convergent output may be different for specimens with air voids compared to those without air voids. Adding air voids can also change the required representative volume element (RVE) size for each scale. The initial stiffness value has been chosen as the simplest factor to use to examine these issues of number of replicates and RVE size.

In order to eliminate the effects of specimen-to-specimen variability, the number of specimens being analyzed must be known for the specimens that have air voids. This information can be found by performing a simple elastic tension test and measuring the initial stiffness for a large number of specimens. This process has been completed for different levels of air void content.

Figure F3b-1.8 shows the average of the initial stiffness values plotted against the number of specimens. It can be observed that each of the curves converge to different values because the air void content is different for each of them. Figure F3b-1.9 shows the error in initial stiffness values versus the number of replicates. It can be seen that the specimens without air voids converge faster than those with air voids. However, both specimens with and without air voids converge fast enough so that by the end of testing five specimens are close to the convergent value with a 5% error.

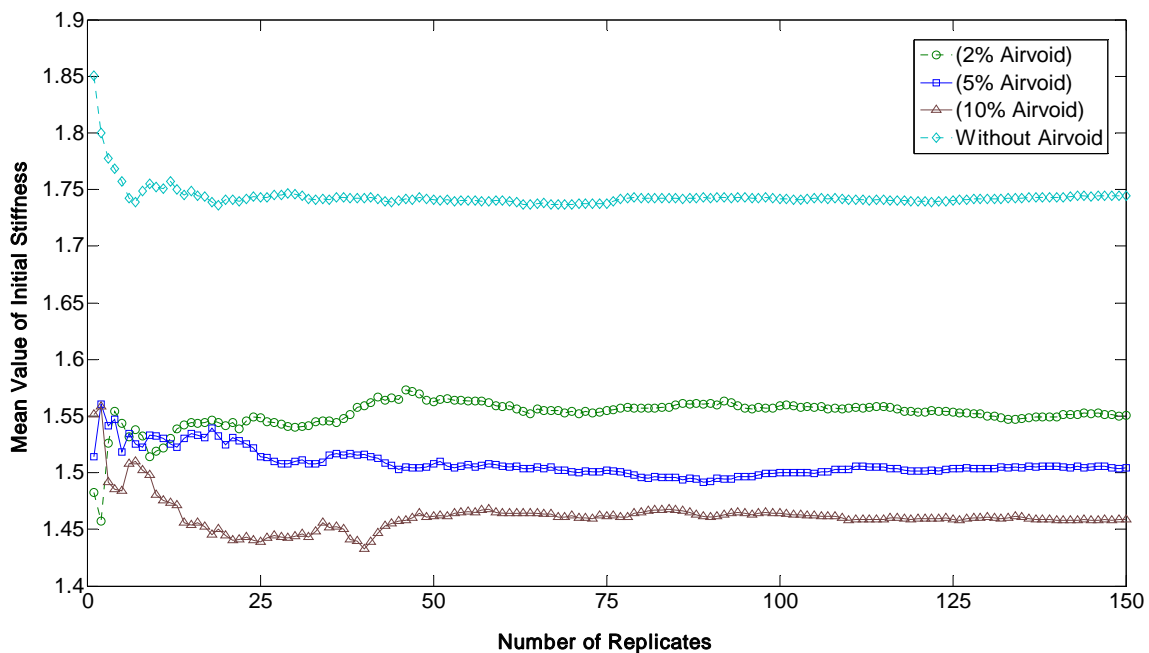


Figure F3b-1.8. Difference in initial stiffness for different levels of air void content.

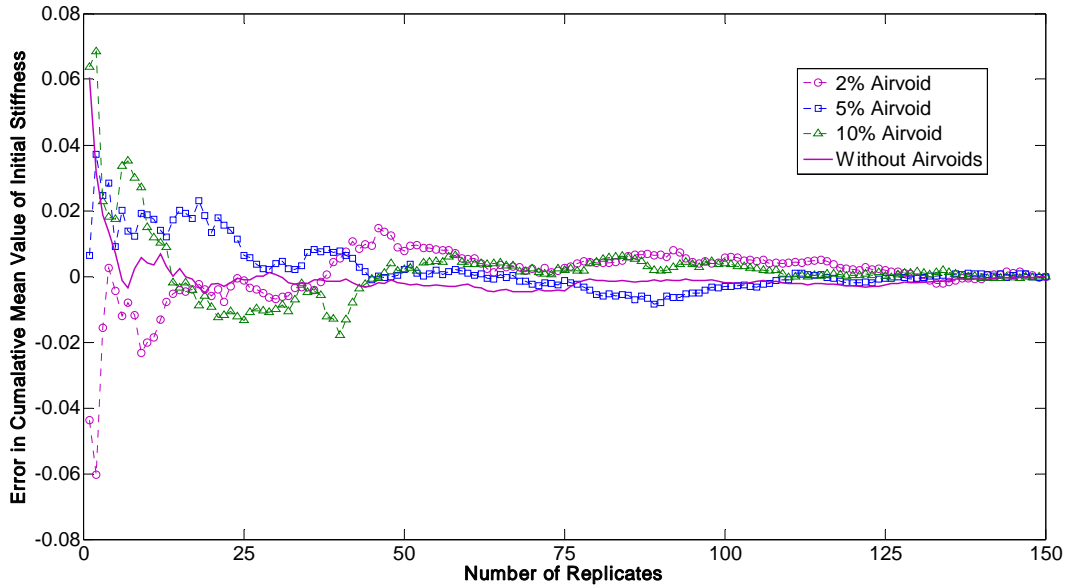


Figure F3b-1.9. Error of the initial stiffness prediction for different levels of air void content.

Previous investigations into the effects of the absence of air voids show that RVE size must be four to five times larger than the maximum aggregate size. Adding voids to the specimen may change the required RVE size. This situation may be checked by predicting the initial stiffness values of RVEs with increasing sizes, averaged over many replicates. The results indicate that four times the largest aggregate size produces an error less than 3 percent. Thus, the original recommendation of four to five times the maximum aggregate size appears to be adequate.

The next step is to ensure that the presented procedure for including air voids is accurate when used in the context of multiple scales. This step involves developing a criterion for scale-splitting the air void gradation. Developing such a criterion, as well as verification using experimental data, is currently in progress.

Continuum Damage to Fracture

Work is continuing on the micromechanical understanding of damage with the eventual goal of linking damage to localization and fracture. Specifically, a quantitative model that can capture the onset of localization (the point of departure from continuum damage theory) is being investigated. Specific results will be reported once the model is successfully developed and tested using some preliminary experimental data.

Significant Problems, Issues and Potential Impact on Progress

None

Work Planned Next Quarter

Cohesive Zone Model

In the next quarter we will work on the following activities:

- SCB fracture tests at additional loading rates;
- Extension of the current rate-independent User Element (UEL) code to incorporate the rate-dependent characteristics of the cohesive zone fracture parameters;
- Submission of journal papers to the 2011 TRB annual meeting;
- Testing of ARC core materials.

Lattice Micromechanical Model

- Quantitative investigation into the effect of air voids on the viscoelastic behavior of asphalt concert.
- Investigation into possible ways to implement the factor of time dependency change in different scales within the lattice modeling framework.

Continuum Damage to Fracture

Continue to develop the micromechanical understanding of damage and quantifiable criteria for the onset of localization.

Work Element F3c: Development of Unified Continuum Model (TAMU)

Work Done This Quarter

In this quarter, the formulations of the constitutive equations associated with the unified continuum damage model are formulated in a consistent mathematical framework based on the laws of thermodynamics. The constitutive model is now complete and includes the ability to predict: (1) nonlinear thermo-viscoelasticity; (2) thermo-viscoplasticity; (3) thermo-viscodamage (i.e. rate- and temperature-dependent damage) for modeling fatigue damage; (4) moisture-induced damage distinguishing between adhesive and cohesive moisture damages; (5) micro-damage healing; and (6) aging. The aforementioned constitutive model capabilities are already implemented in the computational code Pavement Analysis using a Nonlinear Damage Approach (PANDA). Constitutive models (1)-(5) have been verified against a large set of experimental data. The current focus is on more validation of the micro-damage healing and aging models against available data from the literature.

Moreover, a systematic process for the identification of the material parameters associated with the developed models in PANDA is under development. Also, several attempts have been made to relate these material parameters with the fundamental material properties.

The current validation has considered various experimental tests that include creep-recovery, repeated creep-recovery, creep, and uniaxial constant strain rate tests at different temperatures, stress levels, and strain rates in both tension and compression. However, more tests are still needed to fully validate the proposed model. This is critical at high temperatures specially for calibrating the viscoelastic-viscoplastic temperature coupling terms more accurately.

We developed a testing plan (tension and compression) that will be used for the calibration and validation of the PANDA constitutive models. This testing plan in compression is shown below (figure F3c.1 and tables F3c.1 to F3c.9).

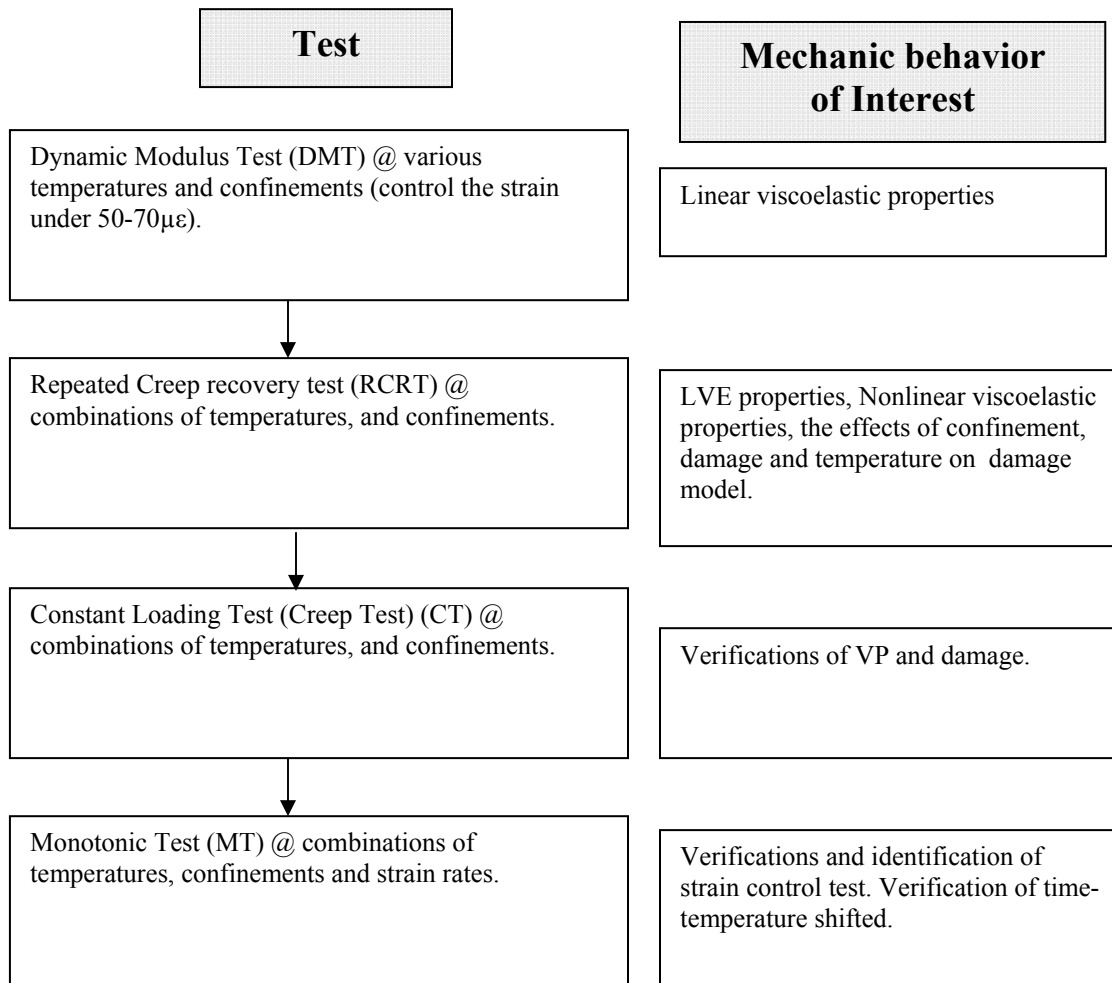


Figure F3c.1. Description of testing matrix in compression.

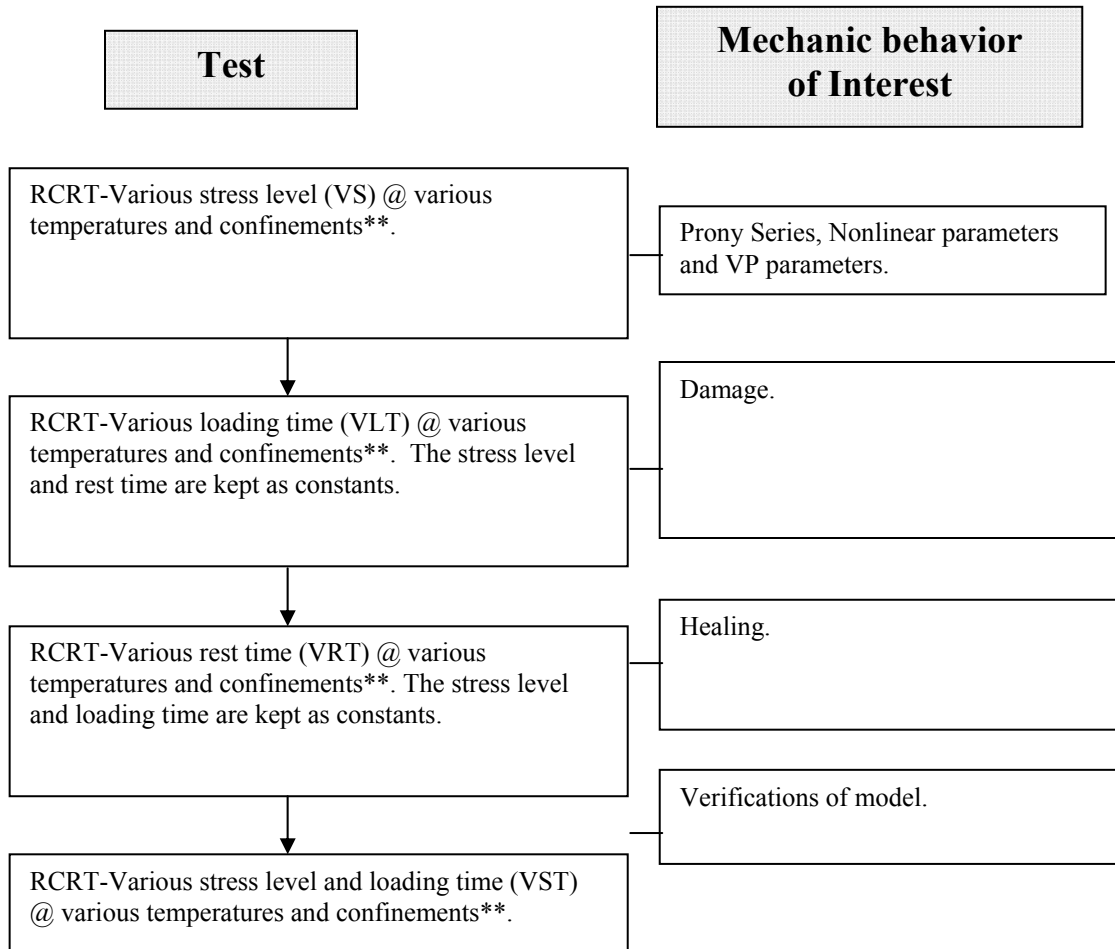


Figure F3c.1. Description of testing matrix in compression (cont.).

Table F3c.1. Dynamic Modulus Test (DMT) @ various temperatures and confinements (control the strain under $50-70\mu\epsilon$).

Temperature (°C)	Confinement Stress (kPa)	Frequency (Hz)
15	0	25
30	140	10
45	500	5
		1
		0.5
		0.1
		0.05
		0.01

Table F3c.2. Repeated Creep recovery test (RCRT) and various stress levels (RCRT-VS).

Temperatures °C	Confining Stress, kPa	Deviatoric Stress	Loading Time (sec)	Recovery Time (sec)
15	0	Starts at 103 kPa and increases by a ratio $1.1^{(n-1)}$, where n is number of cycles (See Table A).	0.1	10
30	140			
45	500			

The loading time in the VS test is 0.1 sec and then following around 10 sec resting time. The resting time should be modified depends on the material behavior. The resting time can be determined by measuring the slope of relaxation strain becomes 0.

Table F3c.3. Repeated Creep recovery test (RCRT) and various loading times (RCRT-VLT).

Temperatures °C	Confining Stress, kPa	Deviatoric Stress, kPa	Loading Time (sec)	Recovery Time (sec)
15	0	400	Starts at 0.1 sec and increases by a ratio $1.2^{(n-1)}$, where n is number of cycles.	10
30	140			
45	500			

Table F3c.4. The multiaxial stress levels for RCRT-VS. The stress levels are determined based on Gibson et al. as shown in figure F3c.2).

No. of cycle	Dev. Stress (kPa)
1	103
2	114
3	125
4	138
5	151
6	167
7	183
8	202
9	222
10	244
11	268
12	295
13	325
14	357
15	393
16	432
17	475
18	523
19	575
20	633
21	696
22	765
23	842
24	926
25	1019
26	1121
27	1233
28	1356
29	1491
30	1641

Table F3c.5. Repeated Creep recovery test (RCRT) and various rest times (RCRT-VRT).

Temperatures °C	Confining Stress, kPa	Deviatoric Stress, kPa	Loading Time (sec)	Recovery Time (sec)
15	0	400	0.1 sec	Starts at 2 sec and increases by a ratio $1.2^{(n-1)}$, where n is number of cycles.
30	140			
45	500			

Table F3c.6. Repeated Creep recovery test (RCRT) and various stress levels and loading times (RCRT-VST).

Temperatures °C	Confining Stress, kPa	Deviatoric Stress, kPa	Loading Time (sec)	Recovery Time (sec)
15	0	To be determined	To be determined	To be determined
30	140			
45	500			

This test will include random combinations of deviatoric stress, loading time and recovery time for verification purposes.

Table F3c. 7: Constant loading test (Creep Test) (CT) at combinations of temperatures, and confinements.

Temperatures °C	Confining Stress, kPa	Deviatoric Stress, kPa
15	0	100
30	140	400
45	500	1500

Table F3c.8 Monotonic test (MT) at combinations of temperatures, confinements and strain rates.

Temperatures °C	Confining Stress, kPa	Strain rate (1/sec)
15	0	Varies depending on temperature, See Table B
30	140	
45	500	

Table F3c.9: Strain rates in the MT test. Strain rates are chosen from NCState data on testing ALF mixtures.

Temperature (°C)	Strain Rate (1/Sec)
15	0.0135, 0.0015
30	0.03, 0.003
45	0.03, 0.003

Significant Results

The analysis has shown that including micro-damage healing effects is essential for predicting the fatigue life and performance of asphalt mixtures without including healing.

Significant Problems, Issues and Potential Impact on Progress

None

Work Planned Next Quarter

The focus will be on completing the extensive calibration and validation of the coupled viscoelastic, viscoplastic, and viscodamage model based on the ALF data.

Aging

Work Done This Quarter

In this quarter, a phenomenological aging model for asphaltic mixtures based on phenomenological aspects derived from experimental data and observations based on oxidation of asphalt binders has been developed. This has been achieved with coordination with Drs. Charles Glover and Amy Epps Martin from Texas A&M. The aging model incorporates the effect of oxygen content, air voids, and damage evolution. The aging model is coupled to the developed unified continuum damage mechanics constitutive equations such that viscoelasticity,

viscoplasticity, and damage evolution are strongly affected by aging. The model has been implemented into PANDA.

Significant Results

None

Significant Problems, Issues and Potential Impact on Progress

None

Work Planned Next Quarter

The focus in the coming quarter is on validating the model against existing experimental data from previous FHWA projects.

Fatigue Year 4		Year 4 (4/10-3/11)											Team	
		4	5	6	7	8	9	10	11	12	1	2		3
Material Properties														
F1a	Cohesive and Adhesive Properties													
F1a-1	Critical review of literature													TAMU
F1a-2	Develop experiment design													
F1a-3	Thermodynamic work of adhesion and cohesion													
F1a-4	Mechanical work of adhesion and cohesion				D			F						
F1a-5	Evaluate acid-base scale for surface energy calculations													
F1b	Viscoelastic Properties													
F1b-1	Separation of nonlinear viscoelastic deformation from fracture energy under cyclic loading				M&A,F,JP			JP						TAMU
F1b-2	Separation of nonlinear viscoelastic deformation from fracture energy under monotonic loading												JP	
F1c	Aging													
F1c-1	Critical review of binder oxidative aging and its impact on mixtures													TAMU
F1c-2	Develop experiment design													
F1c-3	Develop transport model for binder oxidation in pavements						P					P, JP		
F1c-4	Effect of binder aging on properties and performance											P, JP		
F1c-5	Polymer modified asphalt materials						P							
F1d	Healing													
F1d-1	Critical review of literature													TAMU
F1d-2	Select materials with targeted properties													TAMU
F1d-3	Develop experiment design													TAMU
F1d-4	Test methods to determine properties relevant to healing				D			F						TAMU
F1d-5	Testing of materials							JP						TAMU
F1d-6	Evaluate relationship between healing and endurance limit of asphalt binders							JP				P		UWM
F1d-7	Coordinate with AFM analysis				JP									WRI
F1d-8	Coordinate form of healing parameter with micromechanics and continuum damage models													TAMU
Test Methods														
F2a	Binder tests and effect of composition													
F2a-1	Analyze Existing Fatigue Data on PMA													UWM
F2a-2	Select Virgin Binders and Modifiers and Prepare Modified Binder													
F2a-3	Laboratory Aging Procedures													
F2a-4	Collect Fatigue Test Data											DP, P	JP	
F2a-5	Analyze data and propose mechanisms											P		
F2b	Mastic testing protocol													
F2b-1	Develop specimen preparation procedures						F							TAMU
F2b-2	Document test and analysis procedures in AASHTO format						F							
F2c	Mixture testing protocol													
F2d	Tomography and microstructural characterization													
F2d-1	Micro scale physicochemical and morphological changes in asphalt binders									JP				TAMU
F2e	Verify relationship between DSR binder fatigue tests and mixture fatigue performance													
F2e-1	Evaluate Binder Fatigue Correlation to Mixture Fatigue Data													UWM
F2e-2	Selection of Testing Protocols				D		F							
F2e-3	Binder and Mixture Fatigue Testing													
F2e-4	Verification of Surrogate Fatigue Test								D			F, DP		
F2e-5	Interpretation and Modeling of Data							JP					M&A	
F2e-6	Recommendations for Use in Unified Fatigue Damage Model											P		
Models														
F3a	Asphalt microstructural model													WRI
F3b	Micromechanics model													
F3b-1	Model development						JP					P		TAMU
F3b-2	Account for material microstructure and fundamental material properties													
F3c	Develop unified continuum model													
F3c-1	Analytical fatigue model for mixture design													TAMU
F3c-2	Unified continuum model										JP		M&A	
F3c-3	Multi-scale modeling										JP			M&A
	Lattice Model				DP		DP,JP							NCSU
	Continuum Damage to Fracture				DP				JP					

LEGEND

Deliverable codes

- D: Draft Report
- F: Final Report
- M&A: Model and algorithm
- SW: Software
- JP: Journal paper
- P: Presentation
- DP: Decision Point
- [x]

- Work planned
- Work completed
- Parallel topic

Deliverable Description

- Report delivered to FHWA for 3 week review period.
- Final report delivered in compliance with FHWA publication standards
- Mathematical model and sample code
- Executable software, code and user manual
- Paper submitted to conference or journal
- Presentation for symposium, conference or other
- Time to make a decision on two parallel paths as to which is most promising to follow through
- Indicates completion of deliverable x

Fatigue Year 2 - 5		Year 2 (4/08-3/09)				Year 3 (4/09-3/10)				Year 4 (04/10-03/11)				Year 5 (04/11-03/12)				Team
		Q1	Q2	Q3	Q4	Q1	Q2	Q3	Q4	Q1	Q2	Q3	Q4	Q1	Q2	Q3	Q4	
Material Properties																		
F1a	Cohesive and Adhesive Properties																	
F1a-1	Critical review of literature			JP													TAMU	
F1a-2	Develop experiment design																	
F1a-3	Thermodynamic work of adhesion and cohesion																	
F1a-4	Mechanical work of adhesion and cohesion						JP			D	F							
F1a-5	Evaluate acid-base scale for surface energy calculations													JP				
F1b	Viscoelastic Properties																	
F1b-1	Separation of nonlinear viscoelastic deformation from fracture energy under cyclic loading			D,JP	M&A				JP	M&A,F,J	JP		P	JP	M&A,D	F	TAMU	
F1b-2	Separation of nonlinear viscoelastic deformation from fracture energy under monotonic loading			JP	M&A				JP				JP	JP	M&A,D	F		
F1c	Aging																	
F1c-1	Critical review of binder oxidative aging and its impact on mixtures																TAMU	
F1c-2	Develop experiment design			D		F												
F1c-3	Develop transport model for binder oxidation in pavements		P		P,JP		P		P,JP		P		P,JP		D,M&A	F		
F1c-4	Effect of binder aging on properties and performance				JP,P		JP	D	F				P,JP		JP	D	F	
F1c-5	Polymer modified asphalt materials										P					D	F	
F1d	Healing																	
F1d-1	Critical review of literature																TAMU	
F1d-2	Select materials with targeted properties																TAMU	
F1d-3	Develop experiment design																TAMU	
F1d-4	Test methods to determine properties relevant to healing				JP				JP	D	F						TAMU	
F1d-5	Testing of materials						JP				JP			M&A,D	JP,F		TAMU	
F1d-6	Evaluate relationship between healing and endurance limit of asphalt binders	DP				DP	JP	DP			JP		P		JP	D	F	
F1d-7	Coordinate with AFM analysis									JP							WRI	
F1d-8	Coordinate form of healing parameter with micromechanics and continuum damage models															JP,D	F	
Test Methods																		
F2a	Binder tests and effect of composition																	
F2a-1	Analyze Existing Fatigue Data on PMA			DP													UWM	
F2a-2	Select Virgin Binders and Modifiers and Prepare Modified Binder			DP														
F2a-3	Laboratory Aging Procedures																	
F2a-4	Collect Fatigue Test Data		P		JP		P		P				P,DP,JP					
F2a-5	Analyze data and propose mechanisms				P			P				P			P	D	F	
F2b	Mastic testing protocol																	
F2b-1	Develop specimen preparation procedures			D							F						TAMU	
F2b-2	Document test and analysis procedures in AASHTO format			D							F							
F2c	Mixture testing protocol			D,JP	F													
F2d	Tomography and microstructural characterization																	
F2d-1	Micro scale physicochemical and morphological changes in asphalt binders						JP				JP						TAMU	
F2e	Verify relationship between DSR binder fatigue tests and mixture fatigue performance																	
F2e-1	Evaluate Binder Fatigue Correlation to Mixture Fatigue Data						DP,D	F			D	F					UWM	
F2e-2	Selection of Testing Protocols																	
F2e-3	Binder and Mixture Fatigue Testing																	
F2e-4	Verification of Surrogate Fatigue Test												D	F,DP				
F2e-5	Interpretation and Modeling of Data		JP		P		JP		P		JP		M&A					
F2e-6	Recommendations for Use in Unified Fatigue Damage Model												P			D	F	
Models																		
F3a	Asphalt microstructural model							JP								M&A	F	
F3b	Micromechanics model																	
F3b-1	Model development				JP				JP		JP		P	D	DP	F,SW	TAMU	
F3b-2	Account for material microstructure and fundamental material properties													D		F		
F3c	Develop unified continuum model																	
F3c-1	Analytical fatigue model for mixture design														M&A,D	F	TAMU	
F3c-2	Unified continuum model			JP				JP				JP	M&A	D	DP	F,SW		
F3c-3	Multi-scale modeling											JP	M&A	D		F		
	Lattice Model									DP	DP,JP						NCSU	
	Continuum Damage to Fracture									DP		JP						

LEGEND

Deliverable codes

- D: Draft Report
- F: Final Report
- M&A: Model and algorithm
- SW: Software
- JP: Journal paper
- P: Presentation
- DP: Decision Point
- [x]

	Work planned
	Work completed
	Parallel topic

Deliverable Description

- Report delivered to FHWA for 3 week review period.
- Final report delivered in compliance with FHWA publication standards
- Mathematical model and sample code
- Executable software, code and user manual
- Paper submitted to conference or journal
- Presentation for symposium, conference or other
- Time to make a decision on two parallel paths as to which is most promising to follow through
- Indicates completion of deliverable x

PROGRAM AREA: ENGINEERED MATERIALS

CATEGORY E1: MODELING

Work element E1a: Analytical and Micro-mechanics Models for Mechanical Behavior of Mixtures (TAMU)

Work Done This Quarter

In this quarter, major progress was made on the testing of field core specimens and fine asphalt mixtures.

A database was developed to document the identification data of field cores, including the pavement construction date, coring date, geometric size and photographs of cores. All field cores were firstly tested using the Corlok method to determine the total specific gravity and the accessible air voids. Table E1a.1 shows the Corlok test results of the field cores cored from the US 93 in Arizona. Since 4 replicate cores were available from each coring site, an algorithm was used to randomly select a replicate core to be tested by the X-ray Computed Tomography (CT) system to determine the representative air void content and air void distribution at the coring site.

After the X-ray CT test, each field core was trimmed into the construction lifts, and each lift was cut to a prismatic specimen to be tested using the Material Testing System (MTS). The rest of the material left from the test specimen preparation was preserved and tested for the maximum specific gravity of the field core using the Corlok method. The maximum specific gravity and the bulk specific gravity are used together to calculate the average air void content that serves as the initial value to conduct the X-ray CT image analysis in order to determine the air void distribution with pavement depth. Figure E1a.1 shows the measured air void distribution of the field core labeled A14AZ1-1BL2. The air void distribution shown in figure E1a.1 is not uniform with pavement depth but is distributed in an approximately C shape. This is due to the nonuniform compaction temperature with pavement depth. Although the asphalt mixture itself had approximately the same high temperature during compaction, the asphalt mixture was placed on a supporting layer which had a much lower temperature. As a result, the bottom side of the asphalt layer cools rapidly. In the mean time, since the top side of the asphalt layer was exposed to the air, the temperature at the layer surface also cooled in a short time. Only the center of the asphalt layer retained the high temperature. Consequently, the center of the asphalt layer was much easier to compact because of its high temperature so the center had a lower air void content; the top side and the bottom side of the asphalt layer were not as easy to compact due to the significantly decreased temperature so the air void content was much higher on the top side and on the bottom side of the asphalt layer.

Sample ID	Bulk Specific Gravity (g/cm ³)	Maximum Specific Gravity (g/cm ³)	AAV%	AV%
A13 AZ1-1A L1	2.294		6.41	
A13 AZ1-1A L2	2.314		4.25	
A14AZ1-1A L1	2.306		6.17	
A14AZ1-1A L2	2.331		2.04	
A14AZ1-1B L1	2.312	2.450	4.50	5.63
A14AZ1-1B L2	2.295	2.447	5.06	6.23
A13AZ1-2A L1	2.268	2.441	8.24	7.10
A13AZ1-2A L2	2.251	2.419	8.78	6.94
A14AZ1-2A L1	2.245		9.27	
A14AZ1-2A L2	2.252		3.39	
A13AZ1-2B L1	2.298		6.69	
A13AZ1-2B L2	2.263		5.64	
A13AZ1-3B L1	2.293		4.90	
A13AZ1-3B L2	2.306		6.81	
A14 AZ1-3A L1	2.217	2.442	9.73	9.24
A14 AZ1-3A L2	2.262	2.470	3.89	8.40
A14AZ1-3B L1	2.249		9.16	
A14AZ1-3B L2	2.269		7.70	
A14AZ1-4B L1	2.307		6.48	
A14AZ1-4B L2	2.267		8.25	
A13AZ1-4A L1	2.307		7.11	
A13AZ1-4A L2	2.238		10.19	
A14AZ1-4A L1	2.314	2.444	4.68	5.31
A14AZ1-4A L2	2.227	2.497	5.11	10.82

Table E1a.1. Corlok test results of Arizona field cores.

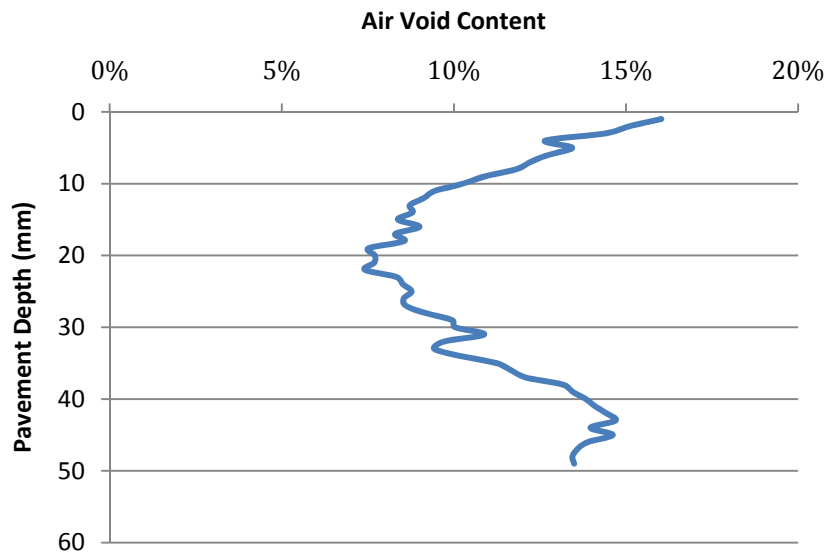


Figure E1a.1. Air void distribution of the Arizona field core A14AZ1-1BL2.

The implication of the nonuniform air void distribution is that the properties of the asphalt mixture vary with the pavement depth, which is verified using the direct tension test. When a monotonically increasing tensile load is applied as shown in figure E1a.2 to the field core specimen labeled A14AZ1-1BL2, the top side had the largest average axial strain and the center had the smallest average axial strain, as shown in figure E1a.3. The test data of measured axial strain confirmed that the properties of the asphalt mixture were not uniform with pavement depth but varying with pavement depth. For an unaged field core such as the tested one labeled A14AZ1-1BL2, the center of the asphalt layer had the highest modulus, while the top side and the bottom side had lower moduli. This finding was consistent with the C shape air void distribution.

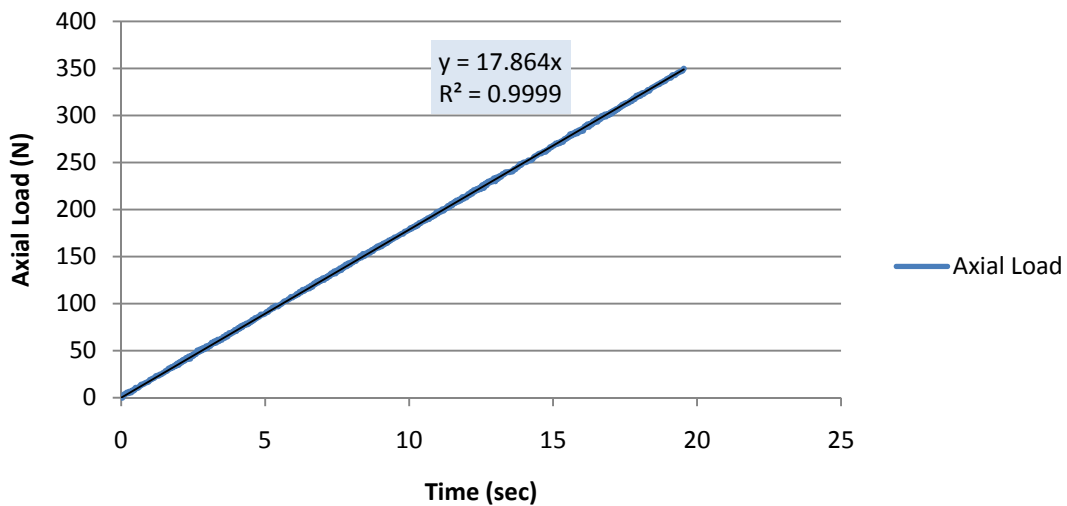


Figure E1a.2. Tensile load applied to the field core specimen A14AZ1-1BL2.

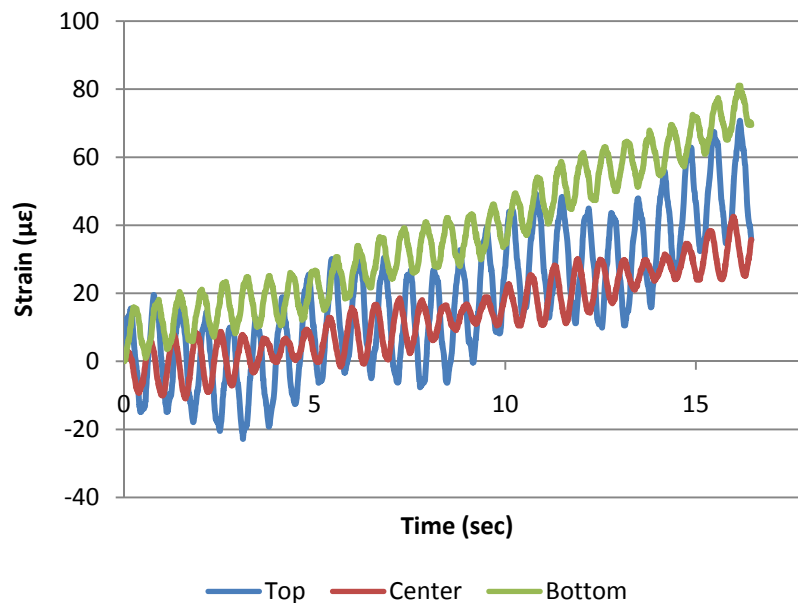


Figure E1a.3. Measured axial strain of the field core specimen A14AZ1-1BL2.

As stated in past quarterly reports, the oscillation of each axial strain curve was caused by the 2 Hz load feed back loop generating a bending moment due to the eccentricity between the applied tensile load and the internal stress distribution. Because the stiffness gradient with pavement depth, the stiffness centroid is not located at the same vertical location as the geometric centroid of the field core specimen. Instead, the stiffness centroid is located vertically above the geometric centroid as illustrated in figure E1a.4. Since the tensile load is applied to the geometric centroid of the specimen, this tensile load generates a bending moment which is the driving force of the strain oscillation.. A numerical method is under development to determine a numerical solution of the stiffness gradient with pavement depth.

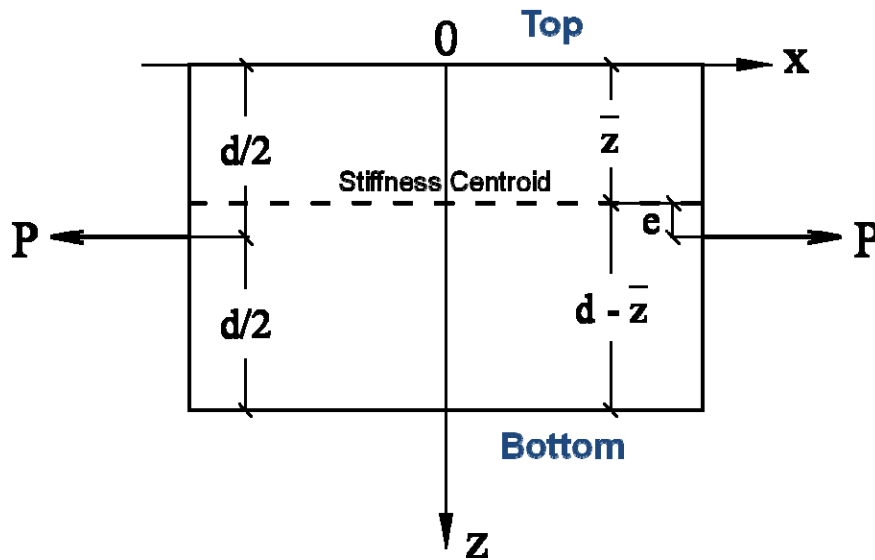


Figure E1a.4. Schematic plot of testing a field core specimen.

In addition to the field cores, the asphalt fine mixture specimens for the Dynamic Mechanical Analyzer (DMA) test were also tested by the X-ray CT system to determine their air void contents. Since the DMA specimens are cored from samples with a 6 in. diameter made by the SuperPave gyratory compactor, the DMA specimens cored from the outer circle of the 6 in diameter specimen have a larger air void content than those cored from the inner circle. This indicates that the closer to the center to the 6 in diameter gyratory specimen, the lower is the air void content. This pattern was found in both samples made with the AAD binder and samples made with the AAM binder, as shown in figure E1a.5.

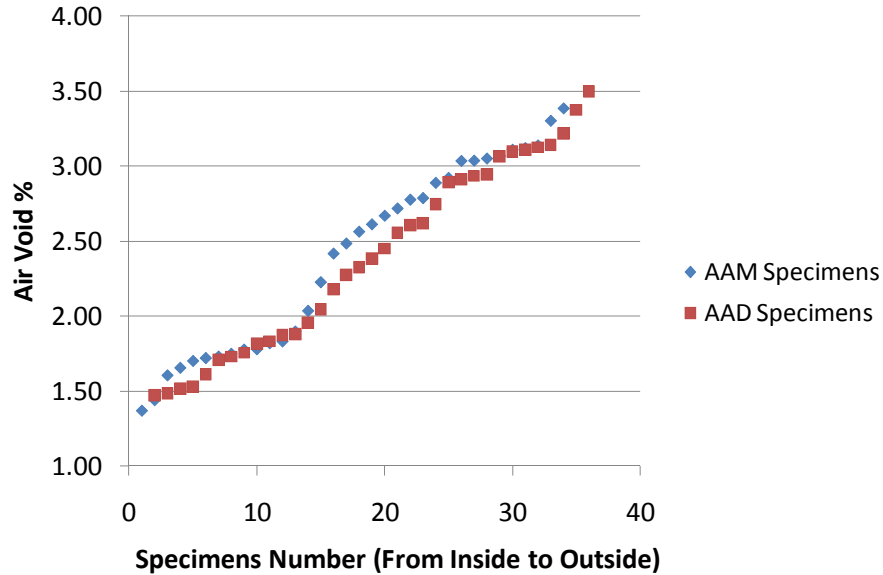


Figure E1a.5. DMA AAM and AAD specimens air void distribution.

After the DMA specimens were cored from the 6 in diameter gyratory samples, the DMA specimens were conditioned in different vacuum desiccators with various levels of constant relative humidity. The constant relative humidity in each vacuum desiccator is created by a solution whose affinity for water regulates the water vapor pressure in the closed system with little temperature fluctuation. Such a solution could be a salt solution or an acid solution. As documented in the literature, various salts and acid concentrations can generate different levels of relative humidity. When a specific solution is chosen for the vacuum desiccator, the corresponding relative humidity is achieved in the DMA specimens placed in the vacuum desiccator after an adequate period of time as illustrated in figure E1a.6.

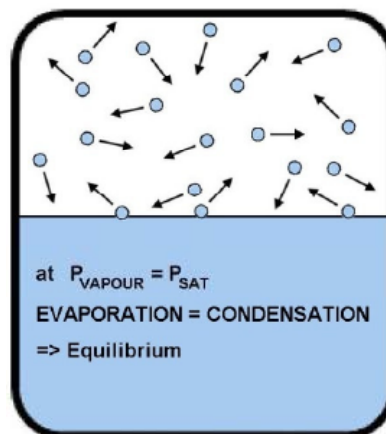


Figure E1a.6. Illustration of constant relative humidity atmosphere in closed system (ChipSensors 2010).

Initially, potassium chloride was planned to be used to condition the relative humidity in the vacuum desiccators. However, it was found that the saturated potassium chloride solution could achieve a relative humidity no lower than 80% at a room temperature. Subsequently, sulfuric acid was considered to achieve relative humidity levels lower than 80% by varying the density of the sulfuric acid solution as shown in figure E1a. 7 (Wilson 1921).

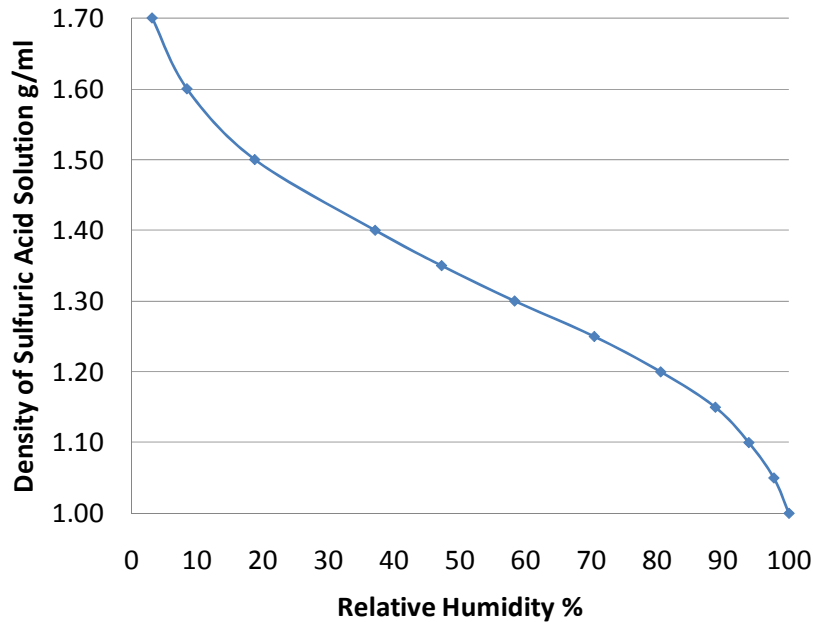


Figure E1a.7. Sulfuric acid solution density vs. relative humidity.

Although it is possible to use the sulfuric acid to achieve different levels of relative humidity, there were safety concerns associated with the sulfuric acid in the laboratory so safer alternative chemical solutions were preferred. Consequently, the three saturated salt solutions listed in table E1a.2 were finally chosen from the literature to condition the relative humidity in the vacuum desiccators (Rockland 1960; Hong 2003). Figure E1a.8 shows the DMA specimens in the vacuum desiccators conditioned at different levels of relative humidity.

Table E1a.2. Relative humidity for different chemical solutions.

Chemical Name	Solubility (g/ml)	Relative Humidity (%)
Sodium Chloride	0.37	75
Magnesium Nitrate	1.25	50
Potassium Acetate	2.81	25



Figure E1a.8. DMA specimens conditioning in desiccators.

At the same time as the equilibrium process in the vacuum desiccators, the fundamental fracture mechanics principles were used to develop a mechanistic method to evaluate the moisture sensitivity and moisture damage of fine asphalt mixtures in terms of the cohesive bond energy of the asphalt mastic and the adhesive bond energy between the asphalt binder or mastic and the aggregates. The bond energies may be back-calculated from the test data of the DMA test.

In order to back-calculate the cohesive bond energy and the adhesive bond energy, equations E1a.1 and E1a.2 were formulated by setting the energy in the damaged material (whose undamaged modulus is E_f that is the true or effective modulus of the asphalt mastic) equal to an equivalent material with a modulus of E'_f that is the damaged or nominal tensile modulus of the asphalt mastic. Equations E1a.1 and E1a.2 establish the relationships between the ratio of the damaged modulus to the initial modulus (E'_f / E_f) for the cohesive and adhesive bonds based on a controlled strain loading. These relationships were developed based on the assumption that only penny shaped cracks exist in the asphalt mastic. The presence of each crack results in two stress-free conical volumes above and below each crack in the specimen (Roylance et al. 2001).

$$\text{Cohesive crack: } \frac{E'_f}{E_f} = \left[1 - \frac{2\pi^2}{3} \frac{m}{A} \frac{\bar{C}^3}{\bar{t}} \left(1 - \frac{3E_f \Delta G_f^c}{\sigma^2 \bar{C}} \right) \right] \quad (1)$$

$$\text{Adhesive crack: } \frac{E'_f}{E_f} = \left[1 - \frac{\pi^2}{3} \frac{m}{A} \frac{\bar{C}^3}{\bar{t}} \left(\left(1 + \frac{E_f}{E_s} \right) - \frac{6E_f \Delta G_f^a}{\sigma^2 \pi \bar{C}} \right) \right] \quad (2)$$

where, \bar{t} is the average asphalt film thickness; A is the cross-sectional area of the material; m is the number of voids; $\bar{\xi} = \frac{m}{A}$ is the damage parameter, which can also be expressed as the volume of voids (air voids and cracks) divided by the total volume; \bar{C} is the average void radius; E_f is the asphalt mastic undamaged modulus; E_s is the solid or aggregate undamaged modulus; ΔG^c is the cohesive bond energy; ΔG^a is the adhesive bond energy; and σ is the applied tensile

stress. The subscript f indicates that the bond energy is associated with the asphalt binder. (Lytton et al. 2005). The viscoelastic characteristics of the DMA specimens are considered by equating the apparent dissipated pseudo-strain energy with the true dissipated pseudo-strain energy which involve the use of the measured moduli and phase angles as they change with repeated loads.

During the calculation, the initial m and \bar{C} may be obtained by conducting X-ray CT image analysis. The true modulus of the specimens E_f may be obtained by conducting the nondestructive repeated direct tension (RDT) test, and E'_f may be obtained by conducting a destructive RDT test. Then the moisture susceptibility of the fine asphalt mixtures may be evaluated by analyzing the reduction in the cohesive and adhesive bond energy in the DMA specimens.

Significant Results

The air void contents of both field cores and DMA specimens were determined using the X-ray CT system. The field core specimens were nondestructively tested using the MTS for their tensile properties at the undamaged state.

The DMA specimens were conditioned in the vacuum desiccators with different levels of relative humidity. Formulations were developed to study the moisture susceptibility of the fine asphalt mixtures.

Significant Problems, Issues and Potential Impact on Progress

In some field cores, the bond between the aggregates and the binder was weak, which made aggregates to pop off during the cutting process. The weaker surfaces showed an unexpected high strain level (higher than $100 \mu\epsilon$) in the direct tension test. In order not to damage the field core specimens, a lower tensile load may be used in future tests.

The X-ray CT program used to scan the DMA specimens is broken and will not be fixed until the end of August.

The new DMA apparatus has not been delivered yet.

Work Planned Next Quarter

An analysis method will be developed next quarter to determine the nonlinear stiffness gradient of field core specimens with pavement depth, which may have the patterns shown in figure E1a.9. The master curves of the magnitude and phase angle of the mixture modulus will be constructed at each pavement depth.

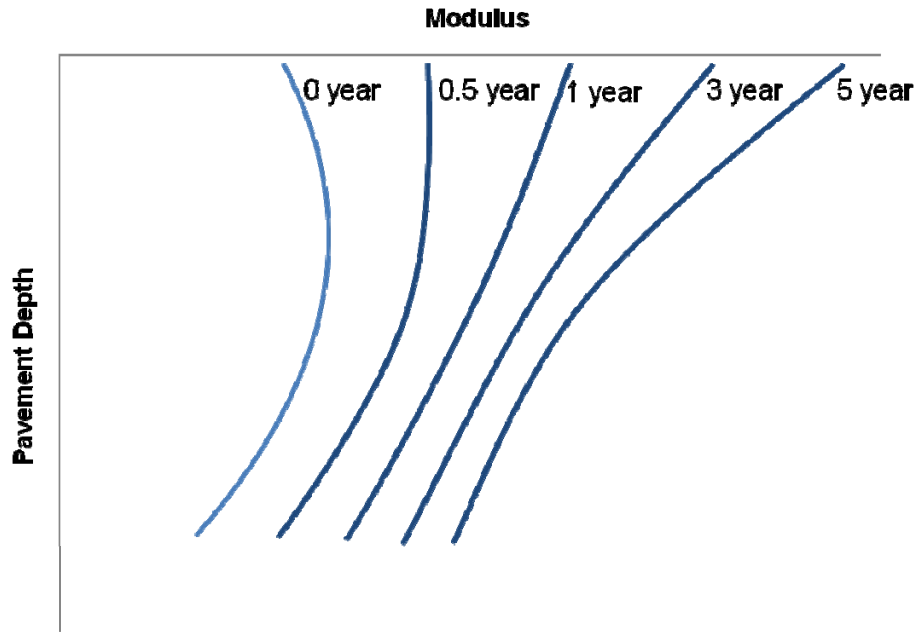


Figure E1a.9. Expected patterns of modulus with aging.

The DMA specimens for the extended experiment will be fabricated. The DMA tests will start from the beginning of August with the arrival of the new DMA test apparatus.

References

ChipSensors, 2010, Available at <http://www.chipsensors.com>, accessed July 2010.

Hong, Tran D., 2003, Saturated salt solutions for humidity control and the survival of dry powder and oil formulations of *Beauveria bassiana* conidia. *Journal of Invertebrate Pathology*, 89, 136–143.

Lytton, R. L., A. E. Masad, C. Zollinger, R. Bulut, and D. N. Little, 2005, Measurements of Surface Energy and its Relationship with Moisture Damage. Technical Report No. FHWA/TX-05/0-4524-2.

Rockland, Louis B., 1960, Saturated Salt Solutions for Static Control of Relative Humidity between 5° and 40° C. *Analytical Chemistry*, 32, 1375.

Royslance, D., 2001, *Introduction to Fracture Mechanics*. Department of Materials Science and Engineering, Massachusetts Institute of Technology, Cambridge, MA.

Wilson, Robert E., 1921, Humidity Control by Means of Sulfuric Acid Solutions, with Critical Compilation of Vapor Pressure Data. *Journal of Industrial and Engineering Chemistry*, 13 (4), 326–331.

Work element E1b: Binder Damage Resistance Characterization (DRC) (UWM)

Subtask E1b-1: Rutting of Asphalt Binders

Work Done This Quarter

Work completed this quarter included additional trial blends of the base binder with the elastomeric polymer, plastomeric polymer, and ground tire rubber (GTR) at the calculated percent modifier based on data collected last quarter. The targeted true grade was $PG\ 76.5 \pm 0.5$ °C. Mixtures containing coarse and fine gradations selected last quarter were prepared using limestone and granite aggregates at three asphalt contents to determine optimum asphalt content for each combination of aggregate type and gradation. Additional limestone mixes of each gradation were compacted at the determined optimum asphalt content, then cut and cored in a fashion similar to preparation for performance testing. The percent reduction in air voids from the total specimen to the cut and cored specimen was determined. All future compactions will account for this reduction by specifying the required air voids for the specimens to be tested for rutting performance. The cut specimens were also imaged and analyzed for number of contact points and aggregate orientation in preparation for future analysis.

Significant Results

Binder Modification

The additional blends of all three modifiers showed that true grade of the rolling thin film oven (RTFO)-aged material is not completely linear and that linear interpolation of percent modifier required to achieve the targeted true grade was not consistent. The elastomeric, plastomeric and GTR at calculated percentages to target 76.5 ± 0.5 °C resulted in 79.3, 74.0 and 79.3, respectively. This provides a better understanding of the relationship of percent modifier to true grade for each modification type and will allow for slight adjustments according to this new, nonlinear relationship to achieve the targeted true grade.

Mixture Analysis

The additional limestone coarse (LSC) and limestone fine (LSF) mixes compacted at the determined optimum asphalt content were split into two sets: one for cutting and coring to determine the percent reduction in air voids from the entirety of the specimen to the cored section, and the second for digital imaging of the cross-section of the mixtures to analyze additional internal characteristics, i.e., aggregate-to-aggregate contact points. Results from each of the specimens are summarized in tables E1b-1.1 and E1b-1.2.

Table E1b-1.1. Limestone mixture density data.

Sample ID	% Air Voids (uncut)	Average	% Air Voids (cored)	Reduction in Air Voids (%)
LSF_9.0_a	8.1	7.8	5.9	1.9
LSF_9.0_b	7.4			
LSF_10.0_a	8.2	8.1	6.7	1.4
LSF_10.0_b	8.0			
LSC_8.0_A	7.0	6.6	5.0	1.6
LSC_8.0_B	6.2			
LSC_9.0_A	7.8	7.7	5.6	2.1
LSC_9.0_B	7.6			

Table E1b-1.2. Limestone mixture imaging data.

Sample ID	Contact Pts.* (uncut)	Average No. Con. Pts.	Normalized to 4"x6" area	Contact Pts. (cored)	Average No. Con. Pts.	% Change**
LSF_9.0_b1	257	275.0	165	136	150	-9.27
LSF_9.0_b2	293					
LSF_10.0_b1	252	283.5	170	146	152.5	-10.52
LSF_10.0_b2	315					
LSC_8.0_B1	539	501.5	301	322	307.5	1.99
LSC_8.0_B2	464					
LSC_9.0_B1	457	513.0	308	255	303	-1.75
LSC_9.0_B2	569					

* Contact points were defined by aggregates ≥ 4.75 mm.

** Change in number of contact points between normalized uncut samples to cored samples.

A clear division is seen between gradations when observing the normalized contact points and the percent change in the number of contact points, regardless of similar percent air voids found in the cored samples. The fine gradation shows a smaller number of contact points and a higher reduction in the number of contact points from the uncut image to the digitally cored image. This is counterintuitive, as the cored samples show a decrease in air voids, which is indicative of an increase in density. Along with this increased densification, a greater number of contact points is expected. It is suspected that this is caused by particle segregation since a constant minimum equivalent diameter (4.75 mm) is used for both the coarse and fine gradations. Perhaps a number of these larger aggregates are moved to outside the cored image/area during gyratory compaction. Further investigation into spatial distribution of aggregates is needed to determine if this is the cause for the significant difference in number of contact points observed before and after coring. At this time, this unique observation is indicative of the potential for internal

aggregate structure to further identify specimen properties beyond density and perhaps explain performance.

Two replicates (a and b; A and B) of mixture specimens for cutting, coring and imaging were prepared as shown in figure E1b-1.1, with one specimen cut and cored and the other sliced vertically for image analysis.



(a)



(b)

Figure E1b-1.1. Photographs. Limestone mixes: (a) before cutting and coring; and (b) after cutting and coring.

The purpose of slicing vertically to image is to verify the sensitivity of the imaging software used for this task and the capability of differentiating between samples of various densities based on the additional characterization of contact points. The percent change shown in table E1b-1.2 related to the number of contact points is based on the digitally cored image relative to the uncut image.

The process of digital coring is illustrated in figure E1b-1.2. This image verification proves the imaging software is a reliable tool for further investigation of internal aggregate structure, which this task intends to monitor in addition to binder properties to provide a more in-depth understanding of both binder properties and aggregate structure influence on pavement performance.

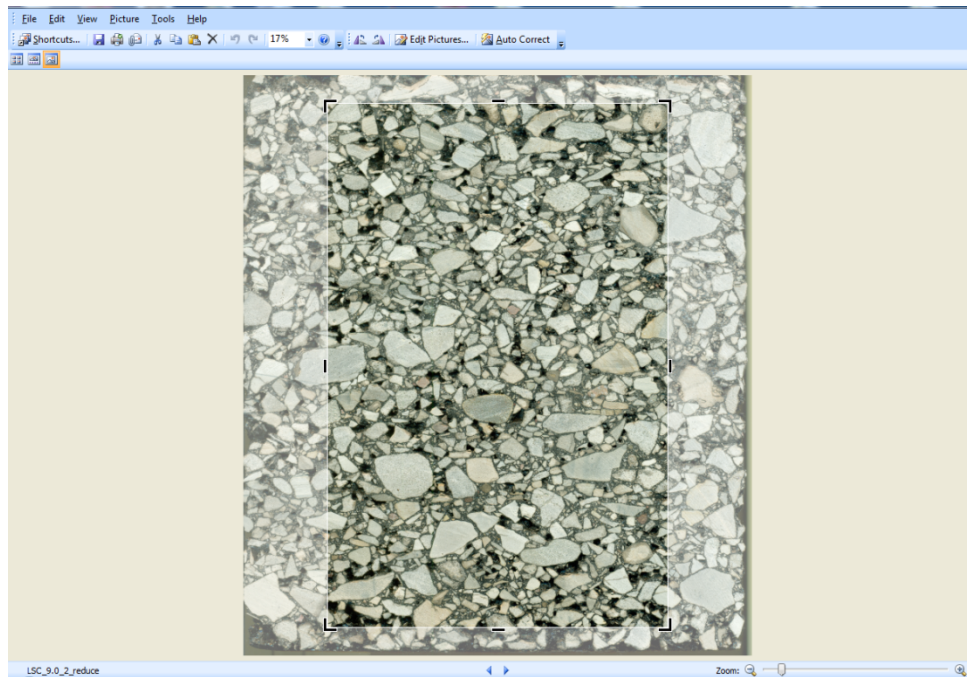


Figure E1b-1.2. Screen shot. Digital coring of imaged specimen.

Significant Problems, Issues and Potential Impact on Progress

The targeted true grade of the modified binders was not met within the \pm tolerance selected, thus additional blends must be produced and true grade confirmed prior to production of mixtures with the modified binder. This is expected to take place immediately and not significantly impact overall progress of the task.

Work Planned Next Quarter

During the coming quarter the research team will address final blends of modified binders, Multiple Stress Creep and Recovery (MSCR) and Repeated Creep and Recovery (RCR) testing of neat binder and its modified forms (elastomeric polymer, plastomeric polymer, and GTR), preparation of fine and coarse limestone mixes with the neat and modified binders, and flow number (FN) testing and image analysis of the prepared mixtures.

Subtask E1b-2: Feasibility of Determining Rheological and Fracture Properties of Thin Films of Asphalt Binders and Mastics using Simple Indentation Tests

Work Done This Quarter

The research team finished the indentation testing according to the experimental plan developed last quarter. The Dynamic Shear Rheometer (DSR) testing needed to compare/validate the indentation test has been completed at both 20 °C and 30 °C. Using the indentation experiments at 20 °C and 30 °C, the creep compliance master curve could be generated as shown in figure E1b-2.1. The actual material properties were obtained by using testing with three different container sizes.

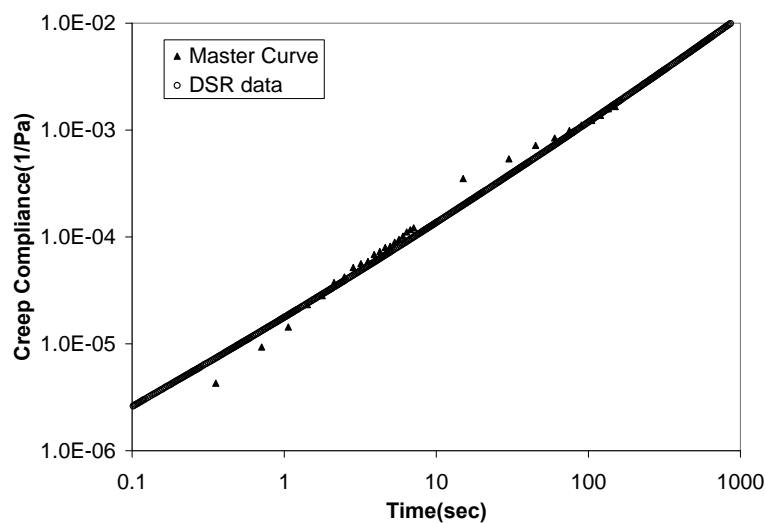


Figure E1b-2.1. Graph. Creep compliance master curves developed from the indentation experiments at 20 °C and 30 °C.

Since conducting the test with three different sizes is tedious, it is desirable to reduce the amount of testing. Hence, a single test with a particular size is preferable provided there is an appropriate method to account for size effects. Finite element (FE) modeling could be used to study this effect in detail. Last quarter, the FE model of the indentation test for a sample with height of 1.7 cm was developed in Abaqus and is being used to generate simulations with different material properties to account for size effects. The research team decided to use 1.7 cm for the height of the sample to minimize the amount of asphalt used for testing. Three approaches are being considered to account for size effects using the FE simulations:

- A single correction factor (χ) which is a function of material properties. Specifically, the single correction factor can be expressed as a function of material creep times τ_i and the weighing constants J_i of the Prony series that describe the viscoelastic behavior of the binder:

$$\chi = f(J_i, \tau_i) \quad (\text{E1b-2.1})$$

- A quasi-elastic approach where the correction factor is expressed as a function of depth of indentation and time. Currently, this method shows very promising results. Simulations of different viscoelastic materials indicate that the correction factor for the displacements in the indentation test can be obtained by a simple equation.
- Using the simulations as a look-up table to account for the size effects that are observed in experiments. The results obtained from the indentation experiment are compared with FE simulations. The material property of the FE modeling simulation that matches closely with the experiment is used as the actual creep compliance.

The importance of the initial contact of the indenter with the asphalt sample surface has been identified and different methods to improve the contact were considered. Currently, the glycerin that is used as lubricant to reduce the frictional forces is used as a marker to identify the contact. The indenter is slowly lowered toward the asphalt surface and the sample is shaken horizontally to see if the glycerin has left any mark. Any mark of the glycerin on the surface confirms that the indenter is in contact with the sample. However, there is a need to improve the system since it is subjective in nature. The research team is developing a counterweight system to address this issue.

In the new procedure, before starting the experiment the indenter shaft is attached to a pulley system with counterweights to make the shaft and indenter float freely. The indenter shaft is then lowered toward the sample surface until it touches the sample. Note that the indenter and shaft are floating freely. Therefore, there is no preloading or pre-indenting of the asphalt surface, which could significantly improve the initial contact. Efforts will focus next quarter on implementing this procedure and changes to the indentation test.

The research team worked on developing a methodology to estimate the nonrecoverable creep compliance (J_{nr}) from the creep compliance calculated from the indentation experiments. A Burgers model, as shown in figure E1b-2.2, was used to fit the creep data obtained from the indentation experiments.

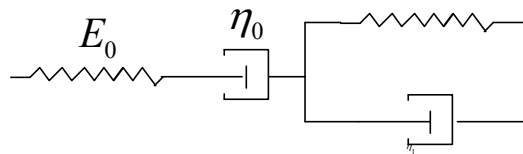


Figure E1b-2.2. Illustration. Burgers model.

The creep compliance for a Burgers model is as shown below:

$$J(t) = \frac{1}{E_0} + \frac{t}{\eta_0} + \frac{1}{E_1} \left(1 - e^{-\frac{E_1 t}{\eta_1}} \right) \quad (\text{E1b-2.2})$$

The J_{nr} is defined as the permanent deformation or the $J(t)$ as $t \rightarrow \infty$. Thus, if the loading at constant stress is for t_1 seconds, then we have:

$$J_{nr} = \frac{t_1}{\eta_0} \quad (E1b-2.3)$$

Choosing t_1 equal to 1 second, then J_{nr} is equal to $\frac{1}{\eta_0}$.

Initially, the indentation experiments conducted at 30 °C were compared with the DSR Multiple Stress Creep and Recovery (MSCR) data at 30 °C. However, it was observed that in the MSCR test at 30 °C, the material does not completely relax in 9 seconds and therefore a poor correlation was obtained. When the MSCR tests at 64 °C were compared to the indentation test at 30 °C, a fairly good correlation was obtained for both stress levels 100 Pa and 3200 Pa, as shown in figures E1b-2.3 and E1b-2.4, respectively.

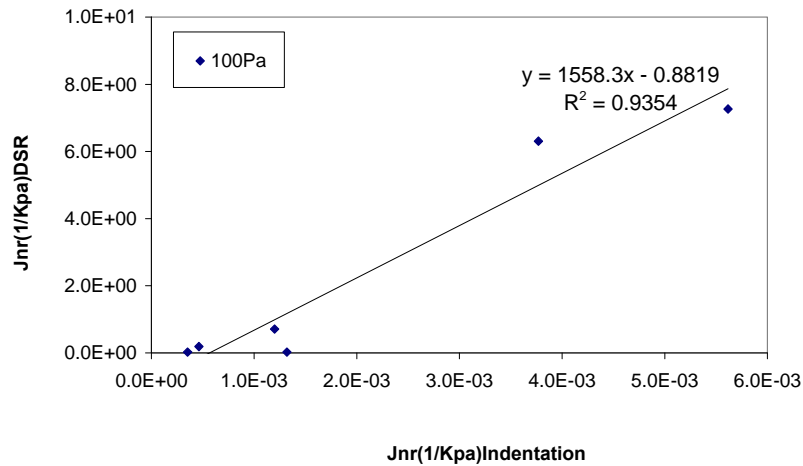


Figure E1b-2.3. Graph. Correlation of the J_{nr} values obtained from indentation with the MSCR values at 64 °C and $\sigma=100$ Pa.

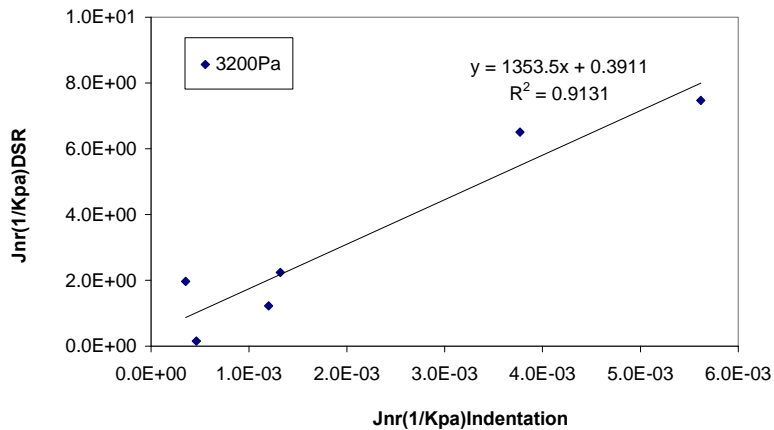


Figure E1b-2.4. Graph. Correlation of J_{nr} values obtained from indentation with DSR data at 64 °C and $\sigma=3200$ Pa.

Significant Results

The initial contact issue of the indentation test could be improved by using the glycerin solution as a marker, but a new counterweight system is designed to improve the system and resolve this problem. The counterweight system can also be used to run tests at higher temperatures since very small net loads can be applied after counterbalancing the self-weight of the indenter. Preliminary results indicate that the J_{nr} values from MSCR test can be correlated with J_{nr} values obtained from indentation measurements by using a Burgers model fit.

Significant Problems, Issues and Potential Impact on Progress

None.

Work Planned Next Quarter

Work in the next quarter will focus on the following tasks:

- The binders used to compare the J_{nr} values were either very stiff or soft. Hence, the gap in performance needs to be filled by testing new binders.
- Use the newly proposed counterweight system to test whether the contact can be improved and also if the tests can be run at temperatures above 30 °C.
- Complete the simulations and propose an appropriate method to account for the size effects.

Work Element E1c: Warm and Cold Mixes

Subtask E1c-1: Warm Mixes

Work Done This Quarter

Efforts focused on measuring the influence of warm mix additives on indicators of asphalt binders' workability and performance. For asphalt workability testing, further development of the procedure for the lubricity test addressed the issues related to repeatability and identified the experimental factors with significant impact on test results. Repeatability issues were addressed by modifying the procedure to test at a constant gap and monitoring normal force. For a given set of testing conditions (temperature and speed), this change has allowed for consistent measurement of both normal force and speed. The research team also focused on identification of the effects of testing speed and temperature. Testing parameters included three levels of temperature (90 °C, 110 °C and 135 °C), three speeds (10 rpm, 20 rpm and 40 rpm), and two replicates. The materials selected for the testing included two binders (PG 64-22 and PG 76-22) and two commercial warm mix additives. At the time of this report the testing matrix was 75% complete.

Asphalt binder performance testing included evaluation of reduced production temperatures on rheological properties and the impacts of warm mix asphalt (WMA) additives on asphalt binder adhesion under dry and wet conditions. A testing matrix was developed to evaluate the impacts of reduced aging temperature during the short-term aging procedure (rolling thin film oven (RTFO)). The aging temperatures used range from 105 °C to 163°C, and the changes in rheological properties were measured at high, intermediate, and low temperatures using standard PG tests. In addition, the Multiple Stress Creep and Recovery (MSCR) test was run at the climatic grade temperature. Materials tested include two sources of asphalt and three WMA additives.

The impacts of WMA additives on adhesion before and after moisture conditioning were evaluated using the Bitumen Bond Strength (BBS) test. Materials evaluated included two binders—PG 64-22 and a styrene-butadiene-styrene (SBS)-modified PG 64-22—and three WMA additives. All testing was conducted on a granite rock substrate with moisture conditioning at 40 °C for 24 hours. This testing is part of a collaborative effort planned by UW–Madison and University Nevada, Reno, which includes evaluation of the impacts of WMA on moisture damage of asphalt mixes.

Significant Results

The coefficient of internal friction (lubricity) was measured for both neat and SBS-modified base binders including Revix and Rediset, two WMA additives classified as surfactants. The relationship between coefficient of friction and temperature is presented in figure E1c-1.1. The plot includes values of coefficient of friction measured at 20 rpm, which was chosen because it allowed for the smallest variation in normal force and torque measurements.

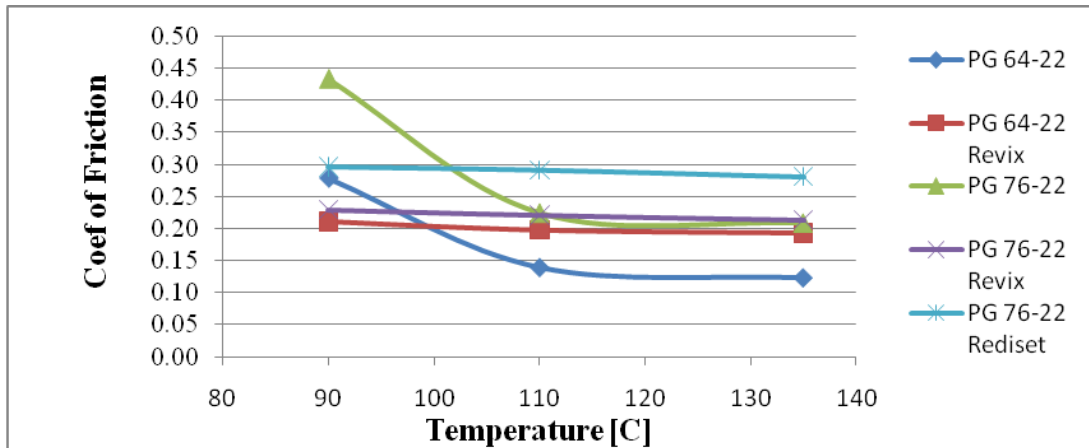


Figure E1c-1.1. Graph. Coefficient of friction versus temperature for conventional and WMA binders.

Results demonstrate that the surfactant-based WMA additives cause less temperature sensitivity and substantial reductions in coefficient of friction at low testing temperatures. This effect is most prevalent in the PG 76-22 series binders, which demonstrate reductions of 33% and 50% for the Rediset and Revix additives, respectively. At higher testing temperatures, the effect of WMA additives on lubricating properties of the binders is not as clear.

The relative impacts of asphalt binder workability parameters, viscosity and coefficient of friction, and mixture gradation on mixture workability as measured by the Construction Force Index (CFI) were evaluated using a regression model. Based on the coefficient of friction results presented in figure E1c-1.1, the regression analysis conducted included only compaction temperatures of 90 °C and 110 °C. The details of the model and a plot of predicted versus measured is presented in table E1c-1.1. As explained in earlier reports, Beta is an indicator of the aggregate gradation curve and is calculated from fitting a Weibull distribution curve to the sieve size analysis.

Table E1c-1.1. Summary of regression statistics – CFI.

Model CFI				
Parameter	Coef	SE Coef	T	P
Constant	-537.9	93.2	-5.77	0.000
Friction	554.5	248.6	2.23	0.040
Viscosity	0.007	0.003	2.15	0.047
Beta	133.4	14.4	9.27	0.000
R²	87.2%			

SE = standard error.

Regression results show that the equation constant and all three material parameters are statistically significant at a 95% confidence level. The R^2 of the model, 87.2%, also indicates that the gradation and binder parameters adequately explain changes in mixture workability. Consistent with previously presented work, the gradation parameter, Beta, appears to have substantially more influence on workability relative to the binder properties. As temperature increases and the sensitivity of the factors that influence asphalt binder workability decreases, it is expected that the effects of gradation will become even more prominent relative to other components of the model.

Preliminary results indicate that the reduced production temperatures associated with WMA have the largest impact on the high-temperature performance of the asphalt binder. Standard PG tests indicate that reducing the RTFO aging temperature from 163 °C to 105 °C results in a decrease in continuous PG grade temperature ranging from 3.5 °C to 6.5 °C; in all cases, this range of values resulted in a one grade high-temperature PG reduction. As shown in figure E1c-1.2, results from the MSCR test demonstrated similar trends.

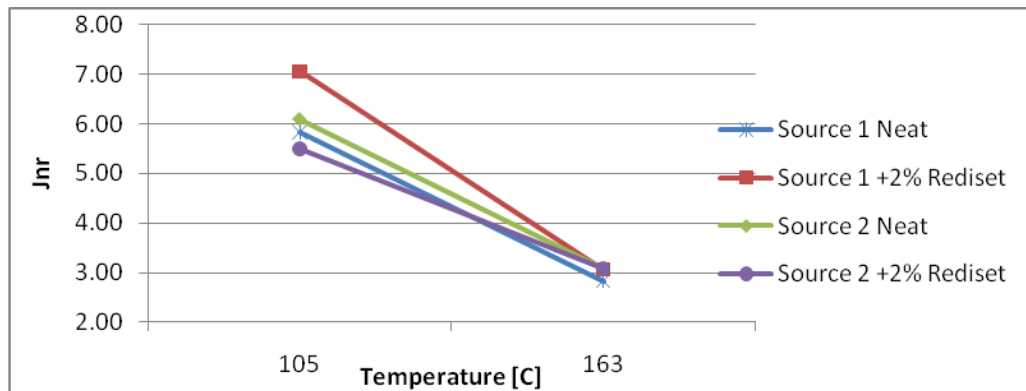


Figure E1c-1.2. Graph. Effect of RTFO aging temperature on nonrecoverable creep compliance (J_{nr}) – MSCR at 3200 kPa and 64 °C.

Results presented in figure E1c-1.2 show that reduced aging temperatures lead to significantly reduced resistance to permanent deformation as measured by the J_{nr} . The only clear effect of WMA additive or asphalt binder source is observed for the “Source 1 +2% Rediset” binder, which shows values of J_{nr} similar to the other materials tested after aging at 163 °C but substantially different after aging at 105 °C. The softer binder produced by lower aging temperatures marginally improved low- and intermediate-temperature properties evaluated on pressure aging vessel (PAV)-aged materials by approximately 1 °C to 2 °C on a continuous PG grading scale.

Statistical analysis of the adhesion testing results indicates that pull-off tensile strength (POTS) is significantly affected by both base binder type and presence of a WMA additive. In addition, it was verified that the effects of WMA additives on tensile strength were statistically significant, with increases in adhesion caused by Rediset and Advera and decreases due to the use of RV-1.

Results in terms of the ratio of wet tensile strength to dry tensile strength are presented in figure E1c-1.3.

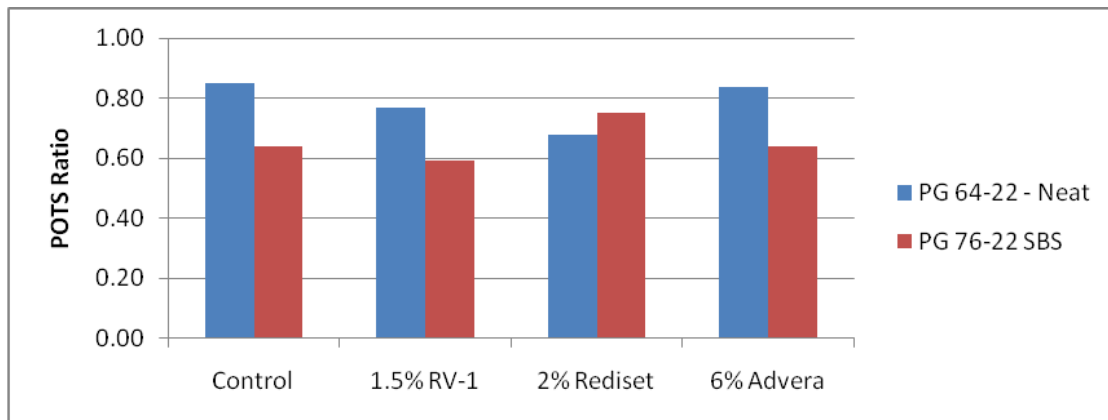


Figure E1c-1.3. Chart. Impact of WMA additives and modification on moisture susceptibility. (POTS Ratio = wet-to-dry POTS.)

Figure E1c-1.3 indicates that the binder type and additive type have some significant effects on moisture effects and POTS values. The use of the PG 76-22 SBS binder and Rediset has the most significant impact on moisture damage. This is partly consistent with the observation that the modified binder demonstrated high dry tensile strength of mixtures, but more moisture susceptibility relative to the neat PG 64-22. Relative to the effect of binder type, WMA additive type has little impact on POTS. The relationship between these results and mixture performance will be evaluated in the future.

Significant Problems, Issues and Potential Impact on Progress

None.

Work Planned Next Quarter

The following activities are planned for next quarter:

- *Lubricity*. Development of the lubricity test procedure will continue. Upon completion of the initial testing matrix, specific testing speeds and temperatures will be selected and the repeatability and reproducibility of the test established. Tests will also be conducted to evaluate the impacts of additive concentration and short-term aging on selected WMA additive/asphalt binder combinations.
- *Asphalt binder performance*. Work will continue in evaluating the moisture damage and aging temperature studies. The research team expects to conduct mixture testing at different short-term aging temperatures to compare to the effects observed in binder testing.

- *Field work.* It is anticipated that Wisconsin DOT will be constructing warm mix projects next quarter. The research team has an agreement in place and agency approval to sample materials and measure emissions/energy consumption on these projects.

Subtask E1c-2: Improvement of Emulsions' Characterization and Mixture Design for Cold Bitumen Applications

Work Done This Quarter

The focus of this quarter's work continued to be on evaluation of the construction properties of emulsions and laboratory measurement of chip seal performance. Emulsion testing included measurement of viscosity and development of adhesion. The dependence of emulsion viscosity on shear rate was evaluated using the Brookfield rotational viscometer at temperatures ranging from 30 °C, 45 °C and 60 °C, and shear rates ranging from 4.65/sec to 458/sec. Each combination was replicated twice and separate samples were used for each temperature. Due to the thixotropic nature of emulsions, each sample was subjected to a shear rate of 46.5/sec for 40 minutes to ensure steady-state viscosity is reached. The No. 21 spindle was used for all tests. This procedure was first proposed in a technical bulletin written by Salomon (Salomon and Palasch 2002). The test was conducted on two emulsions used for surface treatments (CRS-2 and HFRS-2L) and one used in cold mixes (CSS-1).

In terms of adhesion testing, the Bitumen Bond Strength (BBS) testing matrix provided in the Year 3 work plan was completed. Results will be summarized and reported next quarter. In addition, the research team worked with the Emulsion Task Force to finalize an AASHTO standard test procedure for the BBS test. The research team plans to submit the standard to AASHTO with the task force's endorsement.

A study began that focuses on identifying testing conditions and material properties that significantly affect the results of the sweep test. Testing conditions include: aggregate gradation, emulsion application rate, and curing time. Material properties such as aggregate mineralogy, emulsion chemistry and modification are being evaluated. The testing matrix is approximately 75% complete; results will be submitted as a paper to the 2011 TRB Annual Meeting.

Work on use of emulsion in cold mix applications also began. A draft literature review report focused on mix design using the Superpave gyratory compactor (SGC) for cold in-place recycling was submitted by University of Nevada, Reno for review. Also, the aforementioned viscosity test and aggregate coating test were conducted using a CSS-1H emulsion. The coating test was conducted per AASHTO T 195 at four emulsion contents on a fine-graded granite aggregate blend used in HMA.

Significant Results

Viscosity testing was conducted at a variety of temperatures to evaluate the thixotropy at a constant shear rate and shear dependency. To evaluate thixotropy, or change in viscosity over time, the HFRS-2L and CRS-2 emulsions were subjected to a shear rate of 46.5/sec for 40

minutes at a temperature of 30 °C. It was assumed that this period of time was adequate to reach the steady-state viscosity. The dependence of viscosity on time is shown in figure E1c-2.1.

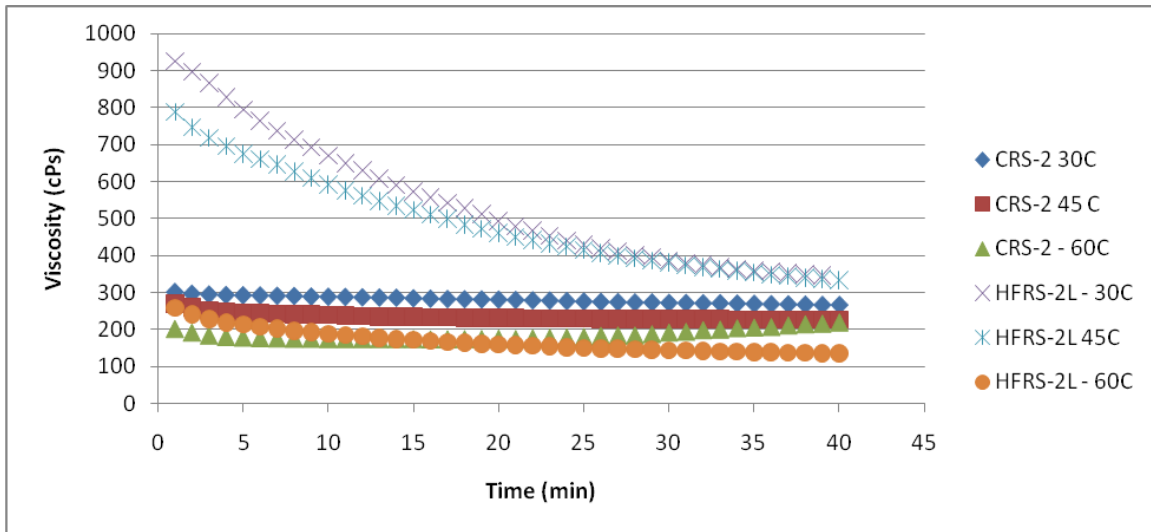


Figure E1c-2.1. Graph. Thixotropy at different temperatures for CRS-2 and HFRS-2L emulsion viscosity (shear rate 46.5/sec; spindle No. 21).

Results presented in figure E1c-2.1 clearly show the effects of emulsion type and testing temperature on thixotropy. The high float emulsion exhibited significantly more time dependence and temperature sensitivity relative to the cationic emulsions. The most prominent differences were observed after increasing the testing temperature to 60 °C. At this temperature, the HFRS-2 displays significantly lower viscosity and less thixotropy. Relative to the HFRS-2L, the viscosity of the CRS-2 showed little dependence on time or temperature. The relationship between viscosity and shear rate for these materials is presented in figure E1c-2.2 at three different temperatures.

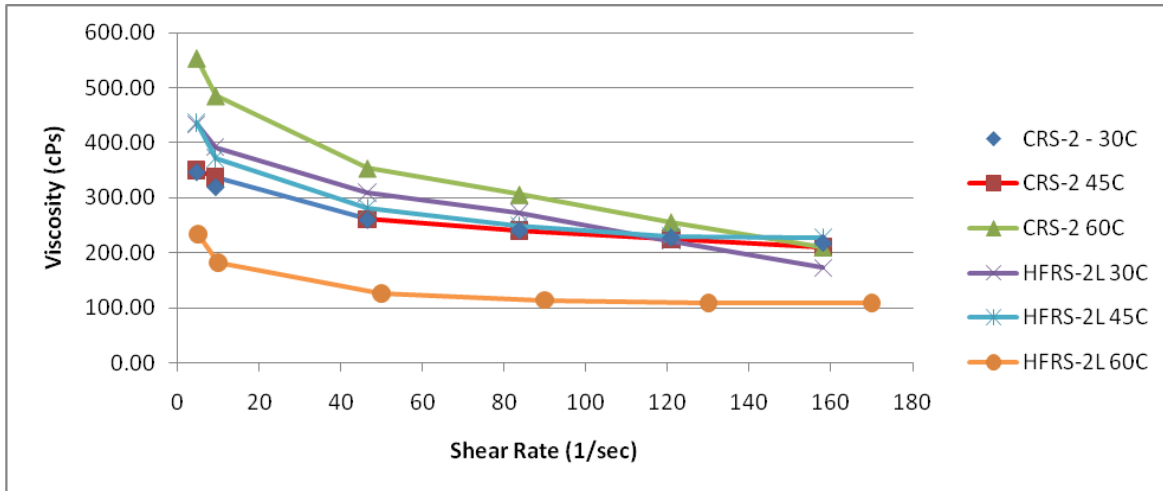


Figure E1c-2.2. Graph. Viscosity versus shear rate for CRS-2 and HFRS-2L emulsion at three testing temperatures.

Results presented in figure E1c-2.2 show that at all three testing temperatures, both emulsions exhibit non-Newtonian behavior. Also, increasing the temperature from 30 °C to 45 °C had little impact on viscosity. However, a relatively large difference between emulsions is observed at 60 °C, with the CRS-2 showing highest viscosity and the HFRS-2L the lowest. Based on previous work by Salomon, it is hypothesized that at 60 °C the viscosity of the CRS-2 increases because the emulsion is starting the breaking process. This is also evident in the plot of viscosity versus time presented in figure E1c-2.1, which shows CRS-2 reach a steady-state viscosity after approximately 20 minutes, after which the viscosity gradually increases—an indicator of emulsion breaking (Salomon and Palasch 2002). The repeatability was acceptable for both the steady-state viscosity and the viscosity measured at different shear rates, with coefficients of variation of approximately 10%.

Preliminary results of the sweep test study to date are provided in figure E1c-2.3. The trends shown indicate both emulsion type and aggregate gradation significantly impact the value of percent aggregate loss measured. Conversely, emulsion application rate had little impact on aggregate loss for both fine and coarse gradations. The terms “fine” and “coarse” refer to the gradation, and the letters “G” and “L” are used to differentiate between granite and limestone aggregates. Results are the average of three replicates; the standard deviation is presented using error bars.

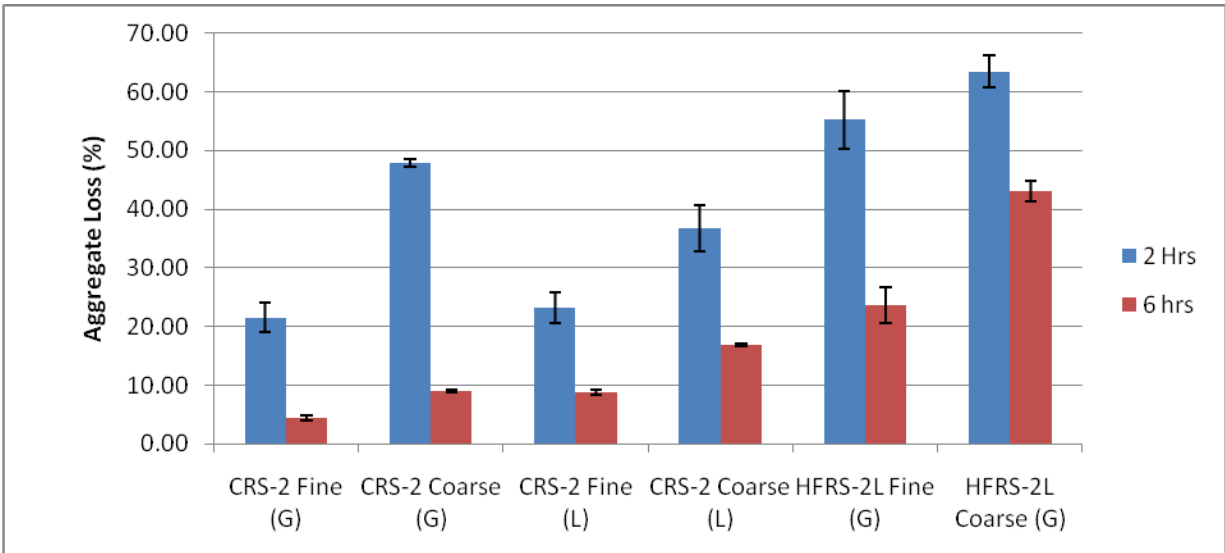


Figure E1c-2.3. Chart. Summary of sweep test results to date (medium application rate).

Results in figure E1c-2.3 indicate that there are significant effects of curing time, emulsion type and aggregate gradation. In all cases, the aggregate loss is lower after 6 hours of curing, indicating that between 2 hours and 6 hours the emulsion is gaining strength and bonding. The most prominent result to note is the effect of emulsion type. For the medium application rate the HFRS-2L and the CRS-2 exhibit similar levels of moisture loss, indicating a similar level of physical curing. However, the HFRS-2L exhibits considerably more aggregate loss, indicating it is possible that the emulsion and aggregate are not compatible. More detailed analysis of these results will be provided pending completion of the testing matrix.

Significant Problems, Issues and Potential Impact on Progress

The research team will delay submittal of any reports until the testing matrix has been completed. The information that was to be provided in an April 2010 draft report, including results of the emulsion construction properties tests and an experimental plan for residue testing, will instead be published in journal papers in August 2010.

Work Planned Next Quarter

Work next quarter will focus on the following tasks:

- *Emulsion construction properties.* BBS and viscosity testing will continue on all new emulsions received from the field.
- *Emulsion residue properties.* Testing will be conducted to compare the rheological properties of residues collected using procedures A and B provided in the draft ASTM emulsion residue recovery standard.

- *Field testing.* The research team will attempt to work with a local contractor to implement laboratory testing protocols on materials sampled from the field and different methods of evaluating field performance of chip seals.
- *Cold mix asphalt.* The research team will continue to coordinate testing activities with UNR.
- *ARC Project Advisory Group and Emulsion Task Force activities.* The research team will continue to hold advisory group meetings and support Emulsion Task Force activities.

Cited References

Salomon, D., and M. Palasch, 2002, Kinetic Properties of Emulsified Asphalts. Technical Bulletin, Idaho Asphalt Supply Inc. Accessed 6/28/2010, <http://www.technopave.com/publications/Kinetic-Properties-of-Emulsified-Asphalts-May-2002.pdf>.

CATEGORY E2: DESIGN GUIDANCE

Work element E2a: Comparison of Modification Techniques (UWM)

Work Done This Quarter

The research team continued testing the binders included in the material library developed for this study. This library includes 17 binders from six sources, five base binder grades and 12 modified binder grades. Tests performed to date include rheological measurements using the Dynamic Shear Rheometer (DSR) according to AASHTO TP5, Multiple Stress Creep and Recovery (MSCR) tests according to ASTM D7405-08a, Binder Yield Energy Test (BYET), frequency sweep testing, Single-Edge Notched Bending (SENB) testing, and Bending Beam Rheometer (BBR) testing. The collected binders were also tested after aging according to laboratory aging techniques such as rolling thin film oven (RTFO) (AASHTO T240) and pressure aging vessel (PAV) (AASHTO R28). Table E2a.1 shows the progress in testing the binders included in the material library.

Table E2a.1. Testing matrix update.

Binder Label	BYET		MSCR		Frequency Sweep		SENB @ -12 °C		BBR @ 2 temp	
	RUN1	RUN2	RUN1	RUN2	RUN1	RUN2	RUN1	RUN2	RUN1	RUN2
A0					X	X	X	X		
A1	X	X			X	X	X	X	X	X
A2					X	X				
A3	X		X	X	X	X	X	X	X	X
A4	X	X	X	X	X	X	X	X	X	X
B0	X	X	X	X	X	X	X	X	X	X
B1	X	X	X	X	X	X	X	X		
B2	X		X	X	X	X				
C0	X	X			X	X	X	X		
C1	X	X	X	X	X	X				
C2	X	X	X	X	X	X				
D0			X	X	X	X	X	X		
D1										
D2										
E0	X	X	X	X						
E1	X	X	X	X	X					
E2	X		X	X	X					

MSCR testing was conducted on RTFO-aged binders at the base binder PG temperature in compliance with the current specifications. The relation between the percent recovery (%R) from MSCR and the BYET was also examined. Frequency sweep test was conducted at 40 °C, 34 °C, 31 °C, 28 °C, 22 °C and 16 °C for binders A1, A2 and A4, while the rest of the binders were tested at 31 °C, 28 °C, 22 °C, 19 °C and 16 °C. Low-temperature properties testing (SENB and BBR) began; however, not enough data were collected to allow for detailed analysis.

Significant Results

The MSCR results for binders tested thus far are summarized in figure E2a.1. In this figure, the specification line followed the guidelines presented at the most recent Binder ETG meeting. The relationship between %R and nonrecoverable creep compliance (J_{nr}) that separates the elastic from nonelastic behavior was defined by the equation E2a.1:

$$Y = 29.371X^{-0.2631} \tag{E2a.1}$$

The figure shows some data points that fall below the required limits for elastic modifiers. However, it also shows that binder B moved from the nonelastic to the elastic region for both one and two modification levels (B1 and B2). Binder E moved to the elastic zone only after two grade pumps (E2), while E1 stayed in the nonelastic zone. Another interesting observation was the change in binder C. Although testing for the base binder is not yet complete, current results show a significant change in the %R between C1 and C2, as the %R increased from about 15% to more than 75%. The first grade jump (C1) was achieved by polyphosphoric acid (PPA) chemical modification. The second jump was achieved by PPA+styrene-butadiene-styrene (SBS)+cross-linking—an elastomer—which explains the jump in the %R.

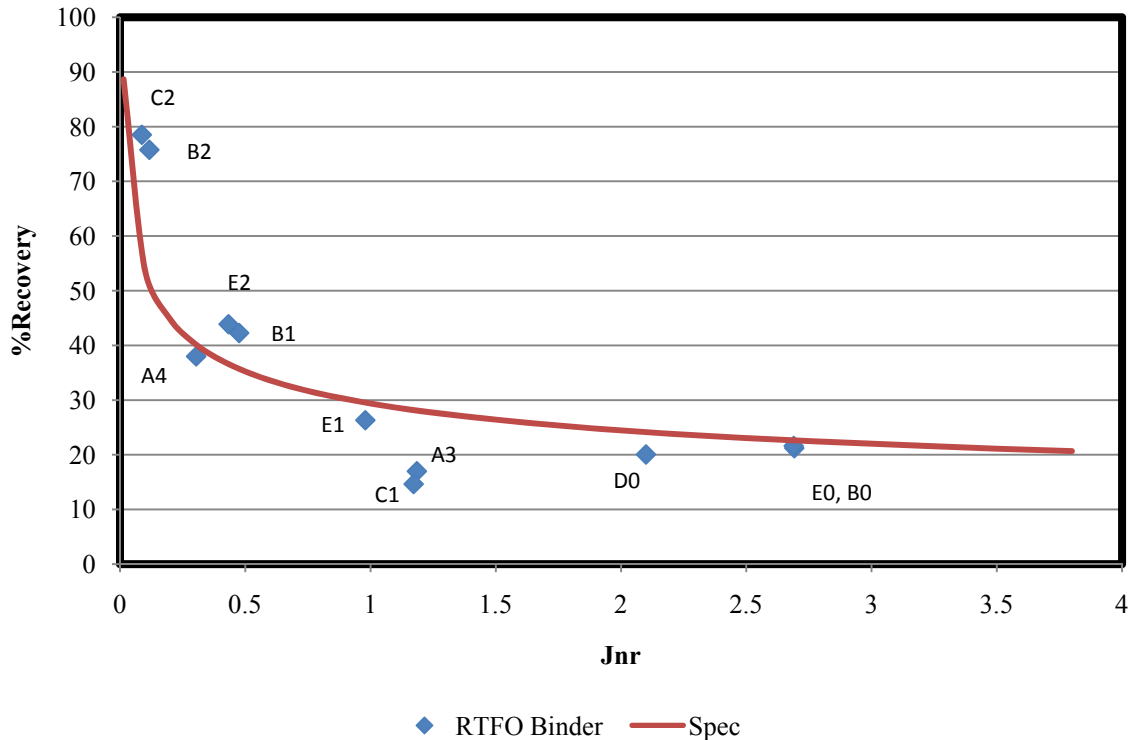


Figure E2a.1. Graph. MSCR results for RTFO binder tested at 3200 Pa and at base binder PG temperature.

To examine the relationship between the MSCR test and the BYET, the %R of the MSCR test at 3.2 kPa and the BYET energy testing results were plotted, as shown in figure E2a.2(a). The figure shows a weak relation between the two parameters with R^2 value of 0.34. However, after examining the BYET test stress-strain curves for the several binders tested, the research team decided that the use of the energy up to the maximum stress point (BYE_{peak}) might not be the best approach, as several binders accumulated considerable amount of damage in the post-peak region of the curve.

A 2000% strain was selected to calculate an alternative BYET energy rather than the maximum stress. This strain level was selected such that all the binders' stress-strain curves are post-peak. It is also important to note that the BYET testing temperature varies from one binder to another, as it is selected to be the binder intermediate PG temperature. Due to the variation in temperature, the binders are actually being tested at significantly different modulus values (G^*). It was also observed that BYET results are very sensitive to changes in modulus. Therefore, the research team decided to normalize the effect of the modulus (G^*) due to variation in BYET testing temperature by dividing the BYET energy by the G^* value for each binder. Based on these changes, three new BYET yield energy values are calculated for each binder:

- BYET energy at 20 strain (BYE₂₀).
- BYET energy/ G^* (BYE_{peak}/ G^*).

- BYET energy at 20 strain/G* (BYE20/G*).

Figures E2a.2(b) through (d) show the MSCR %R results versus these three energies. The use of the energy up to 2000% strain improved the correlation, as the R^2 value increased to 0.69. Normalizing the energy by the G^* increased the correlation to 0.52 for the BYEpeak/ G^* case, and to 0.80 for the BYE20/ G^* case. Therefore, it seems that there might be some relation between the %R in the MSCR and the BYET. However, this is only true when the BYET energy is calculated up to 2000% strain rather than the maximum stress and is normalized to the G^* value.

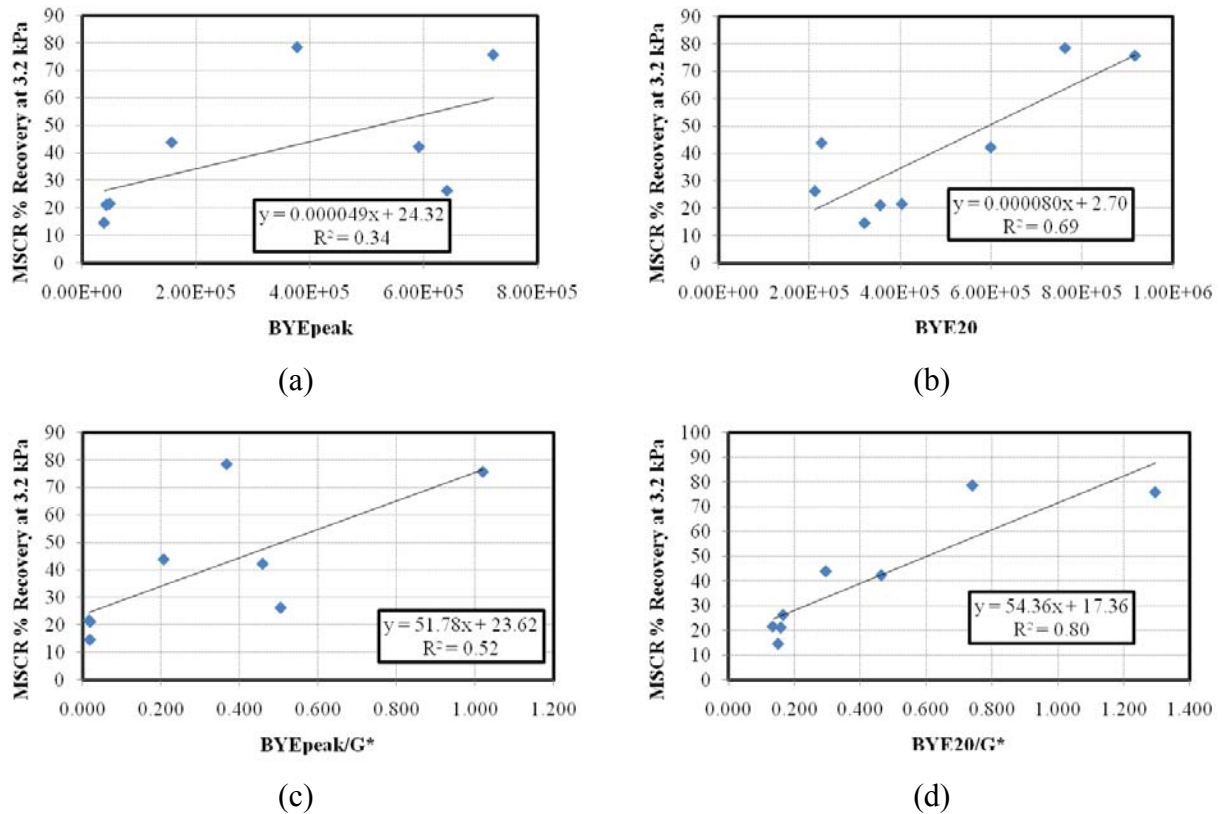


Figure E2a.2. Graphs. MSCR %R (3.2 kPa) versus BYET for: (a) BYEpeak; (b) BYE20; (c) BYEpeak/ G^* ; and (d) BYE20/ G^* .

The frequency sweep testing conducted thus far revealed a change in the master curve for the binders due to modification. In most of the cases, the modified binder master curve deviation from the base binder master curve is more pronounced at lower frequencies rather than high frequencies. Figure E2a.3 shows a plot of the master curves for binders C0, C1 and C2. The modified binders show a higher value of G^* at all frequency levels. More testing is needed to cover the same temperature range for all the binders, which will allow for a more extensive analysis of the modification type/level effect on binder properties.

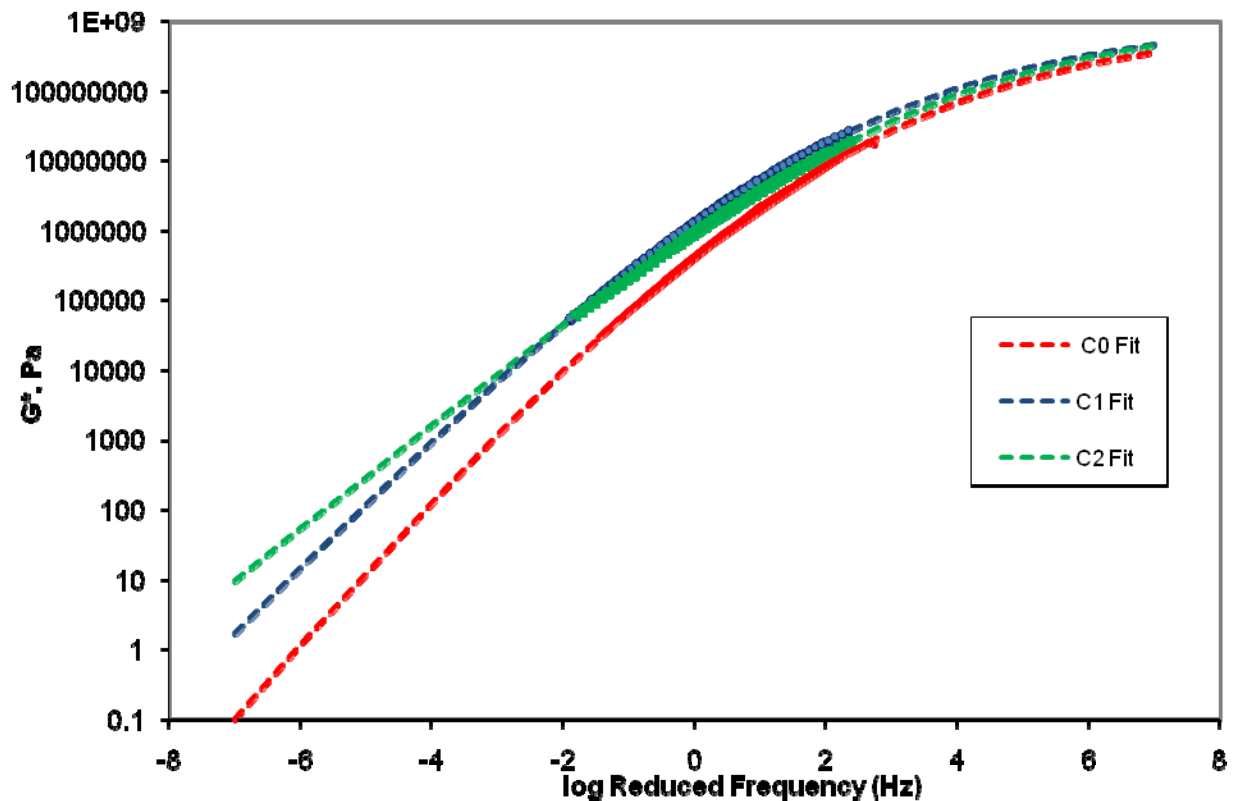


Figure E2a.3. Graph. Frequency sweep master curve for binders C0, C1 and C2.

Significant Problems, Issues and Potential Impact on Progress

None.

Work Planned Next Quarter

Work in the next quarter will focus on finalizing the MSCR and BYET testing for the binders in the testing matrix. The frequency sweep testing will be carried out for all the binders covering the same range of temperatures—16 °C to 40 °C. Finally, low-temperature properties testing will continue in the BBR and the SENB, and testing in the SENB will include a second temperature (-18 °C).

Work element E2b: Design System for HMA Containing a High Percentage of RAP Material (UNR)

Work Done This Quarter

This work element is a joint project between University of Nevada, Reno and University of Wisconsin–Madison and Western Research Institute.

Subtask E2b-1.a

The impact of the current extraction techniques (i.e. ignition, centrifuge, and reflux) on the properties of the extracted recycled asphalt pavement (RAP) aggregates experiment was completed and a report is being finalized for submission.

Subtask E2b-1.b

The recycled asphalt pavement (RAP) binder analysis procedure developed in previous quarters was modified following inconsistent verification results. Sample preparation and testing remains mostly unchanged in the new procedure, but steps allow for more user input in the sample preparation stages to reach comfortable sample workability. A spreadsheet has been developed that allows for all sample preparation calculations and analysis of testing results. A verification procedure was completed for low, intermediate, and high critical testing temperatures for the modified procedure. The artificial RAP material was made by mixing burned R₁₀₀ aggregates with heavily aged (three pressure aging vessel (PAV) cycles) binder at a typical R₁₀₀ RAP asphalt content (10%). The artificial RAP was then tested using the modified procedure and the estimated RAP-blended binder properties were then compared against the true-blended binder properties. Investigation into the feasibility of using the Single-Edge Notched Bending (SENB) test to analyze RAP materials began this quarter.

The modified analysis procedure is based on the idea that if two mortars are prepared with the same gradation and total binder content, but with two different binders, the only difference in the properties between the two can be attributed to the binders used. Thus, when RAP aggregate with rolling thin film oven (RTFO) binder (RRAP) and total RAP with RTFO binder (SRAP) are prepared and tested, the shift in the measured properties (S, m, G*) is due to the RAP binder. If the shift between the SRAP and RRAP remains constant at all testing times (or frequencies) and temperatures, the same shift at the critical time (or frequency) can be applied to the fresh binder at each testing temperature.

Figure E2b-1b.1 illustrates this concept for binder stiffness. The shift is applied by simply multiplying the fresh binder stiffness by the shift factor. From the “new” true grade, a relationship between PG temperature and percent RAP binder can be estimated if the asphalt content of the RAP is known. The fresh binder true grade is known from testing, and if the true grade shift due to a certain percent of RAP binder is assumed constant, prediction of mix PG is possible at RAP binder percentages up to the mortar percentage tested. Extrapolation outside of the testing range should only be done with extreme caution, as a nonlinear relationship may exist outside of the testing range.

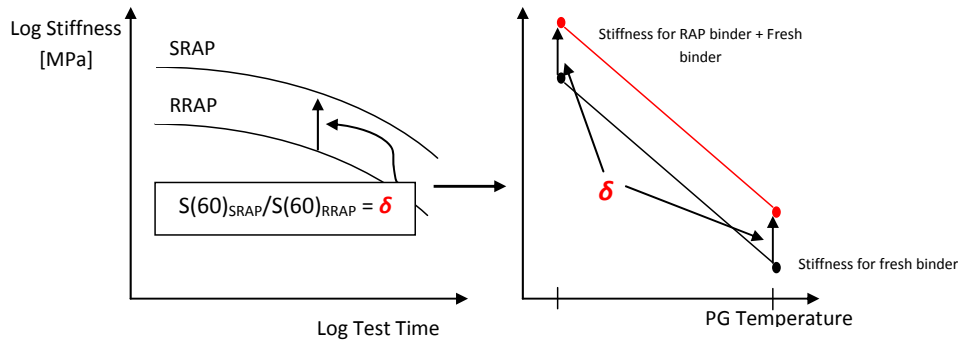


Figure E2b-1b.1. Graphs. Determination of true grade shift (δ) magnitude.

Artificial RAP was produced by mixing R_{100} (passing No. 50 sieve and retained on No. 100 sieve) aggregate material with binder aged for 40 hours in the PAV (two complete PAV aging cycles) at asphalt content similar to what is usually observed in R_{100} RAP material (10.5%). The artificial RAP was tested according to the proposed procedure at low, intermediate and high temperatures treating the artificial RAP as a standard SRAP material. The burned aggregates used for creating the RRAP mortar are the same as those used for creating the artificial RAP material. The RAP binder content was held constant at 15% as a percent of the total binder in all verification testing. Two cases were tested:

Case I: *Artificial RAP_A + PG 64 – 22 fresh binder*

Case II: *Artificial RAP_A + PG 58 – 28 fresh binder*

Results from this testing were verified against blended binder containing 15% artificial RAP binder + 85% fresh binder, aged according to the appropriate testing procedure. Table E2b-1b.1 summarizes the testing conducted in this study.

Table E2b-1b.1. Testing temperatures for verification study.

	Testing Temperatures							
	Low			Intermediate		High		
	-6 °C	-12 °C	-18 °C	25 °C	28 °C	58 °C	64 °C	70 °C
Case I	X	X		X	X		X	X
Case II		X	X	X	X	X	X	

Note: X denotes a testing temperature used.

The low-temperature true grade results are summarized in table E2b-1b.2, where the estimated true grade is the mortar testing spreadsheet estimate, and the measured true grade is the artificial RAP binder + fresh binder blend true grade. The results indicate that the estimated true grade was within 0.5 °C of the measured true grade.

Table E2b-1b.2. Low-temperature true grade verification.

	Test Temp. [°C]	Estimated True Grade [°C]	Measured True Grade [°C]	Difference [°C]
Case I	-6 -12	-18.87	-19.18	0.31
Case II	-12 -18	-25.96	-26.17	0.21

A true grade comparison was completed for intermediate and high temperatures utilizing the Dynamic Shear Rheometer (DSR). The results of the true grade analysis are shown in tables E2b-1b.3 and E2b-1b.4 for intermediate- and high-temperature true grades, respectively. The results indicate that the estimated true grade was within 2.5 °C of the measured true grade for intermediate temperature, while the high-temperature estimation exhibited a higher discrepancy (up to about 6 °C).

Table E2b-1b.3. Intermediate-temperature true grade verification.

	Test Temp. [°C]	Estimated True Grade [°C]	Measured True Grade [°C]	Difference [°C]
Case I	25 28	19.72	21.62	1.90
Case II	25 28	16.82	18.29	1.47

Table E2b-1b.4. High-temperature true grade verification.

	Test Temp. [°C]	Estimated True Grade [°C]	Measured True Grade [°C]	Difference [°C]
Case I	64 70	67.64	73.60	5.96
Case II	58 64	60.16	64.02	3.86

The results shown in table E2b-1b.4 indicate that the estimation method used provides a very conservative estimate of the high-temperature binder properties. The measured true grade in all cases was higher than the estimated true grade; similarly, the actual measurements of the binder properties confirm that the procedure is conservative at high temperatures. All estimated parameter values are lower than the measured blended binder values, indicating there may be additional aggregate-binder interaction that has not been accounted for.

As a result of the discrepancy between the measured and estimated true grade values for the high-temperature testing, additional DSR testing geometries and loading specifications were explored for the verification study. It is believed that the current geometry (25-mm plate tested at a gap of 1 mm and 10% strain) does not capture the binder properties with heavily aged (very stiff) binders and mortars; hence, the relationship between SRAP and RRAP mortars is inaccurate, and the standard geometry produces results outside the linear viscoelastic range of the binder. Trial high-temperature testing geometries for Case I and resulting true grade differences are outlined in table E2b-1b.5.

Table E2b-1b.5. High-temperature trial geometries.

Trial Geometry	Plate Dia. [mm]	Gap [mm]	Strain [%]	Difference in True Grade [°C]
1	25	1	10	5.96
2	25	2	10	2.97
3	25	1	1	4.34
4	25	2	1	5.39
5	8	2	1	7.04

From the trial geometry effect, Trial Geometry 2 was selected for further study as it provided the greatest improvement in verification of true grade for Case I.

The standard Bending Beam Rheometer (BBR) geometry modified with a small notch was used for SENB testing. The minimum total asphalt content for the samples was higher than the BBR testing, as sample preparation requires greater workability in the mortar samples. Preliminary testing confirmed expected trends in both strength and ductility. Figure E2b-1b.2 shows example results from mortar and binder testing. From the load-displacement profile, a clear distinction between RRAP (no RAP binder) and SRAP (blended binder) mortars is observed. The trend is logical, as it shows SRAP, which contains the aged RAP binder, to be more stiff and more brittle (peak at lower displacement). Additional testing temperatures and other RAP sources must be explored to determine if these trends remain the same, and an analysis procedure to isolate the contribution of RAP binder to the fracture parameters needs to be developed.

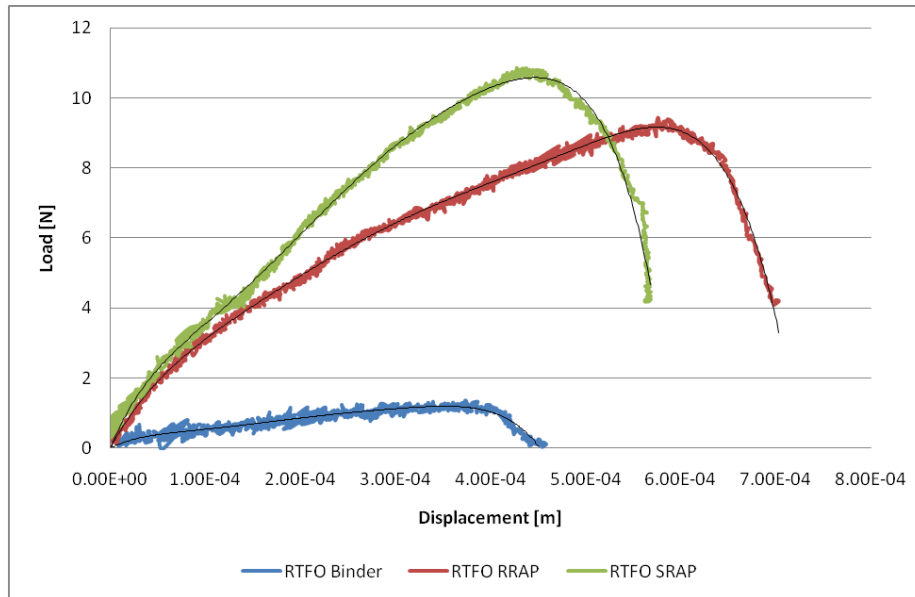


Figure E2b-1b.2. Graph. Preliminary SENB testing results.

Subtask E2b-2 Compatibility of RAP and Virgin Binders

Analysis of the Manitoba RAP field site samples has continued. Extraction of the South Carolina and California RAP samples has been completed. Blending of the extracted RAP samples with two SHRP asphalts after RTFO aging is underway. Compatibility of all RAP/virgin asphalt blends has been delayed by the delivery of the new AFT from Kohler Instruments. The delay is not expected to adversely affect the overall timeline because the AFT analyses can be completed rather quickly once the equipment is fully operational.

Compositional analysis of the Manitoba samples compared with lab prepared blends is also underway. The compositional analysis is expected to give insight into the compositional types that become part of a RAP/virgin asphalt blend which will help guide us to an accurate analysis of RAP stockpiles.

Subtask E2b-5

Asphalt binders were extracted and recovered from the Manitoba RAP mixtures and their rheological properties were evaluated. The asphalt binders were extracted/recovered from the laboratory mixed laboratory compacted (LMLC) and field mixed laboratory compacted (FMLC) virgin and RAP-containing HMA mixtures. Table E2b-5.1 shows the completed testing matrix.

Table E2b-5.1. Testing matrix for the Manitoba extracted/recovered asphalt binders.

Property	Mixture ID *								
	RAP	F-0%-150	F-15%-150	F-50%-150	F-50%-200	L-0%-150	L-15%-150	L-50%-150	L-50%-200
G*/sin δ at high temperature	√	√	√	√	√	√	√	√	√
G* sin δ at intermediate temperature	√	√	√	√	√	√	√	√	√
Stiffness and m-value	√	√	√	√	√	√	√	√	√

* F denotes “Field Mix Lab Compacted”, L denotes “Lab Mix Lab Compacted”, 0%, 15% and 50% denotes the RAP content, and 150 and 200 denotes Pen 150-200 and Pen 200-300, respectively.

Table E2b-5.2 shows the tests results for the extracted/recovered asphalt binders. In some cases, there was some uncertainty in the high temperature grade and the tests are being repeated. Additionally, asphalt binder was extracted directly from the RAP and the rheological properties were determined through the Superpave method (AASHTO M320) and AASHTO method (AASHTO M323). The RAP binder was graded as a PG76-10 and a PG 70-16 according to the Superpave and the AASHTO classification methods, respectively.

The measured critical low, intermediate and high temperatures for the recovered binders from the 15 and 50% RAP mixtures were compared to the calculated corresponding critical temperatures using the blending charts technique.

Additionally, the Manitoba RAP was evaluated using the newly modified RAP binder analysis procedure. The procedure consists of preparing RAP-mortars and evaluating them in the DSR at high and intermediate temperatures and in the BBR at low temperature. The test results are shown in Figures E2b-5.1 and E2b-5.2 for the PEN150 and PEN200 asphalt binders, respectively.

Table E2b-5.2 Testing results for the Manitoba extracted/recovered asphalt binders.

Mix	Critical Temperatures (°C)			PG Grade
	High	Intermediate	Low	
PEN150-200	58,0	14,7	-32,5	58-28
PEN200-300	54,1	12,2	-34,4	52-34
F-0%-150	(*)	15,8	-31,6	(*)-28
F-15%-150	62,6	18,5	-29,5	58-28
F-50%-150	69,1	24,3	-21,2	64-16
F-50%-200	65,1	22,7	-25,1	64-22
L-0%-150	(*)	14,9	-32,6	(*)-28
L-15%-150	(*)	17,8	-30,5	(*)-28
L-50%-150	(*)	23,0	-22,3	(*)-22
L-50%-200	(*)	21,6	-26,6	(*)-22
RAP-Superpave (¹)	76,5	30,9	-14,7	76-10
RAP-AASHTO (¹¹)	72,9	28,2	-21,3	70-16

(*) Test is being repeated.

(¹) RAP binder evaluated according to the Superpave method (AASHTO M320)

(¹¹) RAP binder evaluated according the AASHTO method (AASHTO M323)

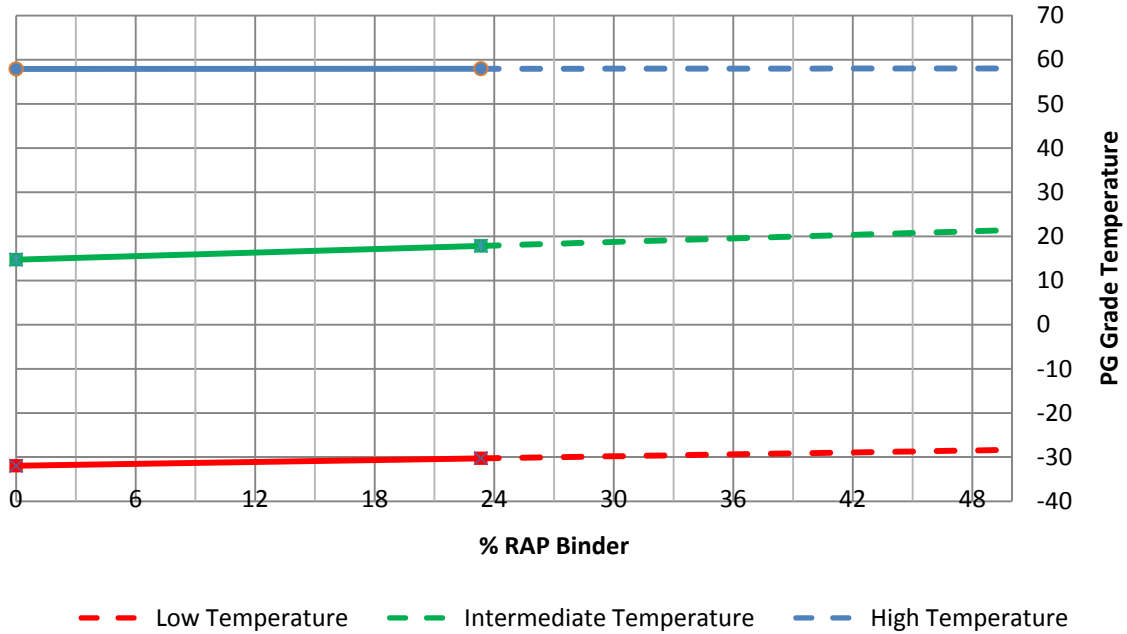


Figure E2b-5.1. Graph. Blending charts for the high, intermediate and low temperatures for the RAP-mortars. Summary for the Asphalt PEN150.

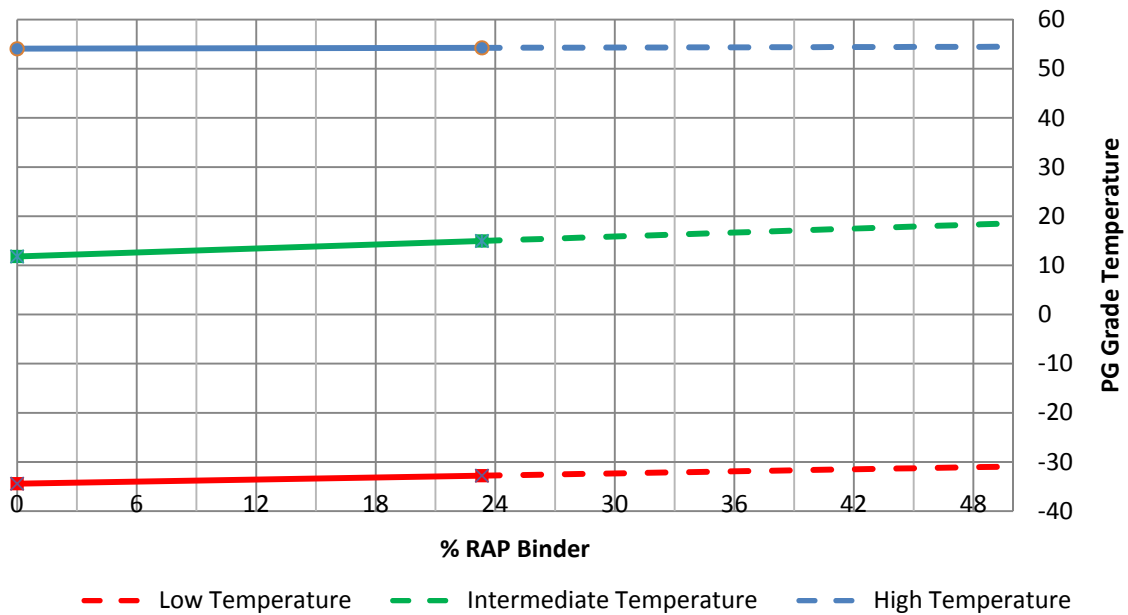


Figure E2b-5.2. Graph. Blending charts for the high, intermediate and low temperatures for the RAP-mortars. Summary for the Asphalt PEN200.

Significant Problems, Issues and Potential Impact on Progress

The Year 4 Gantt chart previously showed an error for a journal paper to be delivered in May 2010. This has been corrected.

The sampling of the material from Granite Construction in UTAH for subtask E2b-3 has been delayed because of no production of Superpave mixes. The work progress is reflected on the Gantt chart.

Under subtask E2b-1.a, there has been some delay in the AIMS testing for the Alabama and Florida aggregates. NCAT is working on completing the testing.

Work Planned Next Quarter

Work will continue on six new RAP sources to conduct the full modified procedure for each. Variability statistics will also be completed for the standard procedure. Two users will complete the full procedure for the same RAP source and virgin binder. One user will also complete the same procedure twice for a RAP material. The variability evaluation plan will be fully developed next quarter. SENB testing will continue for at least two sources and at two temperatures. The research team will also begin assessing the feasibility of using the glass transition temperature testing equipment for investigating RAP materials. The collaboration with the research group at Purdue University's North Central Superpave Center will continue, and testing of the RAPs received from the group will be completed.

Work will continue on the evaluation of the extracted/recovered asphalt binders from the virgin and the RAP-containing asphalt mixtures from Manitoba. The following extracted and recovered asphalt binders will be evaluated:

1. Field mixes (loose)
 - F-0-150
 - F-15-150
 - F-50-150
 - F-50-200
2. Laboratory mixes (loose)
 - L-0-150
 - L-15-150
 - L-50-150
 - L-50-200
3. Field mixed laboratory compacted (E* cylinders)
 - F-0-150
 - F-15-150
 - F-50-150
 - F-50-200
4. Lab mixed laboratory compacted (E* cylinders)
 - F-0-150

- F-15-150
- F-50-150
- F-50-200

5. RAP mix (loose and E* cylinders)

Collect the material for the experimental plan of subtask E2b-3 “Develop a Mix Design Procedure,” and start the testing.

Work element E2c: Critically Designed HMA Mixtures (UNR)

Work Done This Quarter

Work continued to evaluate the applicability of the recommended deviator and confining stresses for the flow number test. A report summarizing the findings of the work completed under subtask E2c.1 is being finalized to incorporate the captions of figures and tables before review and publication.

Work continued to analyze the response data history from 3D-Move analyses. An effort has been done to determine potential predominant loading frequencies for various critical responses.

Work continued on the evaluation of the permanent deformation characteristics of laboratory-produced and field-produced mixtures under the testing conditions identified in Subtask E2c-1. The impact of air-voids, gradation, and binder type on the asphalt mixture critical temperature are under evaluation.

Significant Results

The determined pavement responses such as octahedral stresses and strains were converted from time domain to frequency domain using the Fast Fourier Transformation (FFT). Figure E2c.1 shows the octahedral normal stress under tandem axles in time domain and frequency domain at 0.5 inch below the pavement surface. Figure E2c.1 shows a predominant frequency of 14.4 Hz for which the amplitude of the octahedral stress is at maximum. Similar plots are being developed at different depth for different pavement structures, vehicle speeds, pavement temperatures and mixtures types. These findings are being used to check against the determined pulse durations in the time domain and whether an equivalent elastic modulus for the asphalt layer can be used to generate similar values for selected critical responses such as the tensile strain at the bottom of the HMA layer and the vertical compressive strains in the middle of the HMA sub layers.

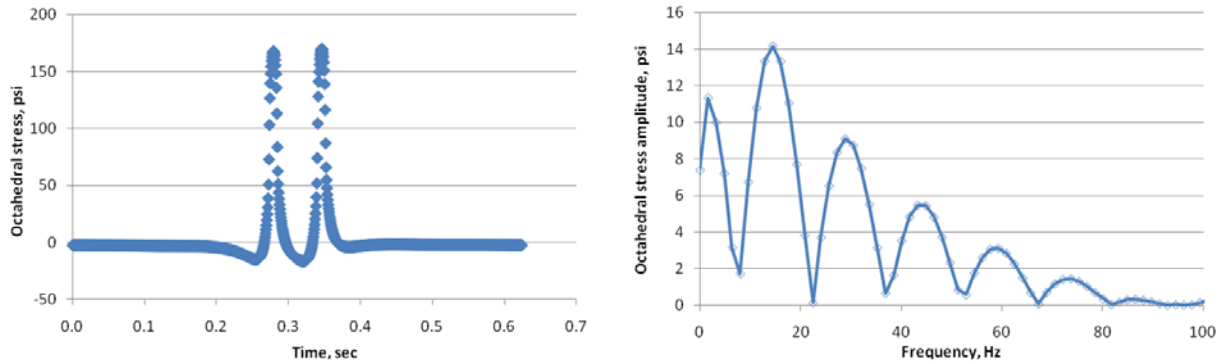


Figure E2c.1. Octahedral normal stress at 0.5 inches below the pavement surface in time domain.

The impact of air-voids and binder type on the asphalt mixture critical temperature is being evaluated using the testing conditions determined under Subtask E2c-1. Three different HMA mixtures with similar gradation and different binder grades (PG64-22, PG58-22, and PG52-22) were tested for flow number at different temperatures and air void levels. Three air void levels are being evaluated:

- 7% to represent typical in-place air void content,
- 4% to represent mix design air void level,
- and 2% to represent excessive in-place air void level.

The FN test was conducted using the determined stress conditions at each testing temperatures for 20,000 cycles or until the specimen reaches 5% strain, whichever occurs first. At each temperature, the corresponding deviator and confining stresses were determined using the testing conditions identified in Subtask E2c-1.

In order to determine the testing conditions the modulus of the mixtures at 2 inches below the pavement surface must be obtained. Hence, a series of dynamic modulus ($|E^*|$) tests were conducted on the PG64-22, PG58-22 and the PG52-22 mix at the target air void levels (i.e. 7, 4, 2%) and the variations of $|E^*|$ were estimated at each of these temperatures using the master curve and shift factors. Figures E2c.2 to E2c.4 show the mixtures' master curves at the reference temperature and for different air void contents. An increase in $|E^*|$ was observed with the decrease in air void contents and an increase in the high performance PG grade.

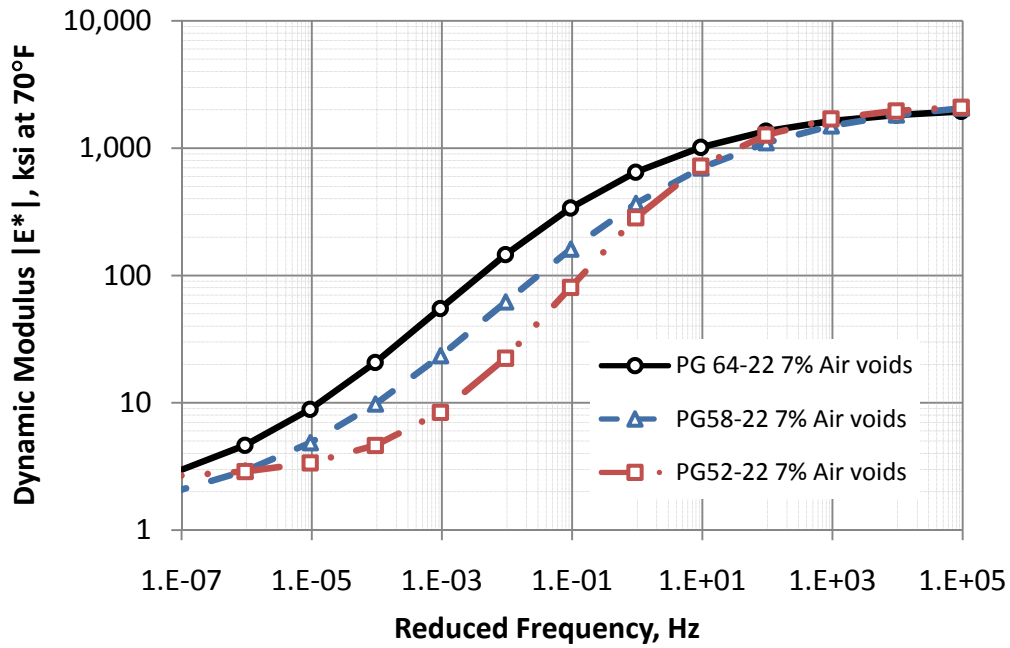


Figure E2c.2. $|E^*|$ at 70°F for the different mixtures at 7% air voids.

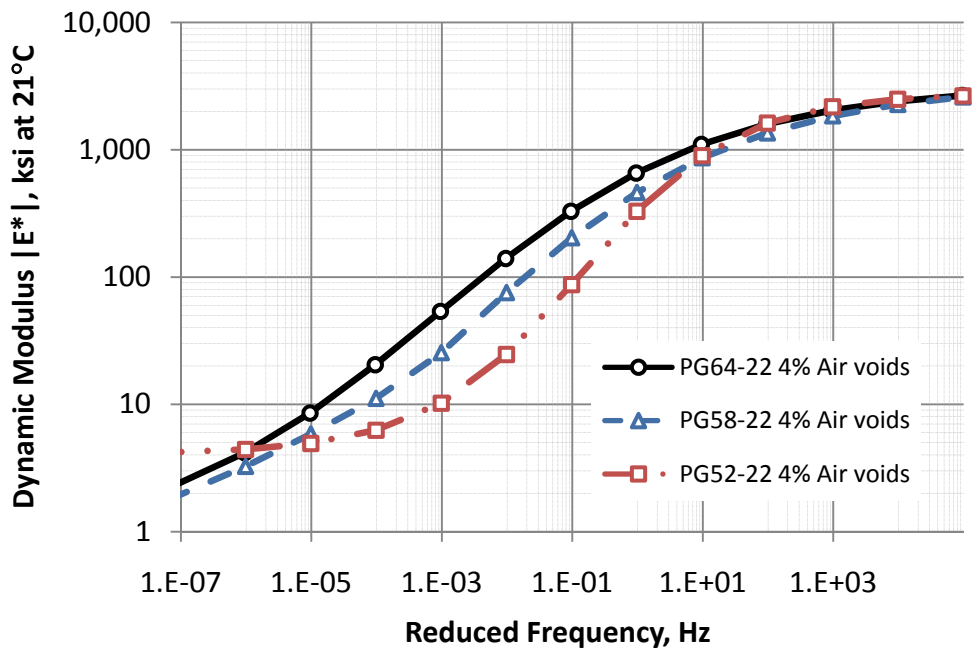


Figure E2c.3. $|E^*|$ at 70°F for the different mixtures at 4% air voids.

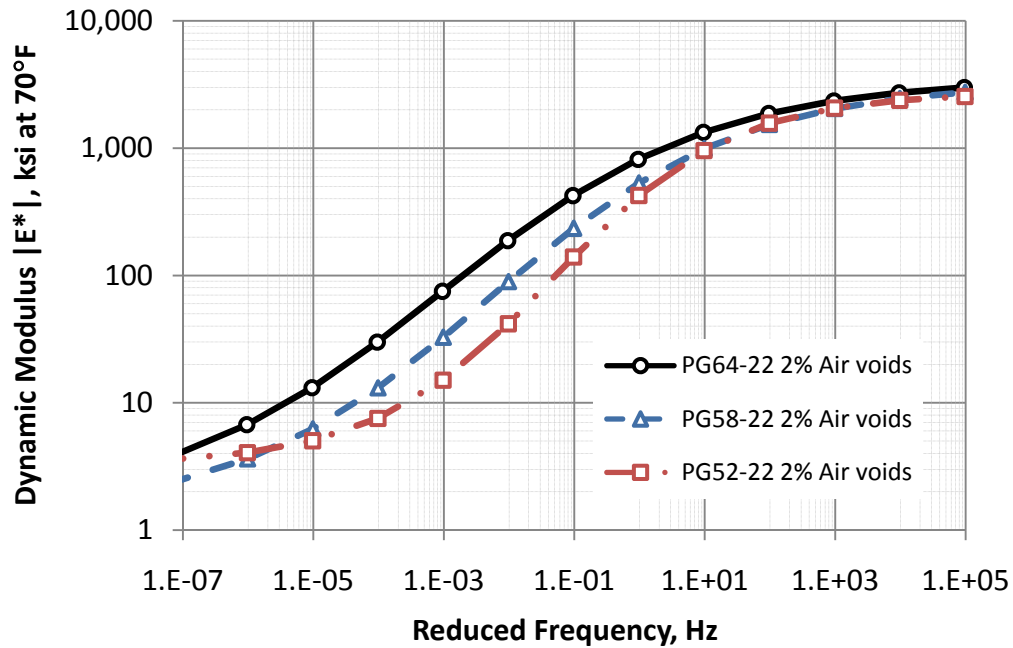


Figure E2c.4. $|E^*|$ at 70°F for the different mixtures at 2% air voids.

Table E2c.1 shows the FN testing conditions and results for all three air-void level for the PG64-22 mixture calculated using the stepwise increase method, the three stage permanent deformation method, and the Francken method. In addition, tables E2c.2 and E2c.3 show the results for the PG58-22 and PG52-22 mixtures respectively. However, at this moment only the stepwise increase method is reported for the PG58-22 and PG52-22 mixtures and further analysis using the other two methods is under development.

Table E2c.1. Flow number test conditions and results – PG64-22 mix.

Testing Temp (°C)	Dynamic Modulus (psi)	Deviator Stress (psi)	Confining Stress (psi)	Rep	Flow Number Three Stage Method		Flow Number Stepwise Method		Flow Number Francken Method	
					Result	Average	Result	Average	Result	Average
PG64-22 Mix at 7% Air Voids										
35	536,355	77	54	1	No FN*	No FN*	No FN*	No FN*	No FN*	No FN*
				2	No FN*		No FN*		No FN*	
40	370,573	76	49	1	10,600	10,300	10,297	9,748	4,795	5,045
				2	9,999		9,198		5,295	
45	250,272	76	44	1	4,499	3,750	4,095	3,995	2,895	2,495
				2	3,000		3,895		2,095	
50	168,416	76	40	1	1,998	1,948	1,999	1,948	1,095	1,045
				2	1,897		1,896		995	
PG64-22 Mix at 4% Air Voids										
40	439,407	76	52	1	No FN*	No FN*	No FN*	No FN*	No FN*	No FN*
				2	No FN*		No FN*		No FN*	
45	314,857	75	48	1	7,999	7,497	7,495	6,947	6,095	5,445
				2	6,995		6,398		4,795	
50	226,523	75	44	1	4,696	4,747	4,895	4,797	4,095	3,845
				2	4,798		4,699		3,595	
PG64-22 Mix at 2% Air Voids										
40	551,586	75	59	1	No FN*	No FN*	No FN*	No FN*	No FN*	No FN*
				2	No FN*		No FN*		No FN*	
45	399,534	75	53	1	13,699	12,097	15,598	13,197	12,820	13,149
				2	10,495		10,796		13,477	
50	290,276	74	48	1	8,796	7,847	9,795	8,695	8,595	7,745
				2	6,897		7,595		6,895	

* A flow number was not found

The PG64-22 mix at 7% air voids exhibited a tertiary stage at a temperature of 40°C. On the other hand, the PG64-22 mix at 4% and 2% air voids exhibited a tertiary stage at a temperature of 45°C. The data indicate the existence of a critical temperature between 35 and 40°C for the PG64-22 mix at 7% air voids and a critical temperature between 40 and 45°C for the PG64-22 mix at both 4% and 2% air voids. However the critical temperature of the PG64-22 mix at 2% air voids was observed at a higher number of load repetitions (i.e. FN) when compared to the critical temperature of the PG64-22 mix at 4% air voids.

The PG58-22 mix exhibited a tertiary stage at 40°C with an air voids level of 7%. As the air void level reduces the critical temperature increases by 5°C as seen in table E2c.2. On the other hand, for the PG52-22 mix at 7% air voids the tertiary stage occurred at 30°C, whereas at 4 and 2% air voids level the critical temperature is between 30 and 35°C.

The results indicate that the HMA critical conditions determined in the FN test are affected by the density of the samples and the PG grade of the asphalt binder. The analysis will continue for the other FN calculation methods and also more testing is going to be undertaken to determine the influence of the pulse time and rest period.

Table E2c.2. Flow Number Test Conditions and Results – PG58-22 mix.

Testing Temp (°C)	Dynamic Modulus (psi)	Deviator Stress (psi)	Confining Stress (psi)	Rep	Flow Number Stepwise Method	
					Result	Average
PG58-22 Mix at 7% Air Voids						
35	368,271	78	46	1	No FN*	No FN*
				2	No FN*	
40	259,395	77	43	1	3,799	4,697
				2	5,595	
PG58-22 Mix at 4% Air Voids						
40	317,119	77	46	1	No FN*	No FN*
				2	No FN*	
45	223,438	76	42	1	1,499	1,550
				2	1,600	
PG58-22 Mix at 2% Air Voids						
40	357,702	76	48	1	No FN*	No FN*
				2	No FN*	
45	250,475	76	44	1	No FN*	No FN*
				2	No FN*	
50	177,971	76	40	1	7,695	9,845
				2	11,995	

* A flow number was not found

Table E2c.3. Flow Number Test Conditions and Results – PG52-22 mix.

Testing Temp (°C)	Dynamic Modulus (psi)	Deviator Stress (psi)	Confining Stress (psi)	Rep	Flow Number Stepwise Method	
					Result	Average
PG52-22 Mix at 7% Air Voids						
25	737,512	80	54	1	No FN*	No FN*
				2	No FN*	
30	478,542	79	48	1	8395	9,095
				2	9795	
35	292,315	79	42	1	2998	2,199
				2	1399	
40	173,809	78	38	1	897	748
				2	598	
PG52-22 Mix at 4% Air Voids						
25	908,595	80	60	1	No FN*	No FN*
				2	No FN*	
30	573,117	79	52	1	16,295	14,895
				2	13,495	
35	340,631	78	45	1	1,995	2,497
				2	2,998	
PG52-22 Mix at 2% Air Voids						
30	632,901	78	55	1	18295	18,745
				2	19195	
35	400,195	78	48	1	3795	3,348
				2	2900	

* A flow number was not found

Significant Problems, Issues and Potential Impact on Progress

Materials for the Flow Number Task Force experiment have not yet been received by UNR.

The write-ups for the figures and tables captions have delayed the submission of the subtask E2c.1 report for review.

Work Planned for Next Quarter

The calculations of the 3D-Move model will continue to cover all the loading conditions that were described in the experimental plan for this work element.

Work will continue on the evaluation of the impact of air-voids, gradation, and binder type on mixtures' critical temperature.

Complete the tables and figures write-ups for the report.

Collect the material for the experimental plan developed by the Flow Number Task Force to develop criteria for asphalt concrete mixture design.

Work element E2d: Thermal Cracking Resistant Mixes for Intermountain States (UNR & UWM)

Work Done This Quarter

This work element is a joint project between University of Nevada Reno and University of Wisconsin–Madison. A thermal cracking meeting was hosted by Granite construction in Reno Nevada on Friday May 7, 2010. The meeting discussed the details of the binders aging model, mixtures aging model, and thermal stresses model. The meeting was attended by Drs. Hussain Bahia from University of Wisconsin, Adam Hand from Granite Construction Inc., Charles Glover from Texas A&M, Raj Siddharthan, Peter Sebaaly and Elie Hajj from University of Nevada Reno. The recommendations and suggestions of the meeting will be discussed next in the appropriate sections.

The UNR team has completed Subtask E2d-1 that is related to the analyses of the air and pavement temperature profiles data from LTPP Seasonal Monitoring Program (SMP) and WesTrack pavement sections. The final sections used for analysis are shown in table E2d.1. A total of 18 sections were used with 13 located within the intermountain region and 7 located outside the intermountain region. Sections were further divided into two pavement depths (12.5 mm and 25 mm).

Table E2d.1 Sections used for analysis.

Sensor Depth (mm)	City, State	Section	Original Construction Date	Climatic classification	Precipitation (mm)	Freezing Index (°C-days)
<i>Sections Within Intermountain Region</i>						
12.5	Kingman, AZ	040113	1/1/1993	Dry, no-freeze, SMP cell #5	205	2
	Kingman, AZ	040114	1/1/1993	Dry, no-freeze, SMP cell #13	205	2
	Delta, CO	081053	2/1/1984	Dry-freeze, cell #3	231	222
	Cody, WY	561007	7/1/1980	Dry-freeze, cell #7	259	512
	Silver Springs, NV	12 (WesTrack)	4/23/1996	Dry-freeze, SMP cell #15	198	105
	Silver Springs, NV	25 (WesTrack)	4/23/1996	Dry-freeze, SMP cell #15	198	105
	Silver Springs, NV	55 (WesTrack)	4/23/1996	Dry-freeze, SMP cell #15	198	105
25	Kingman, AZ	040113	1/1/1993	Dry, no-freeze, SMP cell #5	205	2
	Idaho Falls, ID	161010	10/1/1969	Dry-freeze, cell #15	304	652
	Great Falls, MT	300114	9/18/1997	Dry-freeze, SMP cell #11	360	667
	Battle Mountain, NV	320101	1/1/1993	Dry-freeze, SMP cell #15	229	249
	Hobbs, NM	351112	6/1/1984	Dry, no-freeze, cell #13	397	30
	Faith, SD	469187	5/1/1989	Dry-freeze, cell #3	431	719
	Estelline, TX	481077	1/1/1982	Wet, no-freeze, cell #1	570	68
<i>Sections Outside Intermountain Region</i>						
12.5	Opelika, AL	010101	4/30/1991	Wet, no-freeze, cell #10	1326	13
	Floresville, TX	481122	2/1/1974	Wet, no-freeze, cell #6	763	3
25	Dawsonville, GA	131031	1/1/1987	Wet, no-freeze, cell #10	1422	27
	East Dixfield, ME	231026	7/1/1988	Wet-freeze, cell #8	1149	782
	Oak Lake, Manitoba (Canada)	831801	1/1/1987	Dry-freeze, cell #7	466	1676

The long-term oven aging process continued for the binders as described in the experimental plan for this work element. Table E2d.2 shows the work progress for the binder aging. Additionally, the completed aged binders are under testing for their rheological properties.

Table E2d.2. Binder aging matrix.

Aging Temp (°C)	Aging Period Unit	Aging Period	Binder Grade/Type				
			PG64-22	PG64-28NV	PG64-22 +10%Lime	PG64-22 + 20%Lime	PG64-22+ 3% SBS
135	hours	8	AC	AC	AC	AC	AC
		15	AC	AC	AC	AC	AC
		30	AC	AC	AC	AC	AC
		44	AC	AC	AC	AC	AC
100	hours	44	AC	AC	AC	AC	AC
		90	AC	AC	AC	AC	AC
		150	AC	AC	AC	AC	AC
		240	AC	AC	AC	AC	AC
85	days	7.5	AC	AC	AC	AC	AC
		15	AC	AC	AC	AC	AC
		25	AC	AC	AC	AC	AC
		40	AC	AC	AC	AC	AC
60	days	30	AC	AC	AC	AC	AC
		60	AC	AC	AC	AC	AC
		100	AC	AC	AC	AC	AC
		160	AC	AC	AC	AC	AC
50	days	60	AC	AC	AC	AC	AC
		120	AC	AC	AC	AC	AC
		200	AC	AC			
		320	AC	AC			
AC =	Aging Completed						

This quarter the new Single-Edge Notched Bending (SENB) geometry developed in the last quarter, which adds a notch to the beams made using the common Bending Beam Rheometer (BBR) molds, was used to test a full range of binders with different modifiers at different temperatures. Table E2d.3 shows the test matrix followed using two to three replicates for each condition.

Test results showed that the new SENB method can clearly capture the differences in performance in different binders and modifiers, as shown in figure E2d.1.

Table E2d.3. Test matrix for SENB testing.

Binder	Test Temperature		
	-12 °C	-18 °C	-24 °C
Neat1 (PG 58-28)	√	√	√
Neat2 (PG 58-34)	√	√	√
Neat2 + Styrene-Butadiene-Styrene (SBS)	√	√	√
Neat2 + Polyphosphoric Acid (PPA)	√	√	√
Neat2 + Elvaloy	√	√	√
Neat2 + SBS + PPA	√	√	√
Valero (PG 58-28)	√	√	√
Citgo (PG 58-34)	√	√	√
Marathon (PG 58-34)	√	√	√
Neat (PG 58-34)	√	√	√
Wisconsin (Neat)	√	√	√
New York (Neat)	√	√	√

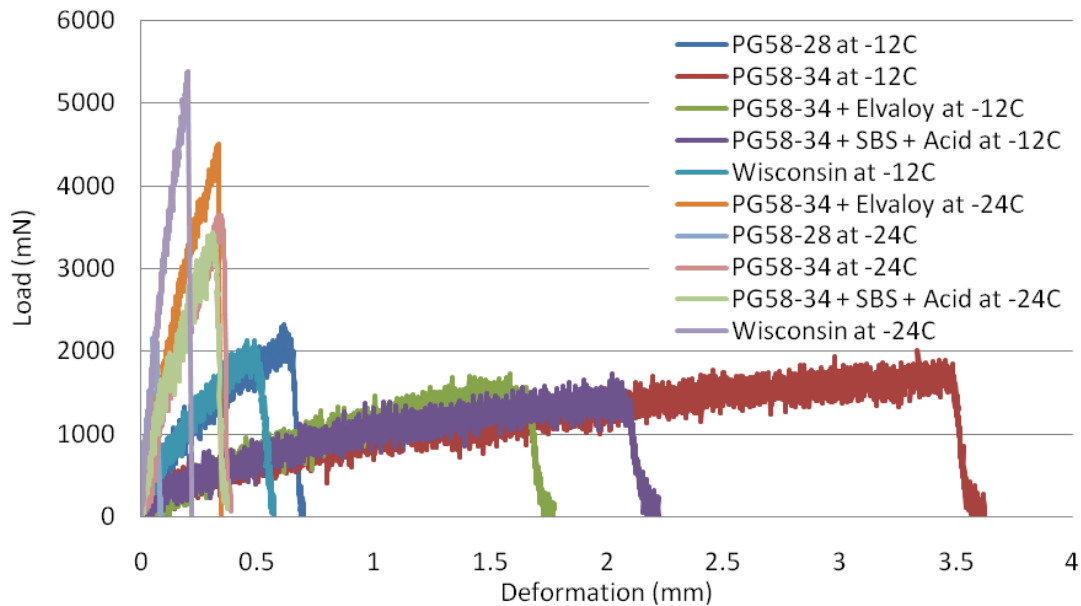


Figure E2d.1. Graph. SENB results at -12 °C and -24 °C for neat and modified binders.

The fixtures for the Thermal Stress Restrained Specimen Test (TSRST) and mixture glass transition temperature (T_g) device were assembled this quarter, as shown in figure E2d.2. The assembly and calibration of the TSRST system is currently a work in progress. Loose mixtures from pavement sections that are being monitored in the field were acquired and the compaction and coring process has started. These mixtures will be used to evaluate if the TSRST- T_g system is capable of differentiating between low-temperature performances of different asphalt

mixtures. TSRST- T_g samples are prepared by gluing together cores from the Superpave gyratory compactor samples to form a 12-inch-long cylinder. Work continues on development of this system and the test procedure.

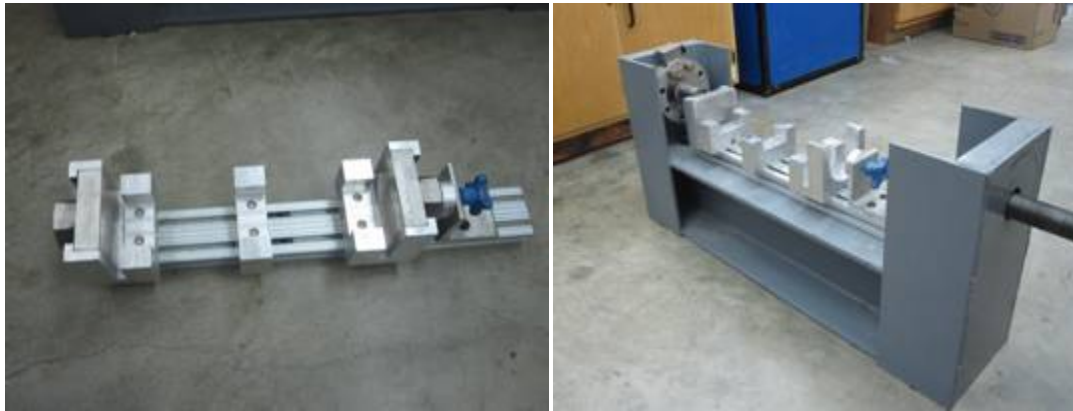


Figure E2d.2. Photographs. Fixtures developed and built for TSRST and T_g tests on asphalt mixtures.

E2d.3.b & c Aggregate Absorption and Mix Characteristics

Under subtasks E2d.3.b and E2d.3.c, significant progress was continued in the E^* compression testing with approximately 80% of the samples being tested. Most of the sources (Nevada, Colorado, Utah, and WesTrack) have most if not all the E^* compression samples tested for all aged (0, 3, 6, and 9 months). California has the least number of samples completed, with many 6 and 9 months samples still in ovens aging. The last of the E^* compression samples are expected out of the oven near the end of the calendar year.

Upon completion of the E^* testing the samples are being extracted and the binder recovered for further testing. Approximately 25% of the samples have been extracted and recovered to date. The testing currently planned for the recovered material includes binder master curves including Low Shear Viscosity (LSV), Fourier Transform Infrared Spectroscopy (FT-IR) for Carbonyl Area (CA) as an indicator of oxidation. From the Thermal Cracking meeting in May it was decided to also add Single Edge Notch Beam (SENB) to the binder tests. A significant amount of the extracted and recovered binders has been sent to UWM to await testing.

At the same Thermal Cracking meeting it was also determined that a fracture test was also needed for the mixture evaluation. The Thermally Stressed Restrained Specimen Test (TSRST) was selected as an appropriate mixture test for this purpose. Since this was just added to the work plan, a significant effort has been exerted on preparing the TSRST samples again for 0, 3, 6, and 9 month durations. Approximately 33% of the samples have been prepared and are currently undergoing oven aging. Along with the TSRST preparation, samples for the coefficient of thermal expansion, α , have also been prepared. The testing is intended to be conducted by UWM as the method is being developed by Dr. Bahia at UWM.

Significant Results

Under Subtask E2d-1, temperature rates were compared amongst the various evaluated sections and significant findings include:

- Maximum air temperatures for all sections were in the 30-40°C range
- Maximum pavement temperatures for all sections were in the 40-60°C range
- Minimum air temperatures ranged from -4.8°C in Kingman, AZ to as cold as -39.9°C in Great Falls, Montana and Oak Lake, Manitoba in Canada
- Minimum air and pavement temperatures not only varied among all sections but they also varied for sections within the intermountain region. This shows that environmental conditions may still vary within the intermountain region
- The intermountain region predominantly lies in a dry-freeze climatic zone with a couple of sections lying in a dry, no-freeze
- Sections classified as freeze sections had minimum air and minimum pavement temperatures that were relatively colder than those that are classified as no-freeze sections
- Temperature rates reduce in magnitude at deeper pavement depths
- Temperature rates reduce in magnitude as temperatures get colder
- Daily temperature rates do not vary greatly between sections. Maximum daily cooling rates ranged from -1.4° to -2.7°C/hr; whereas maximum daily warming rates were in the 3-5°C/hr range.
- At sensor depths of 12.5 mm, the average hourly cooling and hourly warming rates are greater in magnitude for sections within the intermountain region
- There is no clear distinction between cooling and warming rates for sections at a pavement depth of 25 mm. One factor that may contribute to this is that there are three no-freeze sections within the intermountain region considered in this group and two freeze sections outside the region considered at this pavement depth.
- Most no-freeze sections have lower hourly cooling rates than “freeze” sections regardless of region
- Sections classified as freeze generally have colder minimum air and pavement temperatures. This implies that they have greater range of cold temperatures which ultimately lead to higher cooling rates
- The intermountain region is dominated by a freezing climate which explains the relatively higher temperature rates

It was observed that most cooling periods during a day exhibit two distinct rates which constitutes of a higher initial cooling rate followed by a much slower cooling rate as shown in figure E2d.3.

Cooling rate behavior was fairly consistent for all sections regardless of region. High rates were approximately -3.0C/hr whereas low rates were approximately -0.5C/hr . High rates last 2-4 hours whereas low rates lasted longer (more than 6 hours).

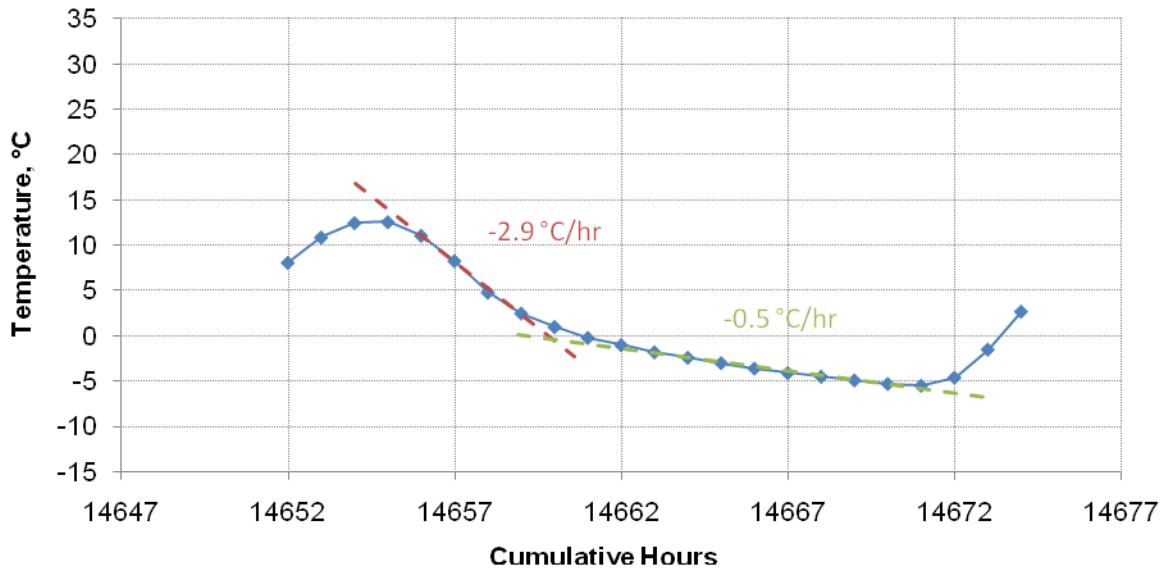


Figure E2d.3. Graph. High rate and low rate calculation of the maximum hourly cooling rate for section 481077 (Estelline, TX) of -3.5C/hour at a minimum pavement temperature of 10C at a sensor depth of 25 mm.

Based on the above conclusions and findings, a few recommendations can be made. There seems to be no significant difference in cooling rate behavior (low and high rates during a cooling cycle) between sections within the intermountain region and sections outside the region. However, findings in this research can still be taken into consideration. In order to accurately simulate the pavement temperature conditions which occur in the intermountain region, actual rates at cold temperatures must be utilized. The range of rates presented should be taken into account when attempting to generate actual field conditions within this region. In order to assess the thermal cracking performance of mixtures, both warming and cooling rates may need to be incorporated during a particular test.

The TSRST cools specimens at a linear cooling rate of 10C/hr . The test only requires that the specimen be cooled and never considers cooling and warming during a test. A new experimental plan is needed to investigate the effects of multiple warming and cooling cycles on the thermal cracking performance of mixtures. Furthermore, a variable cooling rate needs to be implemented to replace linear rates. As mentioned, cooling events are partitioned into two distinct temperature rates; therefore a linear cooling rate may not be the best approach. The initial “high rate” needs to be at least 6 times faster than the “low rate” during a cooling period. The warming rate can be taken as an hourly warming rate. Furthermore, the high rates should occur at much shorter duration than the low rates.

Most maximum rates were well below 10°C/hr. This indicates that the use of a cooling rate of 10°C/hr for tests such as the TSRST is conservative. Temperature rate is just one of many factors that affect an asphalt pavement's performance against thermal cracking. Other factors such as pavement temperature itself may dictate whether a certain rate will crack a pavement. It was found in this research that climatic region plays a role in the magnitude of temperature rates. In regions that experience very cold temperatures ("freeze" sections), high temperature rates will also exist. Therefore, critically low temperatures coupled with high cooling rates will increase an asphalt pavement's susceptibility to thermal cracking. The intermountain region is predominantly within the "freeze" climatic zone. Therefore, asphalt pavements within this region have experienced severe thermal cracking.

Furthermore, other properties of the asphalt pavements used within the intermountain need to be investigated to see if such properties are unique compared to sections outside the intermountain region. Other properties may include, aggregate type, mixture volumetrics, asphalt binder type, air void content, and asphalt layer thickness. This research study focused on environmental conditions. The next phase of this study would be to look into the aforementioned properties of the sections within the intermountain region and to see if they have an effect on thermal cracking performance.

Possible relationships between the results from the SENB, BBR and T_g tests were investigated. Generally, the SENB results for neat binders showed high stiffness and low deformation up to the point of the occurrence of an abrupt brittle failure. On the other hand, modified binders generally deformed to a far greater extent and had a semiductile failure at all temperatures except -24 °C. At this temperature, all modified and neat binders experienced brittle failure. It must be noted that all binders had glass transition temperatures above -24 °C. The variation in the fracture stress was relatively low between different binders. However, there was a very clear relationship between the increase in deformation and the decrease in fracture load.

There is a good correlation between the SENB results (i.e., fracture load, deformation and energy) and the stiffness at 60 seconds from the BBR. However, no clear relationship was observed between the m-value (indicates relaxation) and SENB parameters, as shown in figure E2d.4.

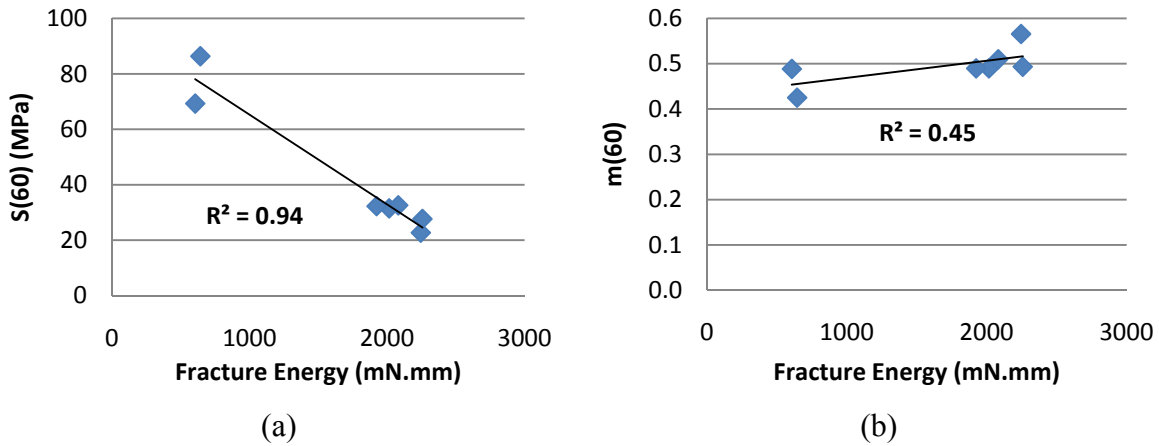


Figure E2d.4. Graphs. Relationship between fracture energy and BBR results at -12 °C: (a) BBR stiffness at 60 sec. versus fracture energy; and (b) m-value at 60 sec. versus fracture energy.

Fracture energy obtained with the SENB correlates fairly well with the T_g of the binder, as shown in figure E2d.5. Note that the relationship between T_g and the BBR parameters (i.e., S and m) is much weaker. One reason for this could be that the effect of glass transition is much more pronounced on the low-temperature fracture at relatively high strain levels, while the BBR measures properties at relatively smaller strain levels.

The research team developed a spreadsheet in Microsoft Excel to process the raw data obtained in the SENB test. The parameters calculated in the spreadsheet include fracture energy, fracture toughness, and maximum deformation, among others.

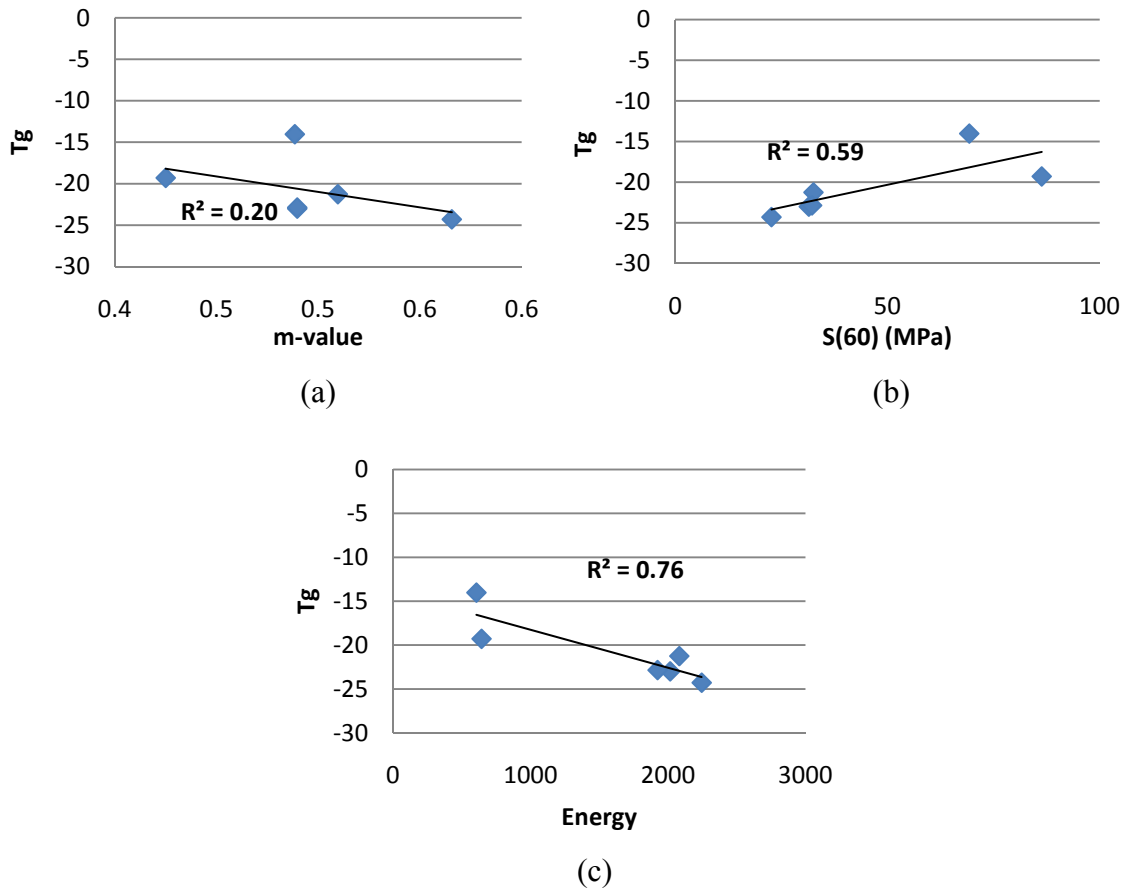


Figure E2d.5. Graphs. BBR and SENB tests performed at -12 °C: (a) T_g versus m-value; (b) T_g versus stiffness at 60 sec.; and (c) relationship between T_g and fracture energy.

With a significant portion of the E^* compression testing being completed for subtasks E2d.3.b and E2d.3.c, some results and conclusions can be made. However, preliminary results seem to indicate additional information may be needed to help differentiate the observed results. It is expected that as more FT-IR and binder LSV results become available more definite conclusions can be drawn from the data.

Significant effort had been extended into the creation of binder master curves from the recovered binders. Several samples had been tested and an acceptable procedure seemed to have been developed, however the DSR at UNR was damaged during other testing. Unfortunately, this occurred prior to complete sets of binders were tested so only limited information is available from that testing. However, an example of the expected results is presented in figure E2d.6 from one of the Nevada data sets.

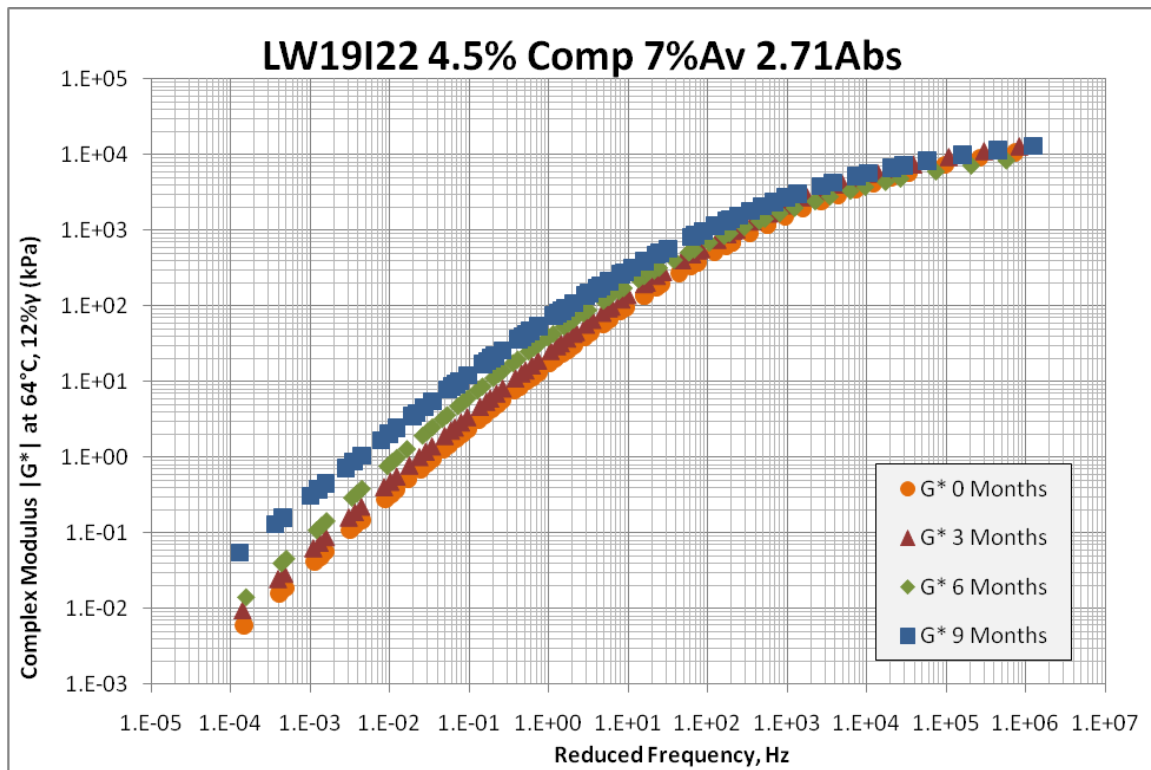


Figure E2d.6 Master curves for recovered binders from Nevada mixes.

An experiment to investigate the effect of size and shape of the TSRST specimen is currently being conducted. Currently, the most common shape for TSRST specimens involve compacting beams and cutting them to 2" x 2" x 10" specimens. Cylindrical specimens compacted using a gyratory compactor were tested and compared to beam specimens (figure E2d.7). Cylindrical specimens were cored from gyratory compacted mixes in three different ways – a) one specimen cored vertically from the center of the compacted specimen (Center Cylinder), b) three specimens cored vertically from the compacted specimen (3in1 Cylinder), and c) two specimens cored horizontally from the compacted specimen (Side Cylinder).



Figure E2d.7. Cylindrical specimen in the TSRST chamber.

All cylindrical specimens had a diameter of 2.25 inches. The heights of the cylindrical specimens that are cored vertically were all 6 inches. The cylinders that were cored horizontally had heights of 5.5 inches. Two binder types were used in this study and had PG grades of PG64-22 and PG 64-28. The low temperature grades of the binders were also determined by extracting and recovering the binder of the tested specimens. Furthermore, 2-D image analysis was conducted to determine if there were any differences as far as aggregate contact points and aggregate orientation of the various specimen types. The testing matrix is shown in table E2d.4. It was determined that coring gyratory compacted samples horizontally would better simulate the actual orientation of an asphalt mixture in the field. Therefore, only cylinders that were cored horizontally from gyratory compacted specimens were used to compare them to beam specimens for the PG 64-28 binder.

Table E2d.4. TSRST experiment test matrix.

Binder	Test	Beam Specimens	Center Cylinder	3in1 Cylinder	Side Cylinder
PG 64-22	TSRST @ Cooling rate of - 10°C/hr	X	X	X	X
	2-D Image Analysis	X	X	X	X
	Extraction/Recovery	X	X	X	X
PG 64-28	TSRST @ Cooling rate of - 10°C/hr	X			X
	2-D Image Analysis	X			X
	Extraction/Recovery	X			X

Table E2d.5 presents initial results of the experiment thus far. It can be observed that cylindrical specimens compare well if not better than beam specimens regarding fracture stress and fracture temperature. Particularly, side cylinders seem to be a promising alternative to beams. Analysis of aggregate orientation and contact points is still being conducted. Furthermore, low temperature grade of tested specimens are still being prepared. Future work includes utilizing the cylindrical geometry to determine the effect of cooling rate on the fracture stress and fracture temperature.

Table E2d.5. TSRST results of various specimen shapes and sizes.

Binder	Specimen	Avg. Fracture Stress, MPa	Coefficient of Variation, %	Avg. Fracture Temperature, °C	Coefficient of Variation, %
PG64-22	Beams	1.8	19.0	-24.2	17.0
	Center Cylinder	1.7	11.0	-23.3	8.0
	3in1 Cylinder	1.4	16.0	-21.6	10.5
	Side Cylinder	1.6	11.0	-25.4	8.4
PG64-28	Beams	1.4	18.0	-31.9	9.4
	Side Cylinder	1.6	12.0	-29.5	3.7

Under subtask E2d-4, UNR is working with TTI for the possibility of modifying the viscoelastic finite element tool (VE2D) developed by TTI to incorporate the findings of this work element. The “VE2D” is used for pavement low temperature cracking analysis and is based on viscoelastic two-dimensional (2D) finite element (FE) method. The “VE2D” is being evaluated for possible incorporation of the following general features:

1. Account for different coefficient of thermal expansions as a function of temperature and time (aging effect)
2. Account for the effect of aging on the asphalt layer property
3. Use the developed temperature model

Significant Problems, Issues and Potential Impact on Progress

Some of the SENB test results showed inconsistencies in the level of noise of the raw data. Figure E2d.8 shows two replicates of the same binder tested one after the other. The results indicate that although both the fracture load and deformation have a coefficient of variance below 10%, Sample 1 has a considerable amount of noise, while the noise in Sample 2 is relatively small. Another interesting observation is the change in noise level during the same test for Sample 1. Similar noise occurrences were randomly seen in other samples. Possible explanations could be interference from cell phones and other electronic devices or fluctuations in the voltage amplitude. Both explanations are currently being investigated.

Although this problem can easily be addressed by using moving average or curve fitting, it is inconvenient for data analysis; therefore, efforts are being made to isolate and eliminate the cause of this random noise.

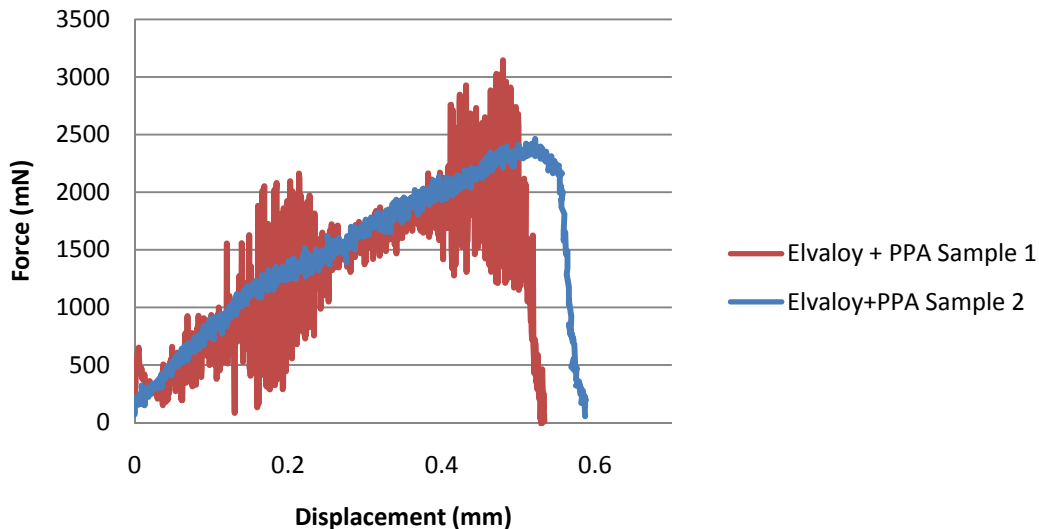


Figure E2d.8. Graph. Comparison of noise level in SENB replicates tested at -18 °C.

The write-ups for the figures and tables captions have delayed the submission of the report for the temperature rates in the intermountain region.

Further progress has been made in the E*-tension area, however mechanical control issues have caused delays in the actual testing. It is believed that all of the necessary components have been obtained (software, hardware, and procedures) they merely need to be installed and implemented. The E* tension samples were produced and aged along with the E* compression samples, so it is expected that the testing will be completed more efficiently than the E* compression, since the samples are already aged. This eliminates the wait time due to oven aging.

With the DSR equipment at UNR being broken no binder master curves or LSV testing can be conducted there. It is not clear when the equipment will be repaired, however efforts are being made to expedite the process.

Difficulties with equipment results and scheduling have caused some delays in the FT-IR testing that had been conducted at UWM. After much consideration by all parties involved, it appears that the FT-IR testing will now be completed by Texas A&M personnel at their facilities. Although the details are not fully established, some samples have already been tested with improved results.

Work Planned Next Quarter

Continue the experiment to evaluate the aging characteristics (oxidation and hardening kinetics) of asphalt binders when aged in forced convection (horizontal airflow) ovens.

The research team will develop the draft procedure for SENB testing now that the planned test matrix has been carried out. The investigation of the relationship between fracture properties above and below the T_g , as well as the relationship between BBR and SENB results will continue. Also, a Flint Hills neat binder (PG 64-22) and Flint Hills binder plus a warm mix additive (e.g., Sasobit) and PPA have also been prepared and will be tested to complete the SENB testing matrix.

Incorporation of the developed fixtures for the TSRST into the T_g device will be completed in the next quarter. Experiments will continue to determine the ideal process for building test samples by coring gyratory-compacted samples. The research team will also focus efforts on modeling the glass transition behavior of asphalt mixtures using finite elements.

Complete the tables and figures write-ups for the report.

The main focus early in the next quarter will be on preparing the TSRST and α samples so that their aging will be complete in time for testing and analysis. The extraction and recovery procedures will continue as will the testing that follows. The FT-IR testing is expected to be moving forward at Texas A&M. The E^* compression testing will continue as the samples complete their aging cycles. Establishment of the E^* tension procedure is expected to finally reach completion in the next few months. And the development of the binder master curves is expected to proceed with little difficulty once the DSR has been repaired. Testing on the TSRST will also begin as samples are available from their respective aging cycles.

Complete the TSRST experiment and submit a paper summarizing the findings of the study. Write an AASHTO draft procedure for the TSRST samples preparation and testing.

Work with TTI to develop a plan on how to modify the viscoelastic finite element tool (VE2D) to incorporate the findings of this work element.

Cited Reference

Hu, S., Zhou, F., and L.F. Walubita, 2009, Development of a viscoelastic finite element tool (VE2D) tailored for asphalt pavement low temperature cracking analysis. *Journal of Road Materials and Pavement Design*, 10 (4), 1-22.

Work element E2e: Design Guidance for Fatigue and Rut Resistance Mixtures (AAT)

Work Done This Quarter

The results of the extended uniaxial fatigue experiment was reanalyzed this Quarter to determine if the fatigue data from tests covering a wide range of temperatures and frequencies do in fact collapse into a unique damage relationship or if the damage relationship is different for different conditions. The major finding from this was the damage relationship depends on the initial stiffness of material tested. Materials with low initial stiffness exhibit higher rates of damage at low numbers of cycles compared to materials with high initial stiffness. However, as damage progresses with increasing cycles, low initial stiffness materials show lower rates of damage accumulation compared to high initial stiffness materials. This initial stiffness effect for the damage relationship has not been reported by other investigators using continuum damage theory, perhaps because the range of temperatures and frequencies used were not as broad as those included in the extended uniaxial fatigue experiment: temperatures from -5 to 30 °C and testing frequencies for 1 and 10 Hz. As a result, the fatigue testing protocol and analysis method for the AMPT uniaxial fatigue test will require modification to capture the initial stiffness effect.

The experimental designs for the Hirsch model, and rutting model experiments were revised and potential material sources were identified. The fatigue model experiment will be revised after the revised testing and analysis protocols are developed.

Work was initiated on a journal paper describing how to estimate binder modulus master curves from measurements made during performance grading. This will allow specification property data to be used with the Hirsch model rather than special frequency sweep data.

Significant Problems, Issues and Potential Impact on Progress

None.

Work Planned Next Quarter

The AMPT fatigue testing protocol and analysis will be revised to account for the effect of initial stiffness on the damage function. The fatigue model experiment will be revised based on the revised testing protocol and analysis procedure.

The journal paper describing how to estimate binder modulus master curves from binder grading test results will be completed.

Materials for the Hirsch model, rutting model, and fatigue experiments will be procured for the laboratory testing.

Engineered Materials Year 4	Year 4 (4/2010-3/2011)												Team
	4	5	6	7	8	9	10	11	12	1	2	3	
(1) High Performance Asphalt Materials													
E1a: Analytical and Micro-mechanics Models for Mechanical behavior of mixtures													TAMU
E1a-1: Analytical Micromechanical Models of Binder Properties				P							P		
E1a-2: Analytical Micromechanical Models of Modified Mastic Systems				P							P		
E1a-3: Analytical Models of Mechanical Properties of Asphalt Mixtures				P, JP			JP (2)		JP (2)		P		M&A
E1a-4: Analytical Model of Asphalt Mixture Response and Damage											P		
E1b: Binder Damage Resistance Characterization													UWM
E1b-1: Rutting of Asphalt Binders													
E1b-1-i. Literature review													
E1b-1-ii. Select Materials & Develop Work Plan													
E1b-1-iii. Conduct Testing				DP									
E1b-1-iv. Analysis & Interpretation									JP				
E1b-1-v. Standard Testing Procedure and Recommendation for Specifications							P					DP	
E1b-2: Feasibility of determining rheological and fracture properties of asphalt binders and mastics using simple indentation tests (modified title)													UWM
E1b-2-i. Literature Review													
E1b-2-ii. Proposed SuperPave testing modifications													
E1b-2-iii. Preliminary testing and correlation of results								JP					
E1b-2-iv. Feasibility of using indentation tests for fracture and rheological properties											P		D
E2a: Comparison of Modification Techniques													UWM
E2a-1: Identify modification targets and material suppliers													
E2a-2: Test material properties							P						
E2a-3: Develop model to estimate level of modification needed and cost index													
E2a-4: Write asphalt modification guideline/report on modifier impact over binder properties								JP					
E2c: Critically Designed HMA Mixtures													UNR
E2c-1: Identify the Critical Conditions													
E2c-2: Conduct Mixtures Evaluations								JP					
E2c-3: Develop a Simple Test													
E2c-4: Develop Standard Test Procedure													
E2c-5: Evaluate the Impact of Mix Characteristics													
E2d: Thermal Cracking Resistant Mixes for Intermountain States													UWMUNR
E2d-1: Identify Field Sections													
E2d-2: Identify the Causes of the Thermal Cracking													
E2d-3: Identify an Evaluation and Testing System								JP				P	
E2d-4: Modeling and Validation of the Developed System								JP					P
E2d-5: Develop a Standard													
E2e: Design Guidance for Fatigue and Rut Resistance Mixtures													AAT
E2e-1: Identify Model Improvements													
E2e-2: Design and Execute Laboratory Testing Program													
E2e-3: Perform Engineering and Statistical Analysis to Refine Models									JP				
E2e-4: Validate Refined Models													
E2e-5: Prepare Design Guidance													
(2) Green Asphalt Materials													
E2b: Design System for HMA Containing a High Percentage of RAP Material													UNR
E2b-1: Develop a System to Evaluate the Properties of RAP Materials			P				JP				P		
E2b-2: Compatibility of RAP and Virgin Binders													
E2b-3: Develop a Mix Design Procedure										D			
E2b-4: Impact of RAP Materials on Performance of Mixtures													
E2b-5: Field Trials								JP					
E1c: Warm and Cold Mixes													UWM
E1c-1: Warm Mixes													
E1c-1-i. Effects of Warm Mix Additives on Rheological Properties of Binders													
E1c-1-ii. Effects of Warm Mix Additives on Mixture Workability and Stability								JP					
E1c-1-iii. Mixture Performance Testing													
E1c-1-iv. Develop Revised Mix Design Procedures													
E1c-1-v. Field Evaluation of Mix Design Procedures and Performance Recommendations													
E1c-2: Improvement of Emulsions' Characterization and Mixture Design for Cold Bitumen Applications													UWMUNR
E1c-2-i. Review of Literature and Standards										D			
E1c-2-ii. Creation of Advisory Group													
E1c-2-iii. Identify Tests and Develop Experimental Plan													
E1c-2-iv. Develop Material Library and Collect Materials													
E1c-2-v. Conduct Testing Plan								JP				P	
E1c-2-vi. Develop Performance Selection Guidelines								JP				P	F
E1c-2-vii. Validate Performance Guidelines													
E1c-2-viii. Develop CMA Mix Design Guidelines													
E1c-2-ix. Develop CMA Performance Guidelines													

Deliverable codes
D: Draft Report
F: Final Report
M&A: Model and algorithm
SW: Software
JP: Journal paper
P: Presentation
DP: Decision Point

Deliverable Description
Report delivered to FHWA for 3 week review period.
Final report delivered in compliance with FHWA publication standards
Mathematical model and sample code
Executable software, code and user manual
Paper submitted to conference or journal
Presentation for symposium, conference or other
Time to make a decision on two parallel paths as to which is most promising to follow through

Work planned
Work completed
Parallel topic

Engineered Materials Year 2 - 5	Year 2 (4/08-3/09)				Year 3 (4/09-3/10)				Year 4 (04/10-03/11)				Year 5 (04/11-03/12)				Team
	Q1	Q2	Q3	Q4	Q1	Q2	Q3	Q4	Q1	Q2	Q3	Q4	Q1	Q2	Q3	Q4	
(1) High Performance Asphalt Materials																	
E1a: Analytical and Micro-mechanics Models for Mechanical behavior of mixtures																	
E1a-1: Analytical Micromechanical Models of Binder Properties			P, JP	JP	P	P	JP		P	P	P	JP	D, JP	F		TAMU	
E1a-2: Analytical Micromechanical Models of Modified Mastic Systems			P, JP	JP	P	P			P	P	JP	D	F, SW, M&A				
E1a-3: Analytical Models of Mechanical Properties of Asphalt Mixtures	P	P, JP	P, JP	JP	P	P	M&A		P, JP(3)	JP (2)	P, M&A	P	JP(2)	D, JP	F, SW, M&A		
E1a-4: Analytical Model of Asphalt Mixture Response and Damage			P, JP	JP	P	P					P	P		D	F, SW, M&A		
E1b: Binder Damage Resistance Characterization																	
E1b-1: Rutting of Asphalt Binders																	
E1b-1-1: Literature review																UWM	
E1b-1-2: Select Materials & Develop Work Plan	DP, P		P														
E1b-1-3: Conduct Testing			P						DP								
E1b-1-4: Analysis & Interpretation			JP	P	JP					JP							
E1b-1-5: Standard Testing Procedure and Recommendation for Specifications										P	DP	P	D	JP	F		
E1b-2: Feasibility of Determining rheological and fracture properties of asphalt binders and mastics using simple indentation tests (modified title)																	
E1b-2i. Literature Review					D												
E1b-2ii. Proposed SuperPave testing modifications or new testing devices					P												
E1b-2iii. Preliminary testing and correlation of results							D		JP								
E1b-2iv. Feasibility of using indentation tests for fracture and rheological properties					JP		P				P, D	F					
E2a: Comparison of Modification Techniques																	
E2a-1: Identify modification targets and material suppliers				DP		DP										UWM	
E2a-2: Test material properties							P			P							
E2a-3: Develop model to estimate level of modification needed and cost index																	
E2a-4: Write asphalt modification guideline/report on modifier impact over binder properties									JP								
E2c: Critically Designed HMA Mixtures																	
E2c-1: Identify the Critical Conditions			JP		D, F		JP	D	F							UNR	
E2c-2: Conduct Mixtures Evaluations								D		JP							
E2c-3: Develop a Simple Test												D, F	JP				
E2c-4: Develop Standard Test Procedure												D, F					
E2c-5: Evaluate the Impact of Mix Characteristics															D, F		
E2d: Thermal Cracking Resistant Mixes for Intermountain States																	
E2d-1: Identify Field Sections																	
E2d-1: Identify Field Sections			D, F	D, F	D	F										UWM/UNR	
E2d-2: Identify the Causes of the Thermal Cracking																	
E2d-3: Identify an Evaluation and Testing System					DP	JP	DP, D			JP	P	JP					
E2d-4: Modeling and Validation of the Developed System										JP	P				D, F		
E2d-5: Develop a Standard															D, F		
E2e: Design Guidance for Fatigue and Rut Resistance Mixtures																	
E2e-1: Identify Model Improvements																	
E2e-1: Identify Model Improvements																AAAT	
E2e-2: Design and Execute Laboratory Testing Program																	
E2e-3: Perform Engineering and Statistical Analysis to Refine Models									JP				P, D, F				
E2e-4: Validate Refined Models													JP				
E2e-5: Prepare Design Guidance														M&A	P, D, F		
(2) Green Asphalt Materials																	
E2b: Design System for HMA Containing a High Percentage of RAP Material																	
E2b-1: Develop a System to Evaluate the Properties of RAP Materials		JP		P	D	D, F	D		P	JP	P					UNR	
E2b-2: Compatibility of RAP and Virgin Binders													D, F	JP			
E2b-3: Develop a Mix Design Procedure								D			D		D, F	JP			
E2b-4: Impact of RAP Materials on Performance of Mixtures															D, F		
E2b-5: Field Trials										JP					D, F		
E1c: Warm and Cold Mixes																	
E1c-1: Warm Mixes																	
E1c-1i: Effects of Warm Mix Additives on Rheological Properties of Binders.																	
E1c-1i. Effects of Warm Mix Additives on Rheological Properties of Binders.																UWM	
E1c-1iii. Effects of Warm Mix Additives on Mixture Workability and Stability		P	D	F, DP						JP						UWM	
E1c-1iii. Mixture Performance Testing							JP		P, DP	DP, P						UW/UNR	
E1c-1iv. Develop Revised Mix Design Procedures																UW/UNR	
E1c-1v. Field Evaluation of Mix Design Procedures and Performance Recommendations														JP	D	P, F	
E1c-2: Improvement of Emulsions' Characterization and Mixture Design for Cold Bitumen Applicators																	
E1c-2i: Review of Literature and Standards		JP, P, D	F		D1	D3	D6				D					UWM	
E1c-2ii: Creation of Advisory Group																	
E1c-2ii: Identify Tests and Develop Experimental Plan				P, DP	D1	D4											
E1c-2iv. Develop Material Library and Collect Materials.																	
E1c-2v. Conduct Testing Plan										JP	P						
E1c-2vi. Develop Performance Selection Guidelines										JP	P, F						
E1c-2vii. Validate Guidelines													JP			P, F	
E1c-2viii. Develop CMA Mix Design Procedure						D2											
E1c-2ix. Develop CMA Performance Guidelines														JP	D	P, F	

Deliverable codes
D: Draft Report
F: Final Report
M&A: Model and algorithm
SW: Software
JP: Journal paper
P: Presentation
DP: Decision Point

Deliverable Description
Report delivered to FHWA for 3 week review period.
Final report delivered in compliance with FHWA publication standards
Mathematical model and sample code
Executable software, code and user manual
Paper submitted to conference or journal
Presentation for symposium, conference or other
Time to make a decision on two parallel paths as to which is most promising to follow through

Work planned
Work completed
Parallel topic
Delayed

PROGRAM AREA: VEHICLE-PAVEMENT INTERACTION

CATEGORY VP1: WORKSHOP

Work element VP1a: Workshop on Super-Single Tires

This work element is complete.

CATEGORY VP2: DESIGN GUIDANCE

Work element VP2a: Mixture Design to Enhance Safety and Reduce Noise of HMA (UWM)

Work Done This Quarter

Work this quarter focused on developing a testing plan to integrate laser profilometer (LP), British Pendulum Skid Resistance Tester, sand-patch, and noise tube measurements to measure asphalt mix surface properties and relate these measurements to noise and friction. The testing plan and experimental matrix are based on available field cores and laboratory gyratory-compacted samples. The testing progression is illustrated in figure VP2a.1.

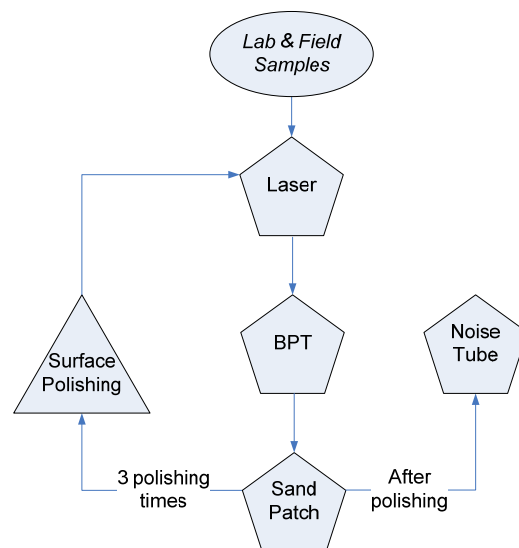


Figure VP2a.1. Diagram. Planned testing progression for analyzing field and lab samples.

Field cores and lab samples are first subjected to LP testing to obtain a surface texture profile. Texture profiles are then analyzed following standard procedures to determine the profile texture

spectrum and mean profile depth (MPD) (ISO 2004; ISO 2005). Testing samples using the British Pendulum Tester (BPT) in accordance with ASTM E303 (2008) yields values for the British Pendulum Number (BPN). A volumetric method commonly known as the sand-patch method is used to investigate the surface mean texture depth (MTD) and follows ASTM E965 (2006). This testing progression repeats three times following surface polishing. After the last iteration of surface texture and profile measurements, a noise tube is used to investigate the sample's acoustic spectrum. Table VP2a.1 describes the factors and levels that will be considered throughout the experiment.

Table VP2a.1. Factors, levels and descriptions for the experimental matrix.

Factors	Levels	Description
Field Sections	8	Includes state highways and U.S. highways from around Wisconsin
Field Samples	2	Two randomly selected field cores extracted from field sites following construction
Lab Samples	3	Loose mix samples obtained from field sites and compacted at given temperatures and pressures
Profiles	4	Number of profiles per sample measured with the LP and BPT

Significant Results

Two analysis techniques may be considered for analyzing LP measurements (Losa 2008; ISO 2004; ISO 2005). The analysis techniques differ in terms of the filter type used to process the digital signal generated by the LP. Alternative 1 utilizes Butterworth's numerical filters while Alternative 2 utilizes moving average filters. Analysis of LP measurements suggests that applying Alternative 1 results in a stronger relationship between field core sample MPD measurements and lab sample MPD measurements. Figure VP2a.2 explores the relationship between field MPD and lab MPD measurements for both analysis methods. Figure VP2a.3 demonstrates the effect of laboratory compaction conditions on the relationship between field and lab MPD measurements.

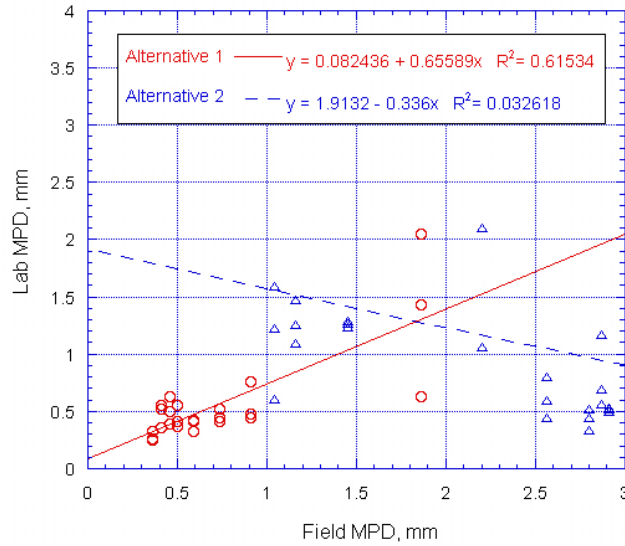


Figure VP2a.2. Graph. Comparison of alternative MPD calculation methods.

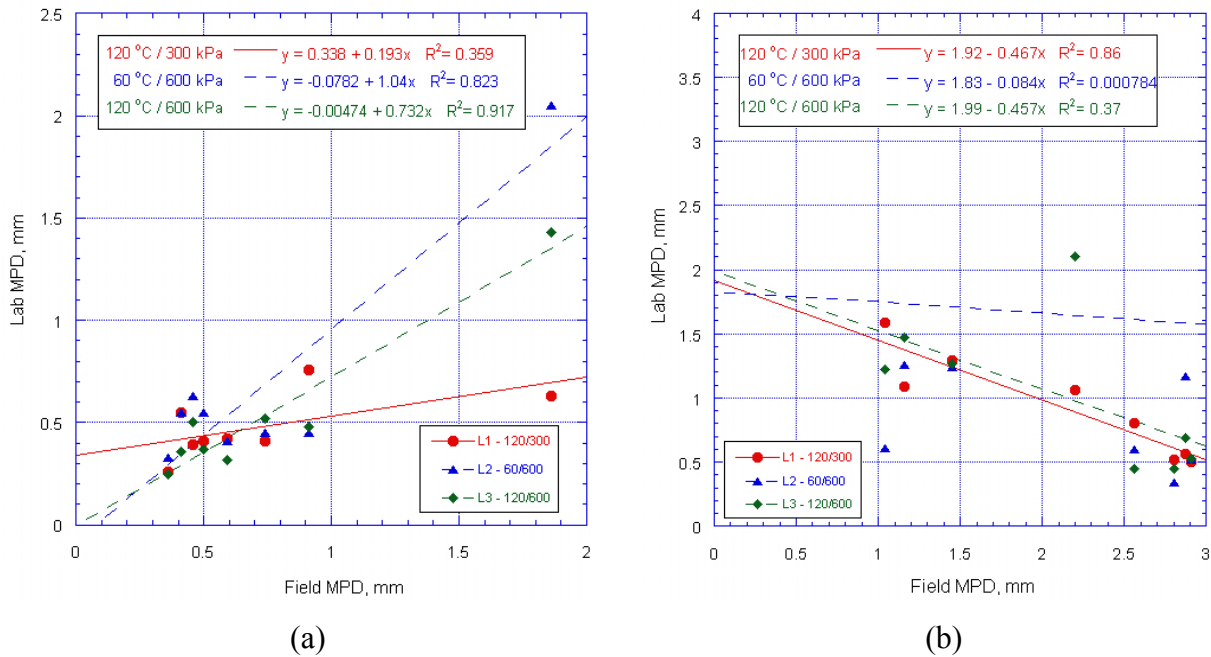


Figure VP2a.3. Graphs. Comparison of laboratory MPD measurements for three compaction conditions for: (a) Alternative 1; and (b) Alternative 2.

Results depicted in figure VP2a.3 demonstrate the effects of varying compaction temperatures and pressures. Table VP2a.2 describes the compaction conditions for the laboratory samples. For Alternative 1, compaction conditions of 120 °C and 600 kPa yield the strongest positive correlation, while compaction conditions of 120 °C and 300 kPa yield the weakest relationship

between field core MPD values and lab sample MPD values. For Alternative 2, compaction conditions of 120 °C and 300 kPa yield the strongest relationship, while compaction conditions of 60 °C and 600 kPa yield the weakest relationship.

Table VP2a.2. Compaction conditions for laboratory samples.

Lab Sample	Temperature (°C)	Pressure (kPa)
L1	120	300
L2	60	600
L3	120	600

LP measurements for lab and field samples may also be considered in terms of texture spectral analysis. Figure VP2a.4 displays the texture spectral analysis for two field samples (F1 and F2) and three lab samples (L1, L2 and L3) from U.S. 45 in rural Wisconsin. Seven other road sections are analyzed in a similar fashion. For this particular road section, field sample 1 (F1) exhibits a similar profile to laboratory sample 2 (L2) and laboratory sample 3 (L3), while field sample 2 (F2) appears most similar to laboratory sample 1 (L1). While the samples may exhibit texture spectrum profiles that are similar in shape, some shift factor is apparent between field and lab samples.

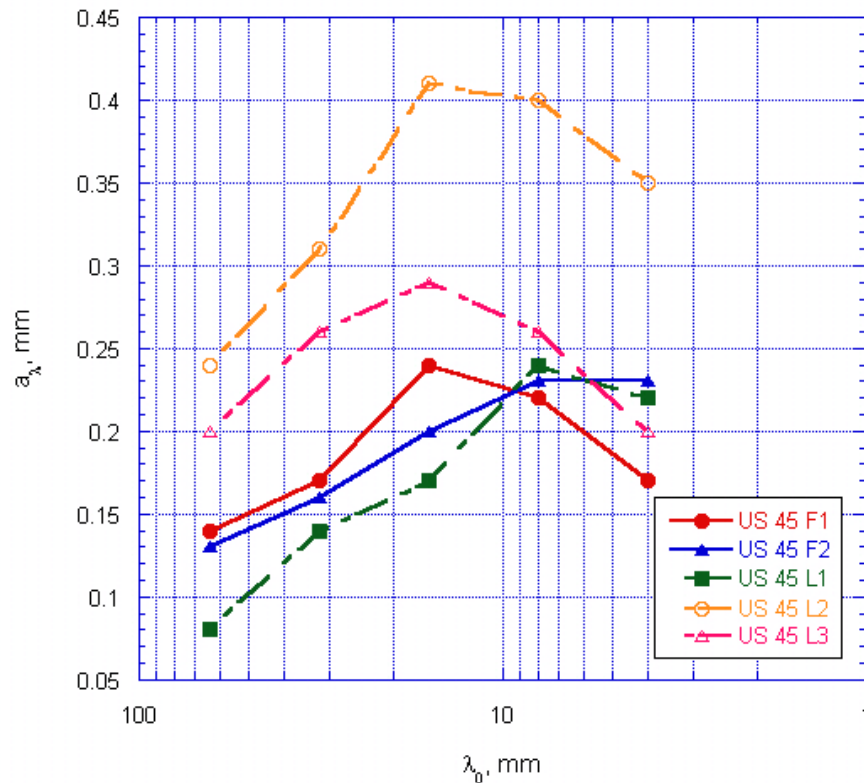


Figure VP2a.4. Graph. Texture spectral analysis comparison for U.S. 45 field and lab samples.

Significant Problems, Issues and Potential Impact on Progress

The noise tube continues to pose issues for research personnel. The team will continue to collaborate with researchers at the University of Pisa to successfully calibrate the noise tube during the next quarter. Once issues related to software installation are resolved, noise measurements should proceed without further hindrance.

To reflect the actual progress of this research, the Gantt chart has been updated to show the planned journal paper deliverable for subtask VP2a-4 will be delivered in August 2010 instead of May 2010.

Work Planned Next Quarter

Work next quarter will focus on the following tasks:

- *Polishing procedures for laboratory and field samples.* Polishing effects depend on particular combinations of rotational speed, contact time, and the material used to polish the sample surface. The effect of polishing will be quantified by LP, BPT and sand-patch measurements.
- *Field measurements for validating experimental results.* Identifying field locations for field samples will validate experimental results. Emphasis will be placed on developing efficient methods for collecting data in the field. Projected field tests include LP, BPT and the sand-patch test.
- *Correlating test methods.* Results from LP, BPT and sand-patch testing will be analyzed and compared to determine which factors lead to higher skid resistance and optimized texture spectrum. These results will allow for comparison to noise measurements.

Cited References

ASTM, 2006, ASTM E965-06, Standard Test Method for Measuring Pavement Macrotexture Depth Using a Volumetric Technique. American Society for Testing and Materials, West Conshohocken, PA.

ASTM, 2008, ASTM E303, Standard Test Method for Measuring Surface Frictional Properties Using the British Pendulum Tester. American Society for Testing and Materials, West Conshohocken, PA.

ISO, 2004, EN ISO 13473-1, Characterization of Pavement Texture by Use of Surface Profiles – Part 1: Determination of Mean Profile Depth. International Organization for Standardization.

ISO, 2005, EN ISO 13473-4, Characterization of Pavement Texture by Use of Surface Profiles – Part 4: Spectral Analysis of Texture Profiles. International Organization for Standardization.

Losa, M., 2008, The Reliability of Tests and Data Processing Procedures for Pavement Macrotexture Evaluation. *Measurement*,

CATEGORY VP3: MODELING

Work element VP3a: Pavement Response Model to Dynamic Loads (UNR)

Work Done This Quarter

Continued the work on the *3D-Move Analysis* software to make it a menu-driven software. Released the beta-version of the *3D-Move Analysis* software in June 2010 and continued the testing of the released version. A Help Menu was created and incorporated in the *3D-Move Analysis* software. Created an internet based forum “3D-Move Discussion Group” to provide guidance and feedback to a user.

The effect of stress distribution and braking condition on pavement responses is under evaluation. The 3D-Move built-in database for the non-uniform contact pressure distribution is being used in this analysis.

Significant Results

3D-Move Release

The beta-version of the 3D-Move Analysis (ver 1.0) was released on June, 2010 and is available to download from the ARC website (www.arc.unr.edu/Software.html). We are continually undertaking product testing under variety of pavement loading and material conditions. Our investigation has revealed under certain pavement layer configurations and vehicle loading conditions (e.g., unrealistic thicknesses and vehicle speeds) can lead to numerical instability as a direct result of under or overflow of computer memory. Though almost all such cases are unrealistic, we have provided controls such that numerical instability is avoided. We intend to upload to the website the modified versions of the software in a periodic manner. Users are requested to check the website periodically for updated versions and use the updates. The latest beta-version (ver 1.1) is available for download from the ARC website. Suggestions and questions regarding the software can be posted in 3D-Move Discussion Group. More details on the avenue to undertake this is provided subsequently.

Help Menu

A Help Menu has been created in html format by using HelpMaker software and it is included with the 3D-Move. The Help Menu can be accessed from the main window of the program. Figure VP3a.1 shows the Help Menu window. The following items are included the Help Menu to assist the user.

- Notes on 3D-Move
- Getting Started
- Analysis Type
- Loading Type
- Materials Type
- Examples

As shown in figure VP3a.1, these items are listed on the left side of window. On the right side of window, descriptions associated with the item selected from the list displayed on the left are displayed. For each item, sufficient details are given along with the figures and tables as needed. Figure VP3a.2 shows the window for Loading Type – Option B.

Three examples (Example A, B and C) are included in the Help Menu and details on these examples can be reviewed by making a selection from the left side of the window. These examples were carefully selected to make a user familiar with many of the important options that are available with the software. Figure VP3a.3 shows the first window associated with Example A. This is a case of three layer static pavement response analysis. The subsequent windows provide a step by step help in undertaking the pavement response analysis relative to this example.

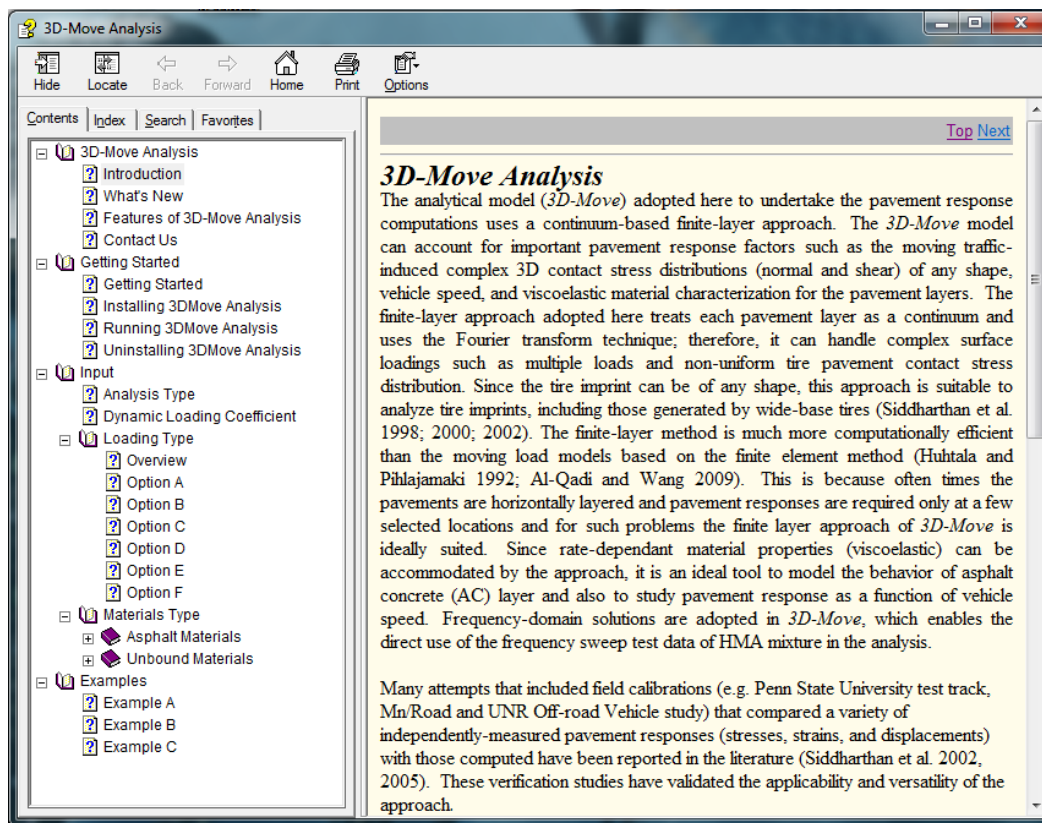


Figure VP3a.1. Help menu window.

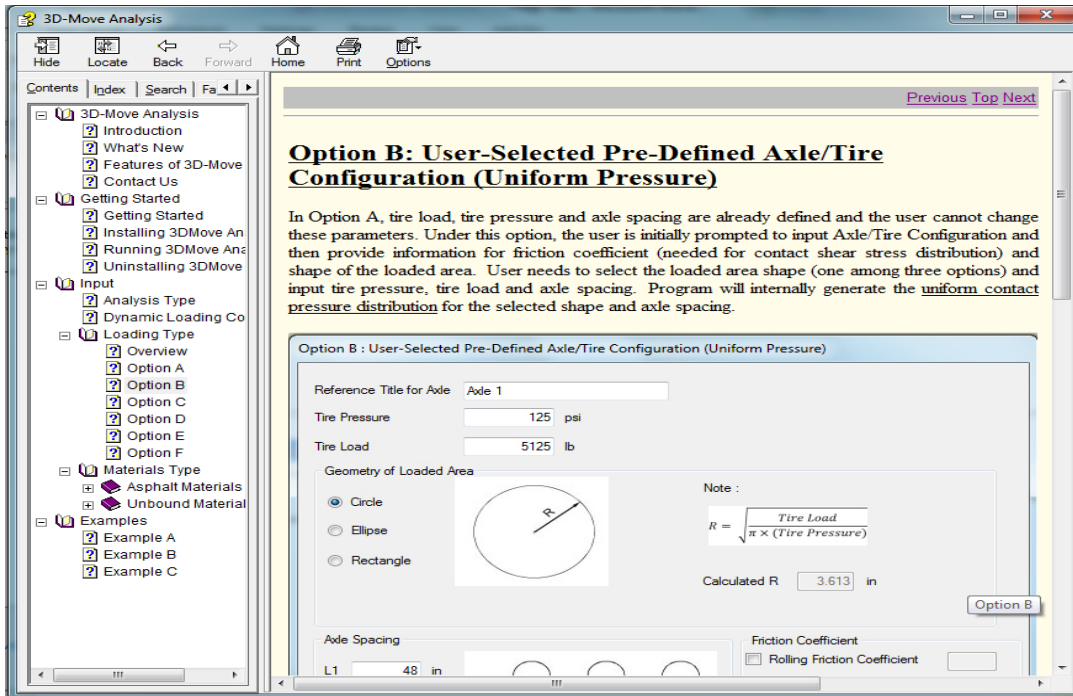


Figure VP3a.2. Help menu window for loading type/Option B.

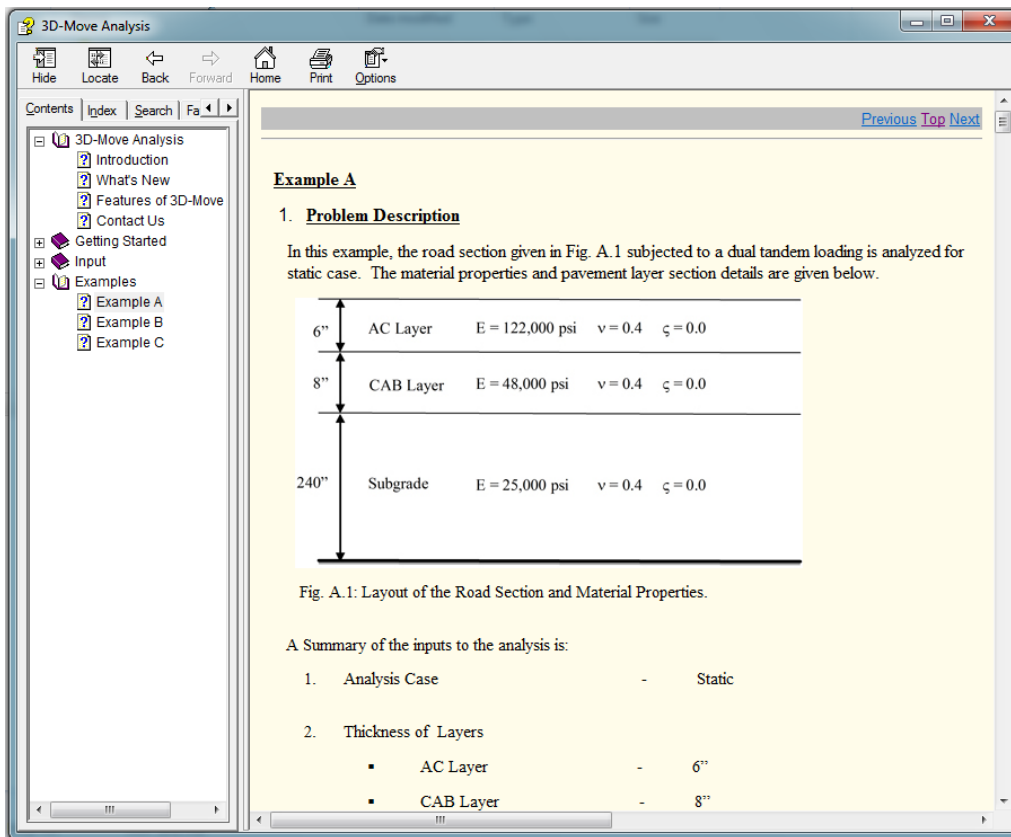


Figure VP3a.3. Step by step help with the Example A.

Discussion and Newsletter Forums

To provide guidance and feedback to a user, an internet based forum “3D-Move Discussion Group” has been created and it can be accessed using the URL <http://3d-move.finddiscussion.com/>. This site is dedicated to collecting the feedback, comments, issues, and concerns etc. of individuals who are evaluating and/or using 3D-Move. There are two forums available at this site: 3D-Move Discussion and 3D-Move Newsletter. The 3D-Move Discussion forum is dedicated for discussion on the features of 3D-Move and providing the solution and feedback to user's questions. Registered users can post questions in the 3D-Move Discussion forum and we will provide the users with answers. The discussions can go on between users and the software administrators and also between users. These discussions will be available at the site for viewing by all registered users (figure Vp3a.4). The other is Newsletter forum. This forum is dedicated to items such as notes on software updates, and also to significant newsworthy information relative to the use of 3D-Move.

The screenshot displays the 3D-Move Discussion Group forum website. The page layout includes a header with the group name and a navigation menu. The main content area features a welcome message, a forum table, and a calendar. The forum table shows two forums: '3D-Move Discussion' with 1 topic and 1 post, and 'Newsletters' with 0 topics and 0 posts. The calendar shows the date July 25, 2010.

Forum	Topics	Posts	Last Posts
3D-Move Discussion	1	1	Welcome Fri 25 Jun 2010 - 14:10 Ellie Hajj
Newsletters	0	0	

Figure VP3a.4. 3D-Move Discussion Group.

Significant Problems, Issues and Potential Impact on Progress

None

Work Planned Next Quarter

Continue working on the 3D-Move model to make it a menu-driven software. Evaluate the beta version for 3D-Move.

New developments relative to integrating performance models in 3D-Move are underway. Specifically, the following widely-used performance models of fatigue and rutting are to be incorporated with the software.

- MEPDG Models
 - AC Fatigue Cracking
 - AC Rutting
 - Base/Subbase Rutting
 - Subgrade Rutting

- VESYS Model
 - Fatigue Cracking
 - Layer Rutting
 - System Rutting

Details on the performance model integration will be included in the next report.

Work will continue on the evaluation of the effect of contact pressure distribution and braking condition on pavement response.

Work out the details for the *3D-Move Analysis* software verification plan in order to evaluate the potential for errors, bugs, and difficulties involved in using the software for pavement analysis purposes. UNR, with the help of FHWA, will solicit users to participate in the verification plan. It is anticipated that the list of participants will include:

- at least three representatives of public agencies,
- at least three representatives of academic researchers,
- at least three representatives of private industries, and
- at least one representative of FHWA.

Vehicle-Pavement Interaction Year 4

	Year 4 (4/2010-3/2011)												Team	
	4	5	6	7	8	9	10	11	12	1	2	3		
(1) Workshop														
VP1a: Workshop on Super-Single Tires														UNR
(2) Design Guidance														
VP2a: Mixture Design to Enhance Safety and Reduce Noise of HMA														UWM
VP2a-1: Evaluate common physical and mechanical properties of asphalt mixtures with enhanced frictional skid characteristics														
VP2a-2: Evaluate pavement macro- and micro-textures and their relation to tire and pavement noise-generation mechanisms														
VP2a-3: Develop a laboratory testing protocol for the rapid evaluation of the macro and micro-texture of pavements														
VP2a-4: Run parametric studies on tire-pavement noise and skid response														
VP2a-5: Establish collaboration with established national laboratories specialized in transportation noise measurements. Gather expertise on measurements and analysis														
VP2a-6: Model and correlate acoustic response of tested tire-pavement systems														
VP2a-7: Proposed optimal guideline for design to include noise reduction, durability, safety and costs														
(3) Pavement Response Model Based on Dynamic Analyses														
VP3a: Pavement Response Model to Dynamic Loads														UNR
VP3a-1: Dynamic Loads														
VP3a-2: Stress Distribution at the Tire-Pavement Interface														
VP3a-3: Pavement Response Model														
VP3a-4: Overall Model														

Deliverable codes

- D: Draft Report
- F: Final Report
- M&A: Model and algorithm
- SW: Software
- JP: Journal paper
- P: Presentation
- DP: Decision Point

Deliverable Description

- Report delivered to FHWA for 3 week review period.
- Final report delivered in compliance with FHWA publication standards
- Mathematical model and sample code
- Executable software, code and user manual
- Paper submitted to conference or journal
- Presentation for symposium, conference or other
- Time to make a decision on two parallel paths as to which is most promising to follow through

	Work planned
	Work completed
	Parallel topic

Vehicle-Pavement Interaction Years 2 - 5	Year 2 (4/08-3/09)				Year 3 (4/09-3/10)				Year 4 (04/10-03/11)				Year 5 (04/11-03/12)				Team
	Q1	Q2	Q3	Q4	Q1	Q2	Q3	Q4	Q1	Q2	Q3	Q4	Q1	Q2	Q3	Q4	
(1) Workshop																	
VP1a: Workshop on Super-Single Tires																	UNR
(2) Design Guidance																	
VP2a: Mixture Design to Enhance Safety and Reduce Noise of HMA																	UWM
VP2a-1: Evaluate common physical and mechanical properties of asphalt mixtures with enhanced frictional skid characteristics				DP													
VP2a-2: Evaluate pavement macro- and micro-textures and their relation to tire and pavement noise-generation mechanisms				DP													
VP2a-3: Develop a laboratory testing protocol for the rapid evaluation of the macro and micro-texture of pavements		M&A															
VP2a-4: Run parametric studies on tire-pavement noise and skid response						JP		D	JP								
VP2a-5: Establish collaboration with established national laboratories specialized in transportation noise measurements. Gather expertise on measurements and analysis																	
VP2a-6: Model and correlate acoustic response of tested tire-pavement systems										JP, P							
VP2a-7: Proposed optimal guideline for design to include noise reduction, durability, safety and costs													P				
(3) Pavement Response Model Based on Dynamic Analyses																	
VP3a: Pavement Response Model to Dynamic Loads																	UNR
VP3a-1: Dynamic Loads			JP														
VP3a-2: Stress Distribution at the Tire-Pavement Interface																	
VP3a-3: Pavement Response Model						SW, v. β						JP		SW, JP			
VP3a-4: Overall Model												SW		D	F		

Deliverable codes

- D: Draft Report
- F: Final Report
- M&A: Model and algorithm
- SW: Software
- JP: Journal paper
- P: Presentation
- DP: Decision Point

Deliverable Description

- Report delivered to FHWA for 3 week review period.
- Final report delivered in compliance with FHWA publication standards
- Mathematical model and sample code
- Executable software, code and user manual
- Paper submitted to conference or journal
- Presentation for symposium, conference or other
- Time to make a decision on two parallel paths as to which is most promising to follow through

- Work planned
- Work completed
- Parallel topic

PROGRAM AREA: VALIDATION

CATEGORY V1: FIELD VALIDATION

Work element V1a: Use and Monitoring of Warm Mix Asphalt Sections (WRI)

Work Done This Quarter

During the last quarter, construction of the WMA site in Manitoba was resumed. Recall that this project was begun last fall but was not completed because of the onset of bad weather. WRI and Manitoba personnel collected over 400 pails of construction materials. Together with the pails collected in the fall of 2009, about 470 pails of materials were collected. The pails are about to be shipped from Canada to the ARC researchers at UNR, UWM, WRI, and also to the MRL in Sparks, Nevada.

Significant Results

None.

Significant Problems, Issues and Potential Impact on Progress

None.

Work Planned Next Quarter

It is planned to begin testing of the Manitoba WMA materials after they arrive from Canada. It is also planned to conduct the annual monitoring the Yellowstone WMA sections and establish and conduct the initial monitoring of the Manitoba WMA sections in the next quarter.

Work element V1b: Construction and Monitoring of Additional Comparative Pavement Validation sites (WRI)

Work Done This Quarter

During the last quarter, FHWA and WRI agreed to consolidate the performance monitoring of the comparative pavement performance sites under the Fundamental Properties of Asphalts and Modified Asphalts III contract with the sites under the ARC contract. Thus, the Arizona, Kansas, Minnesota, and Manitoba RAP sites will all be monitored and reported under this work element. The Yellowstone and Manitoba WMA sites will be monitored and reported under Work Element V1a: Use and Monitoring of Warm Mix Asphalt Sections.

The Kansas comparative pavement performance site was monitored in May 2010. There is beginning to be a noticeable performance difference between the sections. However, the impact

of the different asphalt sources, which were placed in the bottom lift of the pavement, is unclear at this point. Kansas DOT and WRI personnel are continuing to evaluate the sections.

Significant Results

None.

Significant Problems, Issues and Potential Impact on Progress

None.

Work Planned Next Quarter

During the next quarter, it is planned to conduct the annual monitoring of the Minnesota and Manitoba RAP comparative pavement performance sites.

CATEGORY V2: ACCELERATED PAVEMENT TESTING

Work element V2a: Accelerated Pavement Testing including Scale Model Load Simulation on Small Test Track (WRI)

Work Done This Quarter

No activity this quarter. This work element was included in order to accommodate any accelerated testing that may occur during the project.

Significant Results

None.

Significant Problems, Issues and Potential Impact on Progress

None.

Work Planned Next Quarter

No accelerated (field) testing is planned.

Work element V2b: Construction of Validation Sections at the Pecos Research & Testing Center (WRI)

This work element is included to indicate that this may be a possibility for accelerated pavement testing for ARC research because it is a facility in the TAMU system.

CATEGORY V3: R&D VALIDATION

Work element V3a: Continual Assessment of Specifications (UWM)

Work Done This Quarter

In this quarter, the research team continued to collaborate with the Western Cooperative Test Group (WCTG), the Rocky Mountain Asphalt User/Producer Group (RMAUPG), state highway agencies and industry to validate the findings of the research activities of the consortium and to evaluate Superpave PG and PG-Plus tests. The research team focused on building a database of binder performance using current PG specification, PG-Plus and new technologies developed by the ARC. An example of the database sections that have been developed is presented in table V3a.1. Please note that the actual database is much larger and what is shown is for illustration purposes.

Table V3a.1. Example of the database generated in work element V3a.

Binder Information				Ductility				Toughness				Tenacity				MSCR (3.2kPa)												T301 ER						
Binder Code	PG		Modification	Source	Unaged		RTFO		Unaged		Unaged		Testing (RTFO)												25C (RTFO)									
	Hi	Low			Nearest 0.1cm	COV (%)	Nearest 0.1cm	COV (%)	inch-lbs	COV (%)	inch-lbs	COV (%)	Temp (°C)	Jnr (1/MPa)	COV (%)	% Recovery	COV (%)	Temp (°C)	Jnr (1/MPa)	COV (%)	% Recovery	COV (%)	Temp (°C)	Jnr (1/MPa)	COV (%)	% Recovery	COV (%)	%ER	COV (%)					
506A	64	-28	None	Suncor	64.4	11%	31.9	11%	143.9	15%	129.0	17%	64	1.9	110%	43%	5%	58	0.9	145%	57%	4%	64	2.65	87%	39%	54%	58	3.2	233%	58%	34%	82.4%	4%
507A	70	-22	TR	Paramount	61.4	14%	34.5	10%	146.0	15%	127.2	16%	70	0.7	43%	65%	15%	64	0.4	121%	79%	10%	70	26.5	148%	26%	31%	64	8.4	222%	84%	106%	91.7%	3%
508A	76	-28	?	Mountain States	35.0	16%	17.1	17%	141.4	5%	105.9	11%	76	1.1	137%	65%	7%	70	0.3	144%	84%	2%	76	7.37	226%	41%	47%	70	2.1	225%	89%	87%	90.0%	2%
509A	76	-22	?	Terry Asphalt	21.6	9%	4.8	141%	153.1	23%	105.9	27%	76	0.3	37%	84%	4%	70	0.1	54%	89%	2%	76	1.6	85%	56%	26%	70	0.3	84%	77%	27%	87.4%	2%
510A	70	-22	?	McCall Oil	6.6	68%	3.2	98%	95.0	43%	30.5	92%	70	1.5	63%	15%	102%	64	0.7	100%	30%	72%	70	3.0	119%	6.2%	144%	64	1.1	119%	15%	109%	39.1%	68%

Building the database involved the following collaborative activities:

- Binders with different modifications and grades are provided by suppliers.
- PG-Plus test results and field project information are provided by WCTG members. Approximately 40 laboratories around the U.S. are running tests.
- Loose mixture specimens for evaluation are provided by state DOTs/contractors.
- WCTG identifies paving projects for which specific binders and mixtures are used. Future evaluation of the paving projects will be performed and included in the database.

The database includes binder PG and PG-Plus testing results, mixture test results and field performance indicators, which allows for the evaluation of current tests and ARC new binder products. For example, this collaboration can be used to assess if the new fatigue tests being developed are easy and practical to conduct in today's labs. It can also be used to tie fatigue laboratory data from binder and mixture samples to field performance. Materials used in field projects can be tested with newly developed procedures such as the Linear Amplitude Sweep (LAS) and performance of the field section can be used later for validation purposes.

The team continued with binder testing and analysis, identification of suppliers and sites for loose mix acquisition, and coordination with WCTG regarding research priorities. A total of nine binders were tested in 2009-2010. Analysis of the results highlights ongoing issues related to test methods and repeatability between labs. In an effort to establish linkages between tested binders

and constructed field sections, a range of suppliers, contractors and DOT personnel provided direction for acquiring loose mix field samples that may be compacted, tested and analyzed by the UW–Madison research team. Monthly conference calls with the WCTG board of directors helped define research priorities before the next round of binder testing begins in October 2010.

Significant Results

The variability of Superpave PG and PG-Plus tests was estimated based on the nine binders tested in 2009-2010. The coefficient of variation (COV) is a suitable indicator of statistical variability. COV results for Superpave PG tests and Superpave PG-Plus tests are shown in tables V3a.2 and V3a.3, respectively. The variability for the majority of the standard Superpave PG tests is acceptable, with the maximum variability for the majority of tests below 20%. Highly variable results have been observed for $|G^*|$ values aged with the rolling thin film oven (RTFO) and for the Direct Tension Test (DTT). The variability in $|G^*|$ values with RTFO aging at the high PG temperature and at the high PG temperature minus 6 °C is comparatively high. Variability for viscosity and Bending Beam Rheometer (BBR) results falls within acceptable tolerance levels. However, DTT strain measurements showed the maximum COV.

The variability in all Superpave PG-Plus tests is very high, with the exception of elastic recovery at 25 °C. Among all tests, results for Multiple Stress Creep and Recovery (MSCR) tests demonstrate the highest variability. Modifications to existing data collection templates may help in identifying why such high levels of variability exist for this test method.

Table V3a.2. COV for Superpave PG tests.

Test	Maximum	Minimum	Average	Median
Viscosity (20 rpm)	11.0%	2.9%	5.7%	4.9%
Viscosity (1 rpm)	15.0%	3.0%	10.7%	12.0%
$ G^* $ Un-aged	18.0%	3.0%	5.8%	3.9%
$ G^* $ RTFO PG	35.0%	4.0%	9.9%	6.0%
$ G^* $ RTFO PG-6 °C	33.0%	4.0%	10.4%	6.0%
$ G^* $ PAV	21.7%	5.0%	11.1%	10.0%
BBR Stiffness (1 hr)	14.0%	3.0%	7.3%	6.0%
BBR Stiffness (24 hr)	16.0%	3.0%	7.4%	5.6%
BBR m-Value (1 hr)	4.2%	1.7%	2.5%	2.1%
BBR m-Value (24 hr)	4.3%	2.0%	2.9%	2.8%
DTT Stress	26.0%	1.0%	11.8%	9.6%
DTT Strain	67.0%	24.0%	40.7%	38.1%
Maximum	67.0%	24.0%	40.7%	38.1%
Minimum	4.2%	1.0%	2.5%	2.1%

PAV = pressure aging vessel.

Table V3a.3. COV for Superpave PG-Plus tests.

Test	Maximum	Minimum	Average	Median
Ductility Un-aged	59.0%	8.7%	20.2%	15.0%
Ductility RTFO	141.4%	10.3%	43.4%	17.0%
Toughness Un-aged	25.0%	4.6%	16.3%	15.4%
Tenacity Un-aged	80.0%	11.2%	31.1%	21.0%
J _{nr} 3.2 kPa PG	136.9%	5.0%	54.5%	33.0%
J _{nr} 3.2 kPa PG-6 °C	144.6%	7.0%	66.7%	44.0%
J _{nr} 10 kPa PG	225.8%	55.0%	98.6%	80.0%
J _{nr} 10 kPa PG-6 °C	232.9%	57.0%	123.2%	77.0%
%Rec 3.2 kPa PG	236.0%	4.2%	41.0%	16.5%
%Rec 3.2 kPa PG-6 °C	67.0%	1.7%	13.8%	10.0%
%Rec 10 kPa PG	216.0%	22.0%	73.1%	47.0%
%Rec 10 kPa PG-6 °C	188.0%	10.0%	59.1%	31.0%
% ER 25 °C	17.0%	1.0%	5.9%	3.0%
Maximum	236.0%	57.0%	123.2%	80.0%
Minimum	17.0%	1.0%	5.9%	3.0%

J_{nr} = nonrecoverable creep compliance. %Rec = percent recovery. ER = elastic recovery.

Preliminary results under this work element indicate that this effort is fundamental in assessing the practicality and relevance to performance of the current and new testing procedures. The research team has succeeded in building a good collaboration with a group of labs and has worked on a valuable database. This collaboration is helping meet one of the major outcomes of ARC, which is to complement the current PG specification system with new fundamental tests such as MSCR and LAS, and to move away from empirical PG-Plus tests such as ductility and elastic recovery tests.

Significant Problems, Issues and Potential Impact on Progress

Though work element management responsibilities shifted to other personnel within the research group this quarter, this shift did not introduce any significant issues.

Work Planned Next Quarter

With WCTG round-robin binder testing complete for the 2009-2010 testing period, efforts in the next quarter will focus on coordinating binder sampling and testing scheduled to begin in October 2010. In addition, efforts will focus on coordination and collection of loose mix samples corresponding to binders scheduled for testing in 2010-2011. In an effort to reduce variability in test results, research personnel reached consensus with the WCTG board on the need for identifying the make and model of equipment being used in labs to conduct testing. Large variability suggests that there may be differences in test procedures for different models of the testing equipment, and clarifying the equipment used in testing may help reduce variability. Revisions and modifications to reporting forms will encourage labs to identify relevant equipment information.

Work element V3b: Validation of the MEPDG Asphalt Materials Models Using New MEPDG Sites and Selected LTPP Sites (UNR, UWM)

Subtask V3b-1: Design and Build Sections (Start Year 1, Year 2, and Year 3)

Work Done This Quarter

None

Significant Results

None

Significant Problems, Issues and Potential Impact on Progress

Only two agencies have committed to the construction of MEPDG sites: the Washoe RTC in northern Nevada in 2008, The South Dakota DOT in 2009/2010. The researchers are facing significant hesitation from the DOTs to use the MEPDG to design and construct HMA pavements. The level of this work element has been reduced.

Work Planned Next Quarter

None

Subtask V3b-2: Additional Testing (Start Year 2, Year 3, and Year 4)

The reader is referred to subtask V3b-1.

Subtask V3b-3: Select LTPP Sections (Start Year 1 thru Year 5)

Work Done This Quarter

In this quarter, the research group continued the evaluation of the Linear Amplitude Sweep (LAS) test by comparing testing results of LTPP binders with field performance. There are 31 LTPP binders available, out of which eight were previously tested. In this quarter, an additional 14 binders were tested, as shown in table V3b-3.1.

The binders 120902, 370964, 300902, which are shaded in table V3b-3.1, did not have significant damage up to the 20% applied shear strain. The same observation has been made in other work elements that are using LAS for evaluation of modification of binders. Therefore, the research team will explore the possibility of changing the current LAS procedure to apply higher shear strains (i.e., 30% to 40%). Figure V3b-3.1 shows the relation between the fatigue parameter A_{35} and the fatigue cracking measured in the field. Generally, the trend previously observed holds. Higher values of the A_{35} parameter correspond to lower fatigue cracking observed in the pavement. Note that the three binders that did not have significant fatigue damage fall outside the general trend.

Table V3b-3.1. LAS results for LTPP binders.

SHRP ID	PG Grading	Climate Type	Fatigue Testing		A ₃₅	B	2.5%N _f	5%N _f
			Cracking /m ²	Temp /°C				
300903	PG 64-22	DF	0	25	3.674E+06	-4.738	4.784E+04	1794
370901	PG 64-22	WN	0	25	4.920E+06	-4.674	6.796E+04	2663
370902	PG 64-22	WN	0	25	4.806E+06	-4.660	6.720E+04	2659
370903	PG 70-22	WN	0	28	4.039E+06	-4.740	5.248E+04	1964
090960	PG 58-28	WF	0.8	19	2.705E+06	-4.676	3.728E+04	1459
120902	PG 64-16	WN	2.2	28	8.957E+06	-4.684	1.225E+05	4764
090962	PG 58-28	WF	4.3	19	1.792E+06	-4.433	3.087E+04	1429
090903	PG 64-22	WF	5.0	25	2.934E+06	-4.563	4.487E+04	1900
89A901	PG 52-34	WN	8.8	13	3.182E+06	-4.908	3.547E+04	1182
340902	PG 58-28	WF	11.4	19	2.485E+06	-4.751	3.196E+04	1187
350903	PG 58-22	DN	15.7	22	2.340E+06	-4.877	2.680E+04	911
370964	PG 76-22	WN	51.1	31	2.662E+07	-5.004	2.715E+05	8460
300902	PG 64-34	DF	76.2	19	5.832E+07	-6.778	1.174E+05	1074
04B903	PG 70-10	DN	337.9	34	1.196E+06	-4.256	2.422E+04	1269

N_f= fatigue life. DF = dry-freeze. WN = wet-nonfreeze. WF = wet-freeze. DN = dry-nonfreeze.

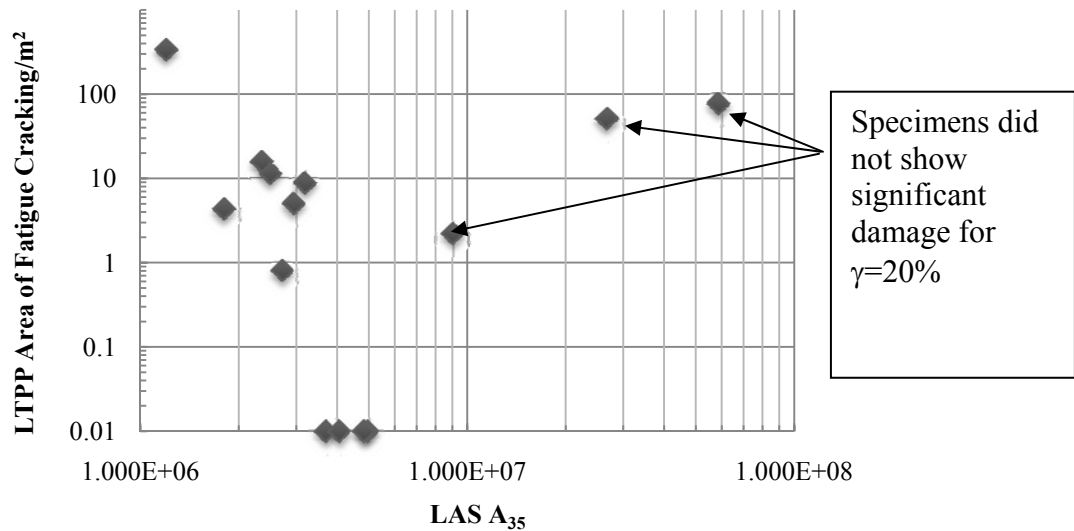


Figure V3b-3.1. Graph. LAS A₃₅ versus measured fatigue cracking of in-service asphalt pavements.

Significant Results

A preliminary investigation on the effect of aging on the LAS results of LTPP binders with a broad range of performance was conducted. Four LTPP binders were tested using LAS at four different levels of aging: original, rolling thin film oven (RTFO), pressure aging vessel (PAV), and double PAV. Table V3b-3.2 shows the results from this aging study. It can be observed that, generally, the parameter A_{35} increases with aging level. On the other hand, the parameter B, which is related to the undamaged viscoelastic properties (i.e., α), decreases with aging.

Table V3b-3.2. Effect of aging on LAS results for LTPP binders.

SHRP ID	PG Grading	Climate Type	Fatigue Cracking /m ²	Testing Temp /°C	Sample Type	A_{35}	B	2.5%N _f	5%N _f
370901	PG 64-22	WN	0.01	25	Original	2.790E+06	-4.349	5.190E+04	2547
					RTFO	4.920E+06	-4.674	6.796E+04	2663
					PAV	1.107E+07	-5.184	9.574E+04	2633
					D PAV	2.198E+07	-5.662	1.227E+05	2424
090960	PG 58-28	WF	0.8	19	Original	1.318E+06	-4.237	2.715E+04	1440
					RTFO	2.705E+06	-4.676	3.728E+04	1459
					PAV	8.163E+06	-5.356	6.032E+04	1473
					D PAV	2.091E+07	-5.870	9.649E+04	1650
350903	PG 58-22	DN	15.7	22	Original	1.539E+06	-4.562	2.353E+04	996
					RTFO	2.340E+06	-4.877	2.680E+04	911
					PAV	1.594E+07	-5.633	9.136E+04	1841
					D PAV	3.221E+07	-6.011	1.306E+05	2025
370964	PG 76-22	WN	51.1	31	Original	3.513E+07	-4.807	4.293E+05	15335
					RTFO	2.662E+07	-5.004	2.715E+05	8460
					PAV	2.750E+07	-5.394	1.964E+05	4674
					D PAV	1.781E+08	-6.094	6.695E+05	9806

D PAV = double PAV; total of 40 hours aging.

Figure V3b-3.2 indicates the effect of aging on the stress-strain response of asphalt binders in the LAS test. It can be clearly seen that fatigue performance improves as the level of aging increases. However, it is important to note that the aging levels used are limited and that the research team is planning to conduct one more test with significantly higher aging level.

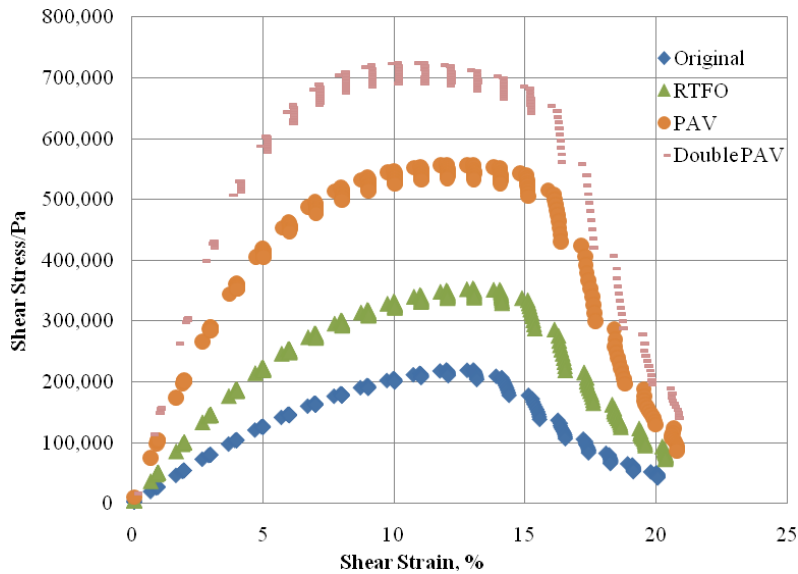


Figure V3b-3.2. Graph. Effect of aging on LAS test for SHRP ID 370901/PG 64-22.

Significant Problems, Issues and Potential Impact on Progress

None.

Work Planned Next Quarter

The research team plans to continue testing the rest of the LTPP binders (eight to be tested) using the LAS. After LAS testing of the LTPP binders is completed, the team will develop limits for parameters A_{35} and B for specification purposes. The research team will continue data collection of LTPP sections for which low-temperature cracking and moisture damage performance is available. Also, the effect of aging on the LAS results will be further investigated.

Subtask V3b-4: Testing of Extracted Binders from LTPP Sections (Start Year 1)

Work Done This Quarter

None.

Work Planned Next Quarter

No work planned.

Subtask V3b-5: Review and Revisions of Materials Models (Start Year 2, Year 3, Year 4, and Year 5)

The reader is referred to subtask V3b-1.

Subtask V3b-6: Evaluate the Impact of Moisture and Aging (Start Year 3, Year 4, and Year 5)

The reader is referred to subtask V3b-1.

Work Element V3c: Validation of PANDA (TAMU)

Work Done this Quarter

The work completed this quarter is described in Work Element F3c.

Work Planned Next Quarter

Please refer to Work Element F3c.

Work Element V3d: Engineered Properties Testing Plan (TAMU)

Work Done this Quarter

The work completed this quarter relates to work described in Work Elements F1b-2, F1c, F2c, F3c, and E1a.

Work Planned Next Quarter

Please refer to Work Elements F1b-2, F1c, F2c, F3c, and E1a.

Validation Year 4	Year 4 (4/2010-3/2011)												Team
	4	5	6	7	8	9	10	11	12	1	2	3	
(1) Field Validation													
V1a: Use and Monitoring of Warm Mix Asphalt Sections													WRI
V1b: Construction and Monitoring of additional Comparative Pavement Validation sites													WRI
(2) Accelerated Pavement Testing													
V2a: Accelerated Pavement Testing including Scale Model Load Simulation on small test track (This work element will include all accelerated pavement testing)													WRI
V2b: Construction of validation sections at the Pecos Research & Testing Center													WRI
(3) R&D Validation													
V3a: Continual Assessment of Specification													UWM
V3a-1: Evaluation of the PG-Plus practices and the motivations for selecting the "plus" tests.													
V3a-2: Detailed analysis of all PG-Plus tests being proposed or in use today, documentation of benefits and costs of these tests, and comparison with new tests													
V3a-3: Development of protocols for new binder tests and database for properties measured				P									
V3a-4: Development of specification criteria for new tests based on field evaluation of construction and performance			P								JP		
V3a-5: Interviews and surveys for soliciting feedback on binder tests and specifications		P							JP				
V3b: Validation of the MEPDG Asphalt Materials Models and Early Verification of Technologies Developed by ARC using new MEPDG Sites and Selected LTPP sites													UNR/UWM/ WRI
V3b-1: Design and Build Sections													UNR
V3b-2: Additional Testing (if needed)													
V3b-3: Select LTPP Sites to Validate New Binder Testing Procedures				DP	JP						P		UWM
V3b-4: Testing of Extracted Binders from LTPP Sections													
V3b-5: Review and Revisions of Materials Models													
V3b-6: Evaluate the Impact of Moisture and Aging													
V3c: Validation of PANDA													TAMU
V3d: Engineered Properties Testing Plan													TAMU

Deliverable codes

D: Draft Report
 F: Final Report
 M&A: Model and algorithm
 SW: Software
 JP: Journal paper
 P: Presentation
 DP: Decision Point

Deliverable Description

Report delivered to FHWA for 3 week review period.
 Final report delivered in compliance with FHWA publication standards
 Mathematical model and sample code
 Executable software, code and user manual
 Paper submitted to conference or journal
 Presentation for symposium, conference or other
 Time to make a decision on two parallel paths as to which is most promising to follow through

	Work planned
	Work completed
	Parallel topic

Validation Years 2 - 5	Year 2 (4/08-3/09)				Year 3 (4/09-3/10)				Year 4 (04/10-03/11)				Year 5 (04/11-03/12)				Team
	Q1	Q2	Q3	Q4	Q1	Q2	Q3	Q4	Q1	Q2	Q3	Q4	Q1	Q2	Q3	Q4	
(1) Field Validation																	
V1a: Use and Monitoring of Warm Mix Asphalt Sections																	WRI
V1b: Construction and Monitoring of additional Comparative Pavement Validation sites																	WRI
(2) Accelerated Pavement Testing																	
V2a: Accelerated Pavement Testing including Scale Model Load Simulation on small test track																	WRI
V2b: Construction of validation sections at the Pecos Research & Testing Center																	WRI
(3) R&D Validation																	
V3a: Continual Assessment of Specification																	UWM
V3a-1: Evaluation of the PG-Plus practices and the motivations for selecting the "plus" tests.		P	D,F														
V3a-2: Detailed analysis of all PG-Plus tests being proposed or in use today, documentation of benefits and costs of these tests, and comparison with new tests				P	D												
V3a-3: Development of protocols for new binder tests and database for properties measured						JP				P							
V3a-4: Development of specification criteria for new tests based on field evaluation of construction and performance					D		P		P			JP	P		JP		
V3a-5: Interviews and surveys for soliciting feedback on binder tests and specifications									P		JP		P		D	F	
V3b: Validation of the MEPDG Asphalt Materials Models and Early Verification of Technologies Developed by ARC using new MEPDG Sites and Selected LTPP sites																	UNR/UWM
V3b-1: Design and Build Sections																	
V3b-2: Additional Testing (if needed)																	
V3b-3: Select LTPP Sites to Validate New Binder Testing Procedures						DP		P		JP, DP		P			D	F	
V3b-4: Testing of Extracted Binders from LTPP Sections																	
V3b-5: Review and Revisions of Materials Models																	
V3b-6: Evaluate the Impact of Moisture and Aging																	
V3c: Validation of PANDA																	TAMU
V3d: Engineered Materials Testing Plan																	TAMU

Deliverable codes

- D: Draft Report
- F: Final Report
- M&A: Model and algorithm
- SW: Software
- JP: Journal paper
- P: Presentation
- DP: Decision Point

Deliverable Description

- Report delivered to FHWA for 3 week review period.
- Final report delivered in compliance with FHWA publication standards
- Mathematical model and sample code
- Executable software, code and user manual
- Paper submitted to conference or journal
- Presentation for symposium, conference or other
- Time to make a decision on two parallel paths as to which is most promising to follow through

- Work planned
- Work completed
- Parallel topic

PROGRAM AREA: TECHNOLOGY DEVELOPMENT

Work element TD1: Prioritize and Select Products for Early Development (Year 1)

Work Done This Quarter

None. This work element has been completed.

Significant Results

Six early technology development projects have been identified and all have received favorable ratings from the ETGs.

Significant Problems, Issues and Potential Impact on Progress

None

Work Planned Next Quarter

None

Work element TD2: Develop Early Products (Year 3)

Work Done This Quarter

Table TD2.1 summarizes the progress on the Products for Early Development. Work has been completed at WRI on the test method for Determination of Polymer in Asphalt. Work on the remaining products is expected to be completed by the end of 2010.

Dr. Donald Christensen of Advanced Asphalt Technologies visited NCAT and presented a seminar on the simplified continuum damage fatigue testing and analysis that is being developed as an Early Development Product. NCAT is considering using continuum damage fatigue testing in some of their projects.

Work Planned Next Quarter

Work will continue of the five Products for Early Development listed in Table TD2.1 with estimated completion dates of 12/31/2010.

Significant Problems, Issues and Potential Impact on Progress

None.

Table TD2.1. Summary of progress on early development products.

Product	ARC Research Program	Format	Estimated Completion Data	ARC Partner	Draft AASHTO Standard?
Simplified Continuum Damage Fatigue Analysis for the Asphalt Mixture Performance Tester	Prior	Test Method	12/31/2010	AAT	Yes
Wilhelmy Plate Test	Prior	Test Method	12/31/2010	TTI	Yes
Universal Sorption Device	Prior	Test Method	12/31/2010	TTI	Yes
Dynamic Mechanical Analysis	Prior	Test Method	12/31/2010	TTI	Yes
Automated Flocculation Titrimetric Analysis	Prior	Test Method	12/31/2010	WRI	Yes
Determination of Polymer in Asphalt	Prior	Test Method	Completed	WRI	Yes

Work element TD3: Identify Products for Mid-Term and Long-Term Development (Years 2, 3, and 4)

Work Done This Quarter

The research team continued to review interim research results to identify potential mid-term and long-term products. A total of 29 mid- and long-term products were identified and brief descriptions of 19 of these products were included in the Revised Annual Work Plan for Year 4. The Revised Year 4 Work Plan is posted on the ARC website, www.ARC.unr.edu.

The 10 mid- and long-term products identified in the Revised Year 4 Work Plan without brief descriptions are listed in table TD3.1. Brief descriptions of these products are included at the end of the Technology Development section.

Significant Problems, Issues and Potential Impact on Progress

None.

Work Planned Next Quarter

The research team will with continue to review interim research products to identify potential long-term development projects. The ARC researchers are planning to discuss the 29 research products with FHWA Co-AOTR’s Mr. Eric Weaver and Dr. Jack Youtcheff to develop a plan to forward the research product briefs to the FHWA Expert Task Groups and/or the AASHTO Subcommittee on Materials for review.

Table TD3.1. ARC Mid-term research products.

Product	ARC Work Element	Format	Estimated Completion Date	ARC Partner
Rigden Voids for fillers	F2e	Test Method	9/30/2011	UWM
Linear Amplitude Sweep (DSR)	F2e	Test Method	3/31/2010	UWM
Elastic Recovery – DSR	F2a	Test Method	12/31/2010	UWM
Binder Yield Energy Test (BYET)	F2e	Test Method	9/30/2010	UWM
Binder Bond Strength Test (BBS)	M1a	Test Method	6/31/2010	UWM
Binder Lubricity Test – DSR	E1c-1	Test Method	12/31/2010	UWM
RAP Binder PG True Grade Determination	E2b	Test Method/Software	12/31/2010	UWM
Single Edge Notch Beam	E2d	Test Method	3/31/2011	UWM
Binder Glass Transition Test	E2d	Test Method	3/31/2011	UWM
Asphalt Mixture Glass Transition Test	E2d	Test Method	3/31/2011	UWM

Work Element TD4: Develop Mid-Term and Long-Term Products (Years 3, 4, and 5)

This activity is planned for later in the project.

Technology Development Product Name

Rigden Voids for Fillers

ARC Research Program

ARC F2e

Format

Test Method

Estimated Completion Date

9/30/2011

ARC Partner

University of Wisconsin-Madison

Product Description

The mineral filler plays an important role in the construction and performance of asphalt pavements. Currently, very little attention has been given to the effect of mineral filler (often referred to as the minus 200 fraction) on the asphalt mixture performance. Although the Superpave mix design method includes a recommendation on the dust-to-binder ratio, some field experience suggests that this ratio may be too restrictive. In certain cases, constructability and performance can be enhanced with the use of additional filler as long as the filler is properly specified.

Mineral filler fractional voids value has been used as an indicator of filler stiffening effect since the introduction of the test by Rigden in 1947. Rigden considered the asphalt required to fill the voids in dry compacted samples as the “fixed asphalt” while asphalt in excess of that amount was defined as “free asphalt”. Research has shown that the percent “free asphalt” is the main factor defining the consistency of the filled systems.

The Rigden voids method is used to determine the voids of dry compacted filler. This test is applicable to natural and imported fillers. This test allows the estimation of the percent volume of free asphalt the filler can carry. The Rigden voids test follows the standardized European Norm EN 1097-4.

Technology Development Product Name

Linear Amplitude Sweep (DSR)

ARC Research Program

ARC F2e

Format

Test Method

Estimated Completion Date

6/31/2010

ARC Partner

University of Wisconsin-Madison

Product Description

The Linear Amplitude Sweep (LAS) test method quantifies fatigue damage accumulation of asphalt binders with a short-duration procedure that can be easily implemented into current practice. The results from the test are analyzed using the framework of Viscoelastic Continuum Damage (VECD). By selecting a specific ramping sequence of strains, and by combining the results with the results of a frequency sweep, it has been shown that estimation of the fatigue performance of asphalt binders can be correlated to mixture performance in the laboratory and to field fatigue performance.

The Linear Amplitude Sweep test is conducted using the Dynamic Shear Rheometer at the continuous intermediate temperature performance grade (PG Grade) of the asphalt binder. The test method can be used with material aged using AASHTO T 240 (RTFOT) and/or AASHTO R 28 (PAV) to simulate the estimated aging for in-service asphalt pavements. Samples for LAS test are prepared consistent with Test Method AASHTO T 315 (ASTM D 7175-05) (DSR). The 8-mm parallel plate geometry with a 2-mm gap setting is used for this test method. In LAS test, the sample is first tested in shear using either stress relaxation or frequency sweep to determine rheological properties, and is then followed by a series of oscillatory load cycles at systematically increasing amplitudes at a constant frequency to cause accelerated fatigue damage. The continuum damage approach is used to calculate the fatigue resistance from rheological properties and amplitude sweep results. The parameters, A and B, which describe the common fatigue law ($N_f = A(\gamma_{\max})^B$) are calculated with this test method.

The accelerated loading scheme is found to produce highly repeatable results and it takes less than 10 minutes to perform. The estimation of binder fatigue performance with the LAS method will be validated against binder time sweep testing, asphalt mixture fatigue results, and with in-

service (field) pavement fatigue performance (LTPP sections). The end product of this technology development element will be in the format of a draft AASHTO test method.

Technology Development Product Name

Elastic Recovery (DSR)

ARC Research Program

ARC F2a

Format

Test Method

Estimated Completion Date

12/31/2010

ARC Partner

University of Wisconsin-Madison

Product Description

Many state highway agencies have implemented what is called Superpave Plus specification (i.e., PG+). Elastic recovery test, using the ductility bath, is one of these PG+ tests. However, high variability in this test procedure has been reported by users. A new protocol for measuring elastic recovery in the DSR is currently being developed. The test is run at 25°C on the RTFO aged binder using the 8 mm parallel plate geometry.

The protocol for running the elastic recovery in the DSR is as follows:

- A constant strain rate of 0.02315/s is imposed for 2 minutes. This step is run in strain controlled mode. The strain at the end of this step is ε_1
- Zero shear stress is applied for a period of 1 hour. This step is run in stress controlled mode and corresponds to the relaxation part of the test. The strain at the end of relaxation is ε_2 .
- Elastic recovery is computed with: $\text{Recovery (\%)} = \frac{\varepsilon_2}{\varepsilon_1} \times 100$

Technology Development Product Name

Binder Yield Energy Test (BYET)

ARC Research Program

ARC F2e

Format

Test Method

Estimated Completion Date

9/30/2010

ARC Partner

University of Wisconsin-Madison

Product Description

The Binder Yield Energy Test (BYET) method measures the asphalt binders' resistance to yield-type failure under monotonic constant shear-rate loading. The BYET method is conducted using the Dynamic Shear Rheometer at the intermediate temperature performance grade (PG Grade) of the asphalt binder. The test method can be used with material aged using AASHTO T 240 (RTFOT) and/or AASHTO R 28 (PAV) to simulate the estimated aging for in-service asphalt pavements.

The Binder Yield Energy Test uses the 8-mm parallel plate geometry with a 2-mm gap setting and samples prepared consistent with Test Method AASHTO T 315 (ASTM D 7175-05) (DSR). The sample is monotonically sheared using a constant shear rate until peak shear strength is achieved and the sample has yielded. This test method is intended to evaluate the amount of energy required to cause yielding in the asphalt binder. The "yield energy" of the material can be used to identify the relative performance of different materials, and the stress-strain response curve can be useful in identifying the presence of polymer modifiers in the material.

Two parameters are obtained from this test method, the area underneath the stress-strain curve up to the point of maximum stress (i.e., "yield energy") and the strain at maximum stress (GMT_{max}). The term "yield energy" (YE) is derived from work done by Kim and Roque on the properties of mixtures tested using indirect tension. The concepts behind energy-based approaches for pavement cracking are based on the idea that there is an energy threshold where a material's resistance to deformation and resistance to damage are both overcome, leading to the propagation of cracking. The energy values can be obtained from monotonic test procedures, where accumulated strain energy, along with the energy dissipated by structural damage, can be summed at the point of failure. The area underneath the stress strain curve until the point of

material failure is known as the specimen's "fracture energy". However, during binder testing at intermediate temperatures under a constant shear rate loading, the material never truly appears to fracture. Rather, it seems to reach a point where it is unable to take on further stress and simply begins to yield, thus the term "yield energy". It is assumed at this point the material has failed, so YE is calculated as the area under the stress-strain curve bounded by the strain level corresponding to the point of maximum stress.

Technology Development Product Name

Binder Bond Strength Test (BBS)

ARC Research Program

ARC M1a

Format

Test Method

Estimated Completion Date

6/31/2010

ARC Partner

University of Wisconsin-Madison

Product Description

The challenge to quantitatively evaluate the adhesive bond between asphalt and aggregate is to identify a test which is simple, quick and repeatable for evaluating adhesion properties of asphalt-aggregate systems. Furthermore, no method is included in the Superpave binder specifications to evaluate adhesive characteristics of asphalt binders. The Binder Bond Strength Test (BBS) is a significantly modified version of the Pneumatic Adhesion Tensile Testing Instrument (PATTI), which is a pull-off tensile test method used successfully in the coating industry and to measure adhesive bond between asphalt and glass.

The BBS method is used to evaluate the asphalt-aggregate bond strength. The main components of the BBS equipment are: pressure hose, portable pneumatic adhesion tester, piston, reaction plate and metal pull-out stub. Before running a test, the piston is placed over the pull-out stub and the reaction plate screwed on it. Then, compressed air is introduced through the pressure hose to the piston. An upward pulling force on the specimen is applied by the pull-out stub. During the test, failure occurs when the applied pressure exceeds the cohesive strength of the asphalt binder or the adhesive strength of the binder-aggregate interface. The pressure at failure is recorded and the pull-off tensile strength (POTS) is calculated. The pull-out stub has a rough surface that can prevent asphalt debonding from the stub surface by providing mechanical interlock and larger contact area between the asphalt binder and stub. The pull-out stub in the BBS test has a diameter of 20 mm with a surrounding edge, used to control film thickness. The stub edge has a thickness of 800 μm .

The BBS test can differentiate the effects of conditioning time, conditioning solution, and modification of binders. These factors significantly affect the pull-off tensile strength of asphalt-aggregate systems. Moreover, preliminary results indicate that the BBS test is repeatable with

measured coefficient of variation for the pull-off tensile strength of less than 10%. The BBS test can be used as a practical method to measure bond strength between aggregate and binders in dry and moisture conditions. The end product of this technology development element will be in the format of a draft AASHTO test method.

Technology Development Product Name

Asphalt Binder Lubricity Test (DSR)

ARC Research Program

ARC E1c-1

Format

Test Method

Estimated Completion Date

12/31/2010

ARC Partner

University of Wisconsin-Madison

Product Description

The conventional laboratory method for evaluation of asphalt binder workability has been unable to demonstrate an ability to exhibit a measured reduction in viscosity due to the presence of warm mix additives consistent with enhanced mixture workability observed in the laboratory and field. The disconnect between the effect of WMA additives on viscosity and asphalt mixture densification over a similar range of temperatures indicates that viscosity reduction is not the only mechanism by which warm mix additives allow for compaction at reduced temperatures. A number of WMA additives that have entered the market have been classified as surfactants. It is believed that these additives enhance mixture workability through improving the lubricating effects of asphalt binders through reduction in the internal friction of the material.

A standard test in the oil industry, ASTM D-5183: Standard Test Method for Determination of the Coefficient of Friction of Lubricants Using the Four Ball Wear Test Machine has been adapted to allow for the test to be conducted in the Dynamic Shear Rheometer (DSR). The apparatus consists of three lower balls which are clamped in a cup; a fourth ball held in a chuck is loaded against them, a sufficient amount of lubricant is added to produce a film between the chuck and clamped assembly. The chuck is rotated in one direction with resistance provided by the fixed balls in the cup below. During the test torque and normal force are monitored under a constant speed and the coefficient of friction of the asphalt binder is measured. The test is conducted in the temperature range of conventional HMA/WMA compaction.

The end product of this Technology development element will be in the format of a draft AASHTO test method.

Technology Development Product Name

RAP Binder PG True Grade Determination

ARC Research Program

ARC E2b

Format

Test Method/Software

Estimated Completion Date

12/31/2010

ARC Partner

University of Wisconsin-Madison

Product Description

State agencies and contractors alike have long recognized the value in utilizing existing asphalt pavement materials in new hot mix asphalt projects. The use of Reclaimed Asphalt Pavement (RAP) in new asphalt mixtures has been found to be both environmentally sound and economical. Blending charts are currently used to accommodate RAP binder properties in mix design. The blending charts system relies on determining the RAP binder properties, which is then combined with the virgin binder properties to produce the charts. Currently, the most commonly used method in retrieving RAP binder properties is extraction and recovery of the asphalt binder using chemical solvents (AASHTO T164 / ASTM D 2172). However, it is well documented that these solvents are not only hazardous to both the user and the environment; they may also alter the aged binder properties significantly. Many contractors are not properly equipped to perform extraction tests using these solvents due to much more stringent environmental law, leading many state agencies to be unwilling to utilize high percentage RAP mixes.

This practice will recommend a non-solvent based test method for analyzing the performance of high percentage RAP mixes, while minimizing time commitment and technical difficulty. RAP passing sieve #50 and retained on #100 sieve (R100) are used. Mortars are prepared by mixing R100 (RAP, and burned) with the virgin binder. A modified bending beam rheometer (BBR) procedure is used to characterize the low temperature properties, while the dynamic shear rheometer (DSR) is used to characterize intermediate and high temperature properties of the mortars and the virgin binder. Analytical procedure is then used to estimate the change in the virgin binder properties due to the addition of the RAP. The output will be a blending chart, indicating the change of the virgin binder low, intermediate, and high PG temperature as function

of the RAP binder percent. The charts will clearly distinguish between the measured and the extrapolated change in the PG.

Technology Development Product Name

Single Edge Notch Beam (SENB)

ARC Research Program

ARC E2d

Format

Test Method

Estimated Completion Date

3/31/2011

ARC Partner

University of Wisconsin-Madison

Product Description

The Single Edge Notch Beam (SENB) test measures the fracture properties of asphalt binders and mastic at low temperatures. The SENB test follows ASTM E399 and assumes that Linear Elastic Fracture Mechanics (LEFM) conditions are true. Asphalt binders samples prepared using the Bending Beam Rheometer (BBR) geometry with a notch on it are tested in three-point bending using displacement controlled mode. Load-displacement curves and fracture mechanics concepts are used to estimate both fracture energy (G_f) and fracture toughness (K_{IC}).

Preliminary results indicate that this test method is capable of differentiate good and poor low temperature performance of both asphalt binders and mastics. Furthermore, the effect of modification on the thermal cracking performance of asphalt binders can be evaluated with this method. Future work includes validation with measured field performance obtained from MnROAD sections and comparisons with test methods currently used by agencies. The end product of this technology development element will be in the format of a draft AASHTO test method.

Technology Development Product Name

Binder Glass Transition Test

ARC Research Program

ARC E2d

Format

Test Method

Estimated Completion Date

3/31/2011

ARC Partner

University of Wisconsin-Madison

Product Description

The glass transition behavior of asphalt binders significantly affects the low temperature performance of asphalt pavements. Furthermore, physical hardening phenomenon of asphalt binders is dictated by its glass transition temperature (T_g). Recent results on aging and glass transition behavior merit a fresh look at the prediction of thermal cracking models. The increasing use of modified binders, particularly polymer and acid modified binders, require a more in depth evaluation of current thermal cracking models for pavement mixtures.

The glass transition temperature (T_g) and the coefficients of thermal expansion/contraction above and below T_g of asphalt binders are measured by means of a dilatometric test system. The apparatus monitors the dilatometric properties of binders while the samples are subjected to a prescribed temperature program. The specific volume vs. temperature data obtained from test can be used to fit a non-linear model that contains the glass transition temperature and the thermal coefficients of contraction/expansion above and below T_g as parameters. Very precise capillary tubes are used to measure volume changes in the sample during the test. The system is automated with precise pressure sensors that continuously measure the change of alcohol height, which is proportional to changes in specific volume of the binder. Furthermore, the dilatometric cells made of aluminum are sealed with military-specified o-rings to minimize the effect of rubber contraction on the test results. Importance of the parameters obtained with this test method will be assessed by running sensitivity analysis of current thermal cracking prediction models to T_g and the coefficients of thermal expansion/contraction above and below T_g . Also, statistical correlations between field performance and T_g of several asphalt binders will be calculated to determine the importance of binder T_g on low temperature cracking performance.

Technology Development Product Name

Asphalt Mixture Glass Transition Test

ARC Research Program

ARC E2d

Format

Test Method

Estimated Completion Date

3/31/2011

ARC Partner

University of Wisconsin-Madison

Product Description

Existing models for thermal cracking predictions over simplify thermo-volumetric properties of asphalt mixtures. Current models assume a single-constant coefficient of thermal expansion/contraction for the mixture. However, glass transition measurements have indicated that these models are not accurate and that there are two coefficients of thermal contraction/expansion: one above and one below the glass transition temperature (T_g). A new procedure for testing the thermal expansion and contraction coefficients as well as the T_g for asphalt mixtures is currently being developed. The goal is to obtain mixture samples from cores extracted from gyratory compacted cylinders. These cores will be glued in one single specimen for T_g testing. The main concern of this approach is the use of an epoxy that may affect the measured coefficient of thermal contraction/expansion and the glass transition temperature.

Preliminary results showed that no significant differences are observed between the thermal response of the asphalt mixture before and after gluing. This result is encouraging but further testing on cylindrical specimens extracted from gyratory compacted samples need to be performed.

The T_g system for asphalt mixtures measures the change in specimen length by means of two LVDTs as function of temperature. The same non-linear model used for asphalt binders can be used for mixtures to estimate T_g and the coefficients of thermal expansion/contraction above and below T_g .

The experimental data collected with this method will be used to modify current models and to provide typical/default values of T_g and contraction coefficients that can be used to predict thermal cracking. The data will be also used to study which material and mixture properties are

statistically important for the prediction of contraction and expansion parameters. Thermal cracking sensitivity analysis will be conducted to determine which of the glass transition parameters are statistically important for thermal cracking, which ones need to be measured, and what is the effect of using estimated rather than measured values

PROGRAM AREA: TECHNOLOGY TRANSFER

CATEGORY TT1: OUTREACH AND DATABASES

Work element TT1a: Development and Maintenance of Consortium Website (Duration: Year 1 through Year 5)

Work Done This Quarter

The ARC website was maintained and updated. The ARC quarterly technical progress report, Jan 1- Mar 31, 2010, was uploaded to the ARC website. The following references were added to the ARC website:

- A list of Publications and Conference Proceedings was added to the ARC website under the “Publications” webpage. A link to the *Abstract* was also provided for each publication.
- A list of Presentations and Posters was added to the ARC website under the “Outreach” webpage. A link to the *Presentation* or *Abstract* was also provided for each reference.
- A list of Theses and White Papers was added to the ARC website under the “Outreach” webpage. A link was also provided for each reference.

A web Tracker (i.e. visitor/site tracker) was added to the ARC website. The “StatCounter” was added to provide hit counters, visitor tracking and website stats. A link “[View My Site Visitors Stats](#)” to access the site visitors’ statistics such as the number of page loads, unique visitors and returning visitors, was added at the bottom of each of the ARC WebPages.

A new webpage “Software” was created to release and download ARC related software. The beta-version of the *3D-Move Analysis* software was uploaded to the ARC website (figure TT1a.1). The *3D-Move Analysis* software can be downloaded for free after filling-up and submitting the software request form (figure TT1a.2). The request form was created to keep track of the users and be able to reach them whenever a new version or an update is released. More details related to the software download registration application are provided under Work Element TT1d.

Software

3D-Move

Free Softwares

3D-Move (Version 1.0) *Now Available Online!*



Announcements

Join Today the "3D-MOVE DISCUSSION GROUP" at 3d-move.finddiscussion.com to provide your feedback or post your questions on the 3D-Move Analysis Software.

The analytical model (*3D-Move*) adopted here to undertake the pavement response computations uses a continuum-based finite-layer approach. The *3D-Move* model can account for important pavement response factors such as the moving traffic-induced complex 3D contact stress distributions (normal and shear) of any shape, vehicle speed, and viscoelastic material characterization for the pavement layers. The finite-layer approach adopted here treats each pavement layer as a continuum and uses the Fourier transform technique; therefore, it can handle complex surface loadings such as multiple loads and non-uniform tire pavement contact stress distribution. Since the tire imprint can be of any shape, this approach is suitable to analyze tire imprints, including those generated by wide-base tires (Siddharthan et al. 1998; 2000; 2002). The finite-layer method is much more computationally efficient than the moving load models based on the finite element method (Huhtala and Pihlajamaki 1992; Al-Qadi and Wang 2009). This is because often times the pavements are horizontally layered and pavement responses are required only at a few selected locations and for such problems the finite layer approach of *3D-Move* is ideally suited. Since rate-dependant material properties (viscoelastic) can be accommodated by the approach, it is an ideal tool to model the behavior of asphalt concrete (AC) layer and also to study pavement response as a function of vehicle speed. Frequency-domain solutions are adopted in *3D-Move*, which enables the direct use of the frequency sweep test data of HMA mixture in the analysis.

Many attempts that included field calibrations (e.g. Penn State University test track, Mn/Road and UNR Off-road Vehicle study) that compared a variety of independently-measured pavement responses (stresses, strains, and displacements) with those computed have been reported in the literature (Siddharthan et al. 2002, 2005). These verification studies have validated the applicability and versatility of the approach.

Download 3D-Move

Getting started with *3D-Move Analysis* is simple on a Win32 operating system (Windows 7, Windows Vista or Windows XP) and it can readily run in that environment. [Download](#)

Figure TT1a.1. Screen capture for ARC Webpage "Software".

To request the Beta version of the 3D-Move software, please fill out the form below:

Software Request Form - 3D-Move

First Name:	<input type="text"/>
Last Name:	<input type="text"/>
Address 1:	<input type="text"/>
Address 2:	<input type="text"/>
City:	<input type="text"/>
State/Region/Province:	<input type="text"/>
Zip/Postal Code:	<input type="text"/>
Country:	<input type="text"/>
Organization:	<input type="text"/>
Telephone:	<input type="text"/>
E-Mail:	<input type="text"/>
Confirm Email:	<input type="text"/>

Figure TT1a.2. Screen capture for 3D-Move Software Request Form.

Significant Results

None

Significant Problems, Issues and Potential Impact on Progress

None

Work Planned Next Quarter

Continue maintaining and updating the ARC website. Update the list of Publications and Conference Proceedings. Update the list of Presentations and Posters and the list of Theses and White Papers.

Work element TT1b: Communications (Duration: Year 1 through Year 5)

Work Done This Quarter

Prepared the seventh ARC Newsletter to be published in July 2010. UNR and UWM contributed to the upcoming Newsletter.

Significant Results

None

Significant Problems, Issues and Potential Impact on Progress

None

Work Planned Next Quarter

Publish the seventh ARC Newsletter.

Work element TT1c: Prepare Presentations and Publications

Presentations

Bahia, H. "Asphalt Binder Lubricity, Impacts of WMA on Emissions and Energy Consumption." Presented to the FHWA Warm Mix Asphalt Technical Working Group, Auburn, Alabama, May 18, 2010.

Grimes, Will, Bill Tuminello, Ryan Boysen, James Beiswenger, Gerry Forney, Niki Kringos, and Troy Pauli. "Nano-Rheology/Nano-Mechanics and Scanning Probe Microscope Imaging Based on Novel Sample Preparation Techniques." Pavement Performance Prediction Symposium, Hilton Garden Inn and University of Wyoming Conference Center, Laramie, Wyoming, July 15, 2010.

Hajj, E. Y. "Impact of current extraction techniques on properties of extracted RAP aggregates." FHWA HMA Recycling Expert Task Group meeting in Auburn, Alabama, May 20, 2010.

Han, Rongbin, Xin Jin, Yuanchen Cui, and Charles J. Glover. "Oxygen Diffusivity in Asphalts and Mastics," presented at the 47th Annual Petersen Asphalt Research Conference, July 14, 2010.

Harnsberger, P. M., and Kristopher Maranchuk, "Construction and Initial Properties of the Manitoba High RAP Site," presented at the 47th Annual Petersen Asphalt Research Conference, July 12, 2010.

Jin, Xin, Rongbin Han, and Charles J. Glover. "A Fast-Rate - Constant-Rate Oxidation Model for Asphalt Binders," presented at the 47th Annual Petersen Asphalt Research Conference, July 14, 2010.

Pauli, Troy, Will Grimes, James Beiswenger, Ryan Boysen, and Gerry Forney. “Phase Field Model Input Parameters, Experimental Approaches. Consortium on Chemo-mechanics of Healing & Ageing Processes in Bituminous Materials.” Delft, The Netherlands, Room 2.66, Faculty Civil Engineering and Geosciences, TU Delft, June 11, 2010.

Prapaitrakul, Nikornpon, Rongbin Han, Xin Jin, and Charles J. Glover. “Transport Model Calculations of Asphalt Binder Oxidation in Pavements,” presented at the 46th Annual Petersen Asphalt Research Conference, July 14, 2009.

Prapaitrakul, Nikornpon, Rongbin Han, Xin Jin, and Charles J. Glover, “A Transport Model of Asphalt Binder Oxidation in Pavements,” presented at the 3rd International Conference on Asphalt Materials, Qingdao, Shandong Province, China, August 6, 2009.

Publications

ASTM D4124-09, 2010, Standard test method for separation of asphalt into four fractions. Annual book of ASTM standards, road and paving materials; vehicle-pavement systems, section 4, vol. 04.03, West Conshohocken, PA: ASTM International.

Greyling, A., T. Miller, K. Jenkins, and H. Bahia. Development of a Standard Test Method for Determining Emulsion Bond Strength Using the Bitumen Bond Strength (BBS) Test – A South African Perspective. Second International Sprayed Sealing Conference, Melbourne, Australia, 2010, submitted.

Han, Rongbin, Xin Jin, and Charles J. Glover. “Modeling Pavement Temperature for Use in Binder Oxidation Models and Pavement Performance Prediction,” submitted July 2009 to *Journal of Materials in Civil Engineering*.

Miller, T. Development of Bond Strength Test for Improved Characterization of Asphalt Emulsions. Masters of Science Thesis, University of Wisconsin–Madison, Madison, Wisconsin, 2010.

Miller, T. D., and H. U. Bahia, 2010, Establishing a Framework for Analyzing Asphalt Pavement Sustainability. *International Journal of Pavement Research and Technology*, 3 (3), 149–155.

Pauli, A.T., R.W. Grimes, A.G. Beemer, J.J. Miller, J.D. Beiswenger, J.E. MacNaughton, T.F. Turner, and J.F. Branthaver, Morphology of asphalts, asphalt chromatographic fractions and model wax-doped asphalts studied in thin-films by atomic force microscopy. *International Journal of Pavement Engineering* (Submitted, in review, April 2010).

Prapaitrakul, Nikornpon, Rongbin Han, and Charles J. Glover, 2009, “A Transport Model of Asphalt Binder Oxidation in Pavements,” *Road Materials and Pavement Design*, Vol. 10 Special Issue, 95-113.

Work element TT1d: Development of Materials Database (Duration: Year 2 through Year 5)

Work Done This Quarter

Last quarter, a workshop was held for ARC members where feedback was gathered on the ARC database management system. This was the first opportunity for the ARC members to use the system and provide vital feedback.

Using the information gathered from the workshop participants, some new software functionality needed to be added. In addition, some software features required redesign in order to improve usability or meet specific organizational goals. Some of these changes were relatively simple, while others required structural changes to the database, procedures that operate on the underlying database, and user interface elements.

These redesign and implementation efforts are discussed in the following sections and correspond to the work planned for this quarter.

- Enhancement of user interface to include bulk editing of property measures
- Validation Section – extensible properties
- Enhancement of role-based authorization
- Enhanced material filtering and sorting
- Redesign of the report management system
- Software download registration application

Because of the redesign efforts, development of the Help system was temporarily suspended. Because changes are required to selected database tables and fields, along with changes to user interface elements, changes will also be required for the corresponding Help system elements.

Significant Results

Property Measures – Bulk Editing

The existing interface for property measures allows entry of all types of data. However, the existing implementation required that users enter data row-by-row. Because of the characteristics of property measures, consortium members noted that such an implementation is prohibitively cumbersome when entering large amounts of data, such as the data shown in the following grid:

Table TT1d.1. Property measures grid.

Temperature, °F	Mixture Phase Angle					
	25 Hz	10 Hz	5 Hz	1 Hz	0.5 Hz	0.1 Hz
40	7.84	8.82	9.59	11.65	12.69	15.57
70	14.45	16.12	17.58	21.57	23.23	27.74
100	29.19	31.21	32.31	34.55	34.40	34.40
130	38.81	37.48	36.46	34.19	32.40	28.43

For this purpose, a rapid entry form supporting multi-dimensional properties and bulk editing has been designed and is presently under development, which will greatly speed the process and reduce error in data entry. The form will automatically generate a grid to be filled in with measures based on consortium defined dimensions and default values, and will also allow users to add additional custom dimension values when needed. Figure TT1d.1 shows the interface for configuring these dimensions. Adding this feature requires significant development effort. Customized and dynamic grids are required to store the multidimensional data. New database tables and controls are required to store the various grid rows and columns.

The screenshot displays a web-based interface titled "Add/Edit Dimensions for Mixture Phase Angle". It contains two distinct configuration sections for dimensions. The first section, labeled "Dimension 1", features a text input field for the name containing "Temperature, F" and a scrollable list box for values containing "15", "40", "70", "100", and "130". A "Submit" button is positioned to the right of the list. The second section, labeled "Dimension 2", features a text input field for the name containing "Hz" and a scrollable list box for values containing "2.5", "10", "5", "1", "0.5", and "0.1". A "Submit" button is also present to the right of this list.

Figure TT1d.1. Multidimensional Editor.

Validation Section – Extensible Properties

In the original application design, validation sites and validation sections were designed to use predefined properties. However, from the workshop feedback, extensible properties were required to further describe the validation site itself or sections and items within the validation site. These characteristics are mentioned in the following list:

- Site properties such as deflection
- Site performance measures
- Mix compaction

This quarter, the design of validation site-based properties is nearing completion. Implementation of this revised design is underway and should be completed this quarter.

Enhanced Role-Based Authorization

The original system design included a role-based system in which users were added to roles. Based on a user's roles, rights were granted to access specific parts of the ARC system. Based on workshop feedback, it was determined that an additional layer of organizational rights needed to be created.

Based on workshop input, ARC users will be divided into ordinary users and organizational super users. Ordinary users will be restricted to editing records that they created. Ordinary users cannot edit records created by other ordinary users. Each organization will have an organizational super user. An organizational super user can edit records created by ordinary users belonging to the same organization. Organizational super users cannot edit records created by ordinary users of another organization. The role of consortium super user will have the rights to edit all data.

The design of this revised authorization is complete and development is presently underway. Development will begin with those tables used frequently by ARC users, such as measures, properties, and validation sites. Some database tables contain primarily static data or lookup data. Implementation of the authorization system for these tables will be performed last.

Enhanced Material Filtering and Sorting

One request by a consortium member was the ability to show all mixes which contain a particular material. This feature, along with other means of displaying and manipulating the data will be provided now that realistic data is being entered and tested.

Development of this new feature set is underway. SQL stored procedures to provide the advanced queries have been created along with the necessary database access code. User interface elements will be added this quarter.

Redesign of the Report Management System

The original system design provided users the ability to upload files such as quarterly reports and other research reports. The implementation was designed such that reports, when uploaded, were submitted for approval. The report super user would approve the report for general access.

Based in input from the workshop, the members requested a more configurable system for uploading reports and related research data, along with linking that data back to particular validation sites, measures, and materials. The revised report management system will have the following additional characteristics:

- In addition to uploading research reports, it is necessary to upload research data having different file types. For example, scanned images, video, or test data might need to be uploaded.
- This research data needs to be associated with particular work elements and work tasks.

- In addition, the system requires that links be created from properties, measures, and validation sites to the associated research data. A specific material or measure must have links to many data items.

The redesign of this sub-system is well underway.

- Because of the large number of files expected to be uploaded, a hierarchical file system will be used to organize files based on the program area, work category, work element, and work sub-task. Supporting files, by default, will be categorized according to the above elements. Users will be able to customize the file structure for custom data.
- Based on the initial design work, many tables contained a field designated to store a URL. As originally designed, this URL field would reference a report stored in the report management system or contain a link to an external URL. This field is repurposed to store an XML document fragment capable of storing references to several URLs (files) along with the capability of storing searchable meta-data.

Development of a custom user control to upload files into a custom directory structure is underway. The development of second user control that will allow users to select URLs from the preceding file system has started and a basic prototype created.

Software Download Registration Application

The ARC consortium has developed a software application named 3D-Move, which is now in Beta testing. This software has been made available to the general public through a registration Web site having the following characteristics:

- Users are required to register before downloading the software.
- Once the user has completed the registration form, the software download Web page appears. From here, users can click a link to download and install the 3D-Move software on their computer.
- A database stores a list of users who have downloaded the software. Note that this database is physically separate from the master ARC database.
- The project manager is notified when the software is downloaded.

The following figure shows the software download form:

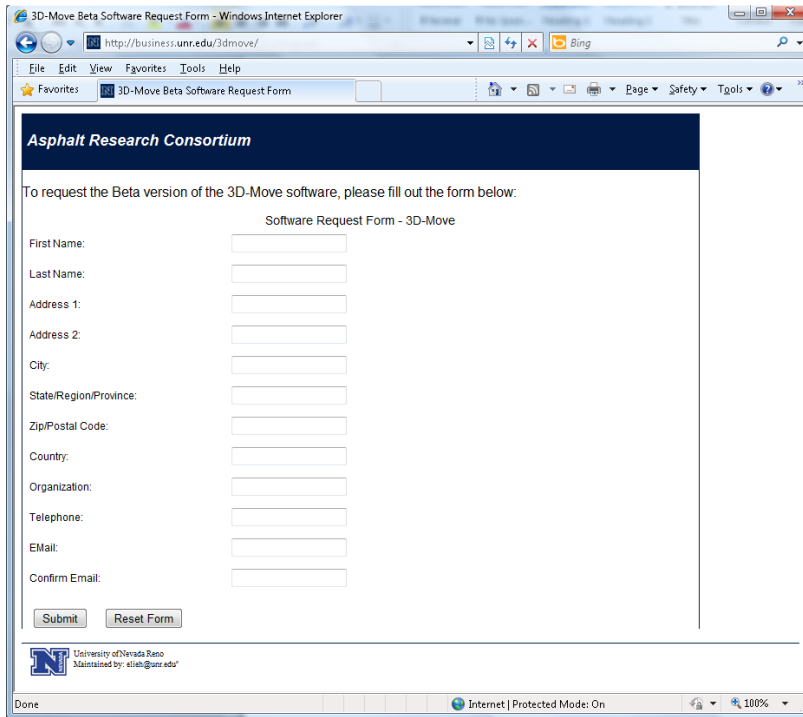


Figure TT1d.2. 3D-Move Software Download Form.

Operational Notes

Formal procedures have been implemented for application and data backups.

- The ARC database is backed up on a nightly basis. Offsite data copies are rotated weekly.
- The ARC application is backed up every other day to a remote site.

Significant Problems, Issues and Potential Impact on Progress

None

Work Planned Next Quarter

Much of the effort this quarter was spent analyzing the design changes from the March workshop. In designing these system changes, all attempts were made to minimize changes to existing database structures so as to minimize the cascading effects to code that depends on the database itself.

This quarter, the implementation of these changes will be carried out.

Work element TT1e: Development of Research Database (Duration: Year 2 through Year 5)

Work Done This Quarter

Uploaded the quarterly technical progress report to the ARC website. Uploaded the following references to the ARC website:

- A list of Publications and Conference Proceedings was added to the ARC website under the “Publications” webpage. A link to the *Abstract* was also provided for each publication.
- A list of Presentations and Posters was added to the ARC website under the “Outreach” webpage. A link to the *Presentation* or *Abstract* was also provided for each reference.
- A list of Theses and White Papers was added to the ARC website under the “Outreach” webpage. A link was also provided for each reference.

Significant Results

None.

Significant Problems, Issues and Potential Impact on Progress

None.

Work Planned Next Quarter

Upload the ARC quarterly technical progress report to the ARC website.

Work Element TT1f: Workshops and Training

Work Done This Quarter

No activity this quarter.

Significant Results

None

Significant Problems, Issues and Potential Impact on Progress

None

Work Planned Next Quarter

None

Technology Transfer Year 4	Year 4 (4/2010-3/2011)												Team	
	4	5	6	7	8	9	10	11	12	1	2	3		
(1) Outreach and Databases														
TT1a: Development and Maintenance of Consortium Website														UNR
TT1b: Communications														UNR
TT1c: Prepare presentations and publications														UNR
TT1d: Development of Materials Database														UNR
TT1d-1: Identify the overall Features of the Web Application														
TT1d-2: Identify Materials Properties to Include in the Materials														
TT1d-3: Define the Structure of the Database														
TT1d-4: Create and Populate the Database														
TT1e: Development of Research Database														UNR
TT1e-1: Identify the Information to Include in the Research Database														
TT1e-2: Define the Structure of the Database														
TT1e-3: Create and Populate the Database														
TT1f: Workshops and Training														UNR

Deliverable codes

D: Draft Report
 F: Final Report
 M&A: Model and algorithm
 SW: Software
 JP: Journal paper
 P: Presentation
 DP: Decision Point

Deliverable Description

Report delivered to FHWA for 3 week review period.
 Final report delivered in compliance with FHWA publication standards
 Mathematical model and sample code
 Executable software, code and user manual
 Paper submitted to conference or journal
 Presentation for symposium, conference or other
 Time to make a decision on two parallel paths as to which is most promising to follow through

 Work planned
 Work completed
 Parallel topic

Technology Transfer Years 2 - 5

	Year 2 (4/08-3/09)				Year 3 (4/09-3/10)				Year 4 (04/10-03/11)				Year 5 (04/11-03/12)				Team
	Q1	Q2	Q3	Q4	Q1	Q2	Q3	Q4	Q1	Q2	Q3	Q4	Q1	Q2	Q3	Q4	
(1) Outreach and Databases																	
TT1a: Development and Maintenance of Consortium Website																	UNR
TT1b: Communications																	UNR
TT1c: Prepare presentations and publications																	ALL
TT1d: Development of Materials Database																	UNR
TT1d-1: Identify the overall Features of the Web Application																	
TT1d-2: Identify Materials Properties to Include in the Materials Database																	
TT1d-3: Define the Structure of the Database																	
TT1d-4: Create and Populate the Database								SW, v. β	SW								
TT1e: Development of Research Database																	UNR
TT1e-1: Identify the Information to Include in the Research Database																	
TT1e-2: Define the Structure of the Database																	
TT1e-3: Create and Populate the Database																	
TT1f: Workshops and Training																	UNR

Deliverable codes

D: Draft Report
 F: Final Report
 M&A: Model and algorithm
 SW: Software
 JP: Journal paper
 P: Presentation
 DP: Decision Point

Deliverable Description

Report delivered to FHWA for 3 week review period.
 Final report delivered in compliance with FHWA publication standards
 Mathematical model and sample code
 Executable software, code and user manual
 Paper submitted to conference or journal
 Presentation for symposium, conference or other
 Time to make a decision on two parallel paths as to which is most promising to follow through

 Work planned
 Work completed
 Parallel topic

